



**mGBP2 engages Galectin-9 for immunity against
*Toxoplasma gondii***

Inaugural dissertation

for the attainment of the doctoral degree
of the Faculty of Medicine
of the Heinrich Heine University Düsseldorf

submitted by
Dr.rer.nat., M.Sc. Biochemistry

Elisabeth Kravets

Düsseldorf 2024

from the Institute for
Medical Microbiology and Hospital Hygiene
of the Heinrich Heine University Düsseldorf

Printed with the permission of the
Medical Faculty of the
Heinrich Heine University Düsseldorf

Dean: Prof. Dr. med. Nikolai Klöcker
Referee: Prof. Dr. Klaus Pfeffer
Co-referee: PD Dr. rer. nat. Albert Zimmermann
Day of the oral examination: 30.01.2025

Index of contents

List of figures	V
List of tables	VII
List of abbreviations	IX
1 INTRODUCTION.....	1
1.1. Interferon- γ	2
1.1.1. IFN- γ : Production und Signalling.....	3
1.2. GTP-binding proteins.....	10
1.2.1. IFN- γ inducible p47 und p65 GTPases.....	13
1.2.2. p65 Guanylate-binding proteins	15
1.3. Galectins.....	27
1.4. Cytoskeleton associated protein 4.....	30
1.5. <i>Toxoplasma gondii</i>	32
1.5.1. Human toxoplasmosis: prevention, screening, diagnosis, and treatment.....	48
1.5.1.1. Prevention and vaccination.....	48
1.5.1.2. Serological screening.....	49
1.5.1.3. Diagnosis.....	49
1.5.1.4. Therapy.....	51
1.5.2. New diagnostic-therapeutic research branches.....	52
1.6. Aim of the work	53
2. MATERIALS UND METHODS	55
2.1. Source of supply	55
2.1.1. Chemicals.....	55
2.1.2. Antibodies	57
2.1.3. Enzymes.....	57
2.1.4. Reagents and Consumables.....	58
2.2. Devices.....	59
2.3. Media and buffers.....	62
2.3.1. Cell culture media and supplements	62
2.3.2. Stock solutions and buffers	62
2.3.3. Media for cell culture	67
2.3.4. Media for bacterial culture	67

2.4. Antibiotics.....	67
2.5. Bacterial strains and cell lines.....	68
2.5.1. Bacterial and <i>Toxoplasma</i> strains.....	68
2.5.2. Cell lines	68
2.6. Primers.....	69
2.7. Plasmid vectors	76
2.7.1. Original vectors.....	76
2.7.2. Plasmids produced during the work	78
2.8. Cell biological methods	79
2.8.1. General cell culture methods.....	79
2.8.2. Cell line cultivation.....	79
2.8.3. Cultivation of primary mouse embryonic fibroblasts.....	79
2.8.4. Cell Count Determination	79
2.8.5. Freezing and thawing of cells	80
2.8.6. Transfection using transfection reagents	80
2.8.7. Lentiviral transduction for the production of stable cell lines	81
2.8.8. Virus production using the 293FT cell line.....	81
2.8.9. Lentiviral transduction of target cells (NIH 3T3, MEF)	82
2.8.10. Stimulation of cells	82
2.8.11. Immunofluorescence staining.....	83
2.8.12. SNAP-tag protein labelling in living cells	83
2.8.13. Gated Stimulated Emission Depletion (STED) measurement.....	84
2.8.14. Cultivation of <i>Toxoplasma gondii</i>	85
2.8.15. <i>In vitro</i> infection with <i>Toxoplasma gondii</i>	85
2.8.16. Determination of recruitment rates of fusion constructs to the PV and the formation of <i>T. gondii</i> rosettes	86
2.9. Molecular biological working methods	86
2.9.1. Analytical plasmid preparation from bacteria.....	86
2.9.2. Preparative plasmid isolation from bacteria.....	86
2.9.3. Genomic DNA extraction from eukaryotic cells.....	87
2.9.4. RNA extraction from eukaryotic cells	87
2.9.5. Reverse transcription of mRNA.....	88
2.9.6. Agarose gel electrophoresis	89
Analytical agarose gel electrophoresis.....	89
Preparative agarose gel electrophoresis and gel extraction.....	90
Determination of DNA fragment sizes.....	90

2.9.7. Enzymatic treatment of DNA	90
Restriction analysis of DNA	90
Dephosphorylation of DNA.....	91
2.9.8. Ligation of DNA molecules.....	91
TOPO TA Cloning® Kit	92
2.9.9. Transformation of <i>E. coli</i> bacteria.....	92
2.9.10. Cryopreservation of bacteria	93
2.9.11. Amplification of DNA molecules by PCR	93
2.9.12. CRISPR/Cas9 knockout strategy.....	94
2.9.13. The Surveyor Mutation Detection® for CRISPR/Cas9 knockout.....	97
2.10. Protein biochemical and biophysical methods.....	100
2.10.1. Preparation of total cell extracts from eukaryotic cells.....	100
2.10.2. Determination of protein concentration using BCA test	101
2.10.3. SDS-polyacrylamide gel electrophoresis (SDS-PAGE).....	101
2.10.4. Coomassie blue staining of protein gels.....	102
Conventional Coomassie R-250 staining	102
Colloidal Coomassie G-250 staining.....	102
2.10.5. Western Blot (Immunoblot).....	102
2.10.6. Immunoprecipitation	103
2.10.7. Silver staining	104
2.10.8. Silver de-staining	105
2.10.9. Reduction and alkylation of SDS gel bands/spots	105
2.10.10. In-gel trypsin digestion of reduced and alkylated spots.....	106
2.10.11. Spots/Band extraction	106
2.10.12. Sample Preparation for Proteomic Analysis	106
2.10.13. Liquid Chromatography and Mass spectrometry	107
2.11. Computer programmes	108
2.11.1. Cloning strategies.....	108
2.11.2. Sequence alignment	108
2.11.3. Quantitative analysis of MS data	109
2.11.4. Software for image analysis.....	109
2.11.5. Statistical analysis	110
2.11.6. Translation software.....	110
3. RESULTS	111
3.1. Identification of interaction partners of mGBP2.....	111
3.1.1. Co-immunoprecipitation analysis.....	111

3.1.2. Mass spectrometry analysis.....	112
3.1.3. Confirmation of Gal9 and Ckap4 as interaction partners of mGBP2 by co-immunoprecipitation analysis	115
3.2. Subcellular localization of Gal9 and Ckap4 and recruitment to the <i>T. gondii</i> PV	118
3.2.1. Confocal and STED analysis of subcellular localization of Gal9 and Ckap4	118
3.3. CRISPR/Cas9 mediated knockout of <i>gal9</i> and <i>ckap4</i> genes in NIH 3T3 fibroblasts.....	121
3.4. Recruitment of mGBP2 to the <i>T. gondii</i> PV in Gal9 deficient cells.	126
3.5. <i>T. gondii</i> replication control by Gal9.....	127
4 DISCUSSION.....	130
5 OUTLOOK.....	136
6 ZUSAMMENFASSUNG.....	137
6 SUMMARY.....	138
7 LIST OF REFERENCES.....	139
Acknowledgement.....	177
Appendix	178
Declaration of independence	199
Curriculum vitae.....	200

List of figures

Figure 1.1: Transduction and regulation of IFN- γ signalling pathways.....	5
Figure 1.2: Structures of GTP-binding proteins.	12
Figure 1.3: GTPase-cycle of GTP-binding proteins.	13
Figure 1.4: Expression of IFN-inducible GTPase families and other characterized anti-microbial effectors.....	14
Figure 1.5: Phylogenetic tree of the p65 mGBPs.....	16
Figure 1.6: Linearized diagram of the three-domain structure of mGBP2.	17
Figure 1.7: Structural and functional properties of a predicted dimer and a tetramer model of mGBP2.	19
Figure 1.8: Structure model of mGBP2.	20
Figure 1.9: Structure functional relationship of the mutations of mGBP2.	25
Figure 1.10: Galectin family members.	28
Figure 1.11: Functions of endogenous galectins.	30
Figure 1.12: The mechanism of Ckap4 regulating cell proliferation.	31
Figure 1.13: Life cycle of <i>T. gondii</i>	34
Figure 1.14: <i>T. gondii</i> entry and control of persistent infection in the brain.....	36
Figure 1.15: Ultrastructure of <i>T. gondii</i> tachyzoite.....	37
Figure 1.16: <i>T. gondii</i> host cell interactions.	40
Figure 1.17: The role of <i>T. gondii</i> virulence factors in modulating innate immune signalling in the host.....	42
Figure 1.18: Control of pro-inflammatory responses during a <i>T. gondii</i> infection.	47
Figure 2.1: Timeline and overview of the CRISPR/Cas9 experimental strategy.	95
Figure 2.2: Target selection and plasmid preparation.	96
Figure 3.1. Identification of mGBP2 interaction partners.	112
Figure 3.2: Identification of mGBP2 interacting proteins using co-immunoprecipitation in combination with label-free quantitative mass spectrometry.	113
Figure 3.3: Verification of Gal9 and Ckap4 as interaction partners of mGBP2 by IP analysis.	116
Figure 3.4: Intracellular colocalization of mGBP2 interaction partners Gal9 and Ckap4 at the PVM of <i>T. gondii</i>	119
Figure 3.5: Localization of Gal9 and mGBP2 during <i>T. gondii</i> infection.....	120
Figure 3.6: CRISPR/Cas9 gene editing of Gal9 and verification of Gal9 inactivation.	122
Figure 3.7: Verification of CRISPR/Cas9 Gal9 inactivation using Surveyor [®] Mutation Detection Kit.....	123
Figure 3.8: Verification of CRISPR/Cas9 Gal9 inactivation by WB analysis.	124

Figure 3.9: Verification of CRISPR/Cas9 Ckap4 inactivation by WB analysis.....	125
Figure 3.10: Gal9 influences the recruitment of mGBP2 to the PVM of <i>T. gondii</i>	126
Figure 3.11: Gal9 is required for the intracellular control of replication of <i>T. gondii</i>	128
Figure 3.12: Inactivation of Gal9 does not influence infection rates of <i>T. gondii</i>	128
Figure 3.13: Gal9 controls the intracellular replication of <i>T. gondii</i>	129
Figure S1: Expression plasmids for interaction partner analysis of mGBP2.....	178
Figure S2: Identification and validation of mGBP2 interaction partners.....	179
Figure S3: Identification of mGBP2 interaction partners.....	180
Figure S4: Verification of MS-identified interaction partners of mGBP2 by IP analysis.....	182
Figure S5: Intracellular colocalization of mGBP2 with the interaction partners Gal9 and Ckap4.	183
Figure S6: Intracellular colocalization of mGBP2 with the interaction partners Gal9 and Ckap4.	184
Figure S7: Intracellular colocalization of mGBP2 with the interaction partners Gal9 and Ckap4.	185
Figure S8: Intracellular colocalization of mGBP2 with the interaction partners Gal9 and Ckap4. STED microscopy.....	187
Figure S9: Intracellular colocalization of mGBP2 with the interaction partners Cathepsin-D and ISG15. Confocal microscopy.	188
Figure S10: CRISPR/Cas9 cloning strategy.	189
Figure S11: Verification of CRISPR/Cas9 Gal9 inactivation by WB analysis.	190
Figure S12: Schematic view of mGBPs, Gal9, and Ckap4 dynamics and multimerization in <i>T.</i> <i>gondii</i> infected cells. For details see Results and Discussion.....	195
Figure S13: Expression plasmids for <i>T. gondii</i> virulence factors.....	196
Figure S14: Intracellular colocalization of mGBP2 with GRA proteins of <i>T. gondii</i> in uninfected cells.....	198
Figure S15: Intracellular colocalization of GRA proteins with SAG1 protein of <i>T. gondii</i>	198
Figure S16: Intracellular colocalization of mGBP2 with GRA proteins of <i>T. gondii</i> in <i>T. gondii</i> infected cells.	198

List of tables

Table 1.1: Serological diagnosis of Toxoplasmosis. Adopted from (Robert-Koch-Institut, 2016). ...	50
Table 2.1: Composition of the cell culture media.....	67
Table 2.2: Composition of the bacteria culture media.	67
Table 2.3: Antibiotics used.....	67
Table 2.4: Bacterial and toxoplasma strains used.....	68
Table 2.5: Cells used.....	68
Table 2.6: Primer for cloning GFP and mCherry fusion constructs.....	69
Table 2.7: Primers for the cloning of truncated GFP-mGBP2 fusion constructs.....	73
Table 2.8: Mutagenesis primers for generating point mutants of mGBP2 in pWPXL-GFP vectors.....	74
Table 2.9: Primers for the introduction of an HA marker at the N-terminus of mGBP2 and subsequent cloning into the pWPI vector.	74
Table 2.10: Primer for CRISPR/Cas9 knockout strategy and Surveyor® nuclease base knock out analysis.....	74
Table 2.11. Sequencing primers.....	75
Table 2.12: Sequences of oligonucleotides and probes for real-time RT-PCR experiments.	76
Table 2.13: Used starting vectors.....	77
Table 2.14: Generated plasmids.....	78
Table 2.15: Reverse Transcription RNA/primer mixture.....	88
Table 2.16: Reverse Transcription (RT) cDNA Synthesis Mix	89
Table 2.17: Restriction digestion.	90
Table 2.18: Standard PCR set-up.....	93
Table 2.19: Programming under standard PCR conditions.	94
Table 2.20: The Surveyor Mutation Detection Kit.....	98
Table 2.21: Set up Surveyor Nuclease reactions for Control G and Control C duplexes.....	98
Table 2.22: PCR products preparation for Surveyor Nuclease assay.	98
Table 2.23: PCR program for Surveyor Nuclease assay.....	99
Table 2.24: Hybridization of PCR amplified DNA for Surveyor Nuclease assay.....	99
Table 2.25: Set up Surveyor Nuclease reactions for digestion of the hetero/homoduplex and reference DNA.....	100
Table 2.26: Set up for silver staining for SDS-PAGE gels.	104
Table 2.27: Washing of SDS gel bands/spots.....	105
Table S1: List and known function of mass spectrometry-identified potential interaction partners of mGBP2.....	180

Table S2: List and validation status of mass spectrometry-identified potential interaction partners of mGBP2.	181
Table S3: Recruitment rates of Gal9 to PV of <i>T. gondii</i> in IFN- γ stimulated WT compared to mGBP2 ^{-/-} MEF 2 h post infection.	190
Table S4: Recruitment rates of mGBP2 to PV of <i>T. gondii</i> in IFN- γ stimulated WT NIH 3T3 fibroblasts compared to cells with specific gene inactivation mutants 2 h post infection. ...	191
Table S5: Recruitment rates of mGBP2 to PV of <i>T. gondii</i> in IFN- γ stimulated WT NIH 3T3 fibroblasts compared to cells with specific gene inactivation mutants, followed by plasmidic gene reconstitution 2 h post infection.	191
Table S6: Replication rates of <i>T. gondii</i> in IFN- γ stimulated NIH 3T3 fibroblasts compared to cells with specific gene inactivation mutants 22 h post infection.	192
Table S7: Replication rates of <i>T. gondii</i> in IFN- γ stimulated, GFP-mGBP2 expressing NIH 3T3 fibroblasts compared to cells with specific gene inactivation mutants, and replication rates in the cells lines followed by plasmidic gene reconstitution 24 h post infection.	193
Table S8: Infection rates of <i>T. gondii</i> in IFN- γ stimulated WT NIH 3T3 fibroblasts compared to cells with specific gene inactivation mutants 2 h post infection.	194
Table S9: List and validation status of <i>T. gondii</i> virulence factors as potential interaction partners of mGBP2.	195

List of abbreviations

ADAR-1	Adenosine deaminase RNA specific-1
AIDS	Acquired immunodeficiency syndrome
Aifm1	Apoptosis-inducing factor 1
AMPK	Adenosine monophosphate-activated protein kinase
Anxa5/6	Annexin A5/A6
APC	Antigen presenting cell
APF	Antiproliferative factor
ATG4b/5	Autophagy related 4b/5
ATP	Adenosine triphosphate
BAG	Bradyzoite antigen
BGB	Blood group B antigen
BMDM	Bone marrow derived macrophages
bp	Base pair(s)
BSA	Bovine serum albumin
CCR5	Cysteine-cysteine chemokine receptor 5
CD	Cluster of differentiation
cDC	Conventional dendritic cell
cDNA	DNA copy of the mRNA (complementary DNA)
<i>C. trachomatis</i>	<i>Chlamydia trachomatis</i>
<i>C. muridarum</i>	<i>Chlamydia muridarum</i>
Ckap4	Cytoskeleton-associated protein 4
CNS	Central nervous system
Copa	Coatomer subunit alpha
CRD	Carbohydrate recognition domain
Cse1	Chromosome segregation 1 Like
CT	C-terminal tail
CTIIA	MHCII transactivator
d	Day
DAPI	4',6-diamidine-2-phenylindole
DC	Dendritic cell
ddH ₂ O	Double distilled or Milli-Q (Millipore) water
Ddx5/6/21	DEAD box protein 5/6/21
Dhx9	DExH-box helicase 9
DKK1	Dickkopf-related protein 1
DMEM	Dulbecco's Modified Eagle Medium
DMSO	Dimethyl sulphoxide
DNA	Deoxyribonucleic acid
dNTP	Deoxyribonucleotides (dATP, dTTP, dCTP, dGTP)
DTT	Dithiothreitol
ECL	Enhanced chemiluminescence
<i>E. coli</i>	<i>Escherichia coli</i>
ECMV	Encephalomyocarditis
EDTA	Ethylenediaminetetraacetic acid
EF	Elongation factor
EF cells	Embryonic fibroblasts
Eif3	Eukaryotic translation initiation factor-3

ER	Endoplasmic reticulum
ERGIC	ER/Golgi intermediate compartment
FCS	Foetal calf serum
FRET	Förster Resonance Energy Transfer
FTase	Farnesyltransferase
FVIII	Coagulation cofactor factor VIII
GAF	STAT1 homodimer
Gal9	Galectin 9
GAS	IFN- γ activated site
GAP	GTPase activating protein
GBP	Guanylate-binding protein
GDI	Guanine dissociation inhibitor
GDP	Guanosine diphosphate
GEF	Guanine exchange factor
GGTase I	Geranylgeranyltransferase I
Gls	Glutaminase
GMP	Guanosine monophosphate
GPI	Glycosylphosphatidylinositol
GRA7/15/25	Dense granule proteins
GTP	Guanosine triphosphate
h	Hour(s)
HAART	highly active antiretroviral therapy
HCC	Hepatocellular carcinoma
HIF1	Hypoxia inducible factor 1
HIV	Human deficiency virus
<i>H. pylori</i>	<i>Helicobacter pylori</i>
HSP	Heat shock protein
IDO	Indoleamine-2,3-dioxygenase
IF	Initiation factor
Ifitm3	Interferon-induced transmembrane protein 3
IFN- γ	Interferon gamma
IFNGR	IFN- γ receptor
IL	Interleukin
ILC	Innate lymphoid cell
IMDM	Iscove 's Modified Dulbecco 's Medium
iNOS	Inducible nitric oxide synthase
IRES	Internal ribosomal entry site
IRF	Interferon regulatory factor
IRG	Immunity-related GTPase
ISG	IFN stimulated genes
ISG15	Interferon-stimulated gene product 15
ISGF3	IFN-stimulated gene factor 3
ISRE	IFN-stimulated response elements
JAK	Janus Kinase
Kank2	KN motif and ankyrin repeat domains 2
kb	Kilobase pair(s)
kgBW	Kilogram body weight
ko	Knockout
kDa	Kilodalton

Kpna2	Karyopherin α -2
Kpnb1	Karyopherin subunit beta 1
Lamp2	Lysosome-associated membrane protein 2
<i>L. monocytogenes</i>	<i>Listeria monocytogenes</i>
LCV	<i>Legionella</i> -containing vacuole
LC3	Light chain 3
LDL	Low-density lipoprotein
LPS	Lipopolysaccharide
LSM	Laser Scanning Microscopy
M	Molar
MAP 4	Microtubule-associated protein
MCS	Multiple cloning site
MDR	Multidrug resistance
MEF	Murine embryonic fibroblast
MEK	Methyl ethyl ketone
M ϕ	Macrophage
MFIS	Multiparameter fluorescence image spectroscopy
Mgat	Monoacylglycerol Acyltransferase
min	Minute(s)
MHC	Major Histocompatibility complex
MMP	Matrix metalloproteinases
mRNA	Messenger RNA
<i>M. tb</i>	<i>Mycobacterium tuberculosis</i>
MTOC	Microtubule organisation centre
MVMp	Minute virus of mice prototype strain
MyD88	Myeloid differentiation primary response gene 88
NADPH	Nicotinamide adenine dinucleotide phosphate
Nampt	Nicotinamide phosphoribosyltransferase
NF- κ B	Nuclear factor- κ B
NK	Natural killer cell
NCS	Newborn-Calf-Serum
NDP52	Nuclear dot protein 52
NO	Nitric oxide
NOX	NADPH oxidase
Npm	Nucleophosmin
NRAMP-1	Natural Resistance-Associated Macrophage Protein-1
o/n	Over night
ORF	Open reading frame
PAMP	Pathogen associated molecular pattern
PBS	Phosphate-buffered saline
p.c.	Post coitus
PCR	Polymerase Chain Reaction
PCV	Pathogen containing vacuole
PFA	Paraformaldehyde
PKP	Protein kinase P
p.o.	Per os
PRR	Pattern recognition receptor
P/S	Penicillin/streptomycin
PTP	Tyrosine phosphatase

PV	Parasitophorous vacuole
PVM	Parasitophorous vacuolar membrane
RNI	Reactive nitrogen intermediates
ROI	Reactive oxygen intermediates
ROP5/16/17/18	Rhoptry protein 5/16/17/18
ROS	Reactive oxygen species
RNS	Reactive nitrogen species
rpm	Rounds per minute
RPMI	Roswell Park Memorial Institute
RT	Room temperature
RT-PCR	Reverse transcription and polymerase chain reaction
SAG	Surface antigen
SARS-CoV-2	Severe acute respiratory syndrome coronavirus 2
SCV	<i>Salmonella</i> -containing vacuole
SDS	Sodium dodecyl sulphate
SDS-PAGE	Sodium dodecyl sulphate polyacrylamide gel electrophoresis
SH2/3	Src homology 2/3
SQSTM1	Sequestosome 1
SOCS	Suppressor of cytokine signalling
SRS	SAG-related sequences
SSH	Suppression-subtractive hybridization
STAT1	Signal Transducer and Activator of Transcription 1
SUSA	SAG-unrelated surface antigens
<i>T. cruzi</i>	<i>Trypanosoma cruzi</i>
<i>T. gondii</i>	<i>Toxoplasma gondii</i>
TE	Toxoplasmic encephalitis
TLR	Toll-like receptor
Thbs1	Thrombospondin 1
TM	Transmembrane
TNF	Tumour necrose factor
TnpoI	Transportin I
VLIG	Very large inducible GTPase
TVN	Tubulo-vesicular network
v/v	Volume/volume
VSV	Vesicular Stomatitis Virus
vWF	von Willebrand factor
Wnt	Wingless/Integrated
w/v	Weight/volume
WT	Wild type

1 Introduction

The immune system of vertebrates is a complex network of cellular and humoral components. It provides protection against a variety of pathogens and the damage they cause, as well as against other harmful substances, such as toxins from pathogens and insects (Murphy, 2009, p. 5). The innate and adaptive immunity are two interlocking mechanisms of pathogen defence that have evolved over time.

The adaptive immunity mediates cellular and humoral response mechanisms by the maturation and expansion of B and T cells, that lead to the formation of a pathogen-specific and efficient elimination of pathogens. This pathogen specificity also builds the "immunological memory," which allows the immune system to respond more quickly and efficiently upon repeated infections or preventive vaccination using "memory" lymphocytes (Abbas, 2007, p. 4; Murphy, 2009, p. 36). However, the adaptive immune response takes several days to establish the necessary specificity and effectiveness for the targeted elimination of a pathogen during a first infection (Murphy, 2009, chapter 1). During this time, the infected organism's innate or native immune system represents the primary anti-microbial defence line, preventing or delaying the spread of infection. The innate immunity is activated directly by pathogens through the recognition of pathogen-associated molecular patterns (PAMPs) and possesses cellular and biochemical defence mechanisms that quickly respond to a wide range of infections and initiate the development of adaptive immunity (Murphy, 2009, p. 19). The epithelial tissue of the skin, the gastrointestinal and the respiratory tract is the main component of the innate immune system, which on the one hand represents the first mechanical barrier for the invading germ, and on the other hand already actively provides anti-microbial defence mechanisms through surface and/or secreted proteins (defensins) (Abbas, 2007, p. 4). Additionally, the complement system, consisting of a number of soluble proteins, plays an important role in both recruiting inflammatory cells to the pathogen (chemoattraction) and directly lysing bacteria, viruses, and eukaryotes (Abbas, 2007, p. 4). However, the central elements of the innate immune system are its cellular components, consisting of phagocytes, natural killer cells (NK), and other inflammatory cells, which provide strong anti-microbial effector mechanisms even before the initiation of an adaptive immune response and thus contribute significantly to the elimination of pathogens or the delay of infection spread. The interaction of these cellular components is directed by cytokines and chemokines, which can regulate immune responses as signalling molecules (Abbas, 2007, p. 4). Phagocytes, such as dendritic cells

(DC) and macrophages (M ϕ), represent the decisive interface between the innate and adaptive immunity and serve as important effector cells of adaptive immune responses. Therefore, understanding the host-pathogen interactions in the context of an immune response requires exploring the mechanisms and effector molecules of the innate immune system, as these represent the first step in eliminating the pathogen. Interferons are among the most important cytokines in pathogen defence.

1.1. Interferon- γ

The mammalian immune system has evolved mechanisms to recognise, eliminate or contain the growth of various pathogens and to eliminate cancer cells. In this respect, interferons (IFNs) play a crucial role. They provide anti-microbial, anti-proliferative and immunomodulatory effects. Type I interferons (IFN- α und IFN- β) are mostly secreted by virus-infected cells. The main source of type II interferon (IFN- γ), besides activated CD4⁺ T_H1 cells, are NK cells and CD8⁺ cytotoxic T cells (Boehm et al., 1997). Other subtypes of T cells, such as T_H0 cells, T_{reg} cells, $\gamma\delta$ -T cells, NK-T cells, as well as M ϕ , DCs and even B cells are also capable of producing IFN- γ (Frucht et al., 2001; Szabo et al., 2003). In NK and T cells, IFN- γ is induced by IL-12 and tumour necrosis factor- α (TNF- α), which are secreted by conventional DCs (cDCs) and M ϕ (Bancroft et al., 1991; Paludan, 2000).

IFN- γ is the central effector of cell-mediated immunity and can coordinate a plethora of antimicrobial functions. It enhances antigen presentation by antigen-presenting cells (APCs) by improving antigen recognition via interaction with T cells, by increasing the production of reactive oxygen species (ROS) and reactive nitrogen intermediates (RNI) and induces antiviral immune responses (Schroder et al., 2004). Additionally, cancer cells are destroyed by IFN- γ activity via induction of an anti-proliferative state (Jorgovanovic et al., 2020) (Jorgovanovic et al., 2020). Immunity to several pathogens is mainly governed by IFN- γ activity. For example, the role of IFN- γ in endowing protection against *Toxoplasma* and *Chlamydial* infections is quite immense (Lima and Lodoen, 2019; Rothfuchs et al., 2004). Additionally, IFN- γ plays a vital role in combating mycobacterial infections by regulating protective functions and sustaining the activity of both CD4⁺ and CD8⁺ cells (Green et al., 2013). The protective benefits of IFN- γ can also be seen in the context of viral infections, as enhanced survival of neurons infected with varicella zoster virus is observed post IFN- γ treatment (Baird et al., 2015). In HIV⁺ (Human Immunodeficiency Virus) patients, the production of IFN- γ by NK cells can effectively restrict the proliferation

of Hepatitis C virus (Kokordelis et al., 2014). During *Staphylococcus aureus* infections, IFN- γ provides improved antibacterial and immune protective effects, along with pro-inflammatory responses that safeguard epithelial monolayers from injury caused by pathogens (Beekhuizen and van de Gevel, 2007). The absence of IFN- γ -activated cellular signalling pathways leads to increased susceptibility of mice to a wide range of pathogens such as *Leishmania major*, *Listeria monocytogenes*, mycobacteria, *Toxoplasma gondii*, and some viruses, as well as increased lethality in sepsis (Cooper et al., 1993; Graham et al., 1993; Muller et al., 1994; Orange et al., 1995; Wang et al., 1994; Zantl et al., 1998). Furthermore, a deregulation of the expansion of certain hematopoietic precursor cell lines is found in IFN- γ -deficient mice (Murray et al., 1998). In humans, it has been observed that genetic defects in IFN- γ receptor (IFNGR) genes lead to susceptibility to infections with *Mycobacteria*, *Toxoplasma*, and *Salmonella* (Dalton et al., 1993; Filipe-Santos et al., 2006; Huang et al., 1993; Jouanguy et al., 1999; Ottenhoff et al., 2002; Schariton-Kersten et al., 1996). Thus, IFN- γ is a potent protective molecule that offers defence against a diverse range of pathogenic entities.

IFN- γ enhances the immune system's ability to combat microbes, but its activity is tightly regulated due to its potential to cause tissue damage, necrosis, and inflammation, leading to disease pathology. Overactivity of both IFN- γ and IL-18 can worsen *Burkholderia* infections (Koo and Gan, 2006), while aberrant IFN- γ production has been associated with autoimmunity and changes in gut flora (Belkaid and Rouse, 2005; Miller et al., 2009). As a result, IFN- γ activity is a double-edged sword, and immune regulatory mechanisms aim to maintain a delicate balance between infection control and disease pathology.

1.1.1. IFN- γ : Production und Signalling

Interferons were initially identified as agents that interfere with viral replication and have potent antiviral activity. However, they have since been found to have a wide range of physiological activities that extend beyond their antiviral effects. IFN- γ secreted by natural killer cells and antigen-presenting cells is believed to play a role in early host defence and autocrine regulation, while T cells are the primary source of IFN- γ during adaptive immunity.

IFN- γ responses are initiated by receptor-mediated signalling. Its interaction with the receptor (IFN- γ R) present on target cells such as macrophages, dendritic cells, and other cell types leads to a signalling cascade that produces protective responses (Bach et al., 1997).

Unlike IFN- α , which has 14 orthologous genes in both humans and mice (Bogdan et al., 2004), IFN- γ is encoded by a single gene located on chromosome 12 in humans and chromosome 10 in mice (Chen et al., 2004; Pestka et al., 2004). IFN- γ has a molecular weight of 34 kDa and in its biologically active form builds a non-covalently bound homodimer (Farrar and Schreiber, 1993; Fountoulakis et al., 1992). IFNGR is expressed on the surface of all nucleated cells, but at varying densities. IFNGR is a heterotetramer consisting of two ligand-binding IFNGR1 subunits (or chains) and two signal-transducing IFNGR2 subunits (or chains) (Figure 1.1). Each of these receptor subunits is constitutively associated with a member of the Janus kinase (JAK) family: IFNGR1 with JAK1 and IFNGR2 with JAK2 (Bach et al., 1997; Chen et al., 2004; Igarashi et al., 1994). Signal transduction begins with the binding of the IFN- γ homodimer to the two chains of IFNGR, initiating a conformational change and dimerization of the two IFNGR1 subunits (Greenlund et al., 1993). Thereby, IFN- γ binds to IFNGR1 with relatively higher affinity compared with IFNGR2. This results in the association of two IFNGR2 subunits with the IFN-/IFNGR1 complex and the subsequent auto- and transphosphorylation and reciprocal activation of JAKs. The activated JAKs phosphorylate the two IFNGR1 chains at Tyr440 in the cytoplasmic domain, creating two docking sites for the Src homology 2 (SH2) domains of the cytosolic signal transducer and activator of transcription 1 (STAT1) molecules (Greenlund et al., 1994; Heim et al., 1995). The STAT1 molecules are phosphorylated at Tyr701 and dissociate from the complex to form homodimers. The STAT1 dimer enters the nucleus where it binds to specific promoter sequences known as the IFN-activated site (GAS). Binding of the dimer to DNA initiates transcription of IFN-stimulated genes (ISGs). Some STAT1-activated genes are also transcription factors, such as IFN-regulated factor-1 (IRF-1) (Sims et al., 1993) and MHC II transactivator (CTIIA), which regulate the expression of secondary activated genes by binding to IFN-stimulated response elements (ISRE). GAS and ISRE sequences often overlap, and genes containing both promoter sequences may be primarily or secondarily regulated. Initial induction of IFN-regulated genes occurs 15-30 min after stimulation (Kerr and Stark, 1991). Activated STAT1 is then acetylated in the nucleus by the histone acetyltransferase CBP and dephosphorylated by the phosphatase TCP45. The dephosphorylated dimer translocates back to the cytosol where it is deacetylated by the

histone deacetylase (HDAC) HDAC3 and made available for the next cycle of phosphorylation/acetylation (Hu and Ivashkiv, 2009; Schroder et al., 2004) (Fig. 1.1).

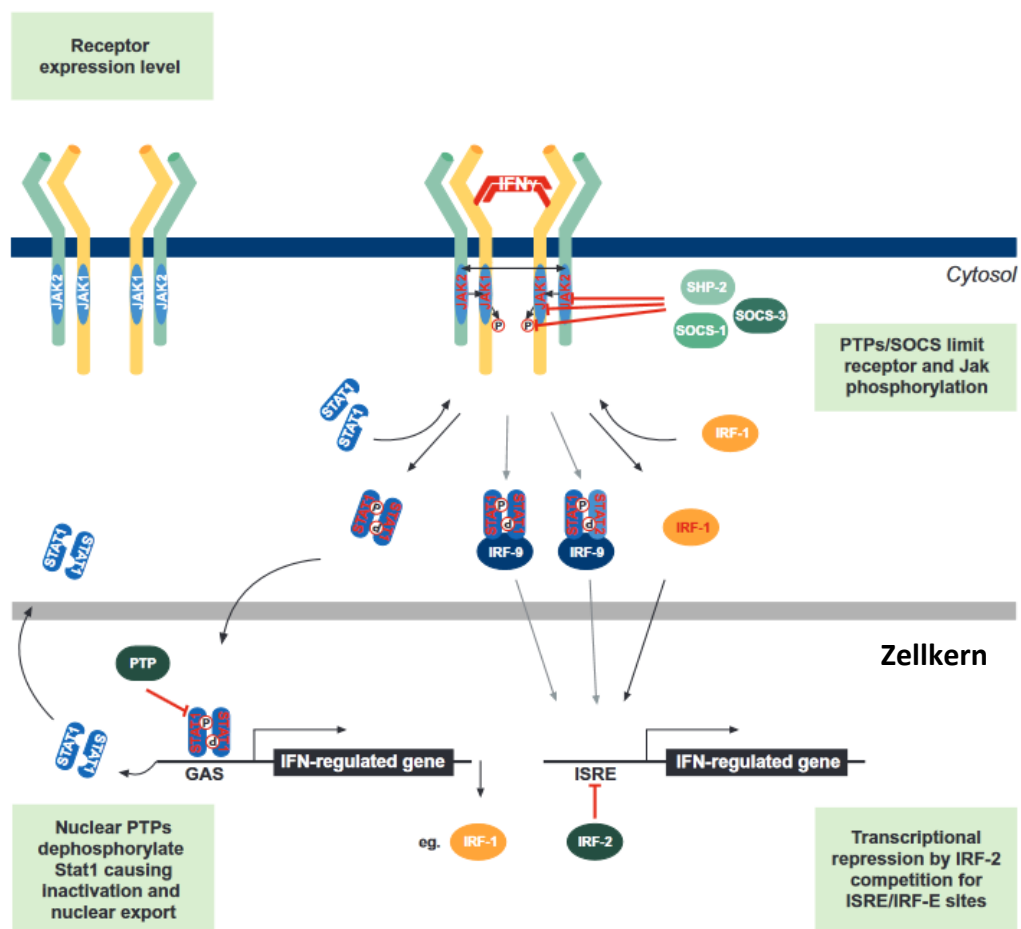


Figure 1.1: Transduction and regulation of IFN- γ signalling pathways.

A homodimer of IFN- γ triggers the formation of a complex consisting of four receptor subunits (IFNGR1, yellow; IFNGR2, green) along with four associated JAKs. Each of these JAKs becomes activated and phosphorylates a subunit of the receptor, thereby creating binding sites for STAT1 molecules, which are also phosphorylated by the JAKs. The phosphorylated STAT1 molecules dissociate from the receptor and form a homodimer, which is transported to the nucleus where it binds to GAS promoter sequences of target genes, including transcription factors such as IRF-1, and activates transcription. Secondary genes are transcribed dependent on IRF-1 by activating the ISRE promoter sequences. In addition, IFN- γ signalling also leads to the formation of STAT1:STAT1:IRF-9 and STAT1:STAT2:IRF-9 (ISGF3) complexes, which bind to ISRE promoter regions. IRF-1 is also able to promote transcription of Stat1 through an unusual ISRE site (IRF-E/GAS/IRF-E). Protein tyrosine phosphatases (PTP), such as Shp2, dephosphorylate the JAKs and IFNGR1. SOCS-1 and SOCS-3 interfere with JAK activity. STAT1 activity is downregulated by dephosphorylation and acetylation in the nucleus. IRF-2 antagonizes transcriptional activation of many (IRF-1-inducible) genes containing ISRE or IRF-E promoter elements by competing for binding sites without promoting gene expression. According to (Schroder et al., 2004) and (Hu and Ivashkiv, 2009).

To terminate signal transduction, the reduction of phosphorylated STAT1 species is initiated by suppressor of cytokine signalling (SOCS-1) proteins through the ubiquitin-proteasome pathway in a negative feedback mechanism (Alexander et al., 1999). SOCS-1 deficient mice die from excessive IFN- γ signalling, which leads to uncontrolled

inflammation and tissue damage (Schroder et al., 2004). SOCS-3, which is induced by IFN- γ , can also negatively regulate IFN- γ dependent signalling (Song and Shuai, 1998). Tyrosine phosphorylation in the JH2 domain of JAK2 inhibits cytokine-induced signal transduction (Feener et al., 2004). Additionally, protein tyrosine phosphatases (PTP), such as Shp2, dephosphorylate JAK1, JAK2, and IFNGR1 (You et al., 1999). The ligand-receptor complex is finally internalized and dissociated intracellularly (Farrar and Schreiber, 1993). In most cells, the IFNGR1 subunit is transported back to the cell surface. In human fibroblasts, internalized IFN- γ is lysosomally degraded (Anderson et al., 1983).

The signalling cascade induced by IFN- γ may partially overlap with that of type I (α/β) IFN signalling via activation of the STAT1-STAT2-IRF-9 complex, also known as IFN-stimulated gene factor (ISGF3). Type I IFNs activate the transcription factors STAT2 and STAT1 via JAK1 and tyrosine kinase 2 (TYK2) (Bach et al., 1997; Chen et al., 2004; Karaghiosoff et al., 2000; Prejean and Colamonici, 2000; Varinou et al., 2003). The ISGF3 complex translocates to the nucleus and initiates transcription of genes that have an ISRE sequence in their promoter regions. Unlike IFN- β , activation of these genes by type I IFN does not require *de novo* protein biosynthesis and is therefore considered a primary response. Association of IRF-9 with the STAT1 homodimer (GAF) can redirect the specificity of the transcription factor from GAS to ISRE promoters (Bluyssen et al., 1995). In turn, type I IFNs can initiate the formation of GAF and thus induce gene expression via GAS elements (Platanias, 2005). Thus, the transcriptional specificity of IFN- γ can be modified at the level of secondary responsiveness, thereby activating typical type I responsive genes (Gao et al., 1993).

Stimulation of cells with IFN- γ activates the transcription of over 2000 genes (Boehm et al., 1997; Degrandi et al., 2009; Degrandi et al., 2007; Taylor et al., 2004), whose gene products exert diverse and essential cellular effects on both innate and adaptive immunity.

As mentioned above, IFN- γ is produced by T_H1 cells, whereas T_H2 cells mainly secrete IL-4 and IL-5. In general, T_H1-mediated cellular immunity is induced by intracellular pathogens such as bacteria and protozoa, whereas T_H2-associated immune responses are mediated via antibody-dependent effector mechanisms, such as in defence against nematodes. IFN- γ thus stimulates innate cell-mediated immunity, specific cytotoxic immunity via recognition of MHC associated antigens and activation of M ϕ . In infection experiments with intracellular pathogens such as *Leishmania*, *Toxoplasma* and *Listeria*, the suppression of the T_H1 response, and more specifically the interference with IFN- γ production and action, leads to

incomplete elimination of the pathogens (Reiner and Locksley, 1995; Sher and Coffman, 1992).

IL-12 is secreted by activated DCs, or by neutrophils induced by lipopolysaccharide (LPS) or other PAMP molecules and M ϕ (Heufler et al., 1996; Macatonia et al., 1995; Trinchieri, 1995). IL-12 induces gene expression (Lederer et al., 1996) and secretion (Trinchieri, 1995) of IFN- γ in antigen-stimulated CD4⁺ T cells and also in NK cells and, in combination with IFN- γ , leads to T_{H1} polarisation of T_H cells (Wenner et al., 1996) and NK cell activation. Conversely, IL-12 is induced by IFN- γ in M ϕ and monocytes (Hayes et al., 1995; Yoshida et al., 1994). The T_{H1} modality is thus stabilised by a positive "feed-back loop". In turn, IFN- γ inhibits the growth and *in vitro* differentiation of T_{H2} cells (Seder et al., 1992).

Macrophages, which serve as versatile guardians of the immune system, act as APCs and are among the first immune cells to encounter invading pathogens. IFN- γ , a cytokine produced by T cells and NK cells, activates M ϕ and enhances their ability to combat microbial infections. This activation results in various immune responses, including improved antigen processing and presentation through upregulation of class II MHC, increased production of ROS and nitrogen species (NOS), induction of autophagy to clear intracellular pathogens, and greater secretion of pro-inflammatory cytokines. IFN- γ also stimulates NK cells, which become better equipped to eliminate tumours, and modulates B cell responses by regulating antibody production. Moreover, IFN- γ facilitates the growth and maturation of other cell types and promotes the migration of leukocytes to sites of infection. This heightened immune activation ultimately leads to the efficient clearance of pathogens through enhanced phagocytosis, pro-inflammatory responses, and lymphocyte recruitment.

IFN- γ possesses a remarkable ability to quickly trigger acidification of phagolysosomes in infected macrophages. The resulting low pH environment within the phagolysosome improves the production of reactive nitrogen species (RNS), and this cooperation between IFN- γ and RNS ultimately eliminates the invading pathogen (Flannagan et al., 2009). Additionally, IFN- γ is a powerful inducer of autophagy, which is now recognized as a new host response to fight against microbial infections (Kroemer and Levine, 2008; Li et al., 2012; Singh et al., 2006). Recently, it has been shown that proteins involved in autophagy play a role in controlling intracellular bacterial and parasitic infections (Zhao et al., 2008). For example, ATG5, which is essential for the conversion of LC3 I to LC3 II and its association with autophagosomes (Mizushima et al., 2002), is required for *in vivo* resistance to *Listeria* and *Toxoplasma* in macrophages (Zhao et al., 2008).

p47 Immunity-related GTPases (IRGs) comprise another very interesting group of IFN- γ -inducible proteins. Stimulation with IFN- γ results in the upregulation of multiple IRGs, which in turn promote the recruitment of autophagic machinery to bacterial phagosomes. For example, human IRGM helps transport various components of the autophagy pathway to vacuoles containing *Mycobacterium tuberculosis* (*M. tb*) (Singh et al., 2006). The primary function of IRGs is to coordinate the trafficking of vacuoles, delivering the pathogen to lysosomes for degradation by enzymes. In *T. gondii* infection, it is involved in the destruction of the parasitophorous vacuole (PV) and elimination of the parasite through the recruitment of the p47 GTPase Irga6 in an autophagosome-independent process (Butcher et al., 2005; Halonen et al., 2001; Ling et al., 2006; Taylor, 2007). The IRG proteins may work in tandem with other proteins, such as sequestosome (SQSTM1/p62), NDP52, and optineurin, which recognize bacteria that have escaped the phagosomal compartment and are tagged with ubiquitin, a small protein that marks cellular material for degradation. Alternatively, another set of IFN- γ -inducible proteins called galectins recognize bacterial glycan moieties. The recognition and subsequent binding of these proteins recruit autophagy proteins, which direct the bound components toward lysosomes (MacMicking, 2012). Activation of *M. tb*-infected macrophages by IFN- γ also stimulates the expression of IRGs, which coordinate the vacuolar traffic and targeting of bacterial cargo for lysosomal hydrolysis (MacMicking et al., 2003). Coordinating vacuolar compartmentalization as a result of orchestrating cell autonomous immune responses is an effective strategy against various intracellular pathogens such as *Toxoplasma gondii*, *Chlamydia psittaci*, *C. trachomatis*, *C. muridarum* and *Salmonella Typhimurium* (Coers, 2017; Coers et al., 2008; Coers et al., 2018; Degrandi et al., 2013; Finethy and Coers, 2016; Haldar et al., 2015; Haldar et al., 2016; Haldar et al., 2013; Huett et al., 2012; Hunn et al., 2011; Johnston et al., 2016; Jouanguy et al., 1999; Kim et al., 2016; Konen-Waisman and Howard, 2007; Kravets et al., 2016; Miyairi et al., 2007; Ohshima et al., 2014; Rupper and Cardelli, 2008; Selleck et al., 2013; Skariah et al., 2022; Steffens et al., 2020).

IFN- γ induces the formation of autophagosomes. These fuse with lysosomes, to which they deliver the cargo of cytoplasmic ubiquitinated proteins and organelles for degradation and recycling (Kroemer and Levine, 2008). Recently, it has been shown that proteins involved in autophagy play a role in controlling intracellular bacterial and parasitic infections (Zhao et al., 2008). For example, ATG5, which is essential for the conversion of LC3 I to LC3 II and its association with autophagosomes (Mizushima et al., 2002), is required for in vivo resistance to *Listeria* and *Toxoplasma* in macrophages (Zhao et al., 2008). In *T. gondii*

infection, it is involved in the destruction of the parasitophorous vacuole and elimination of the parasite through the recruitment of the p47 GTPase Irga6 in an autophagosome-independent process (Halonen et al., 2001; Butcher et al., 2005; Ling et al., 2006; Taylor, 2007)

The 65-73-kDa guanylate binding proteins (p65 GTPases or GBPs), a family of IRF-1 dependent ISGs recently discovered, are crucial for IFN-induced cellular self-defence (Briken et al., 1995; Degrandi et al., 2007; Huang et al., 2019; Skariah et al., 2022; Tretina et al., 2019). GBPs are instrumental in combating intracellular pathogens and form supramolecular protein complexes that include autophagy and ubiquitin proteins. These complexes work in a coordinated and regulated manner to execute specific antimicrobial activities against both vacuolar and cytosolic pathogens (Kravets et al., 2016; Meunier and Broz, 2016; Meunier et al., 2014; Santos and Broz, 2018). GBPs can identify both free and phagosomal entrapped bacteria, and their unique structure enables them to bind and direct bacteria toward lysosomes (Degrandi et al., 2013; Kim et al., 2011). For example, GBP1 facilitates bacterial binding to lysosomes by interacting with SQSTM1. In contrast, GBP7 interacts with autophagy proteins (ATG4B) and drives the extension of the elongation membrane around bacteria to fully sequester them within the autophagosomal compartment for degradation (MacMicking, 2012). Recently, GBP1 has been found to have a protective role in maintaining the intestinal tight junctions. Its expression in these locations helps regulate mucosal immunity by exerting regulatory effects on apoptosis (Schnoor et al., 2009).

It is worth noting that in humans and mice, IFN- γ has the ability to reduce the availability of tryptophan via the Indolamin-2,3-dioxygenase (IDO), which is thought to have a beneficial effect against parasites such as *Toxoplasma gondii* und *Chlamydia psittaci* (Daubener et al., 1999; Daubener et al., 2001; Murray, 2016). IFN- γ exerts its anti-viral effects primarily by inducing the expression of RNA-activated protein kinase R (PKR) and adenosine deaminase RNA specific-1 (ADAR-1), which can interfere with viral replication and genome integrity. Other proteins such as interferon-induced transmembrane proteins (IFITMs) and tripartite motif-containing proteins (TRIMs) are also induced by IFN- γ and exhibit potent anti-viral activity. IFITMs restrict viral uncoating or entry into host cells and protect against various viruses, including Influenza-A, Flaviviruses, HIV-1, Ebola virus, and Coronavirus (Day et al., 2017; Feeley et al., 2011). On the other hand, TRIMs limit viral entry, especially that of retroviruses, and are induced in macrophages and myeloid DCs

(Hatakeyama, 2017). IFN- γ -inducible proteins can utilize components of the autophagic machinery to limit viral replication. For instance, IFN-inducible GTPases use the autophagy pathway's microtubule-associated protein-1-light chain-3 (LC3) protein to block murine norovirus replication. The combined action of IFN-inducible GTPases and GBPs leads to significant inhibition of viral growth in murine cells (Biering et al., 2017).

IFN- γ plays a crucial role in regulating the production of lysosomal components, granules, and substances that exhibit potent antimicrobial activity, including β -defensins, α -defensins, and cathelicidins. Additionally, IFN- γ triggers several efflux systems that reduce essential cation concentrations required for microbial growth within the host. One such immune effector protein, NRAMP1, is upregulated by IFN- γ and expels Mn^{2+} or Fe^{2+} ions, effectively reducing pathogen possession of these ions within the phagosome (Jabado et al., 2000). IFN- γ also enhances the expression of iron-exuding ferroprotein 1 while concomitantly downregulating the transferrin receptor and hepcidin to restrict Fe^{2+} concentration, consequently limiting *Salmonella enterica*, *Listeria monocytogenes* and *M. tb* growth (Abreu et al., 2020).

Thus, IFN- γ is a cytokine with diverse and unique biological activities that are not redundant with other interferons. Its importance in disease pathologies is widely recognized in the scientific literature. The failure of the IFN- γ -IFN- γ R system can greatly impede the host's immune responses to infections. Therefore, IFN- γ is crucial in providing protective immunity in infectious diseases, cancers, and autoimmunity.

1.2. GTP-binding proteins

Some of the most strongly induced genes by IFN- γ encode GTP-binding proteins or proteins that interact with GTP-binding proteins (Degrandi et al., 2007; Martens and Howard, 2006). GTP-binding proteins regulate numerous fundamental cellular processes such as intracellular signal transduction (small Ras-related proteins, heterotrimeric G proteins), protein biosynthesis (elongation and initiation factors), organization of the cytoskeleton and vesicular transport (Rab/Ypt1), control of cell growth and differentiation (p21Ras, dynamin-related proteins), and receptor-mediated endocytosis (dynamin) (Bourne et al., 1990).

Based on sequence homologies, GTP-binding proteins can be classified into five superfamilies: the α -subunits of heterotrimeric G proteins ($G\alpha$), the Ras homologous small

GTPases (Ras, Rho, Ran, Rab, Arf, etc.), the translation factors of protein biosynthesis (IF-2, EF-Tu, EF-G, RF-3, etc.), the signal recognition particle and its receptor (SRP54, Ffh, SR, FtsY, etc.), and the dynamin-related large GTP-binding proteins (e.g. dynamin, p47 and p65 GTPases, Mx, "very large inducible GTPase" (VLIG), atlastin, etc.).

Physiologically, GTPases act as molecular switches. Mechanistically, GTPases share the Mg^{2+} -dependent binding of GTP and subsequent hydrolysis to GDP and/or GMP, which is mediated by five conserved sequence motifs, G1-G5 (Bourne, 1995; Bourne et al., 1991; Bourne et al., 1990), with motifs G1 (GX4GK[S/T]), G3 (DXXG), and G4 (N[T/Q]KXD) conserved in all GTPases. Furthermore, many members of various GTPase families carry post-translational modifications at their carboxy (C) termini, where they can be farnesylated, geranylgeranylated or palmitoylated. Some p47 GTPases are N-terminally myristoylated, and members of the p65 GTPase family are either farnesylated or geranylgeranylated due to a C-terminal CaaX signal sequence (Fres et al., 2010; Stickney and Buss, 2000). The covalently attached isoprenoid unit regulates the subcellular localization of the proteins (Kravets et al., 2012; Vestal et al., 2000).

The comparison of the three-dimensional structures of various GTP-binding proteins shows a great similarity for the GTPase (G) domain (Palfy et al., 2020; Vetter and Wittinghofer, 2001). The minimal basic structure of the G domain is found in Ras proteins (166 amino acids, Vetter and Wittinghofer, 2001). It consists of a six-stranded beta-sheet surrounded by five alpha-helices (Pai et al., 1989; Palfy et al., 2020; Fig. 1.2 A). This topology is varied in the structures of other GTP-binding proteins and Interferon-inducible GTPases by additions and insertions of further structural elements (Fig. 1.2 B).

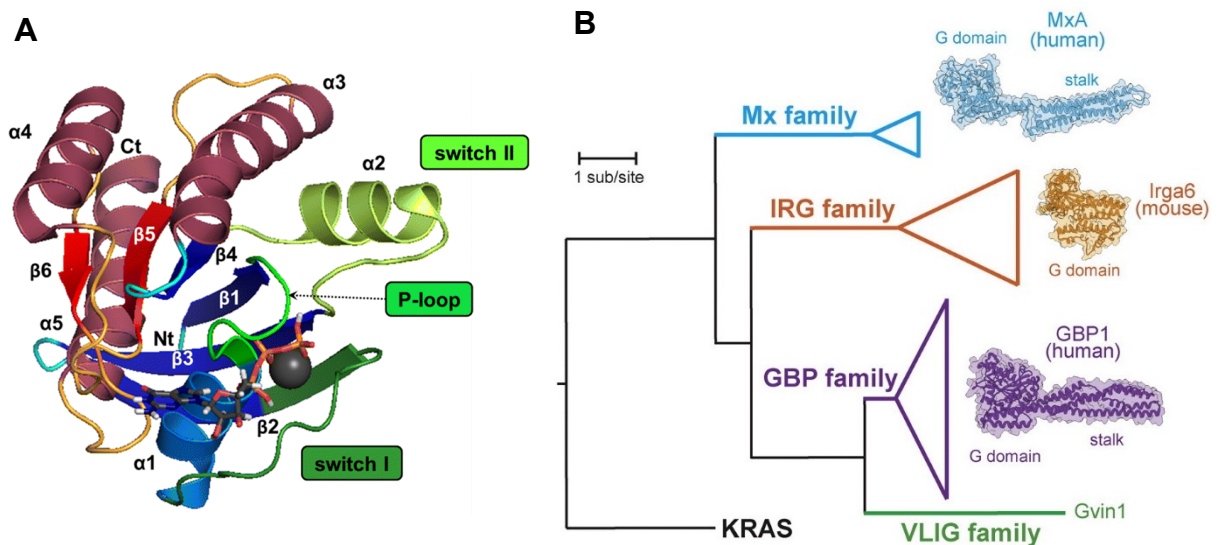


Figure 1.2: Structures of GTP-binding proteins.

Ribbon structure of the minimal G domain of K-Ras-GTP with conserved sequence elements and switch regions (A). The family tree of in Interferon-inducible GTPases with additive domains and their relative position to the G domain of K-Ras are depicted. VLIG: Very large inducible GTPases (B). Adapted from (Palfy et al., 2020; Pilla-Moffett et al., 2016).

The biological activity of GTP-binding proteins is regulated within the cycle of inactive GDP-bound and active GTP-bound states. In the GTP-bound form, the protein adopts the conformation that enables interactions with its effectors. Many GTP-binding proteins have low intrinsic GTPase activity, which can be increased up to 10^5 -fold by GTPase activating proteins (GAP) (Boguski and McCormick, 1993). The GAPs act as negative regulators and terminate signalling by stimulating the hydrolysis of GTP to GDP, thereby deactivating the protein and preventing it from interacting with its effector proteins (Geyer et al., 1996; Zhang et al., 1993). The GAPs provide an arginine to the GTPases *in trans*, which stabilises the negative charge during the transition state ('arginine finger hypothesis') (Ahmadian et al., 1997; Mittal et al., 1996; Scheffzek et al., 1997). A similar role for the intrinsic arginine finger is known for heterotrimeric G proteins and has been described for human GBP1 (hGBP1) and murine GBP2 (mGBP2) (Coleman et al., 1994; Kravets et al., 2012; Praefcke and McMahon, 2004). Mutation of this amino acid leads to an up to 1000-fold reduction in GTPase activity (Ahmadian et al., 1997; Bourne, 1997; Kravets et al., 2012; Praefcke and McMahon, 2004). In addition, GAPs shield the active site from the external medium and can alter the pKa of the phosphate, thereby accelerating catalysis. By exchanging GDP for GTP, the protein regains its active conformation. Nucleotide exchange is often catalysed by guanine nucleotide exchange factors (GEFs), which accelerate the dissociation of GDP from the GTPase through contact with switch regions (Ahmadian et al., 1997; Praefcke and McMahon, 2004). Some proteins, such as the effectors of Ras, Rab and Rho, regulate the GTPase cycle by binding to the GTPase-GDP form and slowing nucleotide dissociation. They are called guanine nucleotide dissociation inhibitors (GDIs) (Fig. 1.3). The binding of GDIs requires prenylation of the GTPase C-terminus. GDIs shield the hydrophobic lipid tail from the aqueous solution, thereby preserving the cytoplasmic pool of prenylated proteins, allowing Rab and Rho proteins to be transported between different membrane-enclosed compartments of the cell. The Ras GTPase response is medically relevant because 25-30% of human tumours are attributed to point mutations in Ras or RasGAP proteins, which can lead to uncontrolled cell growth due to defects in hydrolysis (Ahmadian et al., 1997).

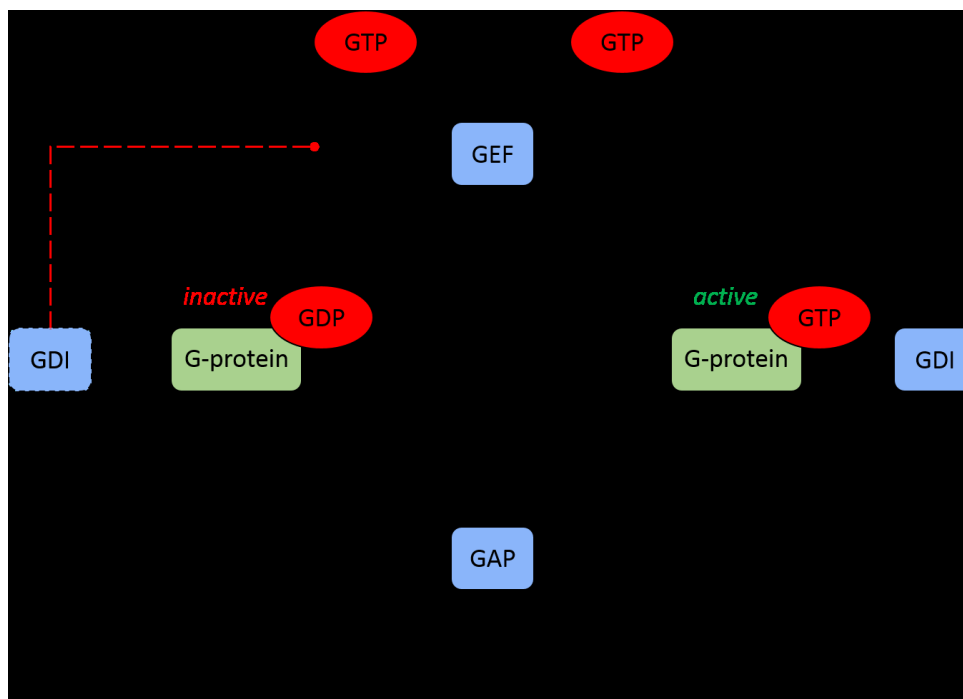


Figure 1.3: GTPase-cycle of GTP-binding proteins.

The exchange of bound GDP for GTP converts the GTP-binding protein into its active state. This process is accelerated by GEFs. The active, GTP-bound protein can bind to its effector proteins. Some of them slow down the dissociation of nucleotides and thus influence the GTPase cycle as GDIs. Inactivation occurs through the hydrolysis of GTP to GDP and/or GMP (not shown) and phosphate (Pi), which can be accelerated by GAPs. According to (Martens and Howard, 2006) .

1.2.1. IFN- γ inducible p47 und p65 GTPases

Microarray and suppression-subtractive hybridization (SSH) analyses conducted on murine embryonic fibroblasts and ANA-1 M ϕ cell line revealed that two distantly related families of GTPases, namely the p65 guanylate-binding proteins (GBPs) and the p47 immunity-related GTPases (IRGs), dominate the IFN- γ response in both cell types (Boehm et al., 1998; Degrandi et al., 2007).

However, these two GTPase families differ in their induction dependence by IFN- γ . The p65 GBP family members are expressed as classical genes of the secondary response, controlled by the transcription factor IRF-1, and are IFNGR dependent. On the other hand, the p47 IRGs, except for Irga6 (IRG-47) and Irgm3 (IGTP), only require activation of GAS sequences by a STAT1 dimer for their expression and are independent of IRF-1, at least in the primary response (Fig. 1.1 and Fig. 1.4). At the protein level, IRGs can be detected as early as 1 hour after stimulation, and they do not rely on *de novo* protein biosynthesis. In contrast, the bands of mGBPs can only be recognized in the Western blot at the earliest 4 hours after induction (Dissertation Konermann, 2008; Taylor et al., 1996).

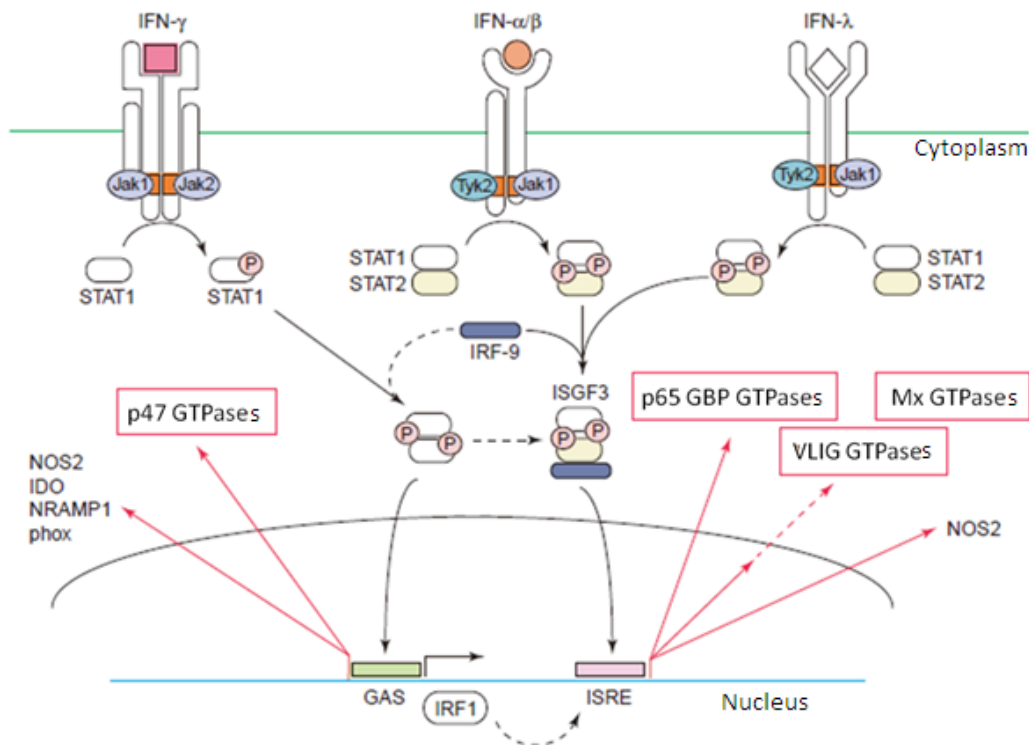


Figure 1.4: Expression of IFN-inducible GTPase families and other characterized anti-microbial effectors.

The binding of IFN- α/β , IFN- λ , or IFN- γ to their respective receptors initiates the JAK-STAT signalling pathway. The specificity of the signal is determined by the combination of certain Jaks with individual STAT dimers. When IFN- γ binds to the IFNGR, it activates JAK1/2, which then recruits and phosphorylates STAT1. The STAT1 dimers are transported into the nucleus where they assemble with histone acetylase to form a complex that activates the GAS elements in the promoters of IFN- γ -inducible genes. This process induces the expression of most members of the p47 GTPase family. The secondary activation of genes, p65 GBPs and VLIG proteins, requires the presence of IRF-1 for full expression, which binds to ISRE sequences. Mx GTPases are mainly induced by IFN- α/β but also by IFN- λ . Signal transduction via JAK1 or Tyk2 kinases leads to the formation of the ISGF3 complex, which binds to the ISRE promoter sequences. The Type I and Type II IFN receptors utilize both signalling pathways synergistically to induce the complete anti-microbial program. The terms used in this context are as follows: GAS: IFN- γ activation site; GBP: Guanylate-binding protein; ISGF: Interferon-stimulated gene factor; ISRE: Interferon-stimulated response element; JAK, Janus kinase; IDO: Indoleamine 2,3-dioxygenase; IRF-1: IFN regulatory factor-1; NOS2: Nitric oxide synthase 2 (iNOS); NRAMP1: natural-resistance associated macrophage protein-1; phox: Phagocyte oxidase; STAT: Signal transducer and activator of transcription; Tyk, JAK protein tyrosine kinase; VLIG: very large inducible GTPases. This information was taken from (MacMicking, 2004).

The significant occurrence of these two protein families during the cellular reaction to IFN- γ stimulation and their diversified structure and biochemistry imply that they serve distinct and clearly defined roles in the innate defence against pathogens. In *Listeria*-infected mice, both protein families are highly induced in the liver and depend on IFNGR (Boehm et al., 1998; Degrandi et al., 2007). Studies utilizing mouse strains deficient in certain IRG genes, including *Irgm1* (LRG-47), *Irgd* (IRG-47), and *Irgm3* (IGTP), have demonstrated the essential role of these proteins in host defence against intracellular pathogens, including *Listeria monocytogenes*, *Mycobacterium tuberculosis*, and *Toxoplasma gondii* (Martens and Howard, 2006; Taylor et al., 2004).

The IRG gene family likely originated in the common ancestor of chordates, similar to the Mx family (Fig. 1.2 B; Li et al., 2009). However, unlike the relatively stable number of Mx genes across vertebrates, the IRG gene family has undergone significant episodes of gene duplication and loss. The expansion and deletion of IRG genes have been particularly apparent in mammals, with rodents possessing up to 20 or more IRG genes, while humans have only 2 (Bekpen et al., 2005; Bekpen et al., 2009; Li et al., 2009). This is likely due to strong selective pressures imposed by the host-pathogen interactions, as organisms need to constantly adapt and evolve to survive the ongoing molecular "arms race" (Daugherty and Malik, 2012). This evolutionary conflict is exemplified by the distinct interactions between the murine IRG resistance system and the virulence factors encoded by *T. gondii*, which comprise a family of polymorphic rhoptry secretory kinases that enable the pathogen to evade IRG immunity (Behnke et al., 2011; Lilue et al., 2013; Reese et al., 2011). Furthermore, the association of human *IRGM* gene variants with the development of inflammatory diseases (Parkes et al., 2007; Rioux et al., 2007) suggests that such evolutionary costs may have played a role in the loss or reduction of the IRG resistance system in many vertebrate species (Pilla-Moffett et al., 2016).

1.2.2. p65 Guanylate-binding proteins

GBPs are a family of 65–73 kDa GTPases that were first isolated as highly expressed proteins in murine and human cells stimulated with IFN- γ (Cheng et al., 1983; Gupta et al., 1979; Knight and Korant, 1979). The GBPs are induced in many different tissues, particularly by IFN- γ , but also by agonists of Toll-like receptors (TLR) and other pro-inflammatory cytokines (Degrandi et al., 2007; Dissertation Konermann, 2008; Nguyen et al., 2002; Praefcke et al., 1999). Infection with *L. monocytogenes* and *T. gondii* leads to upregulation of murine GBPs (mGBPs) (Degrandi et al., 2007). After IFN- γ stimulation, mGBP1, 2, 3, 6, 7, 9, 10 and partially 5 and 8 associate with intracellular *Toxoplasma*, although virulent parasites can prevent the recruitment of mGBP proteins (Degrandi et al., 2007; Kravets et al., 2016; Lindenberg et al., 2017; Virreira Winter et al., 2011). Mice deficient in mGBP2 and mGBP7 reveal a marked immune susceptibility to *T. gondii* (Degrandi et al., 2013; Steffens et al., 2020).

The GBPs have been shown to exhibit a base-specific and affinity-equivalent binding to agarose-immobilized and solubilized guanine nucleotides GTP, GDP, and GMP (Cheng et al., 1983; Cheng et al., 1991). The nucleotide affinities are in the micromolar range and are

significantly lower compared to Ras proteins (Kravets et al., 2012; Praefcke and McMahon, 2004; Wennerberg et al., 2005). The p65 GBPs are highly conserved within vertebrates. So far, seven members of the GBP family and one pseudogene have been identified in humans (Cheng et al., 1983; Degrandi et al., 2007; Nguyen et al., 2002; Schwemmle and Staeheli, 1994). Their genes are encoded in a cluster on chromosome 1 (Olszewski et al., 2006). In mice, eleven GBPs and two pseudogenes have been identified, each clustered on chromosome 3 (gbp1, gbp2, gbp3, gbp5, gbp7, pseudogbp1) or chromosome 5 (gbp4, gbp6, gbp8, gbp9, gbp10, gbp11, pseudogbp2) (Boehm et al., 1998; Cheng et al., 1991; Degrandi et al., 2007; Han et al., 1998; Konermann et al., 2007; Kresse et al., 2008; Vestal et al., 1998; Wynn et al., 1991), (Fig. 8). There are also homologues in other vertebrates (Asundi et al., 1994; Olszewski et al., 2006; Schwemmle et al., 1996; Shenoy et al., 2012). The mGBP proteins exhibit a relatively high degree of similarity among each other (Fig. 1.5).

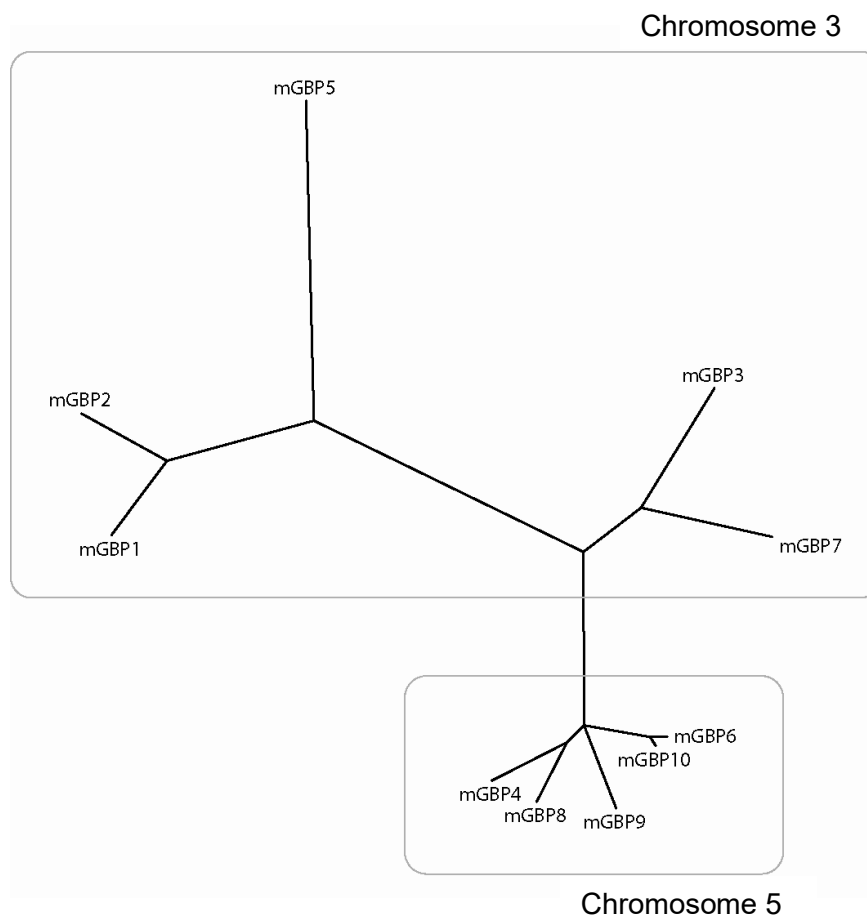


Figure 1.5: Phylogenetic tree of the p65 mGBPs.

The frames illustrate the chromosomal localization of the corresponding gene loci in the mouse genome. From (Degrandi et al., 2007).

Although classified as part of the dynamin superfamily, they are unique members as their primary sequences share little homology with other dynamin proteins (Praefcke and McMahon, 2004). The 3-domain structure is common among GBP proteins (Fig. 1.6). Two of the canonical

GTP-binding motifs typical of Ras, G1 (GX4GKS) and G3 (DXXG), are conserved in GBPs. While other GTPases contain a canonical G4 (N/T)(K/Q)XD motif in their GTP-binding domain (G domain), which is responsible for the specific recognition of the guanine base, GBPs rather contain a TLRD or TVRD sequence for GTP binding (Kresse et al., 2008; Nguyen et al., 2002; Praefcke and McMahon, 2004; Schwemmle and Staeheli, 1994; Fig. 1.6). As typical for dynamin-like proteins GBPs comprise a C-terminal α -helical regulatory domain, an assembly domain, a middle domain, and a GTPase effector domain (GED) with the CaaX motif which is involved in GTP hydrolysis (Cheng et al., 1991; Praefcke et al., 1999; Prakash et al., 2000a; Prakash et al., 2000b; Vopel et al., 2009; Vopel et al., 2010). GBPs have the ability to oligomerize in a nucleotide dependent manner and bind GTP in a concentration dependent manner (Ghosh et al., 2006; Kravets et al., 2012; Legewie et al., 2019; Prakash et al., 2000a).

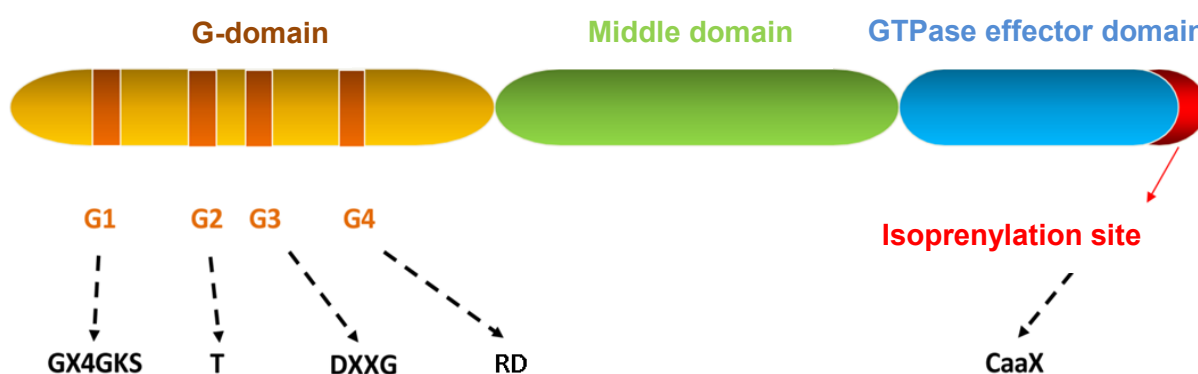


Figure 1.6: Linearized diagram of the three-domain structure of mGBP2.

Within the domains, the nucleotide-binding motifs G1-G4 are depicted with their consensus amino acid sequences. G domain refers to the GTPase domain.

As mentioned above, some GBPs (hGBP1, hGBP2, hGBP5, mGBP1, mGBP2, mGBP5) possess a CaaX motif at their C-terminus, which is recognized by prenyltransferases (Stickney and Buss, 2000). The X residue determines whether a farnesyl (C15) or a geranylgeranyl (C20) isoprenoid is attached via a thioether to the terminal cysteine (Fres et al., 2010; Kinsella et al., 1991; Moores et al., 1991; Seabra and James, 1998; Yokoyama et al., 1991; Zhang and Casey, 1996). Substrates for farnesyltransferase (FTase) have at the C-terminus amino acids such as Met, Ser, Ala, Gln, or Asn (e.g., hGBP1), whereas geranylgeranyltransferase I (GGTase I) primarily modifies CaaX proteins with Leu or Phe residues (e.g., mGBP2). The modification of some GBPs has been demonstrated *in vitro* and *in vivo* (Asundi et al., 1994; Nantais et al., 1996; Schwemmle and Staeheli, 1994; Vestal et al., 1996; Vestal et al., 2000). The nature of the covalently bound isoprenoid unit plays an important role in the subcellular localization of the proteins, their interaction with membranes, and their biological function (Fres et al., 2010; Kravets et al., 2012; Legewie et al., 2019; Santos and Broz, 2018; Zhang and Casey, 1996). Isoprenylated mGBP2 localizes in

granular or vesicle-like structures within the cytosol, the identity of which has not yet been determined. Earlier studies show that mutated mGBP2, which can no longer be isoprenylated, loses this typical subcellular distribution (Kravets et al., 2012; Vestal et al., 2000). The predominantly cytosolic localization of mGBP1 could be partly attributed to incomplete modification at the CaaX motif (Stickney and Buss, 2000).

The GBPs are little aggregation-sensitive in the nucleotide-free state and have the ability to hydrolyse GTP to GMP in two consecutive steps dependent on Mg^{2+} , with GDP appearing as a transient intermediate (Kravets et al., 2012; Neun et al., 1996; Praefcke et al., 1999; Schwemmle and Staeheli, 1994). However, the product ratio of hydrolysis is protein-dependent. GMP is the main product of hydrolysis in hGBP1, mGBP2 and mGBP7, while hGBP2 mainly produces GDP (Kravets et al., 2012; Legewie et al., 2019; Neun et al., 1996; Praefcke et al., 1999). hGBP5 catalyses only the first hydrolysis step and exclusively produces GDP (Wehner and Herrmann, 2010).

For hGBP1, mGBP2 and mGBP7, GTPase activity was shown to be cooperative and to increase at least 100-fold with increasing protein concentration. Dimerization (or oligomerisation) is responsible for the stimulation of hydrolysis and that neither GEFs for activation nor GAPs for deactivation of the proteins are required (Kravets et al., 2016; Kravets et al., 2012; Legewie et al., 2019; Praefcke and McMahon, 2004; Warnock and Schmid, 1996). The wild type protein exhibits low affinities to guanine nucleotides, self-assembles upon GTP binding, forming tetramers in the activated state, and stimulates the GTPase activity in a cooperative manner (Kravets et al., 2012). The hydrolysis of the p47 IRG Irga6 is also cooperative and the specific activity increases with increasing protein concentration. However, it is significantly slower than that of the other large GTP-binding proteins, with cooperativity only occurring at higher protein concentrations (Uthaiiah et al., 2003). In living murine embryonic fibroblasts (MEFs) infected with *T. gondii*, densely packed multimers comprise up to several thousand monomers (Kravets et al., 2016).

Dimerization is mediated in part by the switch regions, whereas in Ras-like G proteins the switch regions are involved in effector domain interaction (Vetter and Wittinghofer, 2001). It has been reported that the guanine cap, particularly the two arginine amino acid residues (R240 and R244), plays a crucial role in the dimerization and self-activation of the GTPase activity of hGBP1 (Wehner et al., 2012). It is proposed that during dimerization, one protein stimulates the GTPase reaction of the other by complex formation and that both monomers of hGBP1 are catalytically active (Kunzelmann et al., 2005; Kunzelmann et al., 2006). In

particular, dimer formation is required for GMP (Abdullah et al., 2010; Kravets et al., 2012). In recent studies, a second interaction surface in the helical domain has been identified for hGBP1, which only becomes accessible during GTP hydrolysis (Vopel et al., 2009; Vopel et al., 2010). This additional contact initiates tetramerization, more precisely, the dimerization of dimers, of the protein. For mGBP2, the formation of a dimer and a subsequent of a tetramer formed by two dimers followed by the formation of higher order oligomers on the base of the tetramer model was described (Kravets et al., 2016; Kravets et al., 2012; Fig. 1.7).

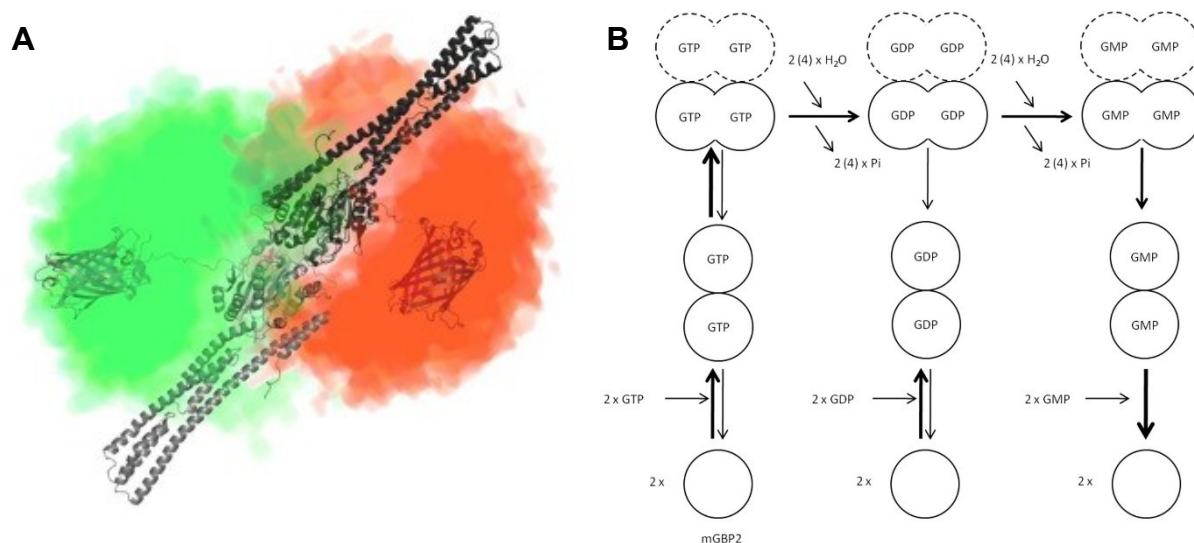


Figure 1.7: Structural and functional properties of a predicted dimer and a tetramer model of mGBP2.

Structural properties of a predicted mGBP2 dimer based on the crystal structure of the hGBP1 dimer (PDB-ID 2BC9). The characteristic Fluorescence Resonance Energy Transfer (FRET) features of the GFP-mGBP2 and mCherry-mGBP2 dimer with flexibly linked fluorescent proteins can be predicted by calculating inter fluorophore distances from the space that is sterically accessible to the fluorescent proteins. The accessible space of attached fluorescent proteins (green (GFP) and red (mCherry)) is depicted as fuzzy cloud (Kravets et al., 2016) (A). Molecular mechanism of GTP-hydrolysis catalysed by the mGBP2 dimer. Both molecules are assumed to be catalytically active and to cleave off phosphate ions from the nucleotide in two successive steps, generating a tetrameric transition state. GDP-hydrolysis is competed by inactivation of the catalytic machinery, most probably by dissociation of the mGBP2 dimer leading to the observed product ratio of GMP and GDP. The dissociation of the GMP-bound dimer is presumably fast and results in high turnover rates. The assembled or active forms of the GDP- and GMP-bound states of mGBP2 are only accessible through precedent binding of GTP (Kravets et al., 2012) (B).

The conformational change of S73 in the Switch I region is relevant for the mechanism of GTP hydrolysis catalysed by hGBP1, which is optimally positioned for coordinating the attacking water molecule (Wittinghofer and Gierschik, 2000). Additionally, an arginine residue (R48) from the P-loop, which protrudes into the solvent in the nucleotide-free and GMP-bound states, is oriented towards the active site by interaction with the second subunit. Overlay with the Ras-RasGAP complex shows that this arginine plays a role comparable to that of the "arginine finger" (Prakash et al., 2000a). The involvement of the proper R48 residue of mGBP2 in protein dimerization has been demonstrated, as a mutation

of this particular residue results in weakened cooperativity of hydrolysis and a significant reduction in specific activity (Kravets et al., 2012; Fig. 1.8). The invariant K51 in the P-loop of hGBP1 contacts a pair of the β - and γ -phosphate oxygens during GTP binding and hydrolysis, while the Mg^{2+} ion coordinates the other pair (Praefcke and McMahon, 2004). Lysine affinity studies have shown that interactions between the β -phosphate and P-loop are the most important elements for strong nucleotide binding, so that structural changes in the P-loop lead to significantly reduced affinities and the inability to hydrolyse GTP (Kravets et al., 2012; Praefcke and McMahon, 2004). The Mg^{2+} ion is octahedrally coordinated by T75 in Switch I and by S52 in the P-loop of hGBP1, as found in canonical GTP-binding proteins (Prakash et al., 2000b). In addition, T75 shields the phosphate groups of the nucleotide and the attacking water molecule from the solvent. In hGBP1, the active site is protected by the phosphate cap. In contrast, in Ras and Rho proteins, the phosphate binding site is open and shielded by the respective GAP proteins (Nassar et al., 1998; Prakash et al., 2000b; Scheffzek et al., 1997). The high flexibility brings the amino acids of the Switch II region into catalytically active positions during GTP hydrolysis. The biochemical characterization of point mutants in the GTP-binding motifs of mGBP2 revealed amino acid residues that decrease the GTPase activity by orders of magnitude and strongly impair nucleotide binding and multimerization ability (Kravets et al., 2012; Fig. 1.8).

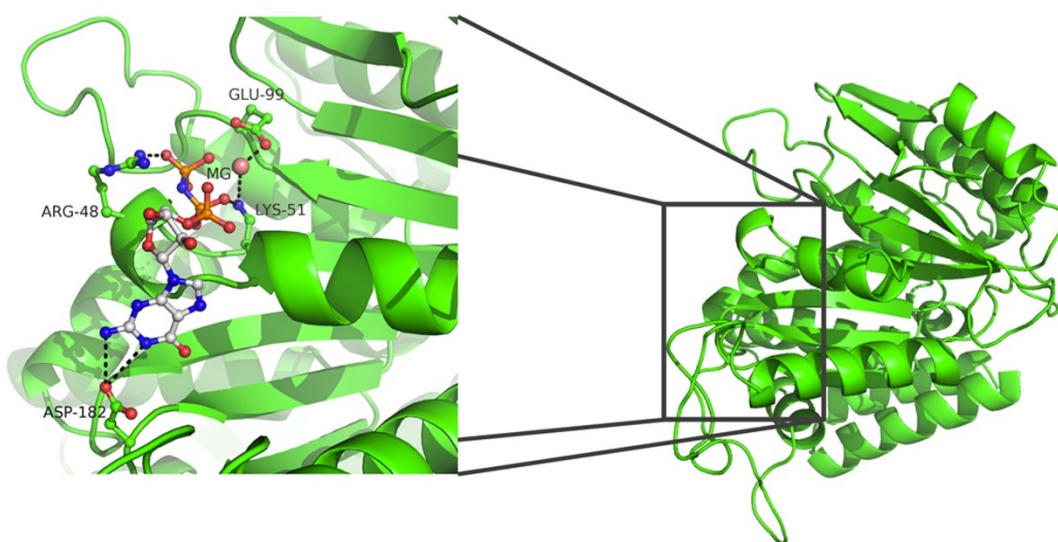


Figure 1.8: Structure model of mGBP2.

Ribbon representation of the mGBP2 model structure (Swissprot). A potential view on the G domain highlighting the amino acids of the catalytic centre and their mutations in the conserved regions are depicted, which are relevant for the mechanism of nucleotide binding and hydrolysis of mGBP2.

Live cell imaging experiments using multiparameter fluorescence image spectroscopy (MFIS) and a Homo-Förster- Resonance Energy Transfer (FRET) assay have shown that the multimerization of mGBP2 in living cells depends on its functional GTPase domain (Kravets et al., 2016; Kravets et al., 2012). These results emphasize the significance of GTP binding, self-assembly, and stimulated hydrolysis activity in determining the proper subcellular localization of mGBP2 in living cells.

1.2.2.1. The physiological function of GBPs

The mGBPs are induced by type I interferons, interleukins IL-1 α and IL-1 β , as well as TNF- α , transiently by LPS, but mainly by IFN- γ as classical secondary responsive, IRF1 dependent, genes, in cells of the immune system and non-immunological cells (Degrandi et al., 2013; Guenzi et al., 2001; Lubeseder-Martellato et al., 2002; Nguyen et al., 2002). In M ϕ and fibroblasts, some members of the mGBPs, especially mGBP2, with a clone frequency of 1.8% in the primary cDNA library, are among the most strongly IFN- γ inducible genes (Boehm et al., 1998).

In human fibroblasts, hGBP1 is also among the most highly inducible proteins after IFN- γ stimulation, with 3×10^5 molecules per cell (Cheng et al., 1985; Nicolet and Paulnock, 1994). The gene encoding mGBP2 has a total length of 17.4 kb (Kresse et al., 2008) and is divided into eleven exons. The open reading frame comprises 1767 bases and encodes a protein of 589 amino acids with a molecular mass of 66.7 kDa. The hGBP1 protein (Cheng et al., 1983) and mGBP2 (Briken et al., 1995) show high similarity with 68% amino acid identity, particularly in the GTPase domain (Olszewski et al., 2006; Kravets et al., 2012).

Despite their strong induction by IFN- γ , little is known about the molecular function of GBPs. Both, mGBP2 and hGBP1 have been reported to participate in various pathways, including those related to cellular proliferation, cell spreading and migration, as well as angiogenesis and immunity (Gorbacheva et al., 2002; Guenzi et al., 2003). In particular, hGBP1 has been associated with reduced tumour angiogenesis in patients with colorectal carcinoma, with the GTPase activity of hGBP1 being described as necessary for the anti-angiogenic effect, unlike the anti-proliferative effect (Guenzi et al., 2001; Naschberger et al., 2008; Weinlander et al., 2008). For mGBP2, an inhibitory role in the cellular mobility of fibroblasts has been demonstrated (Messmer-Blust et al., 2010). Furthermore, hGBP1 has been associated with paclitaxel (Taxol[®]) resistance in ovarian tumour cells and the development of multidrug resistance (MDR) (Duan et al., 2006). Additionally, a role for

hGBP1 in regulating the barrier function of intestinal endothelial cells with an impact on apoptosis has been described (Schnoor et al., 2009).

There is increasing experimental evidence to support the role of p65 GBPs in resistance against intracellular pathogens. Overexpression of hGBP1 was found to regulate the infections of vesicular stomatitis virus (VSV) and encephalomyocarditis virus (EMCV) in cell lines (Anderson et al., 1999), as well as the murine GBP2 (mGBP2), which was later discovered to have a similar effect on these pathogens (Carter et al., 2005). In addition, a splice variant of hGBP3 was demonstrated to mediate anti-influenza activity by repressing the viral polymerase complex (Nordmann et al., 2012). While the loss of GTP binding in hGBP1 and mGBP2 attenuated their ability to restrict viral production of EMCV, these mutations did not affect the restriction of VSV replication, suggesting that distinct GBP restriction mechanisms act specifically on subsets of viruses (Anderson et al., 1999; Carter et al., 2005). Furthermore, it was found that hGBP5 could restrict HIV-1 and other retroviruses by interfering with the processing of the viral envelope glycoprotein, and its antiviral activity required isoprenylation but not protein oligomerization or GTPases activity (Krapp et al., 2016). Although these studies demonstrate that several GBPs can exert some control over viral infections, their role in restriction is relatively weak compared to the antiviral properties of Mx proteins (Haller et al., 2007; Pilla-Moffett et al., 2016).

Initially, GBPs were discovered to play a role in controlling bacterial or protozoan infections, particularly *L. monocytogenes* and *T. gondii*, in which infected mice expressed high levels of numerous GBPs (Degrandi et al., 2007; Kresse et al., 2008). Studies showed that mGBP1, 2, 3, 6, 7, 9, 10 and partially 5 and 8 localized to *T. gondii* parasitophorous vacuoles (PVs) of the avirulent *T. gondii* type II strain (ME49) but failed to associate with PVs formed by virulent *T. gondii* strains (Degrandi et al., 2007; Kravets et al., 2016; Lindenberg et al., 2017; Steffens et al., 2020). mGBP1, mGBP2, and mGBP7 are among the key effector molecules that play a crucial role in the defence against *T. gondii* (Degrandi et al., 2007; Degrandi et al., 2013; Kravets et al., 2016; Saeij and Frickel, 2017; Selleck et al., 2013; Steffens et al., 2020; Virreira Winter et al., 2011; Yamamoto et al., 2012). mGBPs are intricately involved in IFN- γ induced growth restriction and killing of the *T. gondii* in murine macrophages, fibroblasts and astrocytes (Degrandi et al., 2007; Degrandi et al., 2013; Kravets et al., 2016; Lubitz et al., 2013; Pilla-Moffett et al., 2016; Steffens et al., 2020). Similarly, hGBP1 and hGBP2 were found to associate with intracellular *C. trachomatis* and inhibit bacterial growth when overexpressed (Al-Zeer et al., 2013; Tietzel et al., 2009),

although these findings were not confirmed in subsequent studies (Johnston et al., 2016). In order to execute their antimicrobial function, mGBPs can specifically associate with pathogen containing compartments of intracellular microbes which encompass pathogen containing vacuoles (PCVs) as well as viral replication compartments (Coers, 2013; Degrandi et al., 2013; Haldar et al., 2013; Lindenberg et al., 2017; Pilla-Moffett et al., 2016; Steffens et al., 2020), resulting in the innate immune detection and cell-autonomous clearing of PCV-resident pathogens (Coers et al., 2018; Haldar et al., 2015; Kravets et al., 2016; Steffens et al., 2020).

An important property of GBPs that contributes to their role in restriction is their ability to target PVs. Similar to IRGs, GBPs are seen to colocalize with membranous vesicles that are shed from PVs, indicating their involvement in the breakdown of these structures (Selleck et al., 2013; Yamamoto et al., 2012). After IFN- γ induction, mGBP2 molecules assemble in vesicle like structures (VLS) in the cytoplasm and, after *T. gondii* entry into the host cell, mGBP2 attacks the PV membrane (PVM) in orchestrated, supramolecular complexes, ultimately promoting the destruction of PVMs (Degrandi et al., 2013; Kravets et al., 2016). This stage is followed by recruitment of mGBP2 to the plasma membrane of the intracellular parasite, which in turn likely leads to its destruction (Kravets et al., 2016). Multiparameter fluorescence image spectroscopy (MFIS) revealed that mGBP2, on a molecular level, can form homomultimers or heteromultimers with mGBP1, mGBP3 and, to a lesser extent, with mGBP5 within VLS and at the PVM (Kravets et al., 2016). For PV membrane interactions, isoprenylation/farnesylation and/or hydrophobic moieties in the C-terminus of the GBPs are essential (Fres et al., 2010; Kravets et al., 2016; Kravets et al., 2012; Shydlovskiy et al., 2017; Steffens et al., 2020). Eventually, especially mGBP2 and mGBP7, can be found localized at the parasite cell membrane and inside the targeted parasite (Kravets et al., 2016; Steffens et al., 2020) probably also interfering with the integrity of *T. gondii* membranes.

Although GBPs have relatively similar structures, the capacity of individual members to target PVs can vary depending on the PV-resident. Using immunofluorescence assays, mGBP1, mGBP7, and mGBP10 were observed localizing to PVs in macrophages infected with *L. monocytogenes* or *M. bovis* BCG, while mGBP3 did not target these structures (Kim et al., 2011) [100] On the other hand, mGBP3 was found to associate with *T. gondii* PVs, which were, in turn, targeted by mGBP5 to a much lesser extent (Degrandi et al., 2007; Kravets et al., 2016).

In vivo studies have shown that different pathogens elicit varying responses from the host immune system. For instance, mice lacking the cluster of GBPs on chromosome 3 (*Gbp*^{chr3-/-}), which includes mGBP1, mGBP2, mGBP3, mGBP5 and mGBP7 exhibited reduced survival rates upon *T. gondii* infections (Yamamoto et al., 2012), a phenotype that was also observed in mGBP2^{-/-} and mGBP7^{-/-} mice alone (Degrandi et al., 2013; Steffens et al., 2020). However, when infected with *L. monocytogenes*, mGBP2^{-/-} mice showed similar survival rates as wildtype mice (Degrandi et al., 2013; Kresse et al., 2008), while mGBP1^{-/-} mice exhibited significant weight loss and increased *L. monocytogenes* burden (Kim et al., 2011). These findings suggest that different GBPs may have distinct target selection or effector mechanisms during antimicrobial responses.

Despite these early findings discovering the importance of the GBP protein family for a range of infections, the specific functions of individual GBPs in host resistance to various infections remained unclear.

Further examination using siRNA knockdown revealed that many GBPs were required for restriction during *L. monocytogenes* and *M. bovis* BCG infections, but their relative importance varied. For example, mGBP7 was shown to regulate the production of ROS through its supporting of the assembly of the subunits of NADPH oxidase 2 (Nox2) on mycobacterial phagosomes (Kim et al., 2011), while mGBP1 was found to interact with a different set of proteins that included the ubiquitin binding protein p62. Both proteins are involved in the transport of monoubiquitinated proteins to autolysosomes (Kim et al., 2011). However, there are conflicting reports on the exact nature of these protein interactions, and the specificities of these interactions have yet to be explained.

As already mentioned above, the CaaX motif is a C-terminal signal for prenylation, which mediates protein interactions with cellular membranes. GBP1, GBP2, and GBP5 are the only GBPs in both the murine and human families that contain CaaX motifs and these GBPs can be found localizing to various organelles and vesicles (Britzen-Laurent et al., 2010; Kresse et al., 2008). Interestingly, some GBPs lacking an isoprenylation motif are distributed in VLS as well as the CaaX motif might be dispensable for their localization to PVs (Britzen-Laurent et al., 2010; Degrandi et al., 2007; Legewie et al., 2019). In Particular, molecular dynamics simulations indicated that an elongated C-terminal tail (CT) of mGBP7 has transmembrane characteristic and confocal microscopy revealed that the CT tail is required for recruitment of mGBP7 to the PV of *T. gondii* (Legewie et al., 2019). This suggests that there may be alternative lipidation moieties or domains, such as the polybasic region of

hGBP1, that enable GBPs to interact with membranes. Additionally, heterodimerization between GBPs (Britzen-Laurent et al., 2010), as well as with other host proteins, could facilitate the localization of unprenylated proteins to PVs (Haldar et al., 2015; Haldar et al., 2014; Khaminets et al., 2010; Yamamoto et al., 2012). However, the lack of isoprenylation in the CaaX motif mutant of mGBP2, prevents its membrane anchoring, demonstrating that the isoprenoid moiety is essential for localization in the VLS and for the recruitment of mGBP2 to the PVM of *T. gondii* (Degrandi et al., 2013; Kravets et al., 2012).

Furthermore, the ability of GBPs to recruit and to attach to PVs in response to IFN- γ depends on both their capacity for GTP binding and their GTPase activity. Additionally, it was shown that the GTPase domain plays a critical role in the recruitment of mGBP2 to *T. gondii* in response to IFN- γ (Kravets et al., 2012; Fig. 1.9).

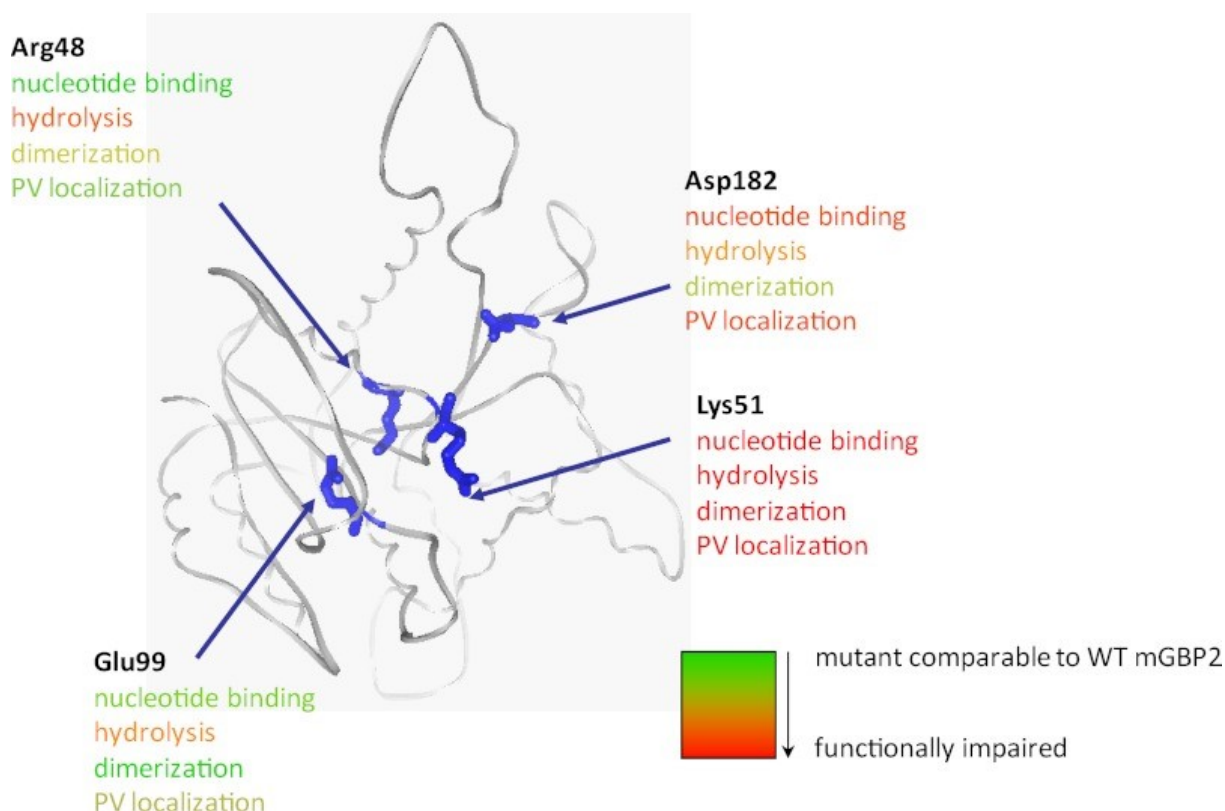


Figure 1.9: Structure functional relationship of the mutations of mGBP2.

A schematic diagram is given summarizing the biochemical and host-pathogen interaction features of mGBP2 mutants with respect to nucleotide binding, dimerization, and PV localization.

The ability of GBPs to attach to PVs depends on their capacity for both GTP binding and GTPase activity. Mutant forms of mGBP2 and mGBP1 lacking GTP binding capacity failed to target *T. gondii* or *C. trachomatis* PVs, while GTP-locked mutants GBPs targeted PVs with the same efficiency as wildtype proteins (Haldar et al., 2013; Kravets et al., 2012;

Virreira Winter et al., 2011). In addition, mGBP2 activation is regulated by Rab guanine dissociation inhibitor (GDI)- α , which specifically interacts with mGBP2 and maintains it in its GDP-bound state. The absence of RabGDI- α increases the targeting of GTP-bound mGBP2 to *T. gondii* PVs and enhances host resistance (Ohshima et al., 2015). GTP binding promotes the homodimerization and heterodimerization of GBPs (Kravets et al., 2016), resulting in different subcellular localization patterns (Britzen-Laurent et al., 2010). For instance, homodimers of unprenylated hGBP3 and hGBP4 localized to the cytoplasm or nucleus, respectively, while heterodimers of these GBPs with prenylated hGBP1, hGBP2, and hGBP5 localized to VLS, the nucleus, or the Golgi, depending on the corresponding homodimers of hGBP1, hGBP2, and hGBP5. These findings suggest that prenylated GBPs, such as hGBP1, direct the targeting of unprenylated GBPs (Britzen-Laurent et al., 2010; Pilla-Moffett et al., 2016).

Furthermore, GBPs have been shown to serve as positive regulators of canonical and noncanonical inflammasome activation, suggesting their role in controlling inflammation (Meunier and Broz, 2016; Meunier et al., 2014; Meunier et al., 2015; Santos et al., 2018). Initial studies showed that mGBP5 overexpression in RAW 264.7 macrophage cell line increased caspase-1-mediated cell death in response to *S. typhimurium* infections, suggesting a role for GBPs in inflammasome activation and pyroptosis. However, a subsequent study by the MacMicking lab reported reduced NLRP3-dependent activities in mGBP5-deficient M ϕ following *S. typhimurium* infection or treatment with potassium efflux agonists (Shenoy et al., 2012). Contradicting these findings, the labs of Broz and Kanneganti, using an independently produced mGBP5^{-/-} mouse line, were unable to replicate the initial results (Man et al., 2015; Meunier et al., 2014; Pilla-Moffett et al., 2016). Possibly, these differences can be attributed to the different genetic backgrounds of the mouse strains analysed (Pilla-Moffett et al., 2016). Despite the uncertainty surrounding the role of mGBP5 in NLRP3 inflammasome activation, studies using *Gbp*^{chr3-/-} mice lacking the entire cluster of mGBP genes on chromosome 3 have firmly established a functional link between mGBPs and the activation of the canonical NLRP3 and AIM2 as well as the noncanonical Caspase-11 inflammasomes. Here, mGBP2 emerged as a critical activator of AIM2 and Caspase-11 inflammasomes (Finethy et al., 2015; Man et al., 2015; Meunier et al., 2014; Meunier et al., 2015; Pilla et al., 2014). A very recent study shows that mGBP1 and mGBP3 are specifically required for inflammasome activation during infection with the cytosolic bacterium *Francisella novicida* leading to pathogen membrane rupture and release of intracellular content for inflammasome sensing (Feng et al., 2022). It is reasonable to

hypothesize that some GBPs may contribute to bacteriolysis and the release of PAMPs, while others may promote inflammasome assembly. These two processes could be linked through shared components to enhance the efficiency of pathogen detection by the inflammasome system (Pilla-Moffett et al., 2016).

1.3. Galectins

Galectins are a family of carbohydrate-binding lectins that are found in a wide range of organisms, from bacteria to humans (Liu and Rabinovich, 2010; Vasta, 2012). (Liu and Rabinovich, 2010). Extracellularly, galectins are able to exhibit bivalent or multivalent interactions with cell-surface glycans on various immune cells and exert various effects. These include cytokine and mediator production, cell adhesion, apoptosis, and chemoattraction. Additionally, they can form lattices with cell-surface glycoprotein receptors, resulting in modulation of receptor functions, including clustering and endocytosis. Intracellularly, galectins can participate in signalling pathways and modulate biologic responses. These include apoptosis, cell differentiation, and cell migration (Farnworth et al., 2008; Liu and Rabinovich, 2010). Numerous studies have demonstrated that galectins have significant functions in modulating the homeostasis and activities of immune cells, highlighting their crucial roles in immune and inflammatory responses. Further evidence supporting the involvement of galectins in these responses has been obtained by studying mice deficient in individual galectins (Beatty et al., 2002; Farnworth et al., 2008; Sano et al., 2003). Current research indicates that galectins play important roles in the development of acute inflammation as well as chronic inflammation associated with allergies, autoimmune diseases, atherosclerosis, infectious processes, and cancer (Liu and Rabinovich, 2010; Rabinovich et al., 2007).

Presently, 15 galectin (Gal) members have been identified in mammals, each with a different structure, tissue distribution, and biological function (Shi et al., 2018). They are classified into three groups based on their structural characteristics: one-CRD or prototype galectins (Gal1, -2, -5, -7, -10, -11, -13, and -14), which are monomers or homodimers of one CRD, chimera galectins (Gal3, which contains a nonlectin part made of proline- and glycine-rich short tandem repeats connected to a CRD) and tandem-repeat galectins (Gal4, -6, -8, -9, -12, and -15), which contains two distinct but homologous CRDs in a single polypeptide chain (Liu et al., 2002; Rabinovich et al., 2007; Yang et al., 2008; Fig. 1.10).




Classification	Structure
<p><i>Proto-type</i></p> <p>Galectin-1, -2, -5, -7, -10, -11, -13, -14 and -15</p>	 <p>One CRD that can dimerize</p>
<p><i>Chimera-type</i></p> <p>Galectin-3</p>	 <p>One CRD connected with a non-lectin domain</p>
<p><i>Tandem repeat-type</i></p> <p>Galectin-4, -6, -8, -9 and -12</p>	 <p>Two distinct CRDs</p>

Figure 1.10: Galectin family members.

The galectin family consists of those containing one CRD; Gal3, which consists of unusual tandem repeats of proline- and glycine-rich short stretches fused onto the CRD; and those containing two distinct CRDs in tandem, connected by a linker. Proto-type-CRD galectins can form dimers; Gal3 forms pentamers upon binding to multivalent carbohydrates; and two-CRD galectins have two carbohydrate-binding sites. Thus, galectins can form lattices with multivalent glycoconjugates. The binding of secreted galectins to cell surface glycans can crosslink glycans on neighbouring cells, leading to cell adhesion. Galectins can also form homogeneous lattices at the cell surface that can activate signalling pathways of functional relevance in the control of receptor endocytosis, host-pathogen interactions, and activation and homeostasis of immune cells (Liu and Rabinovich, 2010; Vasta, 2009).

Galectins are nucleocytoplasmic, can also be exported from cells through a poorly defined unconventional secretion pathway (Haudek et al., 2010; Liu et al., 2002; Vasta, 2009) and can bind directly to bacteria thereby mediating antibacterial effects and modifying inflammatory signalling events (Chen et al., 2014). There is evidence indicating that Gal3 is a negative regulator of LPS-induced inflammation and protects the host from endotoxin shock, excessive induction of inflammatory cytokines and nitric oxide production, but, conversely, favours the survival of *Salmonella* bacteria (Li et al., 2008). Comparably, *T. gondii* infected *Gal3*^{-/-} mice developed reduced inflammatory response in several organs, but displayed a higher parasite burden, emphasizing the regulatory role for galectins in the interface of innate and adaptive immunity (Bernardes et al., 2006). When Mφ obtained from mice infected with *Trypanosoma cruzi* were exposed to increasing amounts of Gal1, a biphasic effect on both parasite replication and cell viability was observed. At low concentrations of this protein, parasite replication was enhanced by reducing interleukin 12 (IL-12) and nitric oxide, and Mφ survival remained unaffected. However, higher concentrations of Gal1 induced inflammation and led to apoptosis, ultimately inhibiting parasite replication (Zuniga et al., 2001). *Gal9*^{-/-} mice were more susceptible to LPS-induced vasculitis, suggesting that Gal9 has suppressive effects on bacterial infection-induced inflammation (Tsuboi et al., 2007). Galectins play a role in the colonization of hosts by protozoan parasites such as *Entamoeba histolytica*, *Plasmodium falciparum*, *Cryptosporidium* species, and *Toxoplasma gondii*. Moreover, galectins present in the host cells, whether they are soluble or membrane-associated, are essential molecules that are crucial in recognizing and establishing beneficial mutualistic interactions with the

colonizing microorganisms (Bhat et al., 2007; Frederick and Petri, 2005; Hager and Carruthers, 2008; von Itzstein et al., 2008). Alternatively, they can initiate innate and adaptive immune responses against pathogens.

Immunomodulatory effects of galectins include recruitment of immune cells to the site of infection, promotion of neutrophil function, and stimulation of the bactericidal activity of infected neutrophils and macrophages (Cooper et al., 2008; Karlsson et al., 1998; Rabinovich and Toscano, 2009). Previously it has been shown that Gal3 can bind *T. gondii* glycosphosphatidylinositols (GPIs) and might be a co-receptor presenting GPIs to TLRs on M ϕ (Debierre-Grockiego et al., 2007; Debierre-Grockiego et al., 2010). Cytoplasmic galectins fulfil functions in several cellular programs including production of proinflammatory cytokines, cell growth and apoptosis (Kashio et al., 2003; Liu et al., 2002; Matsuura et al., 2009). Through binding to multivalent carbohydrates, galectins can multimerize and thereby cluster these surface glycoconjugates resulting in changes in cell migration, receptor endocytosis and various other cellular events (Cerliani et al., 2017; Fulcher et al., 2006; Vasta, 2009; Vasta, 2012).

Glycans are largely restricted to the luminal face but absent from the cytosolic face of intracellular vesicles. If vesicular damage occurs, luminal glycans are exposed to the cytosolic milieu, where they can be recognized by galectins (Boyle and Randow, 2013; Coers, 2017). Furthermore, vacuolar instability of bacterial pathogen containing vacuoles (PCVs) is recognized by host β -galactoside-binding proteins of the galectin family (Chen et al., 2014). Intracellular galectins can serve as danger receptors and can promote autophagy of the invading pathogen (Casals et al., 2018; Meunier et al., 2014). In recent years, there has been growing evidence to suggest that galectins can bind to the surface glycans of potentially harmful microbes and serve as recognition and effector factors in innate immunity. This has led to the establishment of a new paradigm, where galectins not only act as pattern recognition receptors but also as effector factors. Their binding to the microbial surface can hinder adhesion and entry into the host cell, directly destroy the pathogen by disrupting its surface structures, or facilitate phagocytosis, encapsulation, autophagy, and the removal of pathogens from circulation (Vasta, 2020). Figure 1.11 summarise the so far known functions of endogenous galectins.

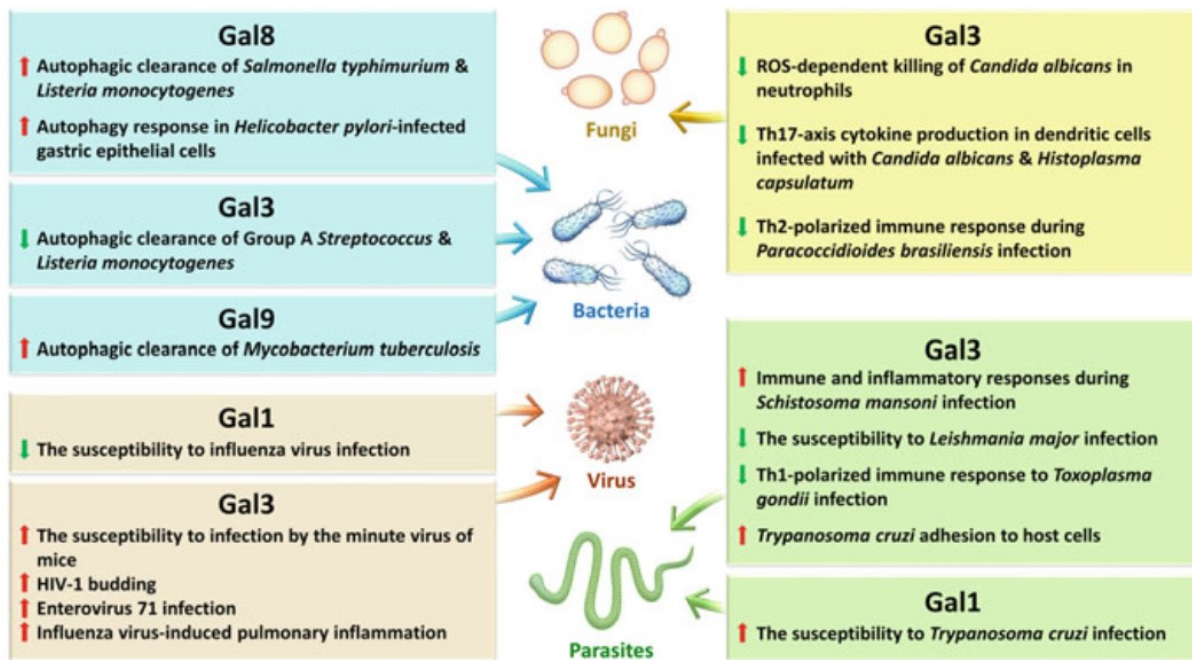


Figure 1.11: Functions of endogenous galectins.

For further information refer to main text.

An intriguing development is the association of galectins with exosomes, which are small vesicles secreted by various cell types resulting from fusion of multivesicular bodies with the plasma membrane and that contribute to various physiological processes (Denzer et al., 2000; Klibi et al., 2009; Liu and Rabinovich, 2010).

Research into galectins has revealed their potential as therapeutic targets for a variety of diseases, including cancer, inflammatory disorders, and infectious diseases.

1.4. Cytoskeleton associated protein 4

Cytoskeleton associated protein 4 (Ckap4), also known as p63, CLIMP-63, or ERGIC-63, is a 63 kDa, reversibly palmitoylated and phosphorylated, type II integral transmembrane (TM) protein that is involved in the regulation organization of the cytoskeleton and its stability (Fig. 1.12). Ckap4 was originally identified as a resident of the endoplasmic reticulum (ER)/Golgi intermediate compartment (ERGIC) (Schweizer et al., 1993) linking the ER to microtubules (Gao et al., 2019; Noda et al., 2014; Vedrenne et al., 2005). There is also steadily accumulating evidence for diverse roles for Ckap4 localized outside the ER, including data demonstrating functionality of Ckap4 as a cell surface receptor for Dickkopf1-cytoskeleton-associated protein 4 (DKK1) (Kikuchi et al., 2017; Kimura et al., 2016) and other ligands (Bates, 2010; Gupta et al., 2006; Kikuchi et al., 2017) resulting in

increased nuclear abundance of Ckap4 in response to the antiproliferative factor (APF) (Tuffy and Lobo Planey, 2012), underlining that Ckap4 is involved in the regulation of cell migration (Osugi et al., 2019) and may play a role in the progression of cancer and other diseases (Batistatou et al., 2003; Sisto et al., 2018). Ckap4 must be palmitoylated to traffic to the cell surface (Li et al., 2020; Zhang et al., 2008).

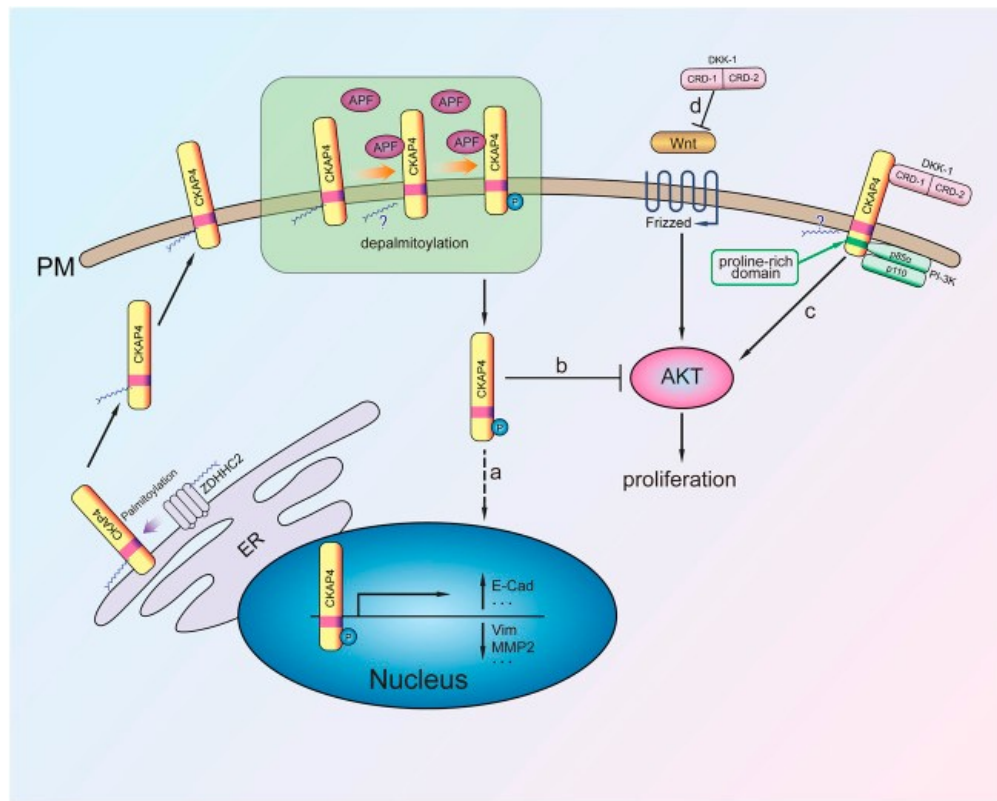


Figure 1.12: The mechanism of Ckap4 regulating cell proliferation.

Palmitoylated Ckap4 translocates from ER to the plasma membrane (PM). At the PM, Ckap4 binds to its ligands APF and DKK-1, and may undergo depalmitoylation. a: APF binding to Ckap4 induces phosphorylation of Ckap4, and the phosphorylated Ckap4 translocates to the nucleus, then changes related genes transcription, and plays an antiproliferation effect. b: The phosphorylated Ckap4 also reduces Protein kinase B (AKT) phosphorylation, which inhibits cell proliferation. c: Upon the cytidine rich domain 1 (CRD-1) of DKK-1 binding to Ckap4, Ckap4 binds to the p85 α subunit of Phosphatidylinositol-3-Kinase (PI3K) to activate PI3K/AKT signalling and stimulate cell proliferation. d: DKK1 is a potent β -catenin-dependent Wingless/Integrated (Wnt) signalling antagonist (Li et al., 2020).

Studies have shown that Ckap4 is involved in the host cell response to viral infections, including the severe acute respiratory syndrome coronavirus type 2 (SARS-CoV-2). Specifically, the endothelial Ckap4 is involved in mediating the secretion of von-Willenbrand-factor (vWF) and thrombosis that is promoted by the Spike protein (Li et al., 2022). Additionally, Ckap4 has been found to contribute to tumour progression associated with human papillomavirus (HPV) (Bernhard et al., 2021). Furthermore, the protein has been implicated in the response to bacterial infections such as *Helicobacter pylori*. In this case, the activation of DKK1/Ckap4 signalling has been found to induce gastric

tumorigenesis through the PI3K/AKT/mechanistic target of rapamycin (mTOR) pathway (Luo et al., 2022).

1.5. *Toxoplasma gondii*

The protozoan *Toxoplasma gondii* (*T. gondii*) is a highly successful obligate intracellular parasite that can persist within host cells for the duration of the host's life and is found worldwide, but the prevalence of *T. gondii* varies greatly in different regions of the world. It can infect at least 350 warm-blooded host species, including humans, due to its low host specificity (Black and Boothroyd, 2000; Hill et al., 2005). Approximately 30-70% of the world's population is infected with the parasite (Canon-Franco et al., 2014; Dubey, 1987; Zhao and Ewald, 2020). Toxoplasmosis is generally benign and often asymptomatic in immunocompetent individuals, however, non-specific flu-like symptoms, lymphadenopathy, and some rare complications might be associated with primary infection. The significance of *T. gondii* in human health was initially recognized with reports of congenital toxoplasmosis in the 1940s. However, recent studies suggest that these asymptomatic infections may have effects on behaviour and other physiological processes (Halonen, Weiss, 2013). Research on *T. gondii* is advancing for two important reasons.

First, *Toxoplasma* can cause health-threatening and fatal implications (Halonen and Weiss, 2013; Jones et al., 2006; Montoya and Remington, 2008; Pinon et al., 2001) in congenitally infected fetuses and immunocompromised individuals (Kim and Weiss, 2008; Luft and Remington, 1992). While the primary infection is mostly asymptomatic in pregnant seronegative women, tachyzoites in the blood may cross the placenta, infect the foetus, and cause retinochoroiditis, intracerebral calcification, encephalitis, hydrocephaly, mental retardation, seizures, myocarditis or even foetal death (Jones et al., 2003; Montoya and Remington, 2008; Olariu et al., 2011; Saadatnia and Golkar, 2012). Clinical manifestations of this infection may be delayed long after birth. The timing of maternal toxoplasmosis acquisition during pregnancy is a critical factor affecting the likelihood of transmission, which increases as pregnancy progresses; the sooner the infection occurs during pregnancy, the lower the risk of congenital infection but the greater the severity of symptoms (Jones et al., 2003; Ortiz-Alegria et al., 2010). Early diagnosis and management of maternal and congenital toxoplasmosis is of the utmost importance to prevent sequelae.

Toxoplasmosis is also a major opportunistic infection in immunodeficiency conditions, i.e. in acquired immunodeficiency syndrome (AIDS) and organ transplant patients. However, the AIDS crisis in the 1980s revealed the prevalence of chronic infection, as patients presented with reactivated latent toxoplasmosis, highlighting the crucial role of an intact immune system for parasite control (Ayoade and Joel Chandranesan, 2023; Wong and Remington, 1993). In individuals with compromised immune systems, the reactivation of a latent infection might result in toxoplasmic encephalitis (TE), which is potentially fatal if not treated properly (Montoya and Liesenfeld, 2004). The use of highly active antiretroviral therapy (HAART) has decreased the occurrence of TE in AIDS patients. However, in countries with a high prevalence of *T. gondii*, TE remains the most frequent cerebral mass lesion among HIV patients (Antinori et al., 2004). Toxoplasmic retinochoroiditis is a major concern in the field of eye diseases globally. Ocular toxoplasmosis is the most common form of infectious posterior uveitis in individuals without compromised immune systems and can occur due to congenital or acquired infections. It may manifest shortly after the initial infection, have a delayed onset, or occur during a reactivation phase (Montoya and Liesenfeld, 2004; Saadatnia and Golkar, 2012).

Furthermore, the possible association of infection of toxoplasmosis with neuropsychiatric disorders such as schizophrenia is also the subject of research (Halonen and Weiss, 2013). Second, *T. gondii* serves as a model system for other related parasites such as *Plasmodium*, the causative agents of malaria; *Eimeria*, the causative agent of avian coccidiosis; and *Cryptosporidium*, another important opportunistic pathogen in patients with AIDS (Kim and Weiss, 2004).

T. gondii belongs taxonomically to the phylum of sporozoans/apicomplexa and here to the subclass Coccidia. It is the only known representative of the genus *Toxoplasma*. The name *Toxoplasma* (*toxon*, Greek for bow, *plasma*, Greek for shape, structure) derives from the crescent-shaped form of the parasite. Characteristic for the pathogen are the infectious sporozoites, an apical complex, and the alternation of generations between sexual and asexual forms.

The complete three-phase life cycle of *T. gondii* was only elucidated in 1970 (Dubey et al., 1970a; Dubey et al., 1970b; Frenkel et al., 1970). The development of *T. gondii* is divided into an enteroepithelial, an exogenous, and an extraintestinal phase, which are associated with the host's change (Dubey, 2004; Dubey, 2009; Dubey et al., 1998; Dubey et al., 1997; Fig. 1.13).

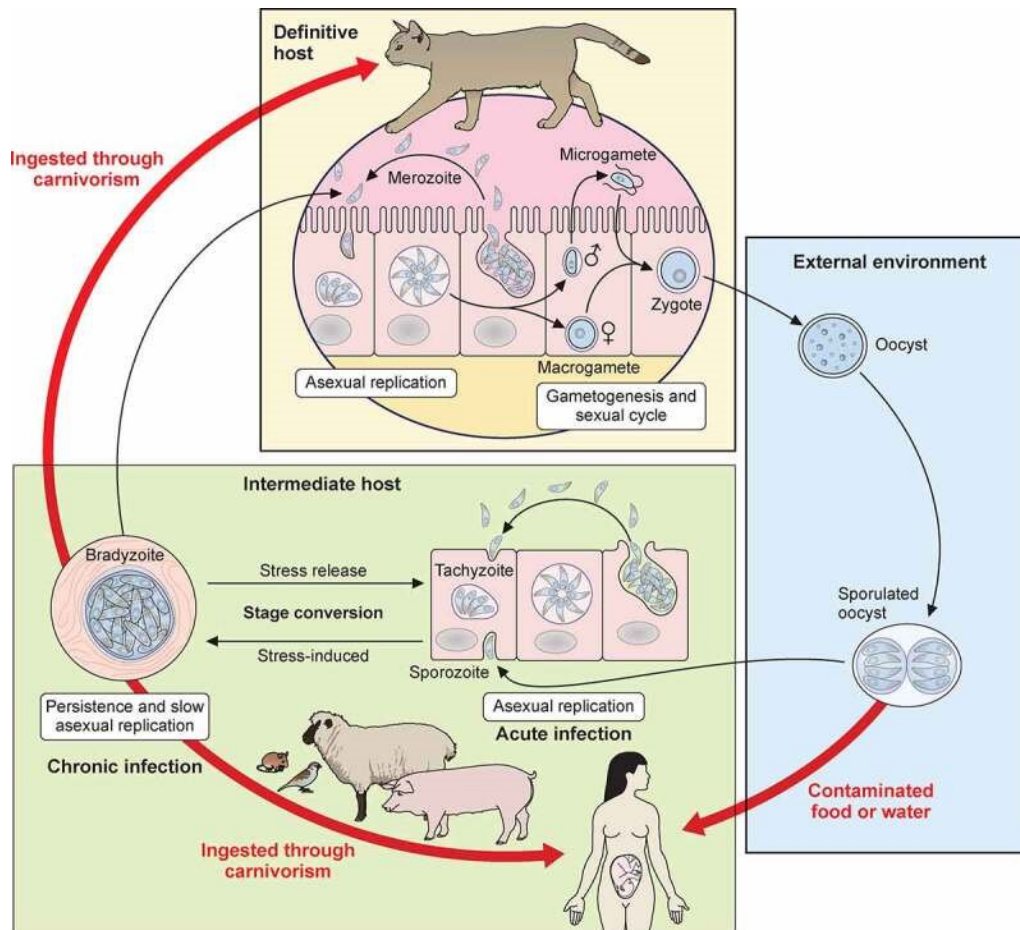


Figure 1.13: Life cycle of *T. gondii*.

Schematic representation of the infective stages and their modes of transmission and replication in their respective hosts (Sanchez and Besteiro, 2021).

The parasite *T. gondii* enters its definitive host through carnivory of infected intermediate hosts (Dubey, 2009). Human contamination can thus happen through food consumption: by ingestion of uncooked or undercooked cyst-containing meat, or of sporulated oocysts-containing vegetables, fruits or water (Belluco et al., 2018). *T. gondii* undergoes a two-phase life cycle, which includes an enteric cycle and an extraenteric cycle. The enteric phase, in which *T. gondii* forms its sexual stages (gametogony), occurs only in the epithelium of the small intestine of domestic cats and some other felid species (definitive host) and ends with the shedding of diploid oocysts in the feces (Gregg et al., 2013; Martorelli Di Genova et al., 2019). In the external phase, the oocyst undergoes reduction division to form eight sporozoites, which are highly infectious for many species of intermediate hosts (mammals, birds) upon ingestion of sporulated oocysts or tissue cysts (Dubey and Frenkel, 1976; Gubbels et al., 2020). For *T. gondii*, three modes of transmission are known: congenital, through ingestion of raw or undercooked meat, and through feces (Dubey et al., 1986).

After the cyst wall dissolves in the stomach, slowly growing gastropeptidase-resistant bradyzoites are released. These bradyzoites then penetrate the small intestinal tissue (Tenter et al., 2000) and differentiate into rapidly proliferating, disease-causing tachyzoites, which lyse their host cells after 48 hours. Tachyzoites bear surface antigens such as Surface Antigen (SAG) 1 and SAG2 (Kasper, 1989). After penetrating the intestinal epithelium, the *Toxoplasma* parasites temporarily reside in the blood or lymph before being transported to the lamina propria. Their asexual reproduction occurs in the cytoplasm of nucleated host cells, preferably in the reticuloendothelial system, muscles, and central nervous system (CNS) (Matta et al., 2021; Schluter and Barragan, 2019; Zhao and Ewald, 2020). Within a parasitophorous vacuole (PV) in the host cell, 16-32 daughter individuals are produced through repeated cell division. Upon bursting of the cell wall, the tachyzoites are released and infect cells in other tissues of the host organism (Frenkel, 1988; Ajioka et al., 2001). This process leads to local tissue damage in the form of focal necrosis and infiltration with reticuloendothelial cells accompanied by inflammatory reactions. Such lesions are mainly found in the CNS, muscles (cardiac and smooth), liver, lymphoreticular system (spleen, lymph node), bone marrow, retina, and placenta (Sanchez and Besteiro, 2021). *T. gondii* does not produce toxins. The acute phase of infection lasts until the host dies or an immune response occurs that eliminates most of the parasites. The intracellular replication of *T. gondii* is curtailed by the host's defence mechanisms, which causes the parasite to revert to the slow-growing stage of bradyzoites in immunocompetent individuals (Belluco et al., 2018). Bradyzoites also express specific antigens such as Bradyzoite Antigen (BAG) 1 or 5 and surface antigen SAG4 (Bohne et al., 1995; Odberg-Ferragut et al., 1996; Parmley et al., 1994; Parmley et al., 1995; Yang and Parmley, 1995). Bradyzoites persist in tissue cysts containing up to 2000 parasites during the chronic phase of infection (Kim and Weiss, 2004). The cysts do not cause acute pathology and can potentially occur in any tissue but have a significantly higher prevalence in neuronal and muscular tissue. *T. gondii* likely persists for the host's lifetime in these tissue cysts (Fig. 1.14). However, reactivation of a chronic infection is possible when immunity collapses or is compromised by intercurrent diseases, injuries, etc (Luder and Rahman, 2017; Montoya and Liesenfeld, 2004).

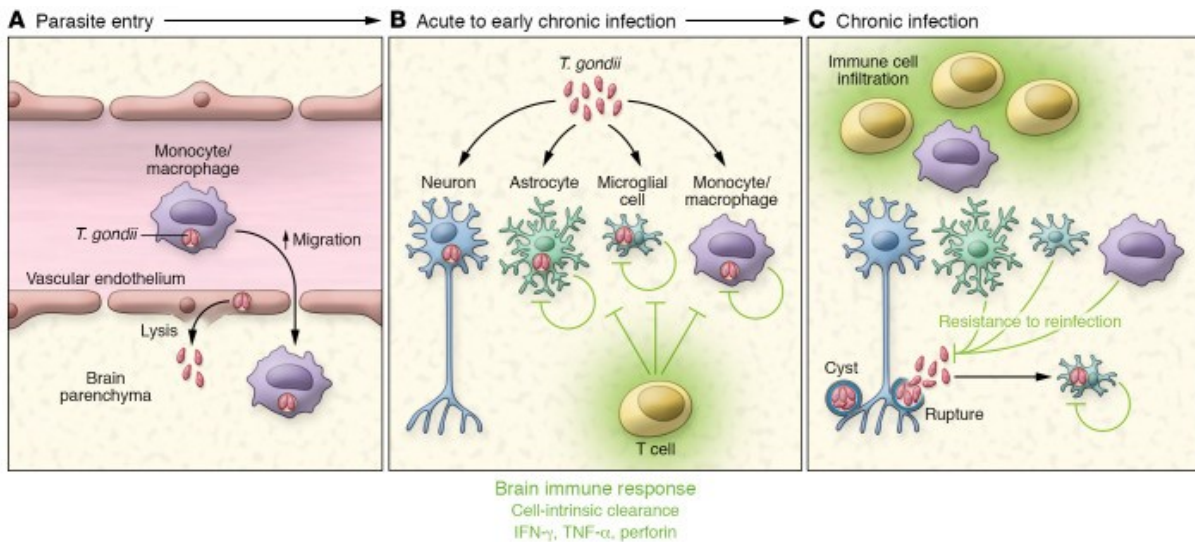


Figure 1.14: *T. gondii* entry and control of persistent infection in the brain.

(A) In acute infection, *T. gondii* is frequently found in immune cells such as monocytes and dendritic cells, exhibiting hypermigratory behaviour. This infection is associated with an increase in blood-brain barrier (BBB) permeability, allowing monocytes to accumulate in the endothelial lumen where they interact with endothelial cells. It has been proposed that migratory immune cells may transport *T. gondii* to the BBB and potentially facilitate its entry into the brain. Additionally, replicating parasites can be observed in brain endothelial cells, and their subsequent lysis could serve as a mechanism for *T. gondii* to breach the blood-brain barrier. (B) During acute infection, parasites can infect various cell types in the brain, including neurons, astrocytes, microglia, and infiltrating immune cells. Astrocytes, microglia, and peripheral monocytes possess cell-autonomous immune pathways that enable them to clear parasites. (C) As the infection progresses to the chronic stage, infected astrocytes and microglia, as well as the parasites within them, are eliminated, resulting in the presence of cysts primarily within neurons. Most of these cysts are not associated with immune infiltrates; however, individual parasites or parasite debris may occasionally colocalize with immune infiltrates. According to (Zhao and Ewald, 2020).

The proinflammatory immune response induced by tachyzoites can also lead to tissue damage. Therefore, achieving a balance between inducing and evading the immune response is crucial for the establishment of chronic *T. gondii* infection.

All three developmental stages, which include rapidly multiplying tachyzoites, dormant bradyzoites, and sporozoites, share common morphological features (Fig. 1.15).

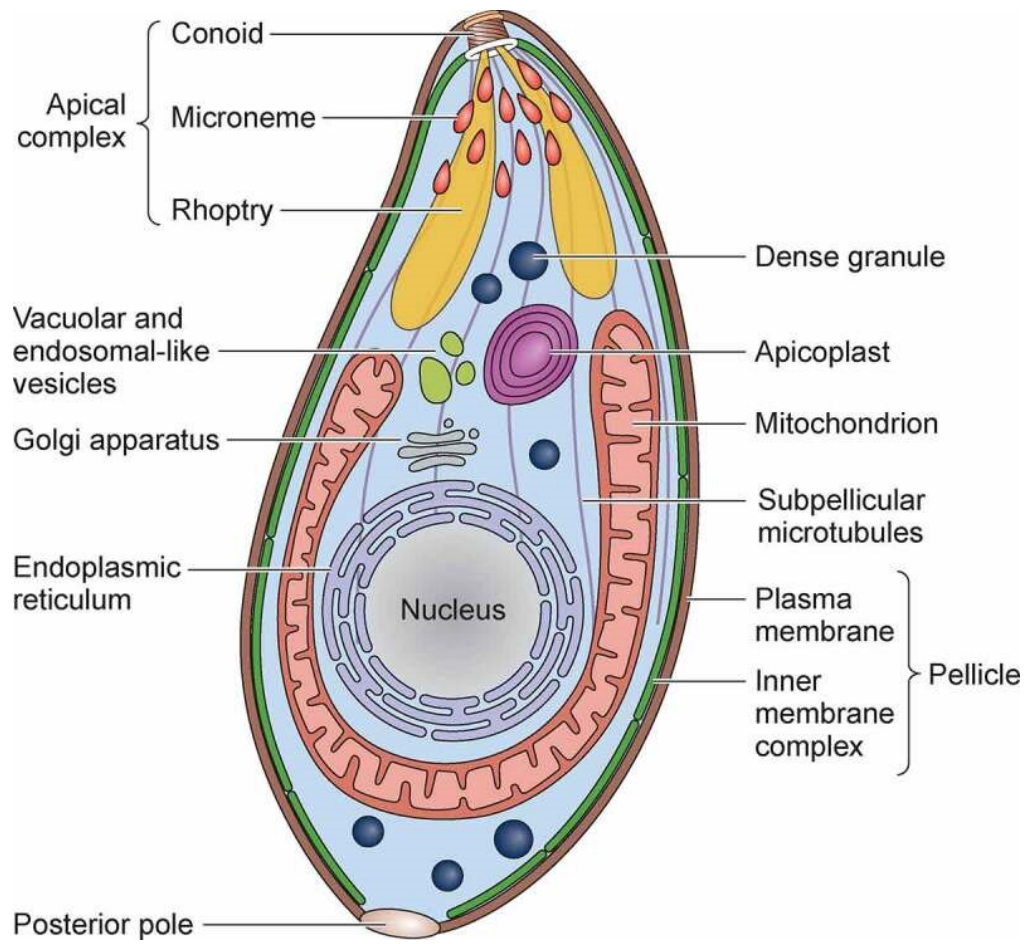


Figure 1.15: Ultrastructure of *T. gondii* tachyzoite.

Tachyzoites, like other invasive stages of *T. gondii*, are highly polarized cells and contain specialized organelles involved in the secretion of virulence factors. According to (Sanchez and Besteiro, 2021)

The parasite possesses typical organelles of eukaryotic organisms and is surrounded by a three-layered pellicle, with the outer membrane fully enclosing it. The two closely spaced inner membranes terminate at the anterior and posterior polar rings. Its microtubule cytoskeleton extends almost the entire cell from the polar ring, and actin and myosin microfilaments are mainly found in the apical part, enabling its motility. The apical complex of *T. gondii* contains characteristic structures like conoid, “dense granules” with GRA proteins, and secretory organelles like rhoptries and micronemes, which secrete proteins facilitating the parasite's penetration and invasion of the host cell (Carruthers and Boothroyd, 2007; Dubey et al., 1998).

The invasion of the host cell by *T. gondii* tachyzoites is an active process that lasts only 15 seconds but consists of many independently regulated steps (Carruthers, 1999; Sibley and Andrews, 2000; Smith, 1995). Initially, the parasite attaches to the cell surface of the host with low affinity. This interaction is mediated by the parasite's surface proteins, most of which are glycosylphosphatidylinositol (GPI)-anchored proteins of the SAG, SAG-related

sequences (SRS), and SAG-unrelated surface antigens (SUSA) families (Boothroyd et al., 1998; Pollard et al., 2008). The actin-myosin skeleton of the parasite is responsible for the gliding motility during invasion (Sibley, 1993). The attachment induces a Ca^{2+} influx into the host cell. The invasion of the parasite is completed by the release of adhesins from micronemes that interact with the surface factors of the host cell (Carruthers and Boothroyd, 2007; Carruthers and Sibley, 1997; Carruthers and Tomley, 2008; Sibley, 2011; Zhou et al., 2005). This is followed by the secretion of contents from the rhoptries into the cytoplasm and the formation of the so-called "Moving Junctions," which drive the invasion process (Alexander et al., 2005; Straub et al., 2009). During the invasion process, the plasma membrane of the host cell is invaginated and ultimately forms the membrane of the parasitophorous vacuole (PV) that surrounds the parasite (Hakansson et al., 2001). Vacuole formation is initiated by secretion of proteins from rhoptries directly into the host cell and into the developing vacuole. Parasitic factors are released that interact either with the PV (ROP2 family and ROP18) or are transported into the cytoplasm (ROP16) or nucleus (PP2C-hn, Gilbert et al., 2007) of the host cell. The PV resists acidification and fusion with endosomes and lysosomes. (Sibley, 2011). Some of these factors, such as ROP16 and ROP18 family members, belong to the polymorphic virulence factors (An et al., 2018; Butcher et al., 2011; Chen et al., 2020; Chen et al., 2022; Du et al., 2022; Khaminets et al., 2010; Kochanowsky et al., 2021; Saeij et al., 2006; Saeij et al., 2007; Wu et al., 2016). Transmembrane proteins and membrane-associated host proteins (except for the GPI-anchored proteins) are removed from the PV and replaced by Rhoptry proteins (Charron and Sibley, 2004; Joiner and Roos, 2002; Mordue et al., 1999a). The modification of the PV membrane (PVM) by *T. gondii* prevents fusion of the vacuole with endocytic compartments of the host and degradation of its content in lysosomes (Hakansson et al., 2001; Mordue et al., 1999b). Thus, the PV represents a safe compartment in which the parasite can carry out its intracellular replication (Lingelbach and Joiner, 1998). After invading host cells, intracellular parasites initiate the reorganization of mitochondria and the ER, and recruit the microtubule-organizing centre (MTOC) and elements of the host cell's cytoskeleton, such as vimentin, to form the PV (de Souza, 2005; Halonen and Weidner, 1994; Martin et al., 2007; Sinai et al., 1997). Mitochondria, which are the site of fatty acid metabolism, serve as a source of lipids for the parasite, such as lipoic acid (Crawford et al., 2006; Sinai and Joiner, 1997), while phospholipids are obtained from the ER (Gupta et al., 2005). The host's microtubules, loaded with LDL cholesterol, then form a connection with the PV and are anchored to it via the protein GRA7 from *T. gondii*'s dense granules (Coppens et al., 2006; Sehgal et al., 2005; Walker et al., 2008). The microtubule-mediated invaginations of the

PVM, also known as the tubulovesicular network (TVN) (Sibley et al., 1995), coated with GRA7, serve as channels for sequestering low-molecular-weight compounds from the endo-lysosomal system (Coppens et al., 2006). Soluble molecules up to 1300 Da pass through the PVM via parasitic membrane channels, ensuring the supply of nutrients to the parasite (Fox et al., 2004; Schwab et al., 1994).

T. gondii primarily infects cells in the S-phase (Youn et al., 1991) and causes cell cycle arrest of infected and adjacent cells between G2 and M phases (Brunet et al., 2008; Molestina et al., 2008). The parasite alters the expression of more than 1000 host genes (Chaussabel et al., 2003), encoding proteins involved in several cellular processes such as inflammation, apoptosis, metabolism, cell growth, and differentiation (Aviles et al., 2008; Naranjo-Galvis et al., 2022; Payne et al., 2003; Sinai et al., 2004). This change in gene expression can occur either through direct interaction of *T. gondii* factors with host transcription factors (Phelps et al., 2008) or by manipulating the signalling pathways of the host cell (Molestina and Sinai, 2005a; Molestina and Sinai, 2005b). The altered gene expression profile can either promote parasite proliferation, immune evasion, and virulence or lead to the development of bradyzoites (Blader and Saeij, 2009; Lima and Lodoen, 2019; Fig. 1.16).

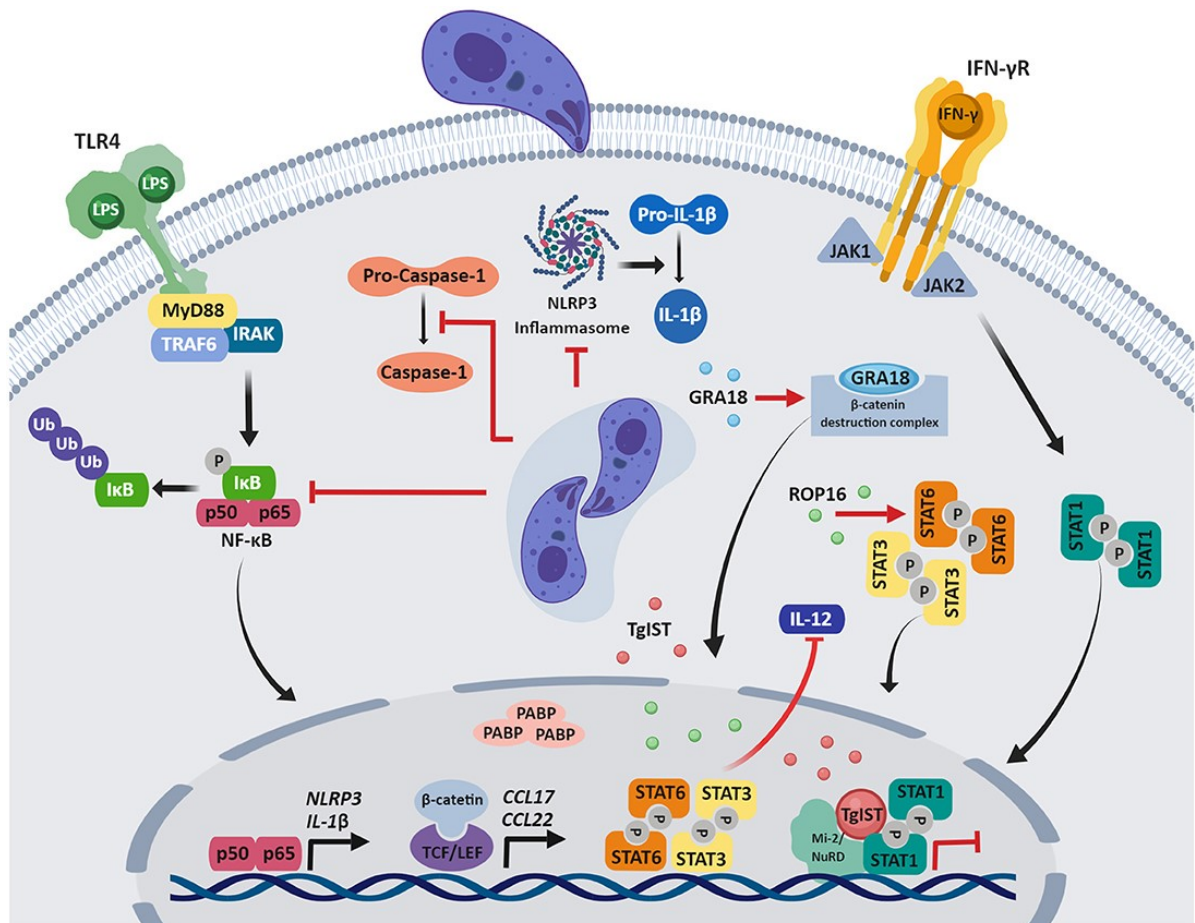


Figure 1.16: *T. gondii* host cell interactions.

Innate immune responses are initiated by Toll-like receptor (TLR) and CCR5 recognition of Toxoplasma-derived factors. *T. gondii* can modulate host immune signalling by interfering with signalling pathways and gene expression, which impairs the innate immune responses of the host. This is achieved through the secretion of parasite effector proteins from the apical secretory organelles, which can be found in the host cytosol (ROP16 and ROP18), associated with the PVM (ROP2 family and ROP18), or even translocated to the host nucleus (PP2c-hn). *Toxoplasma* regulates host transcription either by directly activating host transcription factors or by triggering host signalling cascades that ultimately activate the host transcription factors. Changes in host gene expression can promote parasite growth, immune evasion, virulence, or bradyzoite development. However, it is important to note that the effectiveness of these effector proteins may depend on the specific *T. gondii* strain and the type of cell that is infected, and various mechanisms of immune evasion have been observed (Blader and Saeij, 2009; Lima and Lodoen, 2019).

In North America and Eurasia, the population structure of *T. gondii* is remarkably clonal (Ajzenberg, 2015). Investigations into the antigenic structure and allelic variation of various structural genes have led to the classification of the parasite into three species-specific groups, with 98% similarity on the DNA level between the groups (Ajzenberg et al., 2004; Cristina et al., 1995; Darde et al., 1992; Howe and Sibley, 1995; Sibley and Ajioka, 2008; Sibley et al., 2009). Polymorphisms exhibit a biallelic pattern at nearly all loci, suggesting that they arose in the wild through few recombination events followed by clonal expansion over approximately 10,000 years (Boyle et al., 2006; Sibley and Boothroyd, 1992).

Despite the genetic similarity of *T. gondii* strains, infections cause phenotypic differences in mice. Group I consists of extremely mouse-virulent strains that cause significantly higher parasitaemia (Denkers, 1999; Saeij et al., 2007; Sibley and Boothroyd, 1992). Infection with 10 or fewer tachyzoites already leads to a fatally acute infection. Isolates of groups II and III are weakly virulent in mice. These *T. gondii* strains result in a persistent latent infection with high numbers of tissue cysts at sublethal doses. Several reports show that strains of these groups represent the majority of agents causing human toxoplasmosis (Howe et al., 1997; Howe and Sibley, 1995). Nevertheless, later studies provide evidence that strains of *T. gondii* type II were the most prevalent in immunocompromised patients, while strains of type I were strongly present in cases congenital infections (Fuentes et al., 2001; Halonen and Weiss, 2013).

The three *T. gondii* lineages show variations in their preference for organs and timing of infection in humans. Postnatal ocular infections are commonly associated with type I strains, while type II strains are frequently responsible for congenital infections and the development of toxoplasmic encephalitis (Boothroyd and Grigg, 2002).

The virulence phenotypes of type I, II, and III strains differ in mouse models, with type I being the most virulent, while type II and III are avirulent (Howe et al., 1996; Mordue et al., 2001). Type I strains of *T. gondii*, such as RH and GT-1, exhibit a higher level of motility, which contributes to their virulence in mice (Barragan and Sibley, 2002; Barragan and Sibley, 2003). On the other hand, Type II strains like ME49 and PTG have been found to modulate the migration behaviour of their host cells (Lambert et al., 2011). In addition, type II strains of *T. gondii* induce a significant stronger immune response and increased production of IL-12 (Robben et al., 2004). The virulence differences among various strains are determined by polymorphisms in loci encoding ROP proteins, including ROP18, ROP16, and ROP5 (Behnke et al., 2010; Saeij et al., 2006; Steinfeldt et al., 2010; Su et al., 2002; Taylor et al., 2006). The serine/threonine kinases of the ROP16 family from type I strains phosphorylate STAT3 and STAT6 directly in MΦ, thus prolonging the activation of these transcription factors. This reduces the production of the IL-6/IL-12 p40 and TNF- α cytokines (Hunter and Sibley, 2012; Ong et al., 2010; Saeij et al., 2007; Shapira et al., 2005; Yamamoto et al., 1997). Additionally, the ROP18 and ROP17 family of polymorphic kinases from type I strains form complexes with the ROP5 pseudokinase and act synergistically to control acute virulence in mice (Etheridge et al., 2014). The ROP18 and ROP17 proteins integrate into the PVM and phosphorylate distinct threonine residues in members of the murine p47 IRGs which help prevent IRG recruitment to the PV or lead to IRG disassembly on the PVM thereby mediating resistance to avirulent and virulent *T. gondii* strains (Behnke et al., 2011; El Hajj et al., 2007; Etheridge et al., 2014; Steinfeldt et al., 2010; Taylor et al., 2006; Zhao and Yap, 2014). As a result, the cell's autonomous immune response is weakened (Khaminets et al., 2010; Martens et al., 2005; Steinfeldt et al., 2010; Zhao et al., 2009). The transfer of the Type I allele for ROP18 into a Type III avirulent strain increases the virulence of the latter by more than fourfold (Taylor et al., 2006). Thus, direct mechanisms of immune evasion strategies include residing within a suitable intracellular niche and disrupting intracellular signalling pathways, leading to the inhibition of many host antimicrobial effector mechanisms (Fig. 1.17).

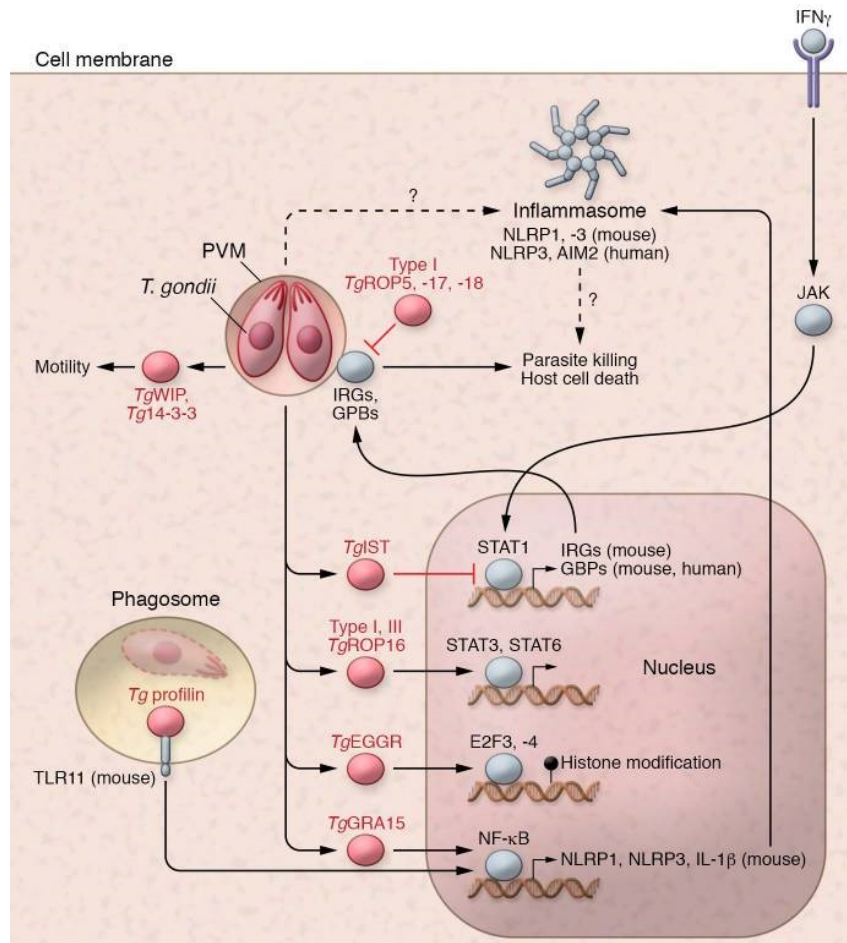


Figure 1.17: The role of *T. gondii* virulence factors in modulating innate immune signalling in the host.

T. gondii replicates within a protective parasitophorous vacuole membrane (PVM) that shields the parasite from cytosolic immune sensors and prevents fusion with endolysosomal compartments containing Toll-like receptors (TLRs). In mice, TLR11 recognizes *Tg* profilin, an actin-modifying protein that becomes exposed when phagocytosed dead or damaged parasites are encountered. Notably, TLR11 is a pseudogene in humans. The dense granule protein *Tg*GRA15II activates TRAF6, which in turn activates IKK, leading to phosphorylation of $\text{I}\kappa\text{B}$ and the release and nuclear translocation of host NF- κB . In mice, NF- κB activation is necessary for the transcriptional regulation of inflammasome components NLRP1, NLRP3, and IL-1 and IL-12 production. However, human monocytes can engage an NLRP3 inflammasome independent of NF- κB prestimulation. *Tg*GRA25, a phosphoprotein that is secreted outside the parasites and is found within the PV is a novel virulence factor and immune modulator. *Tg*GRA24 activates the p38 MAPK pathway to promote expression of IL-12 and IL-18, the upstream regulators of IFN- γ and T cell activation. Upon IFN- γ signalling, STAT1 translocates to the nucleus and upregulates IFN-responsive genes, including immunity-related GTPases (IRGs) in mice and guanylate-binding proteins (GBPs) in both humans and mice. These proteins play a critical role in attacking the parasite vacuole, leading to parasite killing and possibly host cell death. In human cells, GBP1 is necessary for this process, which triggers an alternative apoptosis pathway mediated by AIM2 activation. However, type I *T. gondii* parasites employ rhoptry proteins (*Tg*ROP5I/III, ROP17, and ROP18I) to counteract the function of mouse IRGs (IRGa6 and IRGb6) at the PVM by phosphorylation, thereby inactivating GBP-mediated attack and preventing parasite killing. *Tg*ROP18I also phosphorylates the host transcription factor ATF6 β , which is involved in the unfolded protein response and may also be important for efficient antigen presentation by DCs. Another parasite effector, *Tg*IST, acts as a nuclear repressor of STAT1 transcription. This suppresses transcription of IRF1-dependent cytokines, MHC class II expression and antigen presentation, and inducible nitric oxide synthase (iNOS) expression. *Tg*ROP16I/III, another kinase, phosphorylates STAT3 and STAT6, leading to prolonged activation of these transcription factors and upregulation of IL-4, while inhibiting the induction of IL-12. *Tg*EGGR, on the other hand, influences host gene expression through E2F3- and E2F4-mediated epigenetic modifications, blocking NF- κB -mediated

expression of proinflammatory cytokines like IL-1 β and IL-6. In infected monocytes and dendritic cells (DCs), *Tg*WIP and 14-3-3 proteins promote cell mobility, a putative mechanism of intracellular parasite dissemination *in vivo*. According to (Braun et al., 2013; Butcher et al., 2011; Gay et al., 2016; Hunter and Sibley, 2012; Olias et al., 2016; Ong et al., 2010; Rosowski et al., 2014; Zhao and Ewald, 2020). I, II and III correspond to main *T. gondii* lineages.

Additionally, immune evasion of *T. gondii* can be indirect, such as modifying the expression and release of immunomodulatory cytokines, or by affecting the viability of immune cells (Lang et al., 2007). Several successful mechanisms of immune evasion are based on inhibiting the upregulation of MHC I molecules on the surface of infected cells and downregulation of gene expression of MHC II molecules. In doing so, the parasite prevents the IFN- γ -stimulated STAT1 translocation to the nucleus (Luder et al., 1998; Luder et al., 2001; Olias et al., 2016), which results in reduced antigen presentation to T lymphocytes (Luder et al., 1998; Luder and Seeber, 2001). Alternatively, *T. gondii* blocks STAT1 from binding to the promoters of its target genes by disrupting chromatin remodelling and by preventing its recycling between promoters (Rosowski et al., 2014). In addition, the reduction of inducible nitric oxide synthase (iNOS) expression in infected macrophages favours parasitic replication (Luder et al., 2003). Notably, NO \cdot modulates IFN- γ production and is thus involved in mediating a protective response in toxoplasmosis-susceptible *T. gondii*-infected C57BL/6 mice, but not in resistant BALB/c mice strain during acute infection (Kang et al., 2004).

A *T. gondii* infection can exhibit both pro-apoptotic and anti-apoptotic effects (Carmen et al., 2006; Laliberte and Carruthers, 2008; Mordue et al., 2001). Eliminating of an infected host cell is an important innate defence strategy and inflammasome-dependent pyroptosis has emerged as a cell death pathway critical for resistance (Cirelli et al., 2014). Notably, in mice, *Toxoplasma* also activates the inflammasome via both NLRP1 and NLRP3 and as with human they do not undergo pyroptosis following infection (Gorfu et al., 2014). One conceivable possibility is that subsequent to the activation of caspase 1, a rhoptry or dense granule factor is secreted into the host cell, exerting an augmented capacity to prevent pyroptosis while exhibiting no impact on the synthesis of IL-1 β and IL-18 cytokines. (Blader et al., 2015). Type I strains of *T. gondii* induce apoptosis in neighbouring uninfected cells following IFN- γ stimulation through the activation of iNOS expression and the secretion of NO \cdot (Nishikawa et al., 2007). Cells that have been infected with *T. gondii* display resistance to various triggers of apoptosis, such as Fas-dependent and Fas-independent cytotoxicity mediated by cytotoxic T lymphocytes (CTL), IL-2 deprivation, gamma irradiation, UV irradiation, and the calcium ionophore beauvericin. This broad inhibition of apoptosis

inducers implies the involvement of a mechanism that is shared among multiple, or possibly all, apoptotic pathways (Nash et al., 1998). One of the anti-apoptotic mechanisms involves the inhibition of cytochrome C-mediated activation of caspase 3 through the upregulation of heat shock protein 70 (HSP70) and Bcl2 in infected macrophages (Goebel et al., 2001; Hwang et al., 2010; Molestina et al., 2003; Nash et al., 1998). Conversely, pro-apoptotic members of the Bcl2 family, such as Bad and Bax, are selectively degraded (Carmen et al., 2006; Nelson et al., 2008). Moreover, *T. gondii* prevents programmed cell death in murine fibroblasts, splenocytes, and macrophages by regulating the NF- κ B-dependent expression of anti-apoptotic genes (Molestina and Sinai, 2005b; Payne et al., 2003; Robben et al., 2004; Sinai et al., 2004). Loss of one of the NF- κ B subunits leads to increased susceptibility of the host during acute and chronic infection phases (Caamano et al., 1999). In contrast, Type I strains of *Toxoplasma* delay the nuclear transport of NF- κ B in murine M ϕ and human fibroblasts, despite the phosphorylation and degradation of I κ B α by a parasitic PVM-bound kinase (Butcher et al., 2001; Molestina et al., 2003; Molestina and Sinai, 2005a), as well as the phosphorylation of mitogen-activated protein (MAP) kinases, resulting in reduced expression of IL-12p40 and TNF- α (Butcher et al., 2001; Kim and Weiss, 2004; Shapira et al., 2005). This phenomenon could represent a defence strategy employed by the parasite to postpone the initiation of the pro-inflammatory response in macrophages, allowing the parasite to establish itself within the host cell.

T. gondii stimulates the transcription of genes associated with its parasitic activities, including enzymes involved in glycolysis, the transferrin receptor, and the epithelial growth factor, by modulating the host's own transcription factor Hypoxia-Inducible Factor 1 (HIF1) (Zinkernagel et al., 2007). Moreover, the infection also leads to the upregulation of genes related to the host cell's growth and survival processes, such as those encoding subunits of the EGR and AP-1 transcription factors (Molestina and Sinai, 2005b; Phelps et al., 2008). These transcription factors play important roles in cellular stress responses, including those occurring during infections (Huang et al., 1996).

The immune response against *Toxoplasma* occurs at two distinct time points: during the initial acute infection and upon reactivation of the infection following cyst rupture. In both cases, the host's immune system responds by releasing IL-12 from various immune cells, such as DCs, M ϕ , monocytes, and neutrophilic granulocytes. This IL-12 release then stimulates the secretion of IFN- γ and TNF- α from T and NK cells (Gazzinelli et al., 1993; Reis e Sousa et al., 1997; Scharton-Kersten et al., 1996; Suzuki, 2002).

The absence of IL-12, either due to genetic deficiency (IL-12^{-/-} mice) or systemic depletion, results in 100% mortality in mice infected with *T. gondii* (Gazzinelli et al., 1993; Yap et al., 2000). This lack of IL-12 leads to a significant reduction in IFN- γ expression in both studies. *T. gondii* induces the expression of IL-12 through the activation of the cysteine-cysteine chemokine receptor 5 (CCR5) by cyclophilin-18 (C-18) and the activation of TLR-dependent signalling pathways in DCs and M ϕ (Aliberti et al., 2003; Scanga et al., 2002; Fig. 1.18). Various TLRs recognize *T. gondii*-associated factors, including TLR2 and TLR4, which are activated by dominant surface glycolipids such as GPIs or *T. gondii* HSP70 (Debierre-Grockiego et al., 2007; Mun et al., 2005). TLR9, which serves as a sensor for genomic DNA, is activated by DNA containing CpG motifs (Minns et al., 2006), while TLR11 in mice specifically binds to the parasitic actin-binding structural protein profilin (Gazzinelli et al., 2004; Yarovinsky et al., 2005). It is notable that human TLR11 is a pseudogene, indicating alternative innate sensing mechanisms to detect and destroy *T. gondii* in human cells. TLRs play a critical role in various aspects of host-parasite interactions, including the initiation of pro-inflammatory cytokine response and the expression of co-stimulatory molecules (Pifer et al., 2011). Several studies have indicated that the adapter protein MyD88 in DCs is primarily responsible for the IL-12-induced IFN- γ response during infection with type I strains of *T. gondii* (Hou et al., 2011; Scanga et al., 2002). These findings highlight the important role of DCs in the innate immune response and the development of CD4⁺ T_H1-mediated resistance against *T. gondii* (Gazzinelli et al., 2004). A recent study (Snyder et al., 2021) revealed the existence of MyD88-independent intestinal immune pathways triggered by *T. gondii*. These pathways involve the production of IL-12 by myeloid cells, downstream activation of type I immunity, and the induction of IFN- γ production by innate lymphoid cells (ILC) ILC1, ILC3, and T lymphocytes. Furthermore, during infection, other cytokines such as IL-1 β and IL-18 are induced, and their receptors also interact with MyD88 (Cai et al., 2000; Hunter et al., 1995; Mordue et al., 2001). These cytokines enhance the IL-12-mediated resistance against the type II ME49 strain of *T. gondii*.

IFN- γ is one of the critical mediators of host resistance against both acute and chronic *T. gondii* infections (Denkers and Butcher, 2005; Denkers and Gazzinelli, 1998; Nishiyama et al., 2020; Suzuki et al., 1988; Yap and Sher, 1999). Effector molecules induced by IFN- γ , including iNOS (Scharton-Kersten et al., 1997; Silva et al., 2009), reactive oxygen metabolites (ROS) in phagocytic cells (Boehm et al., 1997), Neutrophil Extracellular Traps (NET) (Miranda et al., 2021), IDO (Pfefferkorn and Guyre, 1984), the IRG GTPases in mice

(Collazo et al., 2001), and the GBP family (Degrandi et al., 2007), are believed to be crucial for the host's ability to resist *T. gondii*. However, the specific mechanisms by which these molecules exert their effects on the parasite are diverse and not fully understood.

NO inhibits the proliferation of *T. gondii* (Adams et al., 1990). iNOS-deficient (iNOS^{-/-}) mice are able to control parasite replication during the acute phase but become highly susceptible and succumb to *Toxoplasma* encephalitis during the chronic phase (Scharton-Kersten et al., 1997; Silva et al., 2009). However, the discovery of complete resistance to *T. gondii* infection, in the iNOS^{-/-} Sprague Dawley (SD) rats, demonstrates a strong link between NO and ROS in immunity to *T. gondii* infection and showcases a potentially novel and effective backup innate immunity system (Wang et al., 2021). IDO reduces the availability of essential tryptophan, thereby impeding the proliferation of intracellular pathogens (Daubener et al., 2001; Pfefferkorn and Guyre, 1984). The p47 GTPases play a crucial role in the IFN- γ -induced inhibition of *Toxoplasma* in murine astrocytes and M Φ (Butcher et al., 2005; Halonen et al., 2001). These GTPases are involved in the destruction of the PV in avirulent strains of *T. gondii* (Martens et al., 2005; Pawlowski et al., 2011) and the stimulation of autophagy in murine cells (Choi et al., 2017; Collazo et al., 2001; Ling et al., 2006; Zhao et al., 2009), and they likely participate in the processing of immunologically relevant molecules (Tiwari et al., 2009). The exact role of GBPs in *T. gondii* infection remains to be fully elucidated. Several GBPs are recruited to the PV of the Type II ME49 strain but not to the PV of the Type I BK strain (Degrandi et al., 2007). Deletion of singular members of this family in mice (mGBP2^{-/-}, mGBP7^{-/-}) and a cluster of these proteins located on chromosome 3 (mGBP^{Chr3}^{-/-}: mGBP1, mGBP2, mGBP3, mGBP5, mGBP7, and mGBP2ps) results in an increased parasite burden in immune organs and leads to elevated mortality and morbidity during infection with the ME49 strain (Degrandi et al., 2013; Steffens et al., 2020; Yamamoto et al., 2012). In humans, there is only one representative of the p47 GTPases (MacMicking, 2004), which is involved in autophagy (Singh et al., 2010). Whether this protein plays a role in the context of *T. gondii* infection has not been investigated.

However, *T. gondii* has developed mechanisms to antagonize IFN- γ -induced immunity (Lang et al., 2007). Infected cells display significantly reduced responsiveness to IFN- γ , as evidenced by decreased expression levels of MHC II, iNOS, and p47 GTPases (Kim et al., 2007; Luder et al., 2001). *T. gondii* disrupts STAT1-mediated transcription in IFN- γ -stimulated cells through the induction of SOCS proteins (Zimmermann et al., 2006), which both inhibit the catalytic activity of JAKs and prevent the recruitment of STAT1 (Murray,

2007). The decrease in STAT1 protein levels observed in *T. gondii*-infected macrophages (Zimmermann et al., 2006) is consistent with the known function of SOCS proteins, which mark STAT1 molecules for proteasomal degradation. Furthermore, studies suggest that *T. gondii* interferes with the binding of STAT1 to the GAS elements present in the promoters of genes responsive to STAT1 (Lang et al., 2006). In the late acute phase of infection, the excessive production of IL-12 is counterbalanced by the induction of IL-10 in macrophages and T_H1 cells (Gazzinelli et al., 1996; Jankovic et al., 2007) as well as the expression of lipotoxin A4 (LXA4) during the chronic phase (Aliberti et al., 2002). This counteraction aims to prevent pro-inflammatory pathology and tissue damage, favouring the establishment of a chronic infection (Aliberti, 2005; Fig. 1.17).

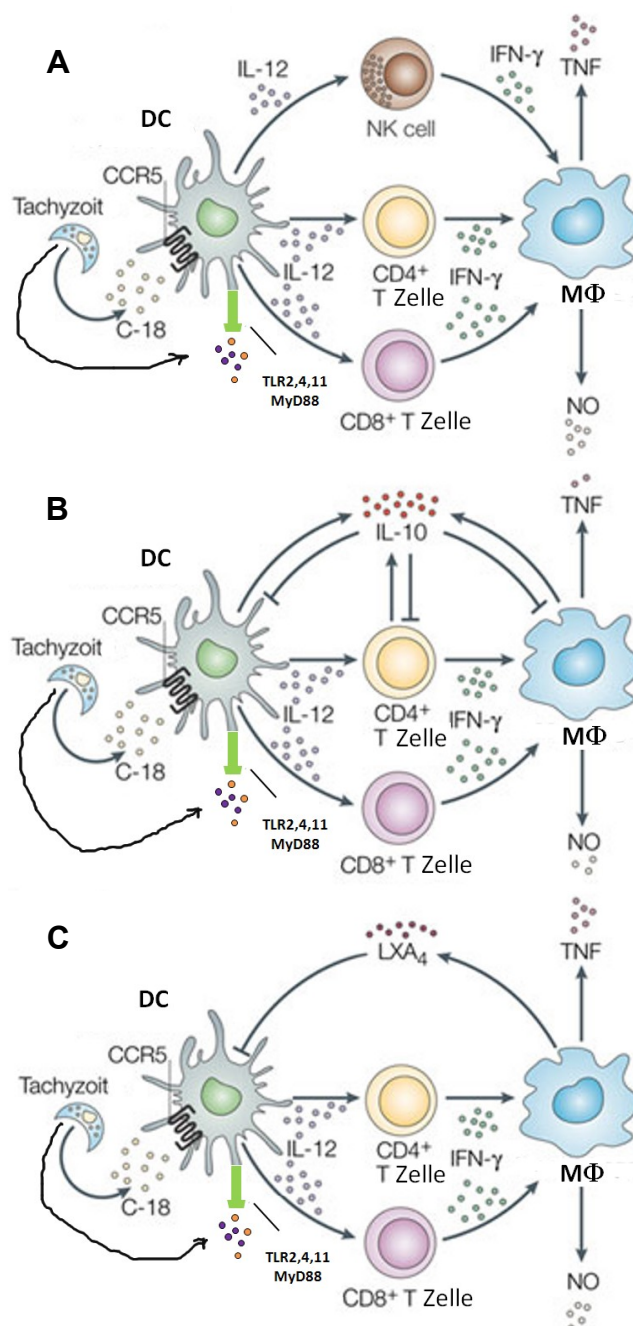


Figure 1.18: Control of pro-inflammatory responses during a *T. gondii* infection.

Following the initial infection, *T. gondii* releases factors like the CCR5 ligand C-18 and TLR agonists. Activation of these receptors leads to the production of IL-12 in DCs. IL-12 production induces or promotes the differentiation/proliferation of CD4⁺ T_H1 cells, CD8⁺ T cells, and NK cells that produce IFN- γ . Subsequently, IFN- γ activates various host cells, including macrophages, to produce microbicidal factors such as NO \cdot or TNF- α (A).

During the later stages of the acute phase, the potential cytotoxic effect is regulated by the production of IL-10 at sites of intense *Toxoplasma* replication, such as the liver or spleen. IL-10 modulates the expression of pro-inflammatory cytokines and chemokines, as well as the microbicidal activity in DCs, T cells, NK cells, and M Φ (B).

In the chronic phase of the infection, the production of lipotoxin LXA₄ helps to regulate the pro-inflammatory cytokine response in specific locations like the central nervous system (CNS) without compromising the microbicidal capacity of macrophages (C). Adapted from (Aliberti, 2005).

1.5.1. Human toxoplasmosis: prevention, screening, diagnosis, and treatment

In terms of clinical presentation, toxoplasmosis can be classified into different categories, including toxoplasmosis immunocompetent patients, congenital infection, acquired or reactivated in immunodeficient patients, parasite transmission during transplantation or accidental inoculation, and ocular infections. Clinically, the lesions may be cerebrospinal, lymphatic, cutaneous, pulmonary, cardiac, etc. A wide differential diagnosis must be considered in all of the above categories, since methods of diagnosis and their interpretation may vary for each clinical presentation (Montoya, 2002). The incubation period is usually given as 2-3 weeks.

1.5.1.1. Prevention and vaccination

Ingesting undercooked meat containing viable tissue cysts is the major route of infection worldwide. In areas with inadequate water hygiene, infection can also occur through the ingestion of soil and water contaminated with oocysts or through direct contact with infectious oocysts (Pereira et al., 2010). The main focus of toxoplasmosis prevention lies in health education aimed at minimizing personal exposure to the parasite (Rorman et al., 2006). It is recommended to avoid consuming raw meat, to ensure to thoroughly clean raw vegetables and fruits, to exercise caution when handling cats, to use gloves while engaging in gardening or earthwork activities, and prior to every meal, and after gardening, earthwork, or visiting the playground, to remember to wash hands thoroughly (Wilking et al., 2016).

Efforts are underway to develop an effective vaccine against *T. gondii*, as primary infection naturally confers lifelong protection against the parasite (Jongert et al., 2009). One successful approach in vaccine development involves using non-virulent mutated strains of the parasite. Although a live attenuated vaccine called Toxovax® is currently used in sheep to prevent abortion caused by congenital infection, it is unsuitable for human use due to the potential risk of reactivation to the pathogenic form (Buxton et al., 1993). Recent research aims to enhance vaccination effectiveness by exploring more potent adjuvant systems, improving methods for antigen delivery and presentation to the immune system, and utilizing immunogenic antigens or their T cell epitopes in combination to increase vaccination efficacy (Innes, 2010; Innes et al., 2019; Jongert et al., 2009).

1.5.1.2. Serological screening

The occurrence of congenital *T. gondii* infection shows significant geographical variation, with incidence rates ranging from less than 0.1 to over 3 cases per 1000 pregnancies (Varella et al., 2009). Fortunately, the prevalence of congenital toxoplasmosis has significantly decreased in the western Europe due to timely therapy provided to pregnant women, fetuses, and newborns (Paquet et al., 2013). Performing serological screening on pregnant women enables the identification of recently acquired *Toxoplasma* infection, facilitating the administration of appropriate chemotherapy to prevent congenital infection and minimize potential complications in newborns. Currently, routine serological screening of pregnant women is implemented exclusively in France and Austria. However, Germany and certain regions in Italy have reported surveillance of congenital toxoplasmosis (Benard et al., 2008). Diagnosis of maternal seroconversion by serological tests is generally straightforward, although it can be challenging if IgM antibodies are detected in the first trimester, requiring referral to a specialized laboratory. Pregnant women with confirmed seroconversion should be referred promptly to an expert centre, where treatment options and prenatal diagnosis can be discussed with them.

1.5.1.3. Diagnosis

Most cases of acute toxoplasmosis are clinically asymptomatic. In cases of cervical lymphadenitis, differential diagnosis should primarily exclude malignancies (such as Hodgkin's lymphoma) and other infectious diseases associated with lymph node enlargement. The presence of ocular toxoplasmosis is recognized by a characteristic observation in the ocular fundus. *Toxoplasma* encephalitis in immunosuppressed patients is characterized by delayed contrast enhancement in the peripheral region (da Cunha Correia et al., 2012).

In immunocompetent individuals, the preferred diagnostic method is the detection of antibodies in serum or plasma, either by the indirect fluorescent assay (Jones et al., 2001; Rorman et al., 2006), or by direct (Peloux et al., 1973), differential (Montoya et al., 2007), indirect latex (Payne et al., 1984), immunosorbent agglutination (Stepick-Biek et al., 1990) tests, or the enzyme immunoassay (EIA) as the most commonly used laboratory *Toxoplasma* diagnostic test (Curdt et al., 2009; Pfrepper et al., 2005), with a particular focus on the quantification of IgG and IgM antibodies. In immunosuppressed patients, antibody testing may be negative and direct detection methods should be prioritized. Currently, a

stepwise diagnostic approach is recommended, with testing during the first trimester of pregnancy when appropriate. Additional diagnostic procedures for *Toxoplasma* include determination of IgG antibody avidity (Hedman et al., 1989), measurement of IgA antibodies, immunoblotting (Remington et al., 2004), and quantitative assays (Robert-Koch-Institut, 2016; Saadatnia and Golkar, 2012). The results can be interpreted according to the following table:

Table 1.1: Serological diagnosis of Toxoplasmosis. Adopted from (Robert-Koch-Institut, 2016).

IgG	IgM	IgG-avidity	probable outcome
positive	negative	–	inactive, latent infection
positive	positive	high	subsiding or latent (inactive) infection
positive	positive	low	acute infection possible further clarification procedures or follow-up are necessary

As mentioned above, any positive *Toxoplasma* IgM antibody result in a pregnant woman should be further investigated by a specialized laboratory, if necessary. The detection of specific IgM and/or IgA antibodies in the peripheral blood of the newborn is considered evidence of a prenatal infection (Gras et al., 2004). The detection of IgG antibodies in the newborn detected by comparative immunoblot (parallel testing of maternal and neonatal serum) (Franck et al., 2008; Magi and Migliorini, 2011) and/or the persistence or increase in concentration of IgG serum antibodies in the postnatal period are also suggestive of prenatal infection (Christoph et al., 2004).

The detection of specific serum antibodies (usually only IgG antibodies) confirms the clinical suspicion of a reactivated infection. Local infection in the eye can also be demonstrated by the detection of local antibody production or specific IgA antibodies in the aqueous humour, e.g. by comparative immunoblotting (aqueous humour versus serum) (Maenz et al., 2014).

Detection of the pathogen or its DNA is confirmatory and should be sought wherever possible. PCR is the most commonly used method for direct detection of the pathogen (Remington et al., 2004). However, although a positive PCR result from tissue or body fluids indicates the presence of *T. gondii*, it does not necessarily prove the activity of the infection (as conventional PCR tests cannot distinguish between tachyzoites and bradyzoites). Conversely, a negative PCR result does not necessarily exclude toxoplasmosis if the parasites are present in low concentrations in a patient sample. PCR from amniotic fluid and

umbilical cord blood can provide information about possible infection of the child in the context of clarifying prenatal *Toxoplasma* infection. A positive result proves infection of the foetus, but a negative result does not rule it out with certainty.

In the immunocompetent patient, PCR from blood samples is not suitable for the diagnosis of acute infection because a negative result does not rule out recent parasitaemia. Positive PCR results from blood samples tend to be incidental findings in the acute phase of infection. Therefore, serology remains the method of choice for detecting acute infection. In immunosuppressed patients, PCR is currently the most reliable method for detecting active infection. Suitable clinical specimens are body fluids (EDTA blood, cerebrospinal fluid, bronchoalveolar lavage) or biopsy material from the site of infection (e.g. in TE) if disseminated infection is suspected. However, a negative PCR result does not exclude acute *Toxoplasma* infection (Robert-Koch-Institut, 2016). CT scan is also useful in the diagnosis of human cerebral toxoplasmosis.

1.5.1.4. Therapy

The main targets of treatment are folic acid metabolism and *Toxoplasma* protein synthesis. Their effect is limited to tachyzoites, while they have little effect on bradyzoite cysts. The most commonly used drugs are spiramycin, pyrimethamine, sulphadiazine, clindamycin and possibly atovaquone. Indications for therapy include active *Toxoplasma* infection in immunosuppressed patients, ocular toxoplasmosis, and pre- and postnatal therapy.

If foetal infection is confirmed through sonographic imaging and PCR testing of amniotic fluid (the indication for amniocentesis should be very strict due to the increased risk of miscarriage (0.6-1%) and should be performed at least four weeks after the infection of the pregnant woman and not before the 18th week of gestation), active prophylactic prenatal treatment should be initiated as early as possible (preferably within three weeks of seroconversion) to reduce the risk of maternal-foetal transmission and to prevent brain and ocular damage (Paquet et al., 2013). The recommended therapies for preventing maternal-foetal transmission are as follows: (1) spiramycin (3.0 g = 9 Mio. IE/d p.o.) for maternal infections before 16 weeks of gestation for 3 weeks, and (2) pyrimethamine (1 × 50 mg on day 1, 1 × 25 mg from day 2) and sulfadiazine (50 mg/kgBW/d) (P-S) with folinic acid (10-15 mg/d) for maternal infections at 16 weeks of gestation or later for at least 4 weeks (Hotop et al., 2012; Paquet et al., 2013). The myelosuppressive effect of drugs must be considered

when administering P-S therapy. A recent study provided evidence that P-S therapy, when administered within the first weeks after infection, is superior to spiramycin therapy in terms of transmission rate and the occurrence of cerebral lesions in the newborn (Mandelbrot et al., 2018).

Neonates are also treated with the combination of pyrimethamine (1 mg/kgBW/d), sulfadiazine (50-100 mg/kgBW/d) and folinic acid (2-3 mg/week), with treatment lasting up to 12 months in symptomatic infants, depending on the severity of the disease, and with continuous administration of the drugs (Pleyer et al., 2019; Robert-Koch-Institut, 2016).

For patients with toxoplasmic retinochoroiditis, clindamycin (1.2-2.4 g/d) is an alternative to combination therapy (Upadhyaya et al., 2023). However, it does not cross the blood-brain barrier in sufficient quantities. In addition, combination therapy with trimethoprim/sulfamethoxazole and atovaquone should be mentioned as a possible therapy for cerebral toxoplasmosis in immunocompromised patients (Hernandez et al., 2017).

Uncomplicated postnatally acquired toxoplasmosis requires monitoring but no therapy (Robert-Koch-Institut, 2016).

1.5.2. New diagnostic-therapeutic research branches

Existing treatments for toxoplasmosis are associated with severe side effects and lack efficacy in eradicating chronic infection. There is an urgent need to develop novel, highly effective anti-toxoplasmosis agents with low toxicity. Recent studies have identified natural products such as 1,2-benzenediol,3-(4-hydroxy-2-methoxy-6-methylphenoxy)-5-methyl- (ACI), 5*S*,6*S*-phomalactone, from the crude extract of *Paraboeremia selaginellae*, an endophytic fungus, or the tuneable luminophore indolo[3,2-*a*]phenazines, as a promising source of novel bioactive compounds for the treatment of toxoplasmosis and other infectious pathogens (Mazzone et al., 2022; Merkt et al., 2021).

Despite its discovery over a century ago (Ferguson, 2009), our understanding of the mechanisms by which this parasite modulates the host to facilitate virulence, growth, immune evasion, and bradyzoite development is only now beginning to emerge. However, many questions remain unanswered. An overarching goal is to develop protective vaccines and to identify novel antiparasitic targets. Advancing our understanding of the fundamental

biological processes and molecular mechanisms underlying host-pathogen interactions will contribute to this goal.

1.6. Aim of the work

The aim of this study was to explore the molecular interaction(s) which enable murine Guanylate-binding-protein 2 (mGBP2) to control *T. gondii* replication. By employing immunoprecipitation (IP) followed by mass spectrometry (MS) analysis, we have identified novel interaction partners of mGBP2 such as galectin-9 (Gal9) and cytoskeleton-associated protein 4 (Ckap4). Furthermore, we demonstrate that the inactivation of Gal9 impairs the cell autonomous IFN- γ induced immune control of *T. gondii* replication. These findings offer important insights into the molecular aspects of cell-autonomous immunity.

2. Materials und Methods

2.1. Source of supply

2.1.1. Chemicals

Chemical	Source of supply
Acetic acid	Merck, Darmstadt
Acetone	Merck, Darmstadt
Acetonitrile	AppliChem, Darmstadt
Agarose	Biozym, Hamburg
Ammonium hydrogen carbonate	Sigma-Aldrich, Taufkirchen
Ampicillin sodium salt	Sigma-Aldrich, Taufkirchen
Ampicillin sodium salt: <i>E. coli</i>	Roth, Karlsruhe
Bactoagar	BD Biosciences, Heidelberg
Bafilomycin	Sigma-Aldrich, Taufkirchen
β -Mercaptoethanol: Cell culture	Invitrogen, Karlsruhe
Bromophenol blue	Merck, Darmstadt
Bovine serum albumin (BSA)	Sigma-Aldrich, Taufkirchen
Calcium chloride	Merck, Darmstadt
Chloroform	Roth, Karlsruhe
Complete Mini Protease Inhibitor Cocktail	Roche, Mannheim
Concanamycin	Sigma-Aldrich, Taufkirchen
Coomassie R-250, G-250	Merck, Darmstadt
4',6-Diamidin-2-phenylindol (DAPI)	ThermoFisher Scientific, Dreieich
Dimethylsulfoxid (DMSO)	Sigma-Aldrich, Taufkirchen
Dipotassium hydrogen phosphate	Merck, Darmstadt
Disodium hydrogen phosphate	Invitrogen, Karlsruhe
Dithiothreitol (DTT)	Gibco, Eggenstein
Enhanced chemiluminescence (ECL), SuperSign Extended Duration	ThermoFisher Scientific, Dreieich
Ethylenediaminetetraacetic acid (EDTA)	Merck, Darmstadt
Ethanol	Merck, Darmstadt
Ethidium bromide	BD Biosciences, Heidelberg
Foetal calf serum (FKS)	Cambrex Corporation, East Rutherford, NJ, USA
Foetal calf serum (FKS) low Endotoxin	SouthernBiotech, Birmingham, USA
Fluoromount-G	Roth, Karlsruhe
Formaldehyde	Merck, Darmstadt
Glycerine	Merck, Darmstadt
Goat serum	DaKoCytomation, Hamburg
4-(2-hydroxyethyl)-1-piperazineethanesulfonic acid (HEPES)	Gibco, Karlsruhe
Hydrochloric acid (HCl)	Merck, Darmstadt R&D Systems, Mainz

Interferon gamma (IFN- γ), murine	Merck, Darmstadt
Isopropanol	Merck, Darmstadt
Lactacystin	Roche, Mannheim
Leupeptin	Roth, Karlsruhe
Lysogeny broth (LB)-agar	Roth, Karlsruhe
LB-medium	Roth, Karlsruhe
Kanamycin	Merck, Darmstadt
Magnesium chloride	ThermoFisher Scientific, Dreieich
MassRuler™ DNA-ladder Mix	Merck, Darmstadt
Methanol	Merck, Darmstadt
Methylene blue	Biomol, Hamburg
MG132	Oxoid, Hampshire, England
Milk powder	Sigma-Aldrich, Taufkirchen
3-(N-Morpholine)-propansulfonic acid (MOPS)	Sigma-Aldrich, Taufkirchen
NP-40 (IGEPAL CA-630®)	Invitrogen, Karlsruhe
NuPage Transfer Buffer (20x)	Merck, Darmstadt
Orange G	Sigma-Aldrich, Taufkirchen
Paraformaldehyde	Roche, Mannheim
Pefabloc SC (4-(2-Aminoethyl)- benzolsulfonylfluorid-hydrochlorid)	Roche, Mannheim
Pepstatin	Roche, Mannheim
PhosSTOP Phosphatase Inhibitor Cocktail Tablets	Roche, Mannheim
PMSF (Phenylmethylsulfonylfluorid)	Millipore, Schwalbach
Polybren, transfection reagent	GE Healthcare, München
Potassium chloride	Merck, Darmstadt
Potassium dihydrogen phosphate	Sigma-Aldrich, Taufkirchen
Potassium hexacyanoferrate	Merck, Darmstadt
Protein marker, High-Range Rainbow	MBI Fermentas, St. Leon-Rot
Protein marker, PageRuler™ Prestained Protein Ladder	GE Healthcare, München
Protein-G-Sepharose	Millipore, Schwalbach
Re-Blot Plus Strong Solution	Carl Roth, Karlsruhe-Mühlburg
Silver nitrate	Carl Roth, Karlsruhe-Mühlburg
Sodium acetate	Merck, Darmstadt
Sodium azide (NaN ₃)	ThermoFisher Scientific, Dreieich
Sodium carbonate (anhydrous)	Merck, Darmstadt
Sodium chloride	VWR, Darmstadt
Sodium dihydrogen phosphate	Roth, Karlsruhe
Sodium dodecyl sulphate (SDS)	Merck, Darmstadt
Sodium fluoride	Merck, Darmstadt
Sodium hydroxide	Sigma-Aldrich, Taufkirchen
Sodium thiosulphate pentahydrate	Merck, Darmstadt
Saponin	
Transfection reagent: jetPRIME®	Polyplus, Berkeley, CA, USA Sigma-Aldrich, Taufkirchen

Tris-(hydroxymethyl)-aminomethan	Sigma-Aldrich, Taufkirchen
Trifluoroacetic acid	Sigma-Aldrich, Taufkirchen
Trypan blue	Serva, Heidelberg
Trypsin, Porcine	Millipore, Merck, Darmstadt
Tween-20	Roth, Karlsruhe
Ultrapure H ₂ O	Invitrogen, Karlsruhe
Water, UltraPure DNase/RNase free	Sigma-Aldrich, Taufkirchen
Wortmannin	Roth, Karlsruhe
Yeast extract	

2.1.2. Antibodies

Antibodies	Source of supply
Alexa Fluor™ 633 goat anti-mouse IgG (H+L)	ThermoFisher Scientific, Dreieich
Anti-β-Actin	Sigma-Aldrich, Taufkirchen
Anti-Ckap4 (STJ1100889)	St John's Laboratory Ltd, UK
Anti-Gal9	
Polyclonal, rabbit (ARP54821_P050)	Aviva Systems Biology, CA, USA
Monoclonal, rabbit (ab275877)	Abcam, Cambridge, UK
Anti-GFP, clones 7.1 and 13.1	Roche, Mannheim
Anti-HA	
Monoclonal, mouse	Roche, Mannheim
Monoclonal, mouse	Sigma-Aldrich, Taufkirchen
Polyclonal, rabbit	Sigma-Aldrich, Taufkirchen
Anti-mGBP2 (EVNGKPVTSDEYLEHC)	Eurogentec, Belgien
Anti-mCherry	Sigma-Aldrich, Taufkirchen
Anti- <i>Toxoplasma gondii</i> [TP3] (SAG1)	Abcam, Cambridge, UK
Cy™2 Goat Anti-Mouse IgG + IgM	Jackson ImmunoResearch, Suffolk, UK
Cy™2 Goat Anti-Rabbit IgG	Jackson ImmunoResearch, Suffolk, UK
Cy™3 Goat Anti-Mouse IgG + IgM	Jackson ImmunoResearch, Suffolk, UK
Cy™3 Goat Anti-Rabbit IgG	Jackson ImmunoResearch, Suffolk, UK
Cy™3 Goat Anti-Rat IgG + IgM	Jackson ImmunoResearch, Suffolk, UK

2.1.3. Enzymes

Enzymes	Source of supply
DNA polymerase, High Fidelity	Roche, Mannheim
DNA polymerase, Expand High Fidelity	Roche, Mannheim
DNA polymerase, Platinum <i>Taq</i>	Invitrogen, Karlsruhe
DNA polymerase, Native Pfx	Invitrogen, Karlsruhe
DNA T4 ligase	NEB, Frankfurt a. M.
DNA T4 polynucleotide kinase	NEB, Frankfurt a. M.

DNA ligation Mix	TaKaRa, Shiga, Japan
Proteinase K	New England BioLabs, Frankfurt a. M.
Restriction enzymes	New England BioLabs, Frankfurt a. M. Roche, Mannheim MBI Fermentas, St. Leon-Rot
Reverse Transcriptase SuperScript	Invitrogen, Karlsruhe
RNAse A	Roche, Mannheim
Shrimp Alkaline Phosphatase (SAP)	USB, High Wycombe, UK

2.1.4. Reagents and Consumables

Reagents	Source of supply
Anti-GFP V _{HH} nanobody eGFPBoosterAtto488	ChromoTek GmbH, Bruchköbel
Anti-RFP V _{HH} nanobody mRFPBoosterAtto647N	ChromoTek GmbH, Bruchköbel
Anti-HA-Agarose HA-7 monoclonal	Sigma Aldrich, Taufkirchen
BCA Protein Assay Kit, Pierce	Thermo Scientific, Rockford, USA
Bis-Tris SDS-Gels (4-12%) NuPAGE™	Invitrogen, Karlsruhe
Bis-Tris SDS-Gels (10%) NuPAGE™	Invitrogen, Karlsruhe
Cellometer strips for cell counting	Nexcelom Bioscience, Lawrence, USA
Cover Glass: Microscope Coverslips 13 mm	VWR, Darmstadt
dNTPs	Invitrogen, Karlsruhe
Films: Hyperfilm™-ECL	GE Healthcare, München
Filter paper Whatman 3MM	Whatman, Dassel
Cannulas	BD Pharma, Heidelberg
Cuvettes	Brand, Wertheim
GFP-Trap®	ChromoTek GmbH, Bruchköbel
Long analytical column (Acclaim PepMapRSLC)	Thermo Scientific, Rockford, USA
Nitrocellulose Blotting Membrane	
Protran BA85	Whatman, Dassel
Amersham Protran 0,45 µm	GE Healthcate, Munich
Oligo(dT) ₂₀ Primer	Invitrogen, Karlsruhe
Plasmid isolation kits	
NucleoBond Xtra Maxi kit	Macherey-Nagel, Düren
Zippy™ Plasmid Miniprep Kit	Zymo Research, CA, USA
High Pure Plasmid Isolation Kit	Roche, Mannheim
mini preparation	American National Can, Chicago, USA
Parafilm M	Zymo Research, Freiburg Roche, Mannheim
PCR-Gel extraction kit	Biozym Scientific GmbH, NUNC, Wiesbaden BD Falcon, Heidelberg
Plastics	Eppendorf, Hamburg Corning Incorporated, NY, USA

PCR Plates FrameStar® Break-A-Way	Sarstedt, Nümbrecht
PCR Strips for doomed or flat caps	Greiner Cellstar, Frickenhausen
ProteoExtract® Subcellular Proteome Extraction Kit	Brand GmbH, Wertheim
Protein-G-Sepharose	Starlab, Hamburg
qPCR MasterMix No ROX	Biozym, Hessisch Oldendorf
Quik-Change II Site Directed Mutagenesis Kit	Calbiochem-Merck, Darmstadt
RFP-Trap®	4titude, Brooks Life Sciences, UK
Rotiphorese® Gel 30% Acrylamid/Bisacrylamid	4titude, Brooks Life Sciences, UK
Running buffer NuPAGE™ MES SDS Running Buffer	Calbiochem-Merck, Darmstadt
Slides	GE Healthcare, München
SNAP-Cell 647-SiR substrate	Eurogentec, Liege, Belgien
Sterile filter	Stratagene, California
Surveyor mutational detection kit	ChromoTek GmbH, Bruchköbel
Syringes	Roth, Karlsruhe
TRIzol®	Invitrogen, Karlsruhe
TOPO TA Cloning® Kit 2.1	VWR, Darmstadt
Ultracentrifuge tubes	NEB, Frankfurt a. M.
	Sartorius, Göttingen
	IDT, USA
	Omnifix, Melsungen
	ThermoFisher Scientific, Dreieich
	Invitrogen, Karlsruhe
	Beckman Coulter, Krefeld

2.2. Devices

Device/Label	Manufacturer
Flue	wrt-Laborbau, Stadtlohn
Analytical balance, Chyo JL-180	Welabo, Düsseldorf
Analytical balance ABT 120 5 DH	Kern, Buchholz
Balance Precisa 600	Oehmen, Essen
Balance EMB 2200-0	Kern, Buchholz
Balance WNB22	Memmert, Schwabach
Cell culture shaker, 3015	GFL, Burgwedel
Cell counting chamber Neubauer improved	BLAUBRAND®, Merck, Darmstadt
Cell Density Meter Ultraspec 10	Amersham Bioscience
Cellometer™ Auto T4	Nexcelom Bioscience, Lawrence, USA
Centrifuges and rotors: for bacteria	Thermo Scientific, Rockford, USA
Evolution RC Centrifuge Sorvall®	Piramoon Technologies Inc., Thermo
F8S-6x1000y FIBERlite Centrifuge	Scientific, Rockford, USA
Sorvall Discovery™ 90 SE Hitachi	Thermo Scientific, Rockford, USA

S100 AT 6	Thermo Scientific, Rockford, USA
S120 AT 3	Thermo Scientific, Rockford, USA
Sorvall Discovery™ M120 SE Hitachi	Thermo Scientific, Rockford, USA
TST 41.14	Kontron, Eching/München
SW41Ti	Beckman, Coulter, Krefeld
Sorvall RC-4 Hitachi	Thermo Scientific, Rockford, USA
Confocal microscope, LSM780	Zeiss, Oberkochen
Confocal microscope, STED, TCS SP8 STED 3X	Leica, Wetzlar
HC PL APO CS2 93x glycerol objective	
Cooling centrifuges: eukaryotic cells	Heraeus Instruments, Hanau
Sorvall® RC26 PLUS	Heraeus Instruments, Hanau
Biofuge fresco	Heraeus Instruments, Hanau
Megafuge 1.0R	Thermo Scientific, Rockford, USA
Counter, 120S Betaplate	Perkin Elmer, Rodgau-Jügesheim
Developer machine Curix 60	Agfa, Köln
Developing chamber	Carl Roth, Karlsruhe-Mühlburg
Digital camera, Powershot G2	Canon, Amsterdam, Niederlande
Digital Graphic printer UP-D898MD	Sony, Stuttgart
ECL & Fluorescence Imager Intas ECL Chemostar	Intas Science Imaging, Göttingen
Electrophoresis chamber for DNA	Hoefer, Amstetten
Electrophoresis chamber for NuPAGE gels: XCell	Invitrogen, Karlsruhe
Electroporation system Pulse Controller Plus	BioRad, Munich
Freezer -20°C	Bosch GmbH, Gerlingen
Freezer -80°C	HettichLab, Tuttlingen
Freezer -80°C Ultra Low	Sanyo, San Diego, CA, USA
Gel documentation system, BioDocAnalyze	Biometra, Göttingen
Gel documentation system Gel Doc XR+	Bio-Rad, München
Heating block, DB 3D Dri Block	Thermo Scientific, Rockford, USA
Heating bath	
Water base	Störk-Tronic, Stuttgart
Metal beats	VWR, Darmstadt
Heating stove, OV3	Biometra, Göttingen
Harvester, Basic 96	Satron instruments, Tampare, Finland
Ice machine	Ziegra, Isernhagen
Incubator: BBD6220 CO ₂ : eukaryotic cells	Thermo Scientific, Rockford, USA
Incubator: bacterial plates: function line	Heraeus Instruments, Hanau
Incubator: <i>E. coli</i> cultures Ecotron, Multitron	Heraeus Instruments, Hanau
Laboratory pump	KNF, Freiburg-Munzingen
Light panel, Kaiser profile basic	TechINN, Pirineus, Spain
Magnetic stirrer: MR3001 K	Heidolph, Schwabach
Magnetic and heater: IKA RCT classis	IKA-Werke, Staufen
Mass spectrometer Orbitrap Elite	Thermo Scientific, Rockford, USA
Microscopes	Zeiss, Oberkochen
Axiovert 100/Axio Observer	
Microwave	Bosch GmbH, Gerlingen

Milli-Q	Millipore, Consett, UK
NanoDrop 1000	PeqLab Life Science, Erlangen
TE2000	Nikon, Düsseldorf
PCR devices	Biometra, Göttingen
T1/3 Thermocycler/T-Gradient	
Rapid Separation Liquid Chromatography system (RSLCnano) UltiMate 3000	ThermoFisher Scientific, Dreieich
Rotator	
Loopster digital	IKA-Werke, Staufen
Rotator SB3 Stuart	IKA-Werke, Staufen
RT-PCR device	BioRad, Munich
CFX96	
pH meter (MP225)	Mettler Toledo, Giessen
Photometer, GeneQuant II	Pharmacia, Braunschweig
Pipettes	Thermo Scientific, Rockford, USA
Pipetting aid (Pipet-Boy, accu-jet)	Brand, Wertheim
Power supply PowerEase	PeqLab Life Science, Erlangen
Protein transfer device (Transblot SD)	Bio-Rad, Munich
Realtime-PCR Machine, iCycler IQ5	Bio-Rad, Munich
Refrigerator	Bosch GmbH, Gerlingen
Roller Mixer	Ratek, Victoria, Australia
Shaker for bacterial cultures	Infors HT, Schweiz
Ecotron	
Multitron Standard	
Shaker for bacteria cultures, GFL-3017	Thermo Scientific, Rockford, USA
Shaker for WB, GFL-3013	Thermo Scientific, Rockford, USA
Shaker for DNA gels Polymax 1040	Heidolph, Schwabach
SilicaTip emitters	New Objective, Woburn, MA, USA
SpeedVac, Vacuum Concentrators	Thermo Scientific, Rockford, USA
Sterile bench, HLB 2472 GS	Heraeus, Hanau
Thermoblocks, Termomixer Compact	Eppendorf, Hamburg
Table-top centrifuges	
Biofuge fresco	Heraeus, Hanau
Centrifuge 5415 C/D	Eppendorf, Hamburg
Trans-Blot® SD Semi-Dry Transfer Cell	Bio-Rad, Munich
Ultrasound device	IKA-Werke, Staufen
Ultra-TURRAX® IKA T25 digital	
Voltage sources	
Power Pack P25	Biometra, Göttingen
PS 500 XT	HIS, San Francisco, USA
Vortex	
Genie 2	Scientific Industries, NY, USA
IKA MS 3 basic/digital	IKA-Werke, Staufen

2.3. Media and buffers

2.3.1. Cell culture media and supplements

Media/ supplements	Source of supply
β -Mercaptoethanol (β -ME)	Gibco, Karlsruhe
Dulbecco's Modified Eagle Medium (DMEM)	Gibco, Karlsruhe
Dulbecco's Phosphate-Buffered Saline (D-PBS)	Gibco, Karlsruhe
Foetal bovine serum Supreme (FBS),	PAN Biotech, Aidenbach
Iscove's Modified Dulbecco's Medium (IMDM)	BioWhittaker, Lonza, Belgium
Newborn calf serum (NCS)	Gibco, Karlsruhe
Hank's Buffered Saline Solution (HBSS)	PAN Biotech, Aidenbach
L-Glutamine	Biochrom, Berlin
Penicillin/streptomycin	Biochrom, Berlin
Trypsin/EDTA 0.25%	Gibco, Karlsruhe

2.3.2. Stock solutions and buffers

Designation	Composition	
Ampicillin stock solution	100 mg/ml	in ddH ₂ O
Coomassie staining		
Coomassie-Blue G-250 for mass spectrometry (MS)	0,02%	Brilliant blue G-250, Merck
	2% (w/v)	Phosphoric acid
	10%	Ethanol
	5%	Al ₂ (SO ₄) ₃
De-staining solution for G-250 Coomassie gels for MS	2% (w/v)	Phosphoric acid
	10%	Ethanol
Fixing solution for G-250 Coomassie gels for MS	2% (w/v)	Phosphoric acid
	30%	Ethanol
DNA electrophoresis		
5 x DNA loading buffer	15%	Ficoll Type 400
	0.05%	Bromophenol blue
	0.05%	Xylene cyanol
10 x DNA loading buffer	1 mg/ml	Orange G
	10 mM	Tris/HCl, pH 7.5
	30%	Gelatine
dNTP-Mix	1 mM	dATP
	1 mM	dCTP

	1 mM	dGTP
	1 mM	dTTP
Immunofluorescence		
Antibody solution	0.2%	Goat serum in 10% blocking solution
Blocking solution	2%	Goat serum in 10% permeabilization solution
DAPI solution	1:2500	in PBS
Fixing solution for cells	4%	Paraformaldehyde (PFA) in PBS
Permeabilization solution	0.02%	Saponin in PBS
Washing solution	0.002%	Saponin in 10% permeabilization solution
In-gel digestion of reduced and alkylated spots		
Washing buffer A keep cold	10 mM	Ammonium bicarbonate (NH ₄ HCO ₃)
Washing buffer B keep cold	100 mM	NH ₄ HCO ₃
Dithiothreitol (DTT) solution keep at -20°C	10 mM 50 mM	DTT NH ₄ HCO ₃
Iodoacetamide (IAA) solution keep at -20°C	55 mM 50 mM	IAA NH ₄ HCO ₃ , pH 7.4
Lentiviral transduction		
HEBS 2x	280 mM 10 mM 1.5 mM 12 mM 50 mM	NaCl KCl Na ₂ HPO ₄ D-glucose HEPES (acid free), pH 7.05, filter sterilize, store at 4°C
HEPES	2.5 mM	filter sterilize, store at 4°C
CaCl ₂	0.5 M	filter sterilize, store at 4°C

PCR

10 x PCR buffer	500 mM	KCl
	100 mM	Tris/HCl, pH 8.3
	15, 20, 25 mM	MgCl ₂
	0.1%	Gelatine

Silver staining

Silver staining solution A	50% (v/v) 10% (v/v)	Ethanol MEK denatured Acetic acid
Silver staining solution B	50% (v/v) 500 mM 8 mM	Ethanol MEK denatured Sodium acetate Sodium thiosulphate
Silver staining solution C	6 mM	Silver nitrate in ddH ₂ O
Silver staining solution D	236 mM	Sodium carbonate anhydrous
Silver staining solution E	236 mM	Sodium carbonate anhydrous Formaldehyde (37%): shake before use
Silver staining solution F	50 mM	EDTA in ddH ₂ O
Silver de-staining solution A	30 mM	Sodium thiosulphate in HPLC-H ₂ O
Silver de-staining solution B	100 mM	Potassium hexacyanoferrate in HPLC-H ₂ O
50 x TAE	2 M 1 M 0.1 M	Tris/HCl Glacial acetic acid EDTA pH 8.0
TAE (Electrophoresis buffer, DNA)	40 mM 20 mM 2 mM	Tris/HCl Glacial acetic acid EDTA pH 8.0
TE buffer	10 mM 1 mM	Tris/HCl EDTA pH 8.0
Trypsin digestion gel bands	100 mM	NH ₄ HCO ₃ , pH 8 in LC-MS H ₂ O

	0.033 µg/µl	Trypsin
WB and IP		
Collecting gel (5%) for SDS	0.7 ml	Rotiphorese® 30
	0.8 ml	Collective gel buffer
	3.5 ml	ddH ₂ O
	5 µl	TEMED
	50 µl	APS
Collective gel buffer for SDS	0.4%	SDS
	0.5 M	Tris/HCl
		pH 8.85
Separating gel (10%) for SDS	2.5 ml	Rotiphorese® 30
	2.5 ml	Separating gel buffer
	4.8 ml	ddH ₂ O
	5 µl	TEMED
	100 µl	APS
Separating gel buffer for SDS	0,4%	SDS
	1.5 M	Tris/HCl
		pH 8.85
TBS-T	150 mM	NaCl
Western Blot (WB) loading buffer (5 x) for Invitrogen gels	10 mM	Tris/HCl
	0.1%	Tween-20
		pH 7.6
	30 mM	Tris/HCl
		pH 6.8
WB loading buffer (5 x) for Bio- Rad gels	45%	Glycerine
	6 M	Urea
	3.2%	SDS
	0.2%	Bromophenol blue
	30 mM	Tris/HCl
		pH 6.8
WB/Cell lysis buffer	140 mM	NaCl
	20 mM	Tris/HCl
	5 mM	MgCl ₂
	1%	NP-40
	1	1 Protease-Inhibitor Cocktail-tablet (EDTA free) (Roche) per 10 ml buffer

	1	1 PhosSTOP tablet (Roche) per 10 ml buffer
	5 mM	NaF
	2.5 mM	PMSF
		pH 7.4
WB/Immunoprecipitation (IP) lysis buffer: fresh preparation only, keep cool on ice	300 mM	NaCl
	50 mM	HEPES
	10 mM	MgCl ₂
	10 mM	KCl
	0.5%	NP-40
	10%	Glycerine
	1	1 Protease-Inhibitor Cocktail-tablet (EDTA free) (Roche) per 10 ml buffer
	1	1 PhosSTOP tablet (Roche) per 10 ml buffer
	1 μM	Leupeptin in DMSO
	0.5 μM	Pepstatin in DMSO
	5 mM	NaF
	2.5 mM	PMSF
	1 mM	Dithiothreitol (DTT)
		pH 7.4
WB running buffer (20 x) for Invitrogen SDS gels	50 mM	MOPS
	50 mM	Tris Base
	1 mM	EDTA
	0.1% (w/v)	SDS
		pH 7.7
WB running buffer (10 x) for Bio- Rad gels	50 mM	Tris/HCl
	196 mM	Glycine
	1.8 mM	EDTA
	0.1% (w/v)	SDS
		pH 8.3
WB Transfer buffer	25 mM	Bicine
	25 mM	Bis/Tris
	1 mM	EDTA
	20%	Methanol

2.3.3. Media for cell culture

Table 2.1: Composition of the cell culture media.

Cell type	Basic medium	FCS*	Penicillin	Streptomycin	β -ME	L-Glutamine
EF cells	DMEM High glucose	10%	100 U/ml	100 μ g/ml	0.05 mM	2 mM
HS27/HFF fibroblasts	IMDM	10%	100 U/ml	100 μ g/ml	0.05 mM	2 mM
NIH 3T3 cells	DMEM High glucose	10% NCS	100 U/ml	100 μ g/ml	0.05 mM	2 mM
293 FT cells	DMEM High glucose	10%	100 U/ml	100 μ g/ml		2 mM

* FCS tested for murine embryonic fibroblasts, NCS tested for NIH 3T3 cells, deactivated for 1 h at 56°C.

2.3.4. Media for bacterial culture

The media (Table 2.2) were sterilized by autoclaving (121°C/2 bar/20 min). To obtain a solid medium, 15 g of agar per litre was added to the medium before autoclaving. Bacteria were grown aerobically at 37 °C. Bacteria on agar plates were sealed with parafilm and stored at 4°C for a maximum of 4 weeks. For long-term storage, liquid cultures grown overnight were mixed 1:1 with 98% sterile glycerol and stored at -80°C or in liquid nitrogen.

Table 2.2: Composition of the bacteria culture media.

Medium	Composition	Quantity
Luria broth (LB)	Tryptone/peptone	10 g
	Yeast extract	5 g
	NaCl	10 g
	ddH ₂ O	ad 1 l
	pH 7.2	

2.4. Antibiotics

For positive selection of plasmid-containing bacteria, ampicillin was added to the culture medium (Tab. 2.3).

Table 2.3: Antibiotics used.

Substance	Stock solution	Final concentration
Ampicillin	50 mg/ml in ddH ₂ O, sterile-filtered	100 μ g/ml

2.5. Bacterial strains and cell lines

2.5.1. Bacterial and *Toxoplasma* strains

Table 2.4 lists the bacterial and *Toxoplasma* strains used in this work, with genotype and reference.

Table 2.4: Bacterial and toxoplasma strains used.

Bacterial strain	Genotype	Reference
<i>E. coli</i> DH5 α TM - T1 ^R	F ⁻ ϕ 80 <i>lacZ</i> Δ M15 Δ (<i>lacZYA-argF</i>) U169 <i>recA1 endA1 hsdR17</i> (r _k ⁻ , m _k ⁺) <i>phoA supE44 thi-1 gyrA96 relA1 tonA</i> (confers resistance to phage T1)	(Hanahan and Meselson, 1983), Invitrogen, Karlsruhe
<i>E. coli</i> TOP10	F ⁻ <i>mcrA</i> Δ (<i>mrr-hsdRMS-mcrBC</i>) Φ 80 <i>lacZ</i> Δ M15 Δ <i>lacX74 recA1 araD139</i> Δ (<i>ara-leu</i>) 7697 <i>galU galK rpsL</i> (Str ^R) <i>endA1 nupG</i>	Invitrogen, Karlsruhe
<i>T. gondii</i> ME49, Type II	obligatory intracellular replicating protozoa	(Parmley et al., 1994)

2.5.2. Cell lines

Table 2.5 lists the cells used in this work, together with their characteristics and references.

Table 2.5: Cells used.

Cells	Properties	Reference
WT EF cells	embryonic fibroblasts at day 14.5 p.c. from WT C57BL/6 embryos	freshly isolated
293FT cells	human primary embryonic kidney cell line transformed with human adenovirus type 5 DNA, additionally transformed with pCMVSPORT6Tag.neo	Invitrogen, Karlsruhe
HS27/HFF	human foreskin fibroblasts	ATCC, CRL-1634 TM
mGBP2 ^{-/-} EF	embryonic fibroblasts at day 14.5 p.c. from mGBP2 ^{-/-} C57BL/6 embryos	freshly isolated, (Dissertation C. Konermann, 2008)
NIH 3T3	murine embryonic fibroblast cell line	ATCC, CRL-1658 TM

2.6. Primers

The oligonucleotides listed in this chapter were synthesized, purified, and lyophilized by Metabion (Martinsried). Tables 2.6, 2.7 and 2.7 list all the primers used to clone the GFP- and mCherry-fusion constructs.

Table 2.6: Primer for cloning GFP and mCherry fusion constructs.

Primer name	Sequence (5'→3')	Application
pWPXL-GFP-w/o-STOP_fwd	ATT GGA TCC AGG CCT AAG CTT ACG	pWPXL-GFP original vector
pWPXL-GFP-w/o-STOP_rev	ATT GAA TTC GAA GTT GAG CTC AGA TCT GAG TCC GGA C	
pWPXL-GFP-mGBP2_fwd	ATA TCC CGG GAG CCT CAG AGA TCC ACA TGT CG	pWPXL-GFP-mGBP2 fusion construct
pWPXL-GFP-mGBP2_rev	ATA TCA TAT GTC AGA GTA TAG TGC ACT TCC CAG	
pWPXL-mCherry-Ckap4_fwd	AAT TGA ATT CCC CTC GGC CAA ACA AAG GGG C	pWPXL-mCherry-Ckap4 fusion construct
pWPXL-mCherry-Ckap4_rev	AAT TCA TAT GTT AGA TCT TTT CAT GGA TCT TCT CAA CTT TCA GAA AC	
pWPXL mut kozak-Ckap4-GFP_fwd	AAT TTG ATC AAT GCC CTC GGC CAA ACA AAG GG	pWPXL-mut-kozak-Ckap4-GFP fusion construct
pWPXL mut kozak-Ckap4-GFP_rev	AAT TTG ATC AAA GAT CTT TTC ATG GAT CTT CTC AAC TTT CAG AAA C	
pWPXL-mCherry-Gal9_fwd	AAT TGA ATT C GC TCT CTT CAG TGC CCA GTC TCC	pWPXL-mCherry-Gal9 fusion construct
pWPXL-mCherry-Gal9_rev	AAT TAC TAG T CT ATG TCT GCA CGT GGG TCA GCT G	
pWPXL mut kozak-Gal9-GFP_fwd	AAT TGG ATC CAT GGC TCT CTT CAG TGC CC	pWPXL-mut-kozak-Gal9-GFP fusion construct
pWPXL mut kozak-Gal9-GFP_rev	AAT TAC GCG TAA TGT CTG CAC GTG GGT CAG	
pWPXL mut kozak-Cathepsin D-GFP_fwd	AAT TAC GCG TAT GAA GAC TCC CGG CGT CTT G	pWPXL-mut-kozak-Cathepsin D-GFP fusion construct
pWPXL mut kozak-Cathepsin D-GFP_rev	AAT TAC GCG TAA GAG TAC GAC AGC ATT GGC AAA GC	
pWPXL-mCherry-ISG15_fwd	AAT TGA ATT CGC CTG GGA CCT AAA GGT GAA GAT GC	pWPXL-mCherry-ISG15 fusion construct
pWPXL-mCherry-ISG15_rev	AAT TCA TAT GTT AGG CAC ACT GGT CCC CTC CC	

pWPXL-mCherry - iNOS_fwd	AAT TCC CGG GAG CTT GCC CCT GGA AGT TTC	pWPXL-mCherry- iNOS fusion construct
pWPXL-mCherry - iNOS_rev	AAT TCA TAT GTC AGA GCC TCG TGG CTT TGG GCT C	
pWPXL-mCherry - Cse1_fwd	AAT TAC TAG TAG AGC TCA GCG ATG CGA ATT TAC AGA	pWPXL-mCherry-Cse1 fusion construct
pWPXL-mCherry - Cse1_rev	AAT TAC TAG TTC ACA ACA GGG TCA CAC TGG CT	
pWPXL-mCherry - Anxa5_fwd	AAT TGA ATT CGC TAC GAG AGG CAC TGT GAC	pWPXL-mCherry- Anxa5 fusion construct
pWPXL-mCherry - Anxa5_rev	AAT TCA TAT GTC AGT CAT CCT CGC CCC CG	
pWPXL mut kozak- Anxa5-GFP_fwd	AAT TGG ATC CAT GGC TAC GAG AGG CAC TG	pWPXL-mut-kozak- Anxa5-GFP fusion construct
pWPXL mut kozak Anxa5-GFP_rev	AAT TAC GCG TAA GTC ATC CTC GCC CCC	
pWPXL-mCherry - Anxa6_fwd	AAT TAC TAG TAG CCA AAA TAG CAC AGG GTG CCA TGT AC	pWPXL-mCherry- Anxa6 fusion construct
pWPXL-mCherry - Anxa6_rev	AAT TAC TAG TTT AGT CCT CTC CGC CAC ACA GAG C	
pWPXL-mCherry - Kpnb1_fwd	AAT TAC TAG TAG AGC TCA TAA CCA TCC TCG AGA AGA CC	pWPXL-mCherry- Kpnb1 fusion construct
pWPXL-mCherry - Kpnb1_rev	AAT TAC TAG TTC AAG CCT GGT TCT TCA GTT TCC TCA GTT C	
pWPXL-mCherry - Kpna2_fwd	AAT TGA ATT CTC CAC GAA CGA GAA TGC TAA CTT ACC AGC	pWPXL-mCherry- Kpna2 fusion construct
pWPXL-mCherry - Kpna2_rev	AAT TCA TAT GTT AGA AGT TAA AGG TCC CAG GAG CTC CAT C	
pWPXL-mCherry - Npm3_fwd	AAT TGA ATT CGC GGC CGG CGC GGC	pWPXL-mCherry- Npm3 fusion construct
pWPXL-mCherry - Npm3_rev	AAT TCA TAT GCT AAG GCC TGC CCC TGT GCT TC	
pWPXL-mCherry - DDX5_fwd	AAT TCC CGG GAT CGA GTT ATT CTA GTG ACC GAG	pWPXL-mCherry- DDX5 fusion construct
pWPXL-mCherry - DDX5_rev	AAT TCC CGG GTT ATT GAG AAT ACC CTG TTG GCA TG	
pWPXL-mCherry - DDX6_fwd	AAT TAC TAG TAA GCA CGG CCA GAA CAG AGA ACC C	pWPXL-mCherry- DDX6 fusion construct

pWPXL-mCherry – DDX6_rev	AAT TAC TAG TTT ACG GTT TCT CGT CTT CTG CAG GC	
pWPXL-mCherry – DDX21_fwd	AAT TGA ATT CCC GGG AAA ACT CCG CAG TGG	pWPXL-mCherry- DDX21 fusion construct
pWPXL-mCherry – DDX21_rev	AAT TCA TAT GTC ACT GAC CAA ACG CTT TAC TAA AAC TCC G	
pWPXL-mCherry – DHX9_fwd	AAT TGA ATT CGG TGA CAT TAA AAA TTT TCT GTA TGC CTG G	pWPXL-mCherry- DHX9 fusion construct
pWPXL-mCherry – DHX9_rev	AAT TGA ATT CTT AAT AGC CAC CAC CAC CCC C	
pWPXL-mCherry – Ifitm3_fwd	AAT TGA ATT CAA CCA CAC TTC TCA AGC CTT CAT CAC CG	pWPXL-mCherry- Ifitm3 fusion construct
pWPXL-mCherry – Ifitm3_rev	AAT TCA TAT GTT AAG TGT GAA GGT TTT GAG CGT TAA GAA CAA TG	
pWPXL-mCherry – Tnp01_fwd isoform 1	AAT TAC TAG TAG TGT GGG ACC GGC AAA CCA AGA TG	
pWPXL-mCherry – Tnp01_fwd isoform 2	AAT TAC TAG TAG AGT ATG AGT GGA AAC CTG ACG AGC	pWPXL-mCherry- Tnp01 fusion construct
pWPXL-mCherry – Tnp01_rev	AAT TAC TAG TTT AAA CAC CAT AAA AAG CTG CAA GAC GCT C	
pWPXL-mCherry – Gls_fwd	AAT TAC TAG TAA TGC GGC TGC GAG GCT CGG	
pWPXL-mCherry – Gls_rev isoform 1	AAT TAC TAG TTT ATA GCA ACC CGT CGA GAT TCT TGT GGA C	pWPXL-mCherry- GLS fusion construct
pWPXL-mCherry– Gls_rev isoform 2	AAT TAC TAG TCT AGC TCC TCT CCC CCA GAC T	
pWPXL mut kozak- Lamp2-GFP_fwd	AAT TGG ATC CAT GTG CCT CTC TCC GGT TAA AGG	pWPXL-mut-kozak- Lamp2-GFP fusion construct
pWPXL mut kozak Lamp2-GFP_rev	AAT TAC GCG TAA AAA TTG CTC ATA TCC AGT ATG ATG GCG C	
pWPXL-mCherry – Nampt_fwd	AAT TGA ATT CAA TGC TGC GGC AGA AGC CGA	pWPXL-mCherry- Nampt fusion construct
pWPXL-mCherry – Nampt_rev	AAT TCA TAT GCT AAT GAG GTG CCA CGT CCT GCT	
pWPXL-mCherry – Thbs1_fwd	AAT TAC TAG TAG AGC TCC TGC GGG GAC TAG GT	pWPXL-mCherry- THBS1 fusion construct
pWPXL-mCherry – Thbs1_rev	AAT TAC TAG TTT AGG AAT CTC GAC ACT CGT ATT TCA TGT CT	

pWPXL-mCherry – Copa_ fwd	AAT TGA ATT CCT AAC CAA ATT CGA GAC GAA GAG CGC GC	pWPXL-mCherry- COPA fusion construct
pWPXL-mCherry – Copa_ rev	AAT TAC TAG TTT AGC GAA ACT GAA GAG GAC TGA TCC TCA GCC	
pWPXL-mCherry – Kank2_ fwd	AAT TGA ATT C GC CCA GGT CCT GCA TGT GCC	pWPXL-mCherry- Kank2 fusion construct
pWPXL-mCherry – Kank2_ rev	AAT TAC TAG T TC ACT CCT CGG CTG AAG ACG AAG C	
pWPXL-mCherry – Aifm1_ fwd	AAT TAC GCG T AT GTT CCG GTG TGG AGG CC	pWPXL-mCherry- Aifm1 fusion construct
pWPXL-mCherry – Aifm1_ rev	AAT TAC GCG TAA ATC TTC ATG AAT GTT GAA GAG TTT AGC TAC TTC	
pWPXL-mCherry – Eif3_ fwd	AAT TGA ATT C GC GGA GTA CGA CCT GAC TAC TCG	pWPXL-mCherry- Eif3 fusion construct
pWPXL-mCherry – Eif3_ rev	AAT TAC TAG T TT AAT AGA AGC CAG AGT CTT GGG TTG CCC	
pWPXL-mCherry – ROP5_ fwd	AAT TAC TAG TAG CGA CGA AGC TCG CTA GAC	pWPXL-mCherry- ROP5 fusion construct
pWPXL-mCherry – ROP5_ fwd	AAT TAC TAG TAG CGA CGG ATG CCA GGA GAC	
pWPXL-mCherry – ROP5_ rev	AAT TAC TAG TTC AAG CGA CTG AGG GCG CAG	
pWPXL-mCherry – ROP5_ rev	AAT TAC TAG TTT ATT TTG ATG ACA GGC TGG TGG ATA TGT C	pWPXL-mCherry- ROP16 fusion construct
pWPXL-mCherry – ROP16_ fwd	AAT TGA ATT CAA AGT GAC CAC GAA AGG GCT TGC	
pWPXL-mCherry – ROP16_ rev	AAT TAC TAG TCT ACA TCC GAT GTG AAG AAA GTT CGG	
pWPXL-mCherry – ROP17_ fwd	AAT TAC TAG TAG AGT TGG TGT TGT GCT TTG TGA TAA TAA CG	pWPXL-mCherry- ROP17 fusion construct
pWPXL-mCherry – ROP17_ rev	AAT TAC TAG TTT ACT CCT TCT GTA ATA AAG CCG CCT CC	
pWPXL-mCherry – ROP18_ fwd	AAT TCC CGG GAC TCG GCA GAT TGA TAC AG	pWPXL-mCherry- ROP18 fusion construct
pWPXL-mCherry – ROP18_ fwd	AAT TCC CGG GAT TTT CGG TAC AGC GGC	
pWPXL-mCherry – ROP18_ fwd	AAT TCC CGG GAG GTT TAG CGA CTC TTC TC	

pWPXL-mCherry – ROP18_rev	AAT TCA TAT GTT ATT CTG TGT GGA GAT GTT CCT GCT G	
pWPXL-mCherry – ROP18_rev	AAT TCA TAT GTT ATT CTG TTT GTA GAT GTT CCT GCT GTT CG	
pWPXL-mut kozak– GRA7-GFP_fwd	AAT TGG ATC CAT GGC CCG ACA CGC AAT TTT TT	
pWPXL-mut kozak– GRA7-GFP_rev	AAT TAC GCG TAA CTC TTC TGT GTC TGT CTG C	pWPXL-mut-kozak- GRA7-GFP fusion construct
pWPXL-mut kozak– GRA7-GFP_rev	AAT TAC GCG TAA CTG GCG GGC ATC CTC	
pWPXL-mut kozak– GRA15-GFP_fwd	AAT TGG ATC CAT GGT GAC AAC AAC CAC GCC	pWPXL-mut-kozak- GRA15-GFP fusion construct
pWPXL-mut kozak– GRA15-GFP_rev	AAT TAC GCG TAA TGG AGT TAC CGC TGA TTG TGT G	
pWPXL-mut kozak– GRA25-GFP_fwd	AAT TTG ATC AAT GAA GCG TTT CTG GTT GTG CGC G	pWPXL-mut-kozak- GRA25-GFP fusion construct
pWPXL-mut kozak– GRA15-GFP_rev	AAT TTG ATC AAA GTT TCT ATC GAA TTC CGG GAG GTT CTC	

Table 2.7: Primers for the cloning of truncated GFP-mGBP2 fusion constructs.

Primer name	Sequence (5'→3')	Application
pWPXL-GFP-mGBP2- G/GM-domain_fwd	ATT CCC GGG AAT GGC CTC AGA	pWPXL-GFP-mGBP2- G/GM/GE-domain- fusion constructs
pWPXL-GFP-mGBP2- G-Domain_rev	GAT TAT CAT ATG ACT CAG CTG ATG GCA CC	pWPXL-GFP-mGBP2- G-domain-fusion construct
pWPXL-GFP-mGBP2- GM-domain_rev	GAT TAT CAT ATG ACT CAT GTG AGT GAC TGA TCC	pWPXL-GFP-mGBP2- GM-domain-fusion construct
pWPXL-GFP-mGBP2- ME-domain_fwd	ATT CCC GGG AAA TGG GTC TCT CC	pWPXL-GFP-mGBP2- ME-domain-fusion construct
pWPXL-GFP-mGBP2- E-domain_fwd	ATC CCG GGA GAG GCA GCA AAG	pWPXL-GFP-mGBP2- E-domain-fusion construct
pWPXL-GFP-mGBP2- ME/E-domain_rev	GAT TAT CAT ATG ACT CAG AGT ATA GTG CAC TTC CC	pWPXL-GFP-mGBP2- ME/E-domain-fusion construct
pWPXL-GFP-mGBP2- GE-domain, G_fwd	ATT CCC GGG AAT GGC CTC AGA GAT CCA CAT GTC GGA ACC C	pWPXL-GFP-mGBP2- GE-domain-fusion construct

pWPXL-GFP-mGBP2- GE-domain, G _ rev	GCT GCC TCG CTG ATG GCA CCA ACA TAG GTC TGC ACC AGG	pWPXL-GFP-mGBP2- GE-domain-fusion construct
pWPXL-GFP-mGBP2- GE-domain, E _ fwd	GCC ATC AGC GAG GCA GCA AAG GAG GTA GAA GAG GAA CGT AC	pWPXL-GFP-mGBP2- GE-domain-fusion construct
pWPXL-GFP-mGBP2- GE-domain, E _ rev	GAT TAT CAT ATG ACT CAG AGT ATA GTG CAC TTC CCA GAC GAT TTG TTT TGC TTC AGG GT	pWPXL-GFP-mGBP2- GE-domain-fusion construct

Table 2.8 lists mutagenesis primers for the introduction of punctate mutations into the GTPase domain and CaaX motif of mGBP2.

Table 2.8: Mutagenesis primers for generating point mutants of mGBP2 in pWPXL-GFP vectors.

Primer name	Sequence (5'→3')	Application
pWPXL-GFP-mGBP2- C586S_rev	ATA TCA TAT GTC AGA GTA TAG TGC TCT TCC CAG AC	Mutagenesis of mGBP2

Table 2.9 lists primers for the introduction of an HA marker at the N-terminus of mGBP2 and subsequent cloning into the pWPI vector.

Table 2.9: Primers for the introduction of an HA marker at the N-terminus of mGBP2 and subsequent cloning into the pWPI vector.

Primer name	Sequence (5'→3')	Application
pWPI-HA-mGBP2_fwd	AAT TTT AAT TAA ATG TAC CCA TAC GAC GTC CCA GAC TAC GCT GCC TCA GAG ATC C	pWPI-HA-mGBP2- fusion construct
pWPI-HA-mGBP2_rev	ATT ATT AAT TAA TCA GAG TAT AGT GCA CTT CCC AGA CGA TTT GTT TTG CTT CAG GGT AT	

Table 2.10 lists primers for generation of CRISPR/Cas9 knockout transfection vectors and Surveyor® Mutation Detection for CRISPR/Cas9 knockout analysis.

Table 2.10: Primer for CRISPR/Cas9 knockout strategy and Surveyor® nuclease base knock our analysis.

Primer name	Sequence (5'→3')	Application
pSpCas9(BB)- 2A-GFP Gal9 fwd	CAC CGC GGG TTA ATG TAT GGA GAC T	CRISPR/Cas9 knockout of Gal9
pSpCas9(BB)- 2A-GFP Gal9 rev	AAA CAG TCT CCA TAC ATT AAC CCG C	

pSpCas9(BB)- 2A-GFP Ckap4 fwd	CAC CGA TCC GCG CCG CCC GAC GGG T	CRISPR/Cas9 knockout of Ckap4
pSpCas9(BB)- 2A-GFP Ckap4 rev	AAA CAC CCG TCG GGC GGC GCG GAT C	
Surveyor-Gal9 fwd	AAC TAG ATT GGG CCT GCC TC	Surveyor® Mutation Detection for CRISPR/Cas9 knockout analysis
Surveyor-Gal9 rev	AGA GAT CCC CCT GAC TCT GT	
Surveyor-Cakp4 fwd	ATG CCC TCG GCC AAA CAA AG	
Surveyor-Cakp4 rev	AAAGCTGGAGTAGGCGACTT	

Table 2.11 lists sequencing primers used at GATC or BMFZ to check cloning success and verify insert sequences.

Table 2.11. Sequencing primers.

Primer name	Sequence (5'→3')	Application
pWPXL_fwd	GAA TTC AGC GGC CGC GTG A	Cloning in pWPXL-GFP-w/o-STOP
pWPXL 166979-rev	GAA TAC CAG TCA ATC TTT CAC	Cloning in pWPXL-GFP-w/o-STOP
pWPXL_rev	CCA CAT AGC GTA AAA GGA GC	Cloning in pWPXL-GFP-w/o-STOP
pWPXL-mCherry_rev	ACC ATC GTG GAA CAG TAC G	Cloning in pWPXL-mCherry-w/o-STOP
pWPXL GFP w/o STOP_fwd	AGA AGC GCG ATC ACA TG	Cloning in pWPXL-GFP-w/o-STOP
pWPXL GFP w/o STOP_fwd	GGA GCA ACA TAG TTA AG	Cloning in pWPXL-GFP-w/o-STOP
T7_fwd	TAA TAC GAC TCA CTA TAG GG	Cloning in pCR 2.1-TOPO
M13_rev	CAG GAA ACA GCT ATG ACC	Cloning in pCR 2.1-TOPO
pWPI 68423_fwd	CAA GCC TCA GAC AGT GGT TC	Cloning in pWPI
pWPI PacI_rev	GTT TGT ATG TCT GTT GC	Cloning in pWPI

Ckap4 central_fwd	CCC GTC CGA CAG ATC TTT GA	Cloning in pWPXL-mCherry-w/o-STOP
Ckap4 central_rev	TCA AAG ATC TGT CGG ACG GGA	Cloning in pWPXL-mCherry-w/o-STOP

Table 2.12 lists the sequences of primers and probes used for real-time RT-PCR.

Table 2.12: Sequences of oligonucleotides and probes for real-time RT-PCR experiments.

Primer name	Sequence (5'→3')	Probe (#)
β -actin_fwd	TGA CAG GAT GCA GAA GGA GA	FAM CTCTGGCT TAMRA (106)
β -actin_rev	CGC TCA GGA GGA GCA ATG	
<i>T. gondii</i> _fwd (MWG)	GCT AAA GGC GTC ATT GCT GTT	FAM ATC GCA ACG GAG TTC TTC CCA GAC GT BHQ (1)
<i>T. gondii</i> _rev (MWG)	GGC GGA ACC AAC GGA AAT	
Gal9_fwd	ACC CTA CCA CCT CGT GGA C	FAM (94)
Gal9_rev	GAC AGG GGC TGC AGA GTT C	
Ckap4_fwd	GGA GGA GGT CCA GCA GGT	FAM (7)
Ckap4_rev	TTG CAAG GGA TTG GAC CTT	
Anxa5_fwd	GCC ATG AAA GGC TTG GGT A	FAM (89)
Anxa5_rev	TGC TTC GGG ATG TCA ACA G	

The β -actin primer probe is part of the Universal Probe Library from Roche, Mannheim, Germany. The *T. gondii* housekeeping gene probe is from Eurogentec, Belgium. Probe numbers are given in parentheses.

2.7. Plasmid vectors

2.7.1. Original vectors

Different initial vectors, including commercially accessible ones, have been employed for the cloning and expression of DNA sequences. A compilation of these vectors can be found in Table 2.13.

Table 2.13: Used starting vectors.

Name	Characteristics	Reference
pCR 2.1-TOPO TA	Vector for direct cloning of PCR products, Amp ^R , Kan ^R , f1 ori, Col E1 ori, lac-promotor, lacZ α -fragment	Invitrogen
pLP/VSVG	Expression vector for lentiviral transduction (envelope), expression of the VSV-G gene (VSV G glycoprotein), CMV promoter, Amp ^R	Invitrogen
pFLAG-CMV-2	Transient expression vector for N-terminal Met-FLAG fusion protein, SV40 origin of replication, CMV promoter, Amp ^R	Sigma-Aldrich
psPAX2	Expression vector for lentiviral transduction (packaging), expression of Gag, Pol, and Env, CMV promoter, Amp ^R	Labor Trono (Yang et al., 2012)
pSpCas9(BB)-2A-GFP (PX458)	CRISPR/Cas9 knockout transfection vector	Addgene, USA
pSV40	Adenovirus vector for immortalizing cells, Amp ^R	Prof. Dr. O. Takeuchi, Research Institute for Microbial Diseases, Osaka University, Japan
pWPI	Expression vector with IRES-eGFP, EF1- α promoter, Amp ^R	Labor Trono, (Zhang and Tandon, 2012)
pWPXL-GFP-w/o-STOP	Expression vector for N-terminal GFP fusion proteins, EF1- α promoter, Amp ^R	
pWPXL-GFP-mGBP2	Lentiviral expression vector for a GFP-mGBP2 construct, EF1- α promoter, Amp ^R	(Dissertation C. Konermann, 2008)
pWPXL-GFP-mGBP2-C586S	Lentiviral expression vector for a GFP-mGBP2 construct in which the isoprenylation site is mutated, EF1- α promoter, Amp ^R	
pWPI-HA-mGBP2	Lentiviral transduction	
pFLAG-CMV2-mGBP2	Transient transfection	
pWPXL-GFP-mGBP2-G	Lentiviral transduction	
pWPXL-GFP-mGBP2-GM	Lentiviral transduction	(Dissertation E. Kravets, 2012)
pWPXL-GFP-mGBP2-GE	Lentiviral transduction	
pWPXL-GFP-mGBP2-ME	Lentiviral transduction	
pWPXL-GFP-mGBP2-E	Lentiviral transduction	

2.7.2. Plasmids produced during the work

Table 2.14 lists all plasmid vectors generated in this work.

Table 2.14: Generated plasmids.

Name	Vector	Insert	Features
pWPXL-mCherry-mGBP2	pWPXL-mCherry-w/o-STOP	mGBP2 ORF	Lentiviral transduction
pWPXL-mCherry-Ckap4	pWPXL-mCherry-w/o-STOP	Ckap4 ORF	Lentiviral transduction
pWPXL-mCherry-Gal9	pWPXL-mCherry-w/o-STOP	Gal9 ORF	Lentiviral transduction
pWPXL-mCherry-ISG15	pWPXL-mCherry-w/o-STOP	ISG15 ORF	Lentiviral transduction
pWPXL-mCherry-Anxa5	pWPXL-mCherry-w/o-STOP	Anxa5 ORF	Lentiviral transduction
pWPXL-mCherry-Anxa6 isoform 1	pWPXL-mCherry-w/o-STOP	Anxa6 ORF	Lentiviral transduction
pWPXL-mCherry- Anxa6 isoform 2	pWPXL-mCherry-w/o-STOP	Anxa6 ORF	Lentiviral transduction
pWPXL-mCherry-COPA	pWPXL-mCherry-w/o-STOP	COPA ORF	Lentiviral transduction
pWPXL-mCherry-DDX5	pWPXL-mCherry-w/o-STOP	DDX5 ORF	Lentiviral transduction
pWPXL-mCherry-DDX6	pWPXL-mCherry-w/o-STOP	DDX6 ORF	Lentiviral transduction
pWPXL-mCherry-DDX21	pWPXL-mCherry-w/o-STOP	DDX21 ORF	Lentiviral transduction
pWPXL-mCherry-Eif3e	pWPXL-mCherry-w/o-STOP	Eif3e ORF	Lentiviral transduction
pWPXL-mCherry-Ifitm3	pWPXL-mCherry-w/o-STOP	Ifitm3 ORF	Lentiviral transduction
pWPXL-mCherry-iNOS	pWPXL-mCherry-w/o-STOP	iNOS ORF	Lentiviral transduction
pWPXL-mCherry-Kpna2	pWPXL-mCherry-w/o-STOP	Kpna2 ORF	Lentiviral transduction
pWPXL-mCherry-Kpnb1	pWPXL-mCherry-w/o-STOP	Kpnb1 ORF	Lentiviral transduction
pWPXL-mCherry-Nampt	pWPXL-mCherry-w/o-STOP	Nampt ORF	Lentiviral transduction
pWPXL-mCherry-Thbs1	pWPXL-mCherry-w/o-STOP	Thbs1 ORF	Lentiviral transduction
pWPXL-mCherry-Tnpo1 isoform 1	pWPXL-mCherry-w/o-STOP	Tnpo1 ORF	Lentiviral transduction
pWPXL-mCherry-Tnpo1 isoform 2	pWPXL-mCherry-w/o-STOP	Tnpo1 ORF	Lentiviral transduction
pWPXL-mut kozak-Cathepsin D-GFP	pWPXL-mut kozak-GFP	Cathepsin D ORF	Lentiviral transduction
pWPXL-mut kozak-Lamp1-GFP isoform 1	pWPXL-mut kozak-GFP	Lamp1 ORF	Lentiviral transduction
pWPXL-mut kozak-Lamp1-GFP isoform 2	pWPXL-mut kozak-GFP	Lamp1 ORF	Lentiviral transduction
pWPXL-mut kozak-Aifm1-GFP	pWPXL-mut kozak-GFP	Aifm1 ORF	Lentiviral transduction

Successful cloning of all constructs was verified by restriction analysis and subsequent sequencing of the insert was performed at GATC or BMFZ.

2.8. Cell biological methods

2.8.1. General cell culture methods

Cell culture work was performed on sterile benches (Laminar AIR Flow) using sterile materials and solutions. In addition, laboratory gloves (latex or nitrile) were consistently worn. Cells were cultured in incubators at 37°C, 10% CO₂ and a fully humidified atmosphere.

2.8.2. Cell line cultivation

MEF, NIH 3T3, and 293FT cells were washed with PBS every 2 days, detached from the cell culture dish using Trypsin/EDTA, and diluted in fresh medium before being plated onto new plates. HS27 cells, used for *Toxoplasma* cultivation, were passaged in T75 flasks (Corning) up to Passage 40. The medium in fully confluent flasks was replaced once a week. Dense T75 flasks were split by washing the cells with PBS, briefly overlaying with Trypsin/EDTA, and incubating them in a CO₂ incubator for 10 minutes. The reaction was then stopped by adding complete medium. Isolated cells were transferred at a 1:6 ratio into T25 flasks.

2.8.3. Cultivation of primary mouse embryonic fibroblasts

Embryonic fibroblasts (EF) were isolated from C57BL/6 embryos at day 14 post-coitum (p.c.). The uteri of donor animals were aseptically removed and placed in a Petri dish containing culture medium. The embryos were carefully dissected from the uteri, and the head and foetal liver were excised. The remaining embryonic tissue was homogenized using a sieve with 100 µm pore size (BD) and cultured in EF medium. Subsequently, the EF cells were seeded into 10 cm culture dishes with an initial density of approximately 5×10^6 cells. Fresh medium was added to the cells every two days to maintain their growth. Once the cells reached confluence, aliquots of EF cells were cryopreserved in liquid nitrogen.

2.8.4. Cell Count Determination

Cell count determination was performed by staining an aliquot of the cell suspension with 0.16% Trypan Blue in a Neubauer counting chamber. Trypan Blue is an acidic azo dye that binds to cellular proteins. It enters the cytosol through damaged cell membranes of dead

cells and stains them deep blue, distinguishing them from live cells. Alternatively, cells were counted using the Cellometer™ Auto T4 (Nexcelom Bioscience, Lawrence, USA), using the appropriate strips.

2.8.5. Freezing and thawing of cells

The cells were expanded to reach higher cell numbers, and before freezing, they were detached using Trypsin/EDTA and the reaction was stopped by adding complete medium. Subsequently, the cell suspension was centrifuged at 1200 rpm for 5 minutes (using a Megafuge) to remove the supernatant. Approximately 5×10^6 to 1×10^7 cells were resuspended in 1 ml of freezing medium (containing a total of 40% FCS or NCS and 10% DMSO), and aliquoted into cryotubes. The cryotubes were incubated at -20°C for 30 minutes and then stored overnight at -80°C , allowing the cells to be preserved for up to 6 weeks. For long-term storage, the cryotubes were transferred to liquid nitrogen. Thawing of the cells was done rapidly at 37°C . The cells were washed once with pre-warmed cell culture medium to remove DMSO, and then seeded in fresh medium.

2.8.6. Transfection using transfection reagents

The transient transfection was performed using jetPRIME® transfection reagents, following the instructions provided by the manufacturers. A total of 2×10^5 cells (NIH 3T3 or MEFs) were seeded in each well of a 6-well plate with 2 ml of medium. After 24 hours, at 60-80% of cell confluence, 3 μg of the expression vector, diluted in jetPRIME® buffer (150 mM NaCl) to a final volume of 200 μl , was prepared, vortexed for 10 seconds, and spun down briefly. Subsequently, 4 μl of jetPRIME® was added to the diluted plasmid DNA, vortexed briefly, and spun down. After incubation for 10 minutes at room temperature, the transfection reagent/DNA mixture was added dropwise to the cells, while gently swirling the plate. The cells underwent a medium change prior to transfection. After 24 hours, the medium was changed, and after an additional 24 hours (48 hours in total), the success of the transfection was assessed by fluorescence microscopy or Western blot analysis (refer to section 2.10.5).

2.8.7. Lentiviral transduction for the production of stable cell lines

Viral gene transfer is an effective method of delivering genetic material to a wide range of target cells. This study used lentiviral vectors that are non-replicative and undergo the lentiviral replication cycle only until integration into the target cell, at which point they become self-inactivating. To produce lentiviral supernatants, three different plasmids were transiently transfected into 293FT cells. One of these plasmids carried the specific gene intended for expression in the target cells. One of these plasmids carried the specific gene intended for expression in the target cells. The pWPXL-GFP-w/o-STOP, pWPXL-mCherry-w/o-STOP plasmids or the pWPI vector, both encoding the gene of interest under the control of an EF1 α promoter, were employed as the initial vectors. These vectors also contained all the necessary *cis*-acting lentiviral sequences essential for transcription, packaging, reverse transcription, and integration processes. The second plasmid used for virus production carried the *gag*, *pol*, and *rev* genes, which are essential for virus packaging. In this study, the second-generation vector psPAX2 was employed, which includes the deletion of additional viral genes like *vpr*, *vif*, *vpu*, or *nef* (Zufferey et al., 1998). The third plasmid carried the genetic information for the G protein of the Vesicular Stomatitis Virus (VSV-G), serving as the envelope protein for pseudotyping the viruses. The transduction efficiency was assessed using fluorescence microscopy or flow cytometry, taking advantage of the green fluorescence emitted by the eGFP protein (referred to as GFP here).

2.8.8. Virus production using the 293FT cell line

The virus production process was conducted using the 293FT cell line, which is well-known for its ability to generate high-titre lentiviruses. This cell line, derived from a human embryonic kidney and transformed with the large SV40 T-antigen, exhibits rapid growth and high transfection rates. Prior to the transfection step, approximately 5×10^6 293FT cells were seeded in a 10 cm cell culture dish containing DMEM medium (refer to section 2.3.1). The transfection mixture consisted of 20 μ g of the expression vector, 15 μ g of the packaging vector psPAX2, and 5 μ g of the envelope protein vector pLP/VSVG. This mixture was prepared by combining the specified amounts and bringing the total volume to 250 μ l using a 2.5 mM HEPES solution. Following the addition of 250 μ l of 0.5 M CaCl₂, the solution was pipetted dropwise into sterile tubes containing 500 μ l of 2x HEBS solution, and the resulting mixture was incubated at room temperature for 35-40 minutes. This allowed the formation of a fine precipitate composed of calcium phosphate and DNA. Meanwhile, a

medium change was performed on the 293FT cells by replacing the culture medium with 10 mL of serum-free medium. Subsequently, the transfection mixture was added to the cells while gently swirling, and the cells were incubated in a temperature-controlled environment at 37°C for 6 hours. Afterwards, the medium containing the DNA precipitate was aspirated, and 6 ml of culture medium containing serum was introduced to the 293FT cells. After a 48-hour incubation period, the virus supernatant was collected. The medium was retrieved from the culture plates and subjected to centrifugation at 2000 rpm for 10 minutes to eliminate any cellular debris. Subsequently, the virus-containing supernatant underwent filtration using a 0.45 µm cell strainer, followed by aliquoting into cryotubes and rapid freezing using liquid nitrogen. The cryotubes were then stored at -80°C for long-term preservation until further utilization.

2.8.9. Lentiviral transduction of target cells (NIH 3T3, MEF)

One day prior to transduction, 3×10^4 MEF or 5×10^4 NIH 3T3 fibroblasts were seeded onto 24-well plates. On the day of transduction, the DMEM medium was removed from the cells, and a mixture of 500 µl virus supernatant and 25 µg Polybrene was added to the cells. The cells were incubated for 30 minutes in a CO₂ incubator at 37°C. Subsequently, the plate was wrapped with Parafilm for sterility and centrifuged at 1200 rpm and 32°C for 2 hours. The Parafilm was then removed, and the cells were incubated with the virus supernatant for an additional 4 hours in the CO₂ incubator. After a medium change (DMEM), the cells were cultured overnight at 37°C. Transduced cells were transferred to larger culture plates every 2 days until reaching a 10 cm culture dish. The success of transduction was assessed using fluorescence microscopy and flow cytometry. After 7-14 days, GFP-positive cells were enriched through flow cytometric sorting (Dr. Daniel Degrandi, Medical Microbiology, Heinrich Heine University, Düsseldorf).

2.8.10. Stimulation of cells

The stimulation of various primary cells and cell lines was performed using the culture media specified in section 2.3.3, with the cells reaching approximately 75% confluence at the time of harvest. For induction, the cells were treated with 100-200 U/ml of murine IFN-γ (R&D) for 16-24 hours. Cell stimulation was achieved by directly adding the appropriate amount of the substance to the culture medium.

2.8.11. Immunofluorescence staining

For intracellular staining, the method of immunofluorescence was applied. Cells were seeded on sterile 13 mm glass coverslips in DMEM medium in 24-well plates the day before staining. On the day of staining, the medium was removed from both non-infected and *T. gondii*-infected cells under the sterile hood. The cells were first washed in PBS for 5 minutes with gentle agitation, then fixed in 4% paraformaldehyde (PFA) in the dark on a shaker at room temperature (RT) for 15 minutes. After another 5-minute wash with PBS, the cells were permeabilized in 0.02% saponin/PBS in the dark at RT for 15 minutes. For permeabilization of the nuclear membrane, 0.05% saponin/PBS was used. Subsequently, the cells were blocked in 0.002% saponin/PBS + 2% goat serum in the dark at RT for 20 minutes. The primary antibody was diluted in 0.0002% saponin/PBS + 0.2% goat serum and incubated in the dark for 1 hour at RT or overnight at 4°C. After three 5-minute washes with 0.0002% saponin/PBS, the cells were incubated with a secondary antibody diluted in 0.0002% saponin/PBS + 0.2% goat serum in the dark at RT for 45 minutes. Following two washes, the cell nuclei were stained with DAPI solution (diluted 1:2500 in PBS) for 3 minutes at RT, followed by a 5-minute wash with PBS. The glass coverslips with the cells were mounted on glass slides using Fluoromount-G and stored at 4°C.

2.8.12. SNAP-tag protein labelling in living cells

The SNAP-tag protein labelling system enables the specific, covalent attachment of virtually any molecule to a protein of interest. The SNAP-tag is based on human O⁶-alkylguanine-DNA-alkyltransferase (hAGT). SNAP-tag substrates are fluorophores, biotin or beads conjugated to guanine or chloropyrimidine leaving groups via a benzyl linker. In the labelling reaction, the substituted benzyl group of the substrate is covalently attached to the SNAP-tag. The system was applied to label the mCherry fusion protein with the SNAP-tag SNAP-Cell 647-SiR substrate, a far-red fluorescent substrate that can be used to label SNAP-tag fusion proteins inside living cells. The cellular labelling was adopted from NEB protocol. One vial of SNAP-tag substrate (30 nmol) was dissolved in 50 µl of DMSO to give a solution of 0.6 mM SNAP-tag substrate in DMSO and vortexed for 10 minutes until complete SNAP-tag substrate dissolution. This stock solution was stored in the dark at 4°C, or for extended storage at -20°C. The labelling stock solution was diluted 1:200 in complete BSA containing culture medium by thorough mixing (necessary for reducing backgrounds) to yield a labelling medium of 3 µM dye substrate. MEFs expressing GFP-

mGBP2 with one of the mCherry fusion constructs as a SNAP-tag fusion protein, were cultured in live cell imaging dishes. The medium on the cells was replaced with the SNAP-tag labelling medium and incubated at 37°C, 5% CO₂ for 30 minutes. Subsequently, the cells were washed three times with tissue culture medium with serum and incubated in fresh medium for 30 minutes. The medium was replaced one more time to remove unreacted SNAP-tag substrate that has diffused out of the cells. SNAP-tag fusion proteins labelled with SNAP-Cell 647-SiR should have an excitation maximum at 645 nm and an emission maximum at 661 nm. It is recommended to analyse the cells under the microscope immediately after the labelling reaction or, if the application allows it, fixing the cells directly after labelling. After labelling the SNAP-tag fusion proteins, the cells can be fixed and permeabilized with standard fixation methods such as para-formaldehyde, ethanol, methanol, methanol/acetone etc., without loss of signal. For a co-staining with an α -SAGI antibody in *T. gondii* infected cell, SNAP-SiR labelled cells were permeabilized, fixed and stained as described in section 2.8.9.

2.8.13. Gated Stimulated Emission Depletion (STED) measurement

The main experimental procedure was executed according to the immunofluorescence staining protocol (refer to section 2.8.9) Briefly, MEFs were seeded and incubated on glass slides, stimulated with IFN- γ for 16 h and subsequently infected with *T. gondii* ME49 for 2 h. After fixation, infected cells were treated with an α -RFP V_HH nanobody conjugated to eGFPBoosterAtto647N and with an α -GFP V_HH nanobody conjugated to eGFPBoosterAtto488 for enhancement of the immunofluorescence of mCherry and GFP, respectively. Finally, glass slides were analysed by STED microscopy (Dr. Sebastain Hänsch, Centre of Advanced Imaging, Heinrich Heine University Düsseldorf). For the live cell STED analysis, SNAP-Cell® 647-SiR, was used to label SNAP-tag® fusion proteins inside living cells (refer to section 2.8.10). It has an excitation maximum at 645 nm and an emission maximum at 661 nm. STED measurements were performed using a TCS SP8 STED 3X (Leica, Wetzlar,) equipped with an HC PL APO CS2 93x glycerol objective (Leica, Wetzlar, NA 1.3) at a scan speed of 1400 Hz. For the acquisition of the gated STED signal of the eGFPBoosterAtto488, 488 nm was used as the excitation laser line, 592 nm as the corresponding depletion laser line and the hybrid detector range was set from 498 nm to 580 nm with a 1 ns to 6 ns time gating. For the acquisition of the gated STED signal of the mRFPBoosterAtto647N, 633 nm was used as the excitation laser line, 755 nm as the corresponding pulsed depletion laser line and the hybrid detector range was set from 640

nm to 750 nm with a 0.8 ns to 6 ns time gating. Detection of the different signals was carried out in a frame sequential measurement setup. Deconvolved data of gated STED measurements were calculated using Huygens software (Huygens professional, Scientific Volume Imaging, Netherlands) with reduced signal to noise factor of 5 for eGFPBoosterAtto488 and 6 for mRFPBoosterAtto647N and a reduced iteration setting of 20 for both channels. Resulting deconvolved images were visually compared to the raw data to ensure the quality of the calculation. To correct for channel shift, a reference double staining of nuclear pores was acquired with similar settings and utilized as a reference for channel shift correction by the Fiji-plugin “multistackreg” (Thevenaz et al., 1998).

2.8.14. Cultivation of *Toxoplasma gondii*

To propagate the avirulent Type II ME49 strain of *T. gondii*, the parasites were cultured in T25 cell culture flasks containing a monolayer of HS27 fibroblasts in IMDM medium. After the parasites had multiplied, the supernatant was collected and centrifuged at $50 \times g$ (600 rpm) and 32°C for 5 minutes, and the supernatant was collected. The remaining supernatant was further centrifuged at $600 \times g$ (1800 rpm) for 15 minutes at 32°C to pellet the parasites. The pellet was then resuspended in fresh IMDM cell medium. For subsequent passages, $0.5-1 \times 10^6$ parasites were added to a T25 cell culture flask containing HS27 fibroblasts.

2.8.15. *In vitro* infection with *Toxoplasma gondii*

3×10^4 cells expressing fusion constructs or empty vector, or remaining untreated, were seeded on glass coverslips in 24-well plates and incubated overnight in a cell culture incubator. After 8 hours, the cells were stimulated with IFN- γ (200 U/mL) or left untreated. After an additional 16 hours, the cells were infected with *T. gondii* (strain ME49) at a ratio of 1:50 (cells:parasites) for various time periods ranging from 0 to 48 hours. Subsequently, the cells were washed twice with PBS, fixed with 4% PFA/PBS solution in the dark for 15 minutes, and washed twice with PBS. If described, the GTPases and intracellular parasites were stained using immunofluorescence techniques (refer to section 2.8.11).

2.8.16. Determination of recruitment rates of fusion constructs to the PV and the formation of *T. gondii* rosettes

3 x 10⁴ NIH 3T3 fibroblasts or MEF cells expressing different fusion constructs, were plated as described in section 2.8.11. They were stimulated with IFN- γ and infected with *T. gondii* for various time periods ranging from 0 to 48 hours. Subsequently, the cells were fixed, and the proteins and intracellular parasites were stained using immunofluorescence techniques (refer to section 2.8.11). Approximately 500-600 intracellular *Toxoplasma* parasites were counted to determine either the recruitment rates of proteins to the parasitophorous vacuole (PV) or the formation of *T. gondii* rosettes. The rates or counts represented either the ratio of parasites associated with the protein of interest to protein-free *Toxoplasma* parasites, or the number of rosettes versus individual parasites in each cell line.

2.9. Molecular biological working methods

2.9.1. Analytical plasmid preparation from bacteria

For analytical plasmid preparation, a single freshly picked *E. coli* colony was incubated in 2 ml antibiotic-containing LB medium in sterile culture tubes overnight at 37°C with shaking at 200 rpm. Plasmid preparation from the overnight culture was performed according to the manufacturer's instructions (Zymo Research, Mini Kit protocol or Roche, Plasmid Isolation protocol). Positive clones containing the desired plasmid DNA were identified by restriction analysis and separation of restriction fragments on an analytical agarose gel, followed by sequencing (performed by GATC or BMFZ). Overnight cultures carrying plasmid DNA with the correct sequence were expanded into 200 ml cultures, and the plasmid DNA was extracted from them (refer to section 2.9.2). Alternatively, the plasmid DNA was amplified by retransformation in *E. coli* (refer to section 2.9.9).

2.9.2. Preparative plasmid isolation from bacteria

For preparative plasmid isolation, a single freshly picked bacterial colony was incubated in 2 ml antibiotic-containing LB medium in sterile culture tubes, shaking at 200 rpm, for approximately 8 hours. The pre-culture was then diluted 1/1000 in 200 ml antibiotic-containing growth medium and incubated overnight at 37°C with shaking. Plasmid preparation from the overnight culture was performed according to the manufacturer's

instructions (Macherey and Nagel, Maxi Kit protocol). The DNA concentration was determined by measuring the absorbance at 260 nm (NanoDrop, Thermo Scientific). The purity of the DNA solution was assessed by calculating the ratio of absorbance at 260 nm and 280 nm, and the presence of plasmid DNA was confirmed through restriction analysis. The plasmid DNA was stored at -20°C.

2.9.3. Genomic DNA extraction from eukaryotic cells

To confirm the successful gene knockout using CRISPR/Cas9, genomic DNA was extracted from potentially mutated NIH 3T3 clonal cell lines. Cell pellets containing 1×10^6 cells from various cell clones were obtained by centrifugation at $1000 \times g$ for 1 minute and resuspended in 100 μ l of cold PBS on ice by gentle pipetting in a 1.5 ml tube. To ensure efficient dispersion of enzymes, 1 μ l of Proteinase K and 3 μ l of RNase A were added to the resuspended pellet and briefly vortexed. Subsequently, 100 μ l of cell lysis buffer was added, and the mixture was vortexed thoroughly. The solution quickly became viscous. The samples were then incubated for 5 minutes at 56°C with agitation at full speed (~ 1400 rpm) using a thermal mixer. To remove debris, samples were centrifuged at $12,000 \times g$ for 10 minutes at 4°C and the supernatants were transferred to new 1.5 mL tubes. DNA precipitation was achieved by adding 100 μ l of cold 100% ethanol (stored at -20°C) to the tube, which was then inverted 5-8 times and left at room temperature for 1-3 minutes. Subsequently, the tubes were centrifuged at $4,000 \times g$ for 2 minutes at 4°C to pellet the DNA. The supernatant was carefully decanted, and the DNA pellet was washed twice by adding 1 ml of cold 75% ethanol (stored at -20°C), inverting the tubes 3-6 times. After allowing the DNA to settle for 1 minute, the tubes were centrifuged at $4,000 \times g$ for 2 minutes at 4°C to pellet the DNA and remove the ethanol. Finally, the pellets were air-dried for 10-15 minutes, and the DNA pellet was dissolved in 20 μ l of sterile water.

2.9.4. RNA extraction from eukaryotic cells

To clone the cDNA of proteins proposed as interaction partners of mGBP2, the first step involved isolating the corresponding mRNAs from WT MEFs and performing reverse transcription. For mRNA extraction, a total of 1×10^7 WT MEFs were harvested (refer to section 2.8.2) and lysed using 1 ml of TRIzol® (Invitrogen). The sample was then left at room temperature for 5 minutes to facilitate dissociation of nucleoprotein complexes. Next, 0.2 mL of Chloroform (49:1) was added per 1 mL of TRIzol® used, and the mixture was

vigorously shaken by hand for 3 minutes. After incubating the sample on ice for 2-3 minutes, it was centrifuged at $12,000 \times g$ for 15 minutes at 4°C to separate the RNA from the rest of the cell lysate. This centrifugation step resulted in the formation of three distinct layers: a red-pink organic layer at the bottom (using TRIzol[®]), an interphase layer, and a top aqueous layer. The top aqueous phase containing the RNA was carefully transferred to a new RNase-free tube using a pipettor. To precipitate the RNA, the extracted aqueous layer was incubated with 0.5 ml of isopropanol at room temperature for 10 minutes. Subsequently, the sample was centrifuged at $10,000 \times g$ for 10 minutes at 4°C , and the supernatant was discarded. A gel-like white pellet of total RNA should be visible at the bottom of the tube. The RNA was then washed by resuspending the pellet in 0.5-1 ml of 75% Ethanol (in DEPC-H₂O) and briefly vortexed. After centrifuging the sample at $10,000 \times g$ for 5 minutes at 4°C , the supernatant was removed. The pellet was air-dried for 5-10 minutes, and then resuspended in 0.1 ml RNase-free water (in DEPC-H₂O) as soon as the entire tube was dry. The RNA was dissolved at 56°C for 10 minutes. The amount of RNA was determined using a NanoDrop spectrophotometer at 260 nm. If the RNA was not immediately used for reverse transcription, it was stored at -80°C to prevent degradation. It is important to avoid subjecting the RNA sample to multiple freeze-thaw cycles. 2-3 μg were applied for cDNA synthesis.

2.9.5. Reverse transcription of mRNA

To generate cDNA for further cloning experiments of genes potentially interacting with mGBP2, the mRNA obtained from WT MEFs was reverse transcribed using the SuperScript[™] III Reverse Transcriptase kit from Invitrogen. The components were combined according to Table 2.15.

Table 2.15: Reverse Transcription RNA/primer mixture.

Component	Volume
up to 5 μg total RNA	x μl
Oligo(dT) ₂₀ Primer, 50 μM	1 μl
dNTP mix, 10 mM	1 μl
DEPC-treated H ₂ O	to 10 μl

The sample was incubated at 65°C for 5 min, followed by cooling on ice for at least 1 minute. Then, 10 μl of cDNA Synthesis Mix (Table 2.16) was added to the RNA/primer mixture, gently mixed, and briefly centrifuged to collect the contents.

Table 2.16: Reverse Transcription (RT) cDNA Synthesis Mix

Component	Volume
10X RT buffer	2 μ l
25 mM MgCl ₂	4 μ l
0.1 M DTT	2 μ l
RNaseOUT™	1 μ l
SuperScript™ III RT (200 U/ μ l)	1 μ l

The sample was incubated for 50 minutes at 50°C to allow reverse transcription to occur. The reaction was terminated by heating at 85°C for 5 minutes, and the tube was cooled on ice. After a brief centrifugation to collect the reaction, 1 μ l of RNase H was added to the tube and incubated for 20 minutes at 37°C. The cDNA synthesis reaction could be stored at -20°C or used for PCR immediately.

2.9.6. Agarose gel electrophoresis

Analytical agarose gel electrophoresis

Agarose gel electrophoresis is a commonly used method for separating DNA fragments based on their size. Nucleic acids are negatively charged over a wide pH range and migrate towards the anode in an electric field. In the agarose gel, the fragments separate according to their size, with the migration speed being inversely proportional to the logarithm (\log_{10}) of the fragment size in base pairs (bp). By incorporating ethidium bromide into the gel mixture, which intercalates into the DNA double helix, the bands fluoresce under UV light (254-366 nm) when the dye is excited by UV radiation. It emits light in the orange-red range (590 nm), allowing the banding pattern to be visualized and analysed photographically. Agarose gel electrophoresis was performed by boiling 1-1.5% (w/v) agarose in TAE buffer until a clear, homogeneous solution was obtained. After cooling the solution to a hand-warm temperature, ethidium bromide (4 μ g/ml) was added. The solution was poured into a gel chamber with the desired combs, and left to solidify into a gel matrix. Subsequently, the gel chamber with the hardened gel was placed into an electrophoresis apparatus and covered with TAE buffer. The DNA samples, mixed with loading buffer at a 1:5 ratio, were pipetted into the wells of the gel, and electrophoresis was conducted at 80-100 V, depending on the gel size. For analytical purposes, the gel was exposed to UV light at 265 nm, and the banding pattern was documented based on ethidium bromide fluorescence.

Preparative agarose gel electrophoresis and gel extraction

Agarose gel electrophoresis has been utilized not only for DNA analysis but also for the selective elution of PCR products and plasmids, including after restriction enzyme digestion. Following agarose gel electrophoresis (as described above), desired DNA fragments could be identified based on their size-specific separation within the gel under long-wavelength UV illumination (325 nm). These fragments were then excised from the gel for further processing. The DNA was extracted from the isolated gel slice using either the "High Pure PCR Product Purification Kit" from Roche or the PCR Gel Extraction Kit from Zymo Research. The extraction procedure followed the instructions provided by the respective kit manufacturer.

Determination of DNA fragment sizes

To estimate the size of DNA molecules and, if necessary, their concentration, an internal standard was included in the gel. In this study, the "MassRuler™ DNA Ladder Mix" from MBI Fermentas was used as the size standard. This ladder mix provided known DNA fragments of different sizes, allowing for the comparison and determination of the sizes of other DNA molecules present in the gel.

2.9.7. Enzymatic treatment of DNA

Restriction analysis of DNA

Type II restriction endonucleases recognize specific palindromic recognition sequences of four to eight base pairs in double-stranded DNA. They catalyse the hydrolysis of phosphodiester bonds in both strands, resulting in DNA molecules with defined ends that are suitable for cloning purposes. The fragments obtained from restriction digestion were also used as probes to identify specific sequences through hybridization. For a complete enzymatic reaction, 2-5 units of restriction enzyme per μg of plasmid DNA and up to 10 units of enzyme per μg of genomic DNA were used. Restriction enzymes from MBI Fermentas, NEB, and Roche were employed. The general approach for restriction digestion is listed in Table 2.17.

Table 2.17: Restriction digestion.

Composition	Volume
DNA	x μl
Buffer (10x)	3 μl
Enzyme	2-5 Units/ μg DNA
ddH ₂ O	ad 30 μl

The amount of enzyme used should not exceed 10% of the reaction volume, as the presence of a high proportion of the enzyme preservative glycerol can interfere with the reaction. For certain reaction setups, it is recommended to add bovine serum albumin (BSA) from the respective manufacturer's kit (20 µg/ml final concentration for enzymes from MBI Fermentas and 100 µg/ml for enzymes from NEB). BSA coats the reaction vessel, allowing the restriction enzyme to remain freely in solution and thereby remain active. The restriction reactions were incubated for 1-2 hours at the optimal temperature for each enzyme activity and analysed by gel electrophoresis (refer to section 2.9.6).

Dephosphorylation of DNA

The alkaline phosphatase is used to dephosphorylate the 5'-ends of a vector, preventing self-ligation of the vector with compatible ends and promoting the desired ligation between the vector and DNA fragment. After the restriction digestion of the plasmid DNA, the restriction enzymes were deactivated at 65°C for 15 minutes and the reactions were cooled on ice for 5 minutes. Subsequently, for dephosphorylation, the reaction mixture was supplemented with two units of alkaline phosphatase (SAP, 2 µL), 4 µL buffer, and 6 µL ddH₂O, followed by incubation at 37°C for 1 hour. The enzyme was then inactivated at 65°C for 10 minutes to prevent any interfering enzyme activity during the subsequent ligation. Alternatively, the cut and dephosphorylated vector was purified through gel electrophoresis and subsequent gel extraction (refer to section 2.9.6).

2.9.8. Ligation of DNA molecules

DNA Ligation Kit <Mighty Mix> by TAKARA BIO INC

The DNA ligase from bacteriophage T4 catalyses the formation of phosphodiester bonds between a 5'-phosphate and a 3'-hydroxyl end of linear DNA molecules. The enzyme can join both cohesive and blunt ends. Efficient ligation of double-stranded DNA molecules requires an appropriate molar ratio of the DNA fragments to be ligated. This ratio should be approximately 1:3 for vector to DNA fragment. The kit provides a ready-to-use reaction mixture containing T4 DNA ligase. For this, vector and DNA insert were mixed in a molar ratio of 1:3 in a volume of 5 µl, and 5 µl of ligase mix was added. Negative controls included reactions with ddH₂O instead of insert DNA, with and without ligase mix. The mixture was incubated for 30 minutes to 1 hour at 16°C.

TOPO TA Cloning® Kit

The TOPO TA Cloning® strategy provides a streamlined approach for cloning by directly inserting *Taq* polymerase-amplified PCR products (refer to section 2.9.11) into a linearized pCR 2.1-TOPO TA plasmid vector exploiting the ability of thermostable DNA polymerases to add a deoxyadenosine to the 3'-end of double-stranded DNA molecules. This vector has compatible deoxythymidine overhangs at the 3'-end. The topoisomerase I enzyme, covalently bound to the TOPO vector (from VSV), binds to the DNA double-strand at a specific sequence (5'-CCCTT) and cleaves the phosphodiester bond of one strand (Shuman, 1991). The energy generated from this reaction is used to create a covalent bond between the 3' phosphate of the cleaved strand and Tyr274 of the enzyme. Subsequently, the 5' hydroxyl end of the PCR fragment can attack this bond, releasing topoisomerase I and completing the ligation process (Shuman, 1994). A volume of 0.5-4 µl of freshly purified PCR product was utilized. To this, 1 µl of salt solution and 1 µl of pCR 2.1-TOPO vector were added, and the total volume was adjusted to 6 µl with ddH₂O. The ligation was carried out for 5 minutes at room temperature, after which 2 µl of the reaction mixture were directly transformed into chemically competent *E. coli* (refer to section 2.9.9).

2.9.9. Transformation of *E. coli* bacteria

Bacteria treated with CaCl₂ can be transformed with plasmid DNA through a brief heat shock (Cohen et al., 1972). The bacterial strains DH5α-T1R (Hanahan and Meselson, 1983) (Hanahan and Meselson, 1983) or TOP10 (Invitrogen) were used for this purpose. 100 µl of competent bacteria (stored at -80°C) were briefly thawed on ice, and the ligation mixture or approximately 100 ng of circular double-stranded DNA was pipetted into the bacteria. Subsequently, the mixture was incubated on ice for 10-30 minutes to ensure even distribution of the DNA. Heat shock was performed at 42°C for one minute. After adding 500 µl of antibiotic-free LB medium, the mixture was incubated at 37°C, 750 rpm, for 1 hour in a shaker to allow expression of the plasmid-encoded antibiotic resistance. The entire mixture was plated onto agar plates containing the appropriate antibiotics and incubated overnight at 37°C. Positive clones were then verified through plasmid isolation (refer to section 2.9.6) and restriction analysis (refer to section 2.9.7)

2.9.10. Cryopreservation of bacteria

For long-term storage of various bacterial strains, glycerol stock cultures were prepared. For this purpose, 500 µl of a bacterial culture in the exponential growth phase were mixed with 500 µl of sterile glycerol (98%) and the solution was gently homogenized. Subsequently, after a brief cold shock in liquid nitrogen, the bacteria were stored at -80°C.

2.9.11. Amplification of DNA molecules by PCR

The polymerase chain reaction (PCR) is used for the selective amplification of specific nucleic acid sequences and is based on the property of DNA polymerases to utilize single-stranded DNA as a template for the synthesis of a complementary strand (Mullis and Brickell, 1992). PCR relies on cyclical temperature changes. After heat denaturation of the double-stranded DNA, specific oligonucleotide primers hybridize to the 5' and 3' flanking sequences of the target DNA fragment through cooling. By heating to 72°C, the thermostable polymerase can then synthesize the complementary strand. A cyclic repetition of heat denaturation, primer hybridization, and extension of the DNA strand over 30-35 cycles leads to an exponential enrichment of the desired DNA fragment. In this study, a DNA polymerase mixture called "High Fidelity" (Roche) (*Taq* and *Tgo*) was chosen for performing PCR. This mixture exhibits high productivity and a low error rate due to the proofreading activity (3'→5' exonuclease activity) of the *Tgo* polymerase. Table 2.18 presents a standard PCR protocol.

Table 2.18: Standard PCR set-up.

Reagent	Volume
DNA	ca. 250 ng
10 x PCR buffer	5 µl
dNTP-mixture (contains 1 mM of each dNTP)	1 µl
Primer fwd (20 pmol)	1 µl
Primer rev (20 pmol)	1 µl
DNA polymerase (2 U/µl)	0,5 µl
ddH ₂ O	ad 50 µl

All PCR reactions were initiated on ice, briefly mixed by flicking, and centrifuged. Table 2.19 presents the conditions under which the PCRs were performed. The temperature for primer hybridization depends on the sequence, and the extension time for each PCR varies based on the size of the PCR product being amplified. Typically, approximately one minute per 1000 amplified base pairs is required.

Table 2.19: Programming under standard PCR conditions.

Function	Time	Temperature		Number of cycles
DNA denaturation	2 min	94°C		
DNA denaturation	30 sec	94°C	}	10 x
Primer hybridisation	30 sec	55-68°C		
Primer extension	variable	72°C		
DNA denaturation	30 sec	94°C	}	20 x
Primer hybridisation	30 sec	55-68°C		
Primer extension	variable + $\sum 20$ s	72°C		
Pause	infinite	4°C		

To generate the deletion mutant mGBP2-GE, two PCRs were initially conducted to produce DNA sequences with long overhangs. The "Expand Long Template PCR System" from Roche was utilized for this purpose. Following purification of the PCR products, 1 μ l of the amplified product from one domain was diluted in 100 μ l of ddH₂O. The mixture was heated to 60°C to denature the double strand, and then 1 μ l of the amplified product from the other domain was added. The mixture was then cooled to room temperature. For the subsequent PCR, 10 μ l of the prepared mixture was used.

2.9.12. CRISPR/Cas9 knockout strategy

CRISPR/Cas9 is a revolutionary gene editing technology that enables precise modifications to be made in the genomic DNA of eukaryotic cells through targeted and specific alterations, utilizing the RNA-guided Cas9 nuclease from the microbial clustered regularly interspaced short palindromic repeats (CRISPR) adaptive immune system (Ran et al., 2013). The Type II CRISPR system comprises the Cas9 nuclease, a crRNA array encoding the guide RNAs, and an essential auxiliary trans-activating crRNA (tracrRNA) that aids in the processing of the crRNA array into individual units (Garneau et al., 2010). Furthermore, the crRNA and tracrRNA can be fused together to create a chimeric, single-guide RNA (sgRNA). The RNA-guided nuclease function of CRISPR/Cas9 is reconstituted in mammalian cells through the heterologous expression of human codon-optimized Cas9 and the requisite RNA components (Cho et al., 2013). Efficient genome engineering is achieved by simply specifying a 20-nt targeting sequence within its guide RNA. The guide sequence pairs with the DNA target, directly upstream of a requisite 5'-NGG adjacent motif (PAM). Cas9 nuclease mediates a double strand break (DSB) -3 bp upstream of the PAM. Here, the Cas9-mediated genome editing was provided via nonhomologous end joining (NHEJ) DNA DSB damage repair, which leaves scars in the form of insertion/deletion (indel) mutations and

can be harnessed to mediate gene knockouts, as indels occurring within a coding exon can lead to frameshift mutations and premature stop codons (Perez et al., 2008). Subsequently, the modified cell lines were utilized for downstream functional studies (Fig. 2.1, Ran et al., 2013).

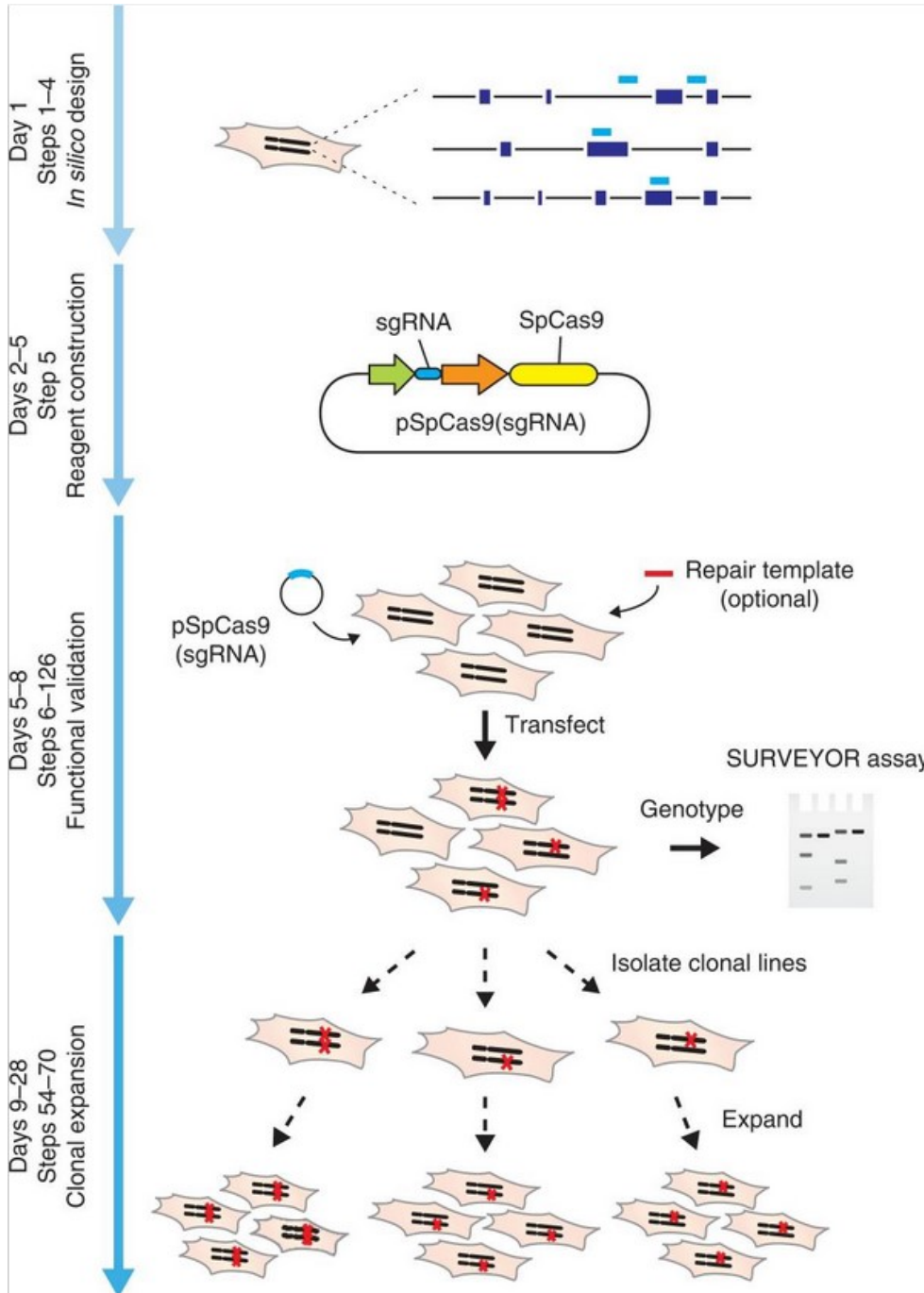


Figure 2.1: Timeline and overview of the CRISPR/Cas9 experimental strategy.

The experimental timeline and overview are presented, outlining the steps involved in reagent design, construction, validation, and cell line expansion. *In silico* design of custom sgRNAs (light blue bars) and genotyping primers is conducted using the CRISPR Design Tool (<http://tools.genome-engineering.org>). The sgRNA guide sequences are subsequently cloned into an expression plasmid containing both the sgRNA scaffold backbone (BB) and Cas9, known as pSpCas9(BB). This resulting plasmid is denoted as pSpCas9(sgRNA). Verified pSpCas9(sgRNA) plasmids, along with optional repair templates to facilitate the high-fidelity HDR, are then transfected into cells to assess their ability to induce targeted cleavage. Finally,

transfected cells can undergo clonal expansion to generate isogenic cell lines with predetermined mutations. According to (Ran et al., 2013).

The Galectin 9 gene (lectin, galactose binding, soluble 9, Lgls9) as well the Ckap4 gene (P63; CLIMP-63; 778 5630400A09Rik) were disrupted by applying the CRISPR/Cas9 technology in NIH 3T3 fibroblasts. The knockout was performed by transfection of the pSpCas9(BB)-2A-GFP (PX458) plasmid (Addgene, USA), expressing a sgRNA (Gal9: fwd CAC CGC GGG TTA ATG TAT GGA GAC T, rev AAA CAG TCT CCA TAC ATT AAC CCG C, Ckap4: fwd CAC CGA TCC GCG CCG CCC GAC GGG T, rev AAA CAC CCG TCG GGC GGC GCG GAT C) corresponding to the sequence contained in the first exon of either Gal9 or Ckap4 gene (Fig. 2.2).

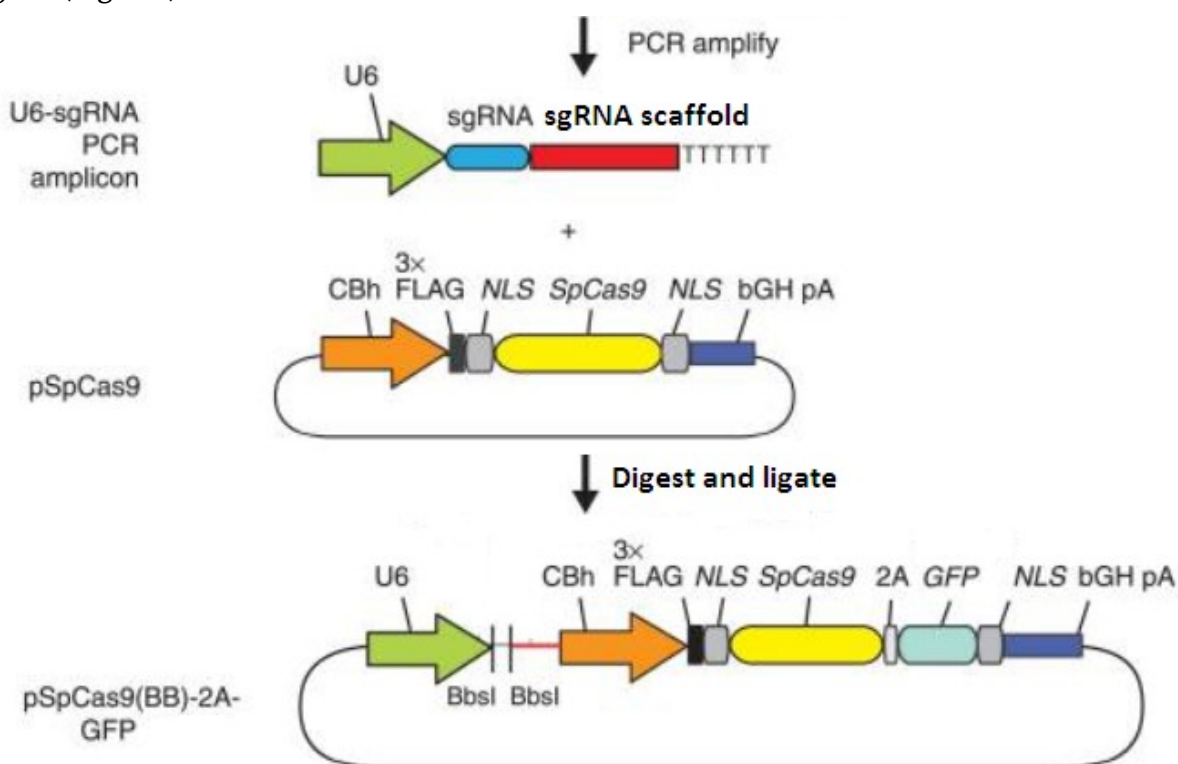


Figure 2.2: Target selection and plasmid preparation.

To facilitate the generation of a U6-driven sgRNA expression plasmid, a PCR amplification approach was employed. A PCR template containing the U6 polymerase III promoter was utilized along with a fixed forward primer (U6-for GAG GGC CTA TTT CCC ATG ATT CC), sgRNA-encoding DNA can be appended onto the U6 reverse primer (U6-rev CCA CAA AGC AGG AAA GGT GTT CG) and synthesized as an extended DNA oligo (Ultrasmer oligos from IDT). The guide oligos were designed with overhangs to enable ligation into a pair of BbsI restriction sites present in pSpCas9(BB). It is important to note that the orientation of the top and bottom strands of the guide oligos matches that of the genomic target, where the top oligo represents the 20-bp sequence preceding the 5'-NGG motif in the genomic DNA. The resulting amplicon could be co-transfected with a Cas9 expression plasmid pSpCas9. Through digestion of pSpCas9(BB) with BbsI, the Type II restriction sites (depicted in blue outline) can be replaced, allowing for the direct insertion of the annealed oligos. Additionally, in our experiments, pSpCas9(BB) contains a GFP marker that aids in the selection of transfected cells. According to (Ran et al., 2013).

The initial step involved the preparation of the appropriate PX458 vectors. The BB plasmids underwent digestion using the BbsI restriction enzyme. Following this, the sgDNA-containing oligos (each at a concentration of 100 μ M) were subjected to phosphorylation using T4 polynucleotide kinase for 30 minutes at 37°C. The enzyme was then inactivated at 95°C for 5 minutes, and the probes were allowed to cool to RT. The phosphorylated oligos were subsequently ligated to pSpCas9(BB) at RT for 1 hour, utilizing overhangs that facilitate ligation by T4 ligase into a pair of BbsI restriction sites present in the BB plasmid. The synthesized vector was transformed into *E. coli* (refer to section 2.9.9). Successful cloning was confirmed through sequencing using the U6_f primer (5'-TGG ACT ATC ATA TGC TTA CCG TAA C-3').

After sequence verification, the sgRNA encoding plasmids were transfected into NIH 3T3 fibroblasts according to jetPRIME® transfection protocol (Polyplus, New York City) (refer to section 2.8.6). The transfection efficacy was analysed by fluorescence microscopy and flow cytometry (FACS). Subsequently, GFP positive cells were sorted (executed by Dr. Daniel Degrandi, Medical Microbiology, Heinrich-Heine University, Düsseldorf) and single cell colonies, achieved by serial dilution, were cultivated. Mutated clones of the Gal9 gene were identified by Surveyor® Mutation Detection (Integrated DNA Technologies, Inc., USA) (Gal9: for AAC TAG ATT GGG CCT GCC TC, rev AGA GAT CCC CCT GAC TCT GT, expected PCR fragment: 923 bp, expected digested fragments: 747, 176 bp, Ckap4: for ATG CCC TCG GCC AAA CAA AG, rev AAA GCT GGA GTA GGC GAC TT, expected PCR fragment: 950 bp, expected digested fragments: 890, 60 bp) (refer to section 2.9.13) The knockout of both genes, respectively, was confirmed by PCR amplification (refer to section 2.9.11), subcloning and sequencing of the corresponding gene stretches from different single cell colonies. Additionally, WB analysis was performed with a polyclonal rabbit anti-mouse antibody against Ckap4 (STJ110088, St John's Laboratory Ltd, UK) and a polyclonal rabbit anti-mouse antibody against Gal9 (ARP54821_P050, Aviva Systems Biology) (refer to 2.10.5).

2.9.13. The Surveyor Mutation Detection® for CRISPR/Cas9 knockout

The knockout success of the CRISPR/Cas9 system was analysed in various generated NIH 3T3 cell lines compared to wild-type (WT) by utilizing the Surveyor Mutation Detection®

kit. The following components are included in the IDT kit and set up as indicated in Tables 2.20 and 2.21.

Table 2.20: The Surveyor Mutation Detection Kit.

Component
Surveyor Nuclease S
Surveyor Enhancer S
0.15 M MgCl ₂ Solution
Stop Solution
Control C
Control G

The kit should be stored at -20°C in a manual defrost freezer.

Table 2.21: Set up Surveyor Nuclease reactions for Control G and Control C duplexes.

Tube no.	Volume required (μl)					
	Hybridized control G/C	Hybridized control C	0.15 M MgCl ₂	Surveyor Enhancer S	Surveyor Nuclease S	Stop Solution (Add after Incubation)
1		6	0.6	1	1	0.9
2		12	1.2	1	1	1.5
3		18	1.8	1	1	2
4	6		0.6	1	1	0.9
5	12		1.2	1	1	1.5
6	18		1.8	1	1	2

Mutation detection and confirmation with Surveyor Nuclease involves four steps. In the first steps, PCR amplification is performed to generate amplicons from both the mutant (test) and WT (reference) DNA. For this purpose, the following components were added in the order listed in Table 2.22 to each of the two 0.2-ml tubes (keep on ice). One tube was used for test sample DNA and the other for reference DNA.

Table 2.22: PCR products preparation for Surveyor Nuclease assay.

Reagent	Volume/amount
Test sample or reference DNA	10 ng plasmid DNA or 100 ng genomic DNA
10X Polymerase Buffer	5 μl
dNTP-mixture (2.5 mM each)	4 μl (final concentration of each dNTP is 0.2 mM)
sense primer (~120 ng of a 25-mer)	15 pmol
antisense primer	15 pmol
DNA polymerase (2.5 units/ μl)	1 μl
ddH ₂ O	to 50 μl

2 μl of Control G and 2 μl of Control C DNA are amplified in separate 50- μl reactions using a proofreading DNA polymerase and the PCR program described in Table 2.23, where $T_a =$

65°C and the 72°C extension time is appropriate for the polymerase used (e.g., 1 min for Optimase Polymerase).

Table 2.23: PCR program for Surveyor Nuclease assay.

Function	Time	Temperature	Number of cycles
DNA denaturation	2 min	94°C	
DNA denaturation	30 sec	94°C	x 30
Annealing (T _a)	30 sec	65°C	
Extension	30 sec/250 bp	72°C	
Extension	5 min	72°C	
Pause	Hold	4°C	

The annealing temperature (T_a) was determined by calculating the T_m for each primer using the OligoAnalyzer Tool on the IDT webpage: www.idtdna.com/calc/analyzer.

After amplification, a 2-5 µl aliquot of each amplified DNA was analysed against a DNA mass ladder on a 2% (w/v) high resolution agarose and the band intensities were compared, using a UV transilluminator at 250 to 300 nm, with those of the DNA ladder to establish the DNA concentration.

Secondly, the test and reference DNA samples were mixed in equal amounts (15 µl of each if the amplified DNA concentrations are ≥40 ng/µl, ≥200 ng total DNA) in a 0.2 ml tube and subjected to heating and cooling in a thermal cycler and run the program as described in Table 2.24. This step allows for the formation of hetero- and homo-duplexes through hybridization.

Table 2.24: Hybridization of PCR amplified DNA for Surveyor Nuclease assay.

Temperature	Time
95°C	10 min
85°C	1 min
75°C	1 min
65°C	1 min
55°C	1 min
45°C	1 min
35°C	1 min
25°C	1 min
4°C	Hold

The hybridization produces a population of molecules containing 50% homoduplex, 25% heteroduplex with a C/G mismatch, and 25% heteroduplex with a G/C mismatch. Also, 30 µl of Control C homoduplex should be self-annealed in a separate tube.

Subsequently, the mixture containing the annealed hetero- and homo-duplexes was treated with Surveyor Nuclease. For this, 0.5 ml reaction tubes were set on ice with the indicated amounts of PCR product and the amount of Surveyor Nuclease and additional $MgCl_2$ (Table 2.21 and 2.25). A negative control was also prepared by treating the reference DNA alone in a similar manner.

Table 2.25: Set up Surveyor Nuclease reactions for digestion of the hetero/homoduplex and reference DNA.

Component	Amount
Hybridized DNA	200-400 ng in 8-40 μ l
0.15 M $MgCl_2$	1/10th volume
Surveyor Enhancer S	1 μ l
Surveyor Nuclease S	1 μ l

The tubes were incubated at 42°C for 60 min, then 1/10th volume of Stop Solution was added.

Finally, the resulting DNA fragments were analysed using agarose gel electrophoresis (refer to section 2.9.6). The presence of additional bands on the gel indicates the formation of new cleavage products resulting from the presence of one or more mismatches. The size of these cleavage products provides information about the location of the mismatch or mismatches.

2.10. Protein biochemical and biophysical methods

2.10.1. Preparation of total cell extracts from eukaryotic cells

To prepare whole-cell extracts, a range of 1×10^6 to 1×10^7 cells were subjected to trypsinization, followed by washing with PBS. The cells were then resuspended in 100 μ l of cell lysis buffer per 1×10^6 cells and incubated on a rotating wheel at 4°C for 20-30 minutes. The inclusion of the non-ionic detergent NP-40 (IGEPAL CA-630®, Sigma Aldrich) in the buffer facilitated the extraction of soluble nuclear proteins and cytoplasmic proteins from eukaryotic cells. After centrifugation at 13,000 rpm and 4°C for 20 minutes, the supernatant was transferred to a fresh reaction tube, while the remaining cellular debris was discarded. The protein content was determined using the BCA assay (refer to section 2.10.2). The lysates were denatured by adding 5x loading buffer and boiling for 10 minutes at 95°C. Subsequently, the resulting protein lysates could be separated and analysed using SDS-polyacrylamide gel electrophoresis (SDS-PAGE) (refer to section 2.10.3) and Western blotting (refer to section 2.10.5).

2.10.2. Determination of protein concentration using BCA test

The Bicinchoninic acid (BCA) test (Smith et al., 1985) is a colorimetric method used to quantify protein concentrations in unknown samples. It is highly sensitive and resistant to interference from detergents, but can be disrupted by complexing and reducing agents. The test relies on the ability of proteins, specifically the amino acids cysteine, tyrosine, and tryptophan, to reduce Cu^{2+} to Cu^{+} in an alkaline, copper-containing solution (known as the Biuret reaction). The resulting monovalent copper ion forms a coloured complex with two molecules of BCA. By measuring the absorbance at 562 nm, which corresponds to the maximum absorption of the complex, the protein concentration in the samples can be determined using a calibration curve generated with a standard protein (such as BSA). In this study, the BCA test was conducted following the instructions provided by the manufacturer, utilizing the BCA Protein Assay Kits (Pierce). Protein concentrations of 20-40 μg were used for Western blot analyses.

2.10.3. SDS-polyacrylamide gel electrophoresis (SDS-PAGE)

SDS (sodium dodecyl sulphate) is an anionic detergent that strongly binds to hydrophobic regions of proteins (1 g of protein binds to 1.4 g of SDS) and induces their denaturation. This process introduces a highly negative charge, effectively masking all intrinsic charges on the proteins. Consequently, during electrophoresis, the linear protein-SDS complexes migrate exclusively towards the anode, regardless of the protein's amino acid composition or isoelectric point. By utilizing the sieving properties of a polyacrylamide gel, the protein's mobility becomes a linear function of the logarithm of its molecular weight. Thus, the relative molecular weight of a protein can be determined using a protein standard. In this study, protein separation was performed using 4-12% Bis-Tris gradient gels or 10% Bis-Tris gels from Invitrogen. Denatured samples were loaded into the gel pockets and separated at voltages ranging from 100 to 120 V using appropriate running buffers. To determine the relative molecular weight of the proteins, a molecular weight marker (such as PageRuler™ Prestained Protein Ladder from MBI Fermentas or High-Range Rainbow from GE Healthcare) was also applied. Electrophoresis was conducted until the bromophenol blue dye in the sample buffer reached the lower boundary of the gel. The gel pockets were labelled with malachite green dye.

2.10.4. Coomassie blue staining of protein gels

To quickly visualize the proteins separated by SDS-PAGE gel electrophoresis, the Coomassie Blue staining method was utilized. Coomassie R-250 was used as the dye for control gels, whereas Coomassie G-250 was employed for gels prepared for subsequent mass spectrometric analysis. Both dyes interact with the basic and aromatic side chains of amino acids, leading to non-specific staining of all proteins. Coomassie G-250 exhibits higher sensitivity compared to Coomassie R-250.

Conventional Coomassie R-250 staining

During this staining process, the proteins were stained overnight in a solution containing Coomassie R250. The next day, the gels were de-stained for several hours in a de-staining solution, followed by a 5-minute wash in ddH₂O.

Colloidal Coomassie G-250 staining

The gels were initially fixed using a 2% (v/v) phosphoric acid in 50% (v/v) ethanol solution for 30 minutes. Subsequently, the gels were immersed in a staining solution containing aluminium sulphate and Coomassie G-250 for 1 hour. After staining, the gels were washed in ddH₂O.

2.10.5. Western Blot (Immunoblot)

The technique of Western blotting, first introduced in 1979 by (Towbin et al., 1979) and (Renart and Sandoval, 1984), is used to transfer proteins separated in a gel (e.g., SDS-PAGE) onto a solid support, such as a nitrocellulose or polyvinylidene fluoride membrane. This allows for subsequent detection of the immobilized proteins using specific antibodies. Following SDS-PAGE gel electrophoresis (refer to section 2.10.3), the proteins separated on a polyacrylamide gel were transferred onto a nitrocellulose membrane using the Trans-Blot® SD Semi-Dry Transfer Cell apparatus from Bio-Rad. To initiate the transfer process, the gel, membrane, and filter paper (Whatman 1 mm) were briefly equilibrated in transfer buffer containing 20% methanol. Subsequently, the components were layered in a bubble-free manner onto the anode graphite plate moistened with transfer buffer as followed:

1. 3 layers Whatman paper
2. Membrane
3. SDS gel
4. 3 layers Whatman paper

The transfer process took 2 hours at a constant current of 40 mA per gel. Subsequently, the membrane was blocked for 1 hour at RT in either 5% skim milk powder or 5% bovine serum albumin (BSA) with 0.2% NaN₃, both dissolved in TBS-T buffer. This blocking step aimed to prevent non-specific binding of the antibody. The primary antibody was diluted in either a 3% milk powder solution or 5% BSA, according to the manufacturer's instructions, and incubated overnight at 4°C with the membrane, gently shaking in sealed bags or slowly rolling in Falcon tubes. After three 5-minute washes with TBS-T to remove any non-specifically bound primary antibody, the membrane was then incubated with the secondary antibody conjugated to horseradish peroxidase (HRP), also dissolved in 3% skim milk powder-TBS-T, for 1 hour at RT. Following this, the membrane was washed three times for 10 minutes each with TBS-T at RT. The specific binding of the antibody and, consequently, the target protein were detected using an ECL system (GE Healthcare). The membrane was wetted with the detection solution (composed of equal parts of solutions A and B) in the dark, incubated for 3 minutes, and then placed in a plastic film. Chemiluminescence was detected by ECL & Fluorescence Imager (Intas ECL Chemostar, Intas Science Imaging, Göttingen).

2.10.6. Immunoprecipitation

Immunoprecipitation was used to detect protein interactions of mGBP2. For this purpose, either HA-mGBP2 fusion protein expressing mGBP2^{-/-} MEFs versus mGBP2^{-/-} MEFs transduced with the empty expression vector as control, or GFP-mGBP2 versus only GFP-stable expressing mGBP2^{-/-} MEF cells were cultured. Cells were stimulated with 100 U/ml IFN- γ overnight. After 16 hours, 2-3 x 10⁶ cells were left uninfected or were infected with *T. gondii* ME49 for 2 hours. The cells were harvested with trypsin and washed three times with ice cold PBS. Subsequently cells were resuspended and lysed in 0.5 ml IP lysis buffer and rotated on a rotator at 4°C for 30 minutes. Following centrifugation at 13,000 rpm for 20 minutes, the supernatant was transferred to a new tube, and the precipitating antibody (anti-HA or anti-GFP) was added to the sample volume at a dilution of 1:20 and incubated overnight at 4°C on the rotator. In the case of precipitating antibodies, Protein-G-Sepharose (GE Healthcare) was washed four times with lysis buffer at 4,500 rpm on the following day. Then, 60 μ l of Protein-G-Sepharose was added to the lysates and incubated on the rotator at 4°C for 4 hours. For antibodies directly coupled to agarose, the agarose was washed four times with lysis buffer at 4°C and 4,500 rpm. Then, 60 μ l of antibody-coupled agarose was added to the lysates and incubated overnight at 4°C on the rotator. Alternatively, Green

Fluorescent Protein (GFP)-Trap[®] agarose (an affinity resin for IP of GFP-fusion proteins, consisting of a GFP Nanobody/V_HH coupled to agarose beads) or mCherry-Trap[®] agarose was added to the samples and incubated for 4 hours at 4°C on a rotator. Subsequently, the samples were centrifuged at 4,500 rpm and 4°C, the supernatant was removed and stored as a reserve at -20°C. After four washes with lysis buffer at 4°C and 4,500 rpm, the pellet was completely dried and supplemented with 40-60 µl of 5x loading buffer. The samples were boiled for 10 minutes at 95°C, then centrifuged at 13,000 rpm for 2 minutes, and the supernatant was transferred to a fresh tube. 20 µl of each sample was loaded onto an SDS gel (4%-12%) and a Western blot was performed as described in sections 2.10.4 and 2.10.5. The protein of interest was detected by incubating the blot membrane with the appropriate antibody, diluted according to the manufacturer's recommendations, overnight at 4°C. After three 5-minute washes in TBS-T, the nitrocellulose membranes were incubated with the corresponding HRP-conjugated secondary antibodies for 1 hour at room temperature, followed by another wash step (3 times for 10 minutes in TBS-T) and wetting the membranes with the ECL detection solution for three minutes. The signals were detected as described in section 2.10.5.

2.10.7. Silver staining

Silver staining was used for detailed visualisation of the proteins separated by SDS-PAGE gel electrophoresis. The technique is based on the simple principle that selective reduction of silver into metallic silver occurs at the initiation site in the close proximity of protein molecules. Silver staining was modified for 1D SDS-PAGE gels according to (Heukeshoven and Dernick, 1988). The staining process sequentially consists of protein fixation, sensitization, washing, silver impregnation, and finally development of image. Depending upon the amount of silver incorporated into the protein bands, different colour of gel is produced on silver staining. The detailed steps and times are summarized in Table 2.26.

Table 2.26: Set up for silver staining for SDS-PAGE gels.

Dyeing step	Volume per gel	Solution	Treatment time	Comments
Fixation	50 ml	A	15 min – o/n	Light protection
Incubation	50 ml	B	15 min – 2 h	
Soaking	each 50 ml	ddH ₂ O	3× 5-15 min	
Staining	50 ml	C	15 min – 30 min	Incubate up to 2h
Soaking	50 ml	C	few seconds	

Rinsing	50 ml	D	1 min	Shake well to remove any precipitated silver from the gel
Development	50 ml	E	1-7 min	Decide individually
Stop	50 ml	F	minimum 20 min	
Washing	50 ml	ddH ₂ O	minimum 10 min	

From the staining step on, dispose of everything in the canister for Ag waste under the fume cupboard!!!

2.10.8. Silver de-staining

The standard de-staining protocol was used to decolourise silver spots/bands. Solutions 1 and 2 are ready to use in the fridge, they just need to be mixed prior to de-staining. Approximately 15 - 60 μ l of the working solution (a 1:1 mixture of decolorizing solution 1 and solution 2) are applied onto the gel spot, ensuring that the spot is completely covered (for approximately 1 minute). Then, the solution is removed and discarded. Subsequently, a wash with ddH₂O is performed.

2.10.9. Reduction and alkylation of SDS gel bands/spots

Carefully excised bands or spots from de-stained gels are transferred to a digestion tube. The gel pieces are subsequently subjected to alternate incubations in Wash Buffer A and B as specified in Table 2.27. Ensuring complete coverage of the spots with liquid (20-50 μ l) is crucial during this process.

Table 2.27: Washing of SDS gel bands/spots

Reagent	Treatment time
Washing buffer A	3-10 min
Washing buffer B	3-10 min
Washing buffer A	3-10 min
Washing buffer B	3-10 min
Washing buffer A	3-10 min
Washing buffer B	3-10 min
Drying gel pieces in the SpeedVac	

To perform reduction and alkylation, the gel pieces were subjected to an incubation in 50 μ l of 10 mM dithiothreitol (DTT) in 50 mM ammonium bicarbonate (NH₄HCO₃) for 45 minutes at 56°C. After removing any excess solution, 50 μ l of 55 mM iodoacetamide (IAA) in 50 mM NH₄HCO₃ was promptly added. The gel pieces were then incubated for 30 minutes at room temperature in a dark environment. Finally, the IAA solution is carefully

removed. Subsequently, the gel pieces underwent a washing step using the indicated volumes as described in Table 2.28.

2.10.10. In-gel trypsin digestion of reduced and alkylated spots

The working solution is freshly prepared or stored it in the refrigerator; it can be used for approximately 7 days. A 5 μl aliquot of Trypsin solution is diluted with 32.5 μl of NH_4HCO_3 (100 mM, pH 8) to achieve a final Trypsin concentration of 0.033 $\mu\text{g}/\mu\text{l}$. 2 μl of Trypsin or the appropriate amount are applied directly onto the gel piece (with a ratio of 1:50 to 1:100, adjust the volume if needed). Wait for 1 minute until the gel piece becomes transparent and returns to its original size. If it does not, an additional 2 μl of Trypsin (or an appropriate volume) of Solution A should be added. Cover the digestion tube and incubate overnight at 37°C.)

2.10.11. Spots/Band extraction

The extraction solution, comprising a 1:1 ratio of 0.1% TFA and acetonitrile, should be freshly prepared. 10 - 40 μl of the extraction solution are applied onto the spot, covering the spot/band adequately based on its size. The samples are ultrasonicated in an ice bath for 15 minutes and the resulting supernatant is transferred to a labelled HPLC sample vial. The procedure is repeated by adding another 10 - 40 μl of the extraction solution onto the spot and another 15-minute ultrasonication is performed. The obtained supernatant is combined with the previously collected supernatant. Acetonitrile is removed by evaporating the samples using a SpeedVac (Thermo Scientific, Rockford, USA). Finally, the sample vial is filled with 0.1% TFA up to a volume of 17 μl or the desired volume for injection.

2.10.12. Sample Preparation for Proteomic Analysis

MEFs were plated at the amount of 1×10^6 per 75 cm^2 flask, harvested from 6 individual cell culture dishes, prepared, and measured independently ($n = 6$ per group). At a cell density of about 80%, cells were stimulated with 200 U/mL IFN- γ for 16 h prior to infection with 1×10^7 freshly harvested ME49 *T. gondii* for 2 h or left uninfected. Subsequently, cells were washed five times with serum-free medium to reduce the amount of potential contaminating serum proteins and harvested for proteomic analysis (refer to section 2.8.2). This procedure was performed with six biological replicates. The cell viability was

monitored using trypan blue staining and cells analysed by an automated cell counter (Cellometer™ Auto T4, Nexcelom Bioscience, Lawrence, USA) (Grube et al., 2018). After harvesting cells by scraping them in ice cold PBS and buffer removal by centrifugation, lysis buffer and antibody loaded resins were used to extract proteins as described in section 2.10.6. Five µg of protein per sample was loaded onto a 4–12% Bis-Tris SDS-polyacrylamide gel and run for about 10 min for a one-shot analysis (refer to section 2.10.5) whereas 20 µg of protein was separated for about an hour for the analysis of 15 different gel slices per lane. After silver staining (refer to section 2.10.7) protein bands were cut out and processed as described in sections 2.10.9 and 2.10.10. and (Poschmann et al., 2014). Briefly, bands were de-stained and washed, proteins reduced by 10 mM DTT and alkylated with 55 mM iodoacetamide. Subsequently, proteins were digested for 16 h at 37 °C with 0.1 µg of trypsin in 100 mM ammonium hydrogen carbonate in water. Tryptic peptides were extracted twice with a 1:1 (v/v) solution of acetonitrile and 0.1% TFA and, after acetonitrile removal, resuspended in 0.1% (v/v) TFA (executed by Dr. Gereon Poschmann, MPL, Heinrich Heine University, Düsseldorf.)

2.10.13. Liquid Chromatography and Mass spectrometry

A label-free mass spectrometry, based quantification approaches enabled by a highly reproducible and stable Liquid-Chromatography Mass Spectrometry / Mass Spectrometry (LC-MS/MS) system was chosen for a quantitative analysis of the mGBP2 interactome. Six individual replicates of co-immunoprecipitation samples (refer to section 2.10.12) per group (HA-mGFP2, control-vector, HA-mGFP2 + ME49 *T. gondii* and control-vector + ME49 *T. gondii* or GFP-mGFP2, GFP only, GFP-mGFP2 + ME49 *T. gondii* and GFP only + ME49 *T. gondii*) were prepared from transduced IFN-γ stimulated mGBP2^{-/-} MEFs (refer to section 2.8.7). Samples were prepared for mass spectrometric analysis essentially as described in section 2.10.12 (Grube et al., 2018). Briefly, proteins were stacked into an acrylamide gel (about 4 mm running distance), subjected to silver staining, de-stained, reduced and alkylated and digested with trypsin. Resulting peptides were extracted from the gel and approximately 500 ng peptides per sample prepared in 0.1% trifluoroacetic acid.

First, peptide samples were separated on an UltiMate 3000 Rapid Separation Liquid Chromatography system (RSLCnano, Thermo Fisher Scientific, Dreieich, Germany). Peptides were initially trapped on a 2 cm long trap column (Acclaim PepMap100, 3 µm C18 particle size, 100 Å pore size, 75 µm inner diameter, Thermo Fisher Scientific) for 10 min

at a flow rate of 6 $\mu\text{l}/\text{min}$ with 0.1 % (v/v) trifluoroacetic acid (TFA) as mobile phase. Subsequently, they were separated on a 25 cm long analytical column (Acclaim PepMapRSLC, 2 μm C18 particle size, 100 Å pore size, 75 μm inner diameter, Thermo Fisher Scientific) at 60°C using a 2 h gradient from 4 to 40% solvent B (solvent A: 0.1% (v/v) formic acid in water, solvent B: 0.1% (v/v) formic acid, 84% (v/v) acetonitrile in water) at a flow rate of 300 nl/min .

Separated Peptides were injected with distal coated SilicaTip emitters (New Objective, Woburn, MA, USA) into an Orbitrap Elite mass spectrometer (Thermo Fisher Scientific) via a nanosource electrospray interface. The mass spectrometer was operated in positive, data dependent mode with a spray voltage of 1.4 kV and capillary temperature of 275°C. First, a full scan from m/z 350 to 1700 was recorded with a resolution of 60000 (at 400 m/z) in the orbitrap analyser with a target for automatic gain control set to 1,000,000 and a maximal ion time of 200 ms. Then, up to 20 two- and threefold charged precursor ions with a minimal signal of 500 were isolated (isolation width 2) in the linear ion trap part of the instrument. Here, ions were collected for a maximum of 50 ms with an automatic gain control set to 30,000, fragmented by collision induced dissociation with a normalized collision energy of 35 and analysed at a resolution of 5,400 (at 400 m/z). Already fragmented precursors were excluded from fragmentation for the next 45 seconds. Quantitative analysis of MS data was performed with Progenesis QI for proteomics analysis software for your LC-MS (version 2.0, Nonlinear Dynamics, Newcastle upon Tyne, UK) and Perseus software (version 1.6.2.2, MPI for Biochemistry, Planegg, Germany) (refer to section 2.11.3).

2.11. Computer programmes

2.11.1. Cloning strategies

The Vector NTI Advance™ program (Invitrogen) and Geneious bioinformatic software (Dotmatics) were used to develop strategies for cloning expression and recombination vectors.

2.11.2. Sequence alignment

Sequence alignments were carried out using SeqMen (DNASar), Vector NTI Advance™ (Invitrogen), Geneious (Dotmatics) or ClustalW software.

2.11.3. Quantitative analysis of MS data

Quantitative analysis of MS1 based precursor ions was carried out with Progenesis QI for proteomics (version 2.0, Nonlinear Dynamics, Newcastle upon Tyne, UK). The software first detects and aligns precursor ion signals (features) then associates information from MS2 based precursor identification and finally computes protein intensities on basis of associated features. Automatic processing was used without manual alignment adjustment. Here, one run of the control-vector + ME49 could not automatically aligned and was not further considered in the analysis. Searches were triggered by Proteome Discoverer (version 1.4.1.14, Thermo Scientific) and the percolator node was used for identification validation at 1% false discovery rate. Spectra were searched with the Mascot search engine (version MASCOT 2.4.1, Matrix Science, London, UK) considering cysteine carbamidomethylation as fixed and protein N-terminal acetylation and methionine oxidation as variable modification as well as tryptic cleavage specificity with a maximum of two missed cleavage sites. Mass precision was set to 10 ppm for precursor and 0.4 Da for fragment spectra. Database searches were carried out using the mus musculus (UP000000589) and toxoplasma gondii (UP000002226) reference proteome data sets downloaded on 18th January 2018 from UniProtKB including 52548 respectively 8404 entries. Only “high confident” peptide spectrum matches were used for further processing and peptide spectrum matches associated with proteins identified with at least two unique peptides. As we noticed a bias towards higher protein intensities in the mGBP2 overexpressing cells (arising from mGBP2 and associated proteins), no global normalization was performed but a normalization of protein intensities based on the sum of the Ig heavy chain proteins P18525, P18524. Calculated protein intensities were further processed within the Perseus (version 1.6.2.2, MPI for Biochemistry, Planegg, Germany) software environment. Here, Student’s t-tests were calculated on \log_2 transformed normalized intensities using the significance analysis of microarrays method for cutoff determination (S0 set to 0.8, 5% false discovery rate, a minimum of 4 valid values per group). The mass spectrometry proteomics data have been deposited to the ProteomeXchange Consortium via the PRIDE [PubMed ID: 30395289] partner repository with the dataset identifier PXD027029.

2.11.4. Software for image analysis

Deconvolved data of gated STED measurements were calculated using Huygens software (Huygens professional, Scientific Volume Imaging, Netherlands). Colocalization analyses of

confocal images was performed with ZEN imaging system from ZEISS and Fiji ImageJ software and Imaris Image Visualization and Analysis Software. INTAS Science Imaging was used for ECL emission detection and Image Lab gel documentation software was utilized for ethidium bromide fluorescence in the GelDoc XR+ system (Bio-Rad).

2.11.5. Statistical analysis

Statistical analysis of the data was conducted using GraphPad Prism® 5 or 9 software. The standard paired t-test was employed for statistical analysis. The results are presented as mean \pm standard deviation. Significance between experimental groups was determined based on a p-value of less than 0.05, indicating that the probability of error for the statement was less than 5%.

2.11.6. Translation software

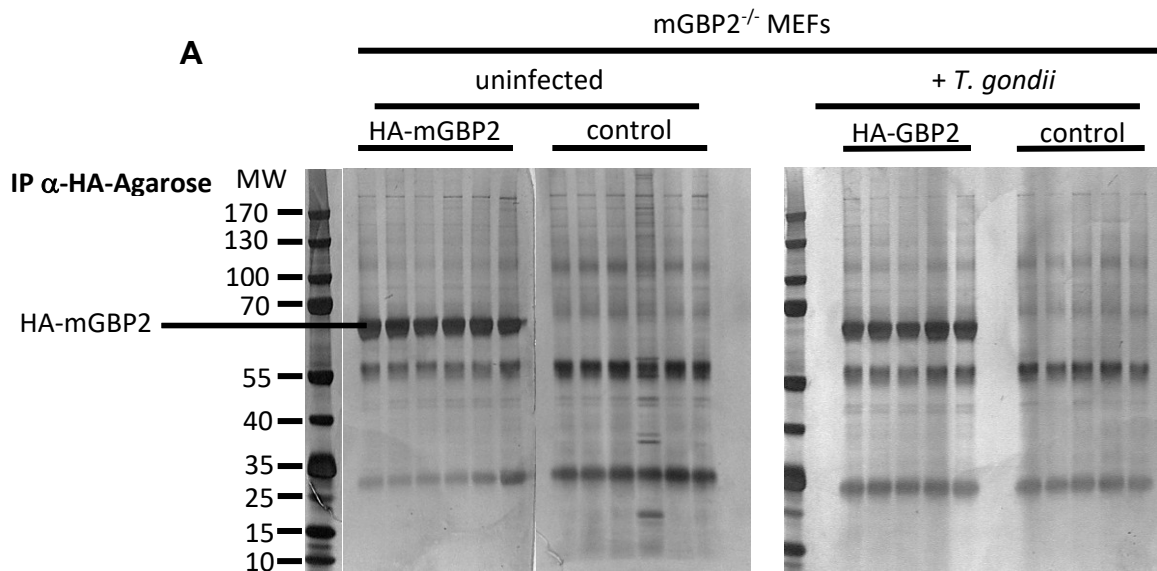
DeepL translate and DeepL write were used for German language interpretation and language enhancement.

3. Results

3.1. Identification of interaction partners of mGBP2

3.1.1. Co-immunoprecipitation analysis

Previously, we could show that mGBP2 interacts with itself and other mGBP family members forming homo- and heteromultimers, respectively, in vesicle-like structures (VLS) and at the *T. gondii* parasitophorous vacuole membrane (PVM), utilizing immunoprecipitation analysis and Förster Resonance Energy Transfer (FRET) techniques (Kravets et al., 2016). For a profound understanding of the functions of mGBP2 in *T. gondii* infection, we searched for other interaction partners of mGBP2. To this end, mGBP2^{-/-} murine embryonic fibroblasts (MEFs) (Degrandi et al., 2013) expressing HA-tagged mGBP2 were constructed (Fig. S1), stimulated with IFN- γ , and either infected with the type II strain *T. gondii* ME49 or left uninfected. An HA-tag specific IP (Fig. 3.1) was performed followed by MS based quantitative protein analysis (Fig. 3.2). mGBP2^{-/-} MEFs transduced with an empty expression vector (Fig. 3.1) served as negative controls. Alternatively, IP experiments followed by MS analysis were performed in IFN- γ stimulated, *T. gondii* infected or uninfected, GFP-mGBP2 transduced cells versus GFP-only expressing mGBP2^{-/-} MEFs (Fig. S2).



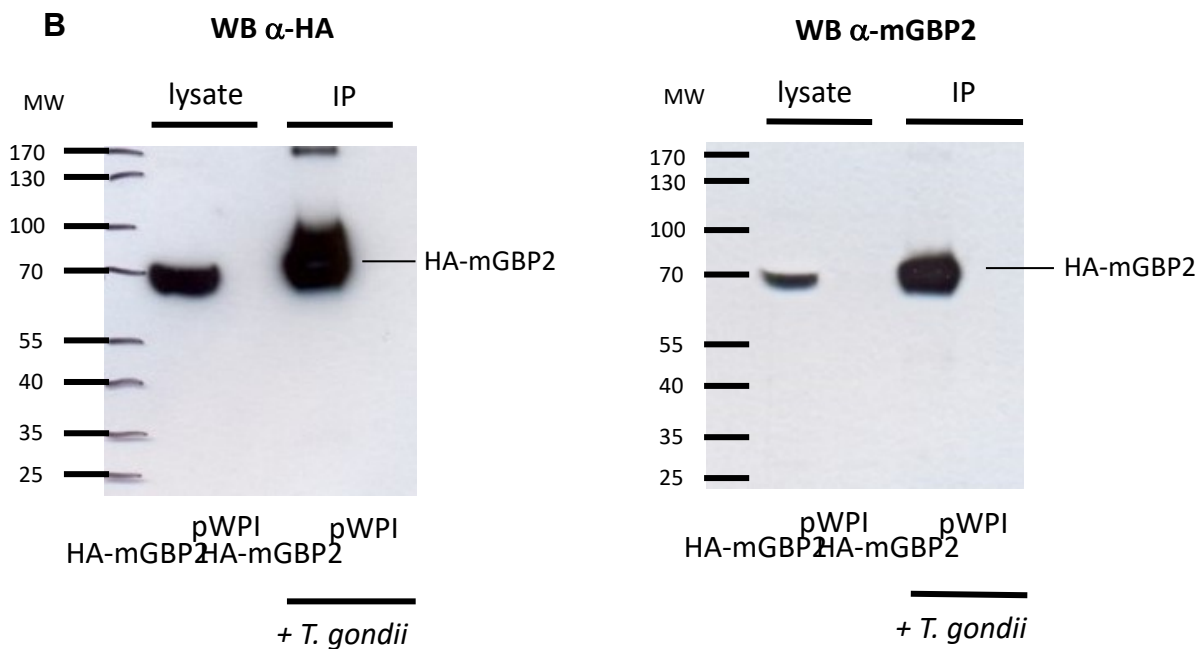


Figure 3.1. Identification of mGBP2 interaction partners.

mGBP2^{-/-} MEFs were reconstituted with HA-mGBP2 or a control vector and stimulated with IFN- γ for 16 h, infected for 2 h with *T. gondii* ME49 or left uninfected. Subsequently, cells were lysed and postnuclear supernatants were incubated o/n with α -HA antibody coupled agarose beads at 4°C for IP. Five to six replicates were analysed per condition and putative mGBP2 interacting proteins were identified from uninfected and *T. gondii* ME49 infected cells. One part of IP samples was separated via 10% SDS-PAGE and labelled using silver staining (A). Another part of the IP samples was subjected to Western Blotting and immune staining with an α -mGBP2 antiserum or an α -HA antibody (B). A third part of these IP samples was transferred to the MS analysis (Fig. 3.2).

3.1.2. Mass spectrometry analysis

After successful precipitation and protein detection of HA-mGBP2 in IFN- γ stimulated and *T. gondii* infected or uninfected mGBP2^{-/-} MEFs, the IP samples were subjected to silver staining and subsequently digested with trypsin, as described in sections 2.10.7-13. No additional specific bands were observed when the cells were additionally treated with various proteasome and autophagy inhibitors (Fig. S3). The resulting peptides were then extracted from the gel and prepared for analysis using liquid chromatography and mass spectrometry (MS). Following that, the precursor ions were identified, aligned, compared against relevant databases (the mus musculus (UP000000589) and toxoplasma gondii (UP000002226) reference proteome data), and subjected to quantitative analysis using Progenesis QI for proteomics and Perseus software.

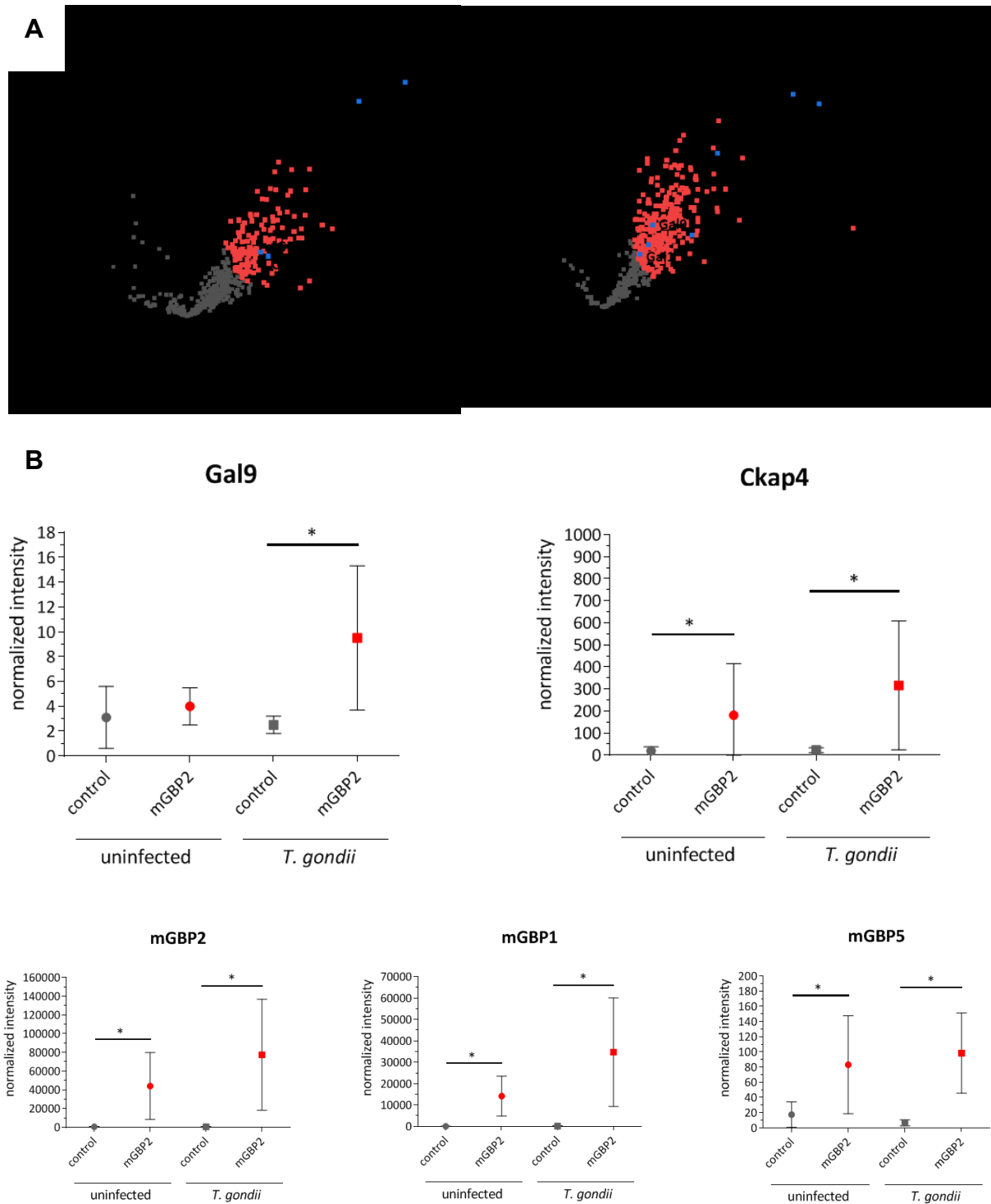


Figure 3.2: Identification of mGBP2 interacting proteins using co-immunoprecipitation in combination with label-free quantitative mass spectrometry.

An HA-mGBP2 fusion protein was expressed in mGBP2^{-/-} MEFs. mGBP2^{-/-} MEFs transduced with the empty expression vector were used as controls. MEFs were stimulated with IFN- γ (16 h) and left uninfected or were infected with *T. gondii* ME49 for 2 h. IPs were performed with an anti-HA antibody from cell lysates. Immunoprecipitated proteins were analysed by label-free quantitative mass spectrometry. Five to six replicates were analysed per condition and putative mGBP2 interacting proteins were identified from uninfected and *T. gondii* ME49 infected cells. Volcano plots were used to visualise the immunoprecipitated proteins. The data analysis was conducted using an unpaired Student's t-test, and proteins exhibiting significant differences at a $p < 0.05$ were highlighted in red (A). Mean values of normalized intensities are shown in the bar plots \pm standard deviations (B).

Table 2.1: Statistical analysis of mGBP2 interacting proteins using co-immunoprecipitation in combination with label-free quantitative mass spectrometry. In the table, details from the protein identification are shown: the confidence scores from the MASCOT search engine (Bollineni et al., 2018; Stratmann et al., 2016), the number of identified unique peptides per protein as well as p-values from Student's t-tests. Furthermore, the enrichment ratios (intensity ratio between mGBP2 expressing cells and vector control) are given (a correction for multiple testing has been performed using the significance analysis of microarray approach, 5% false discovery rate, S_0 0.8, a minimum of 4 valid values per group).

accession	gene names	unique peptides	confidence score
Q01514	mGBP1	19	1702.6
Q9Z0E6	mGBP2	55	4193.6
Q8CFB4	mGBP5	6	199.1
Q8BMK4	Ckap4	13	747.1
O08573	Gal9	2	79.9

uninfected			
gene names	p-value	ratio mGBP2/control	significance mGBP2/control
mGBP1	3.3E-08	186	+
mGBP2	1.3E-07	66.8	+
mGBP5	9.1E-03	4.8	+
Ckap4	1.2E-02	9.2	+
Gal9	1.3E-01	1.5	

<i>T. gondii</i> infected			
gene names	p-value	ratio mGBP2/control	significance mGBP2/control
mGBP1	2.8E-06	199.7	+
mGBP2	1.5E-06	125.4	+
mGBP5	6.3E-05	15.1	+
Ckap4	1.0E-02	14	+
Gal9	5.6E-03	3.8	+

Statistical analysis revealed that 148 proteins from the uninfected and 294 proteins from the *T. gondii* infected cells were co-purified with HA-mGBP2. In addition to the bait protein mGBP2, other members of the mGBP family were enriched as prey proteins (Fig. 3.2). Among them, a clear co-purification of mGBP1 and mGBP5, previously independently identified by MFIS as mGBP2 interacting members (Kravets et al., 2016), was observed in uninfected and infected HA-mGBP2 expressing MEFs (mGBP1 enrichment factor > 185 in both experimental conditions, mGBP5 enrichment factor 4.8 from uninfected and 15.1 from infected cells) (Fig. 3.2), validating the reliability of the co-IP and MS analysis.

Furthermore, Ckap4 was specifically enriched in mGBP2 immunoprecipitation experiments.

Members of the galectin family were significantly enriched in IPs from *T. gondii* infected cells. From the list of potential mGBP2 interactors, Gal9 was further analysed as it was found to be significantly enriched in IP samples from type II *T. gondii* ME49 infected cells (Fig. 3.2), and interestingly, a role for several other galectin family members had already been proposed in microbial infections (Shi et al., 2018). Furthermore, Ckap4 showed a high enrichment factor (uninfected: 9.2 / *T. gondii* infected: 14) comparable to the known mGBP2 interacting proteins mGBP1 and mGBP5 (Fig. 3.2). In addition, further putative interaction partners of mGBP2 were identified by MS analysis (Tab. S1 and S2). The validation of these interactions and the investigation of the functions of these proteins will be the subject of future studies (Fig. S9).

3.1.3. Confirmation of Gal9 and Ckap4 as interaction partners of mGBP2 by co-immunoprecipitation analysis

To validate and characterise the interactions of Gal9 and Ckap4 with mGBP2 in detail, mCherry-fused proteins of Gal9 or Ckap4 were co-expressed with full-length GFP-mGBP2 or with GFP-mGBP2 truncation mutants containing the GTP-binding domain and the middle domain (GM), the middle domain and the C-terminal effector domain (ME) or only the C-terminal effector domain (E) in mGBP2^{-/-} MEFs (Degrandi et al., 2013; Kravets et al., 2012). These cell lines were infected with *T. gondii* followed by co-IP using either GFP or vice versa mCherry protein as the target. Co-expressing WT GFP-mGBP2 and mCherry-mGBP2 mGBP2^{-/-} MEF cell line served as positive control in IP experiments. Interestingly, in multiple repetitions, the strongest band consistently corresponded to the C-terminal domain. Through this approach, we successfully validated the interaction between mGBP2 and Gal9 and Ckap4, highlighting the essential role of the E-domain of mGBP2 in these interactions. (Fig. 3.3 and Fig. S4).

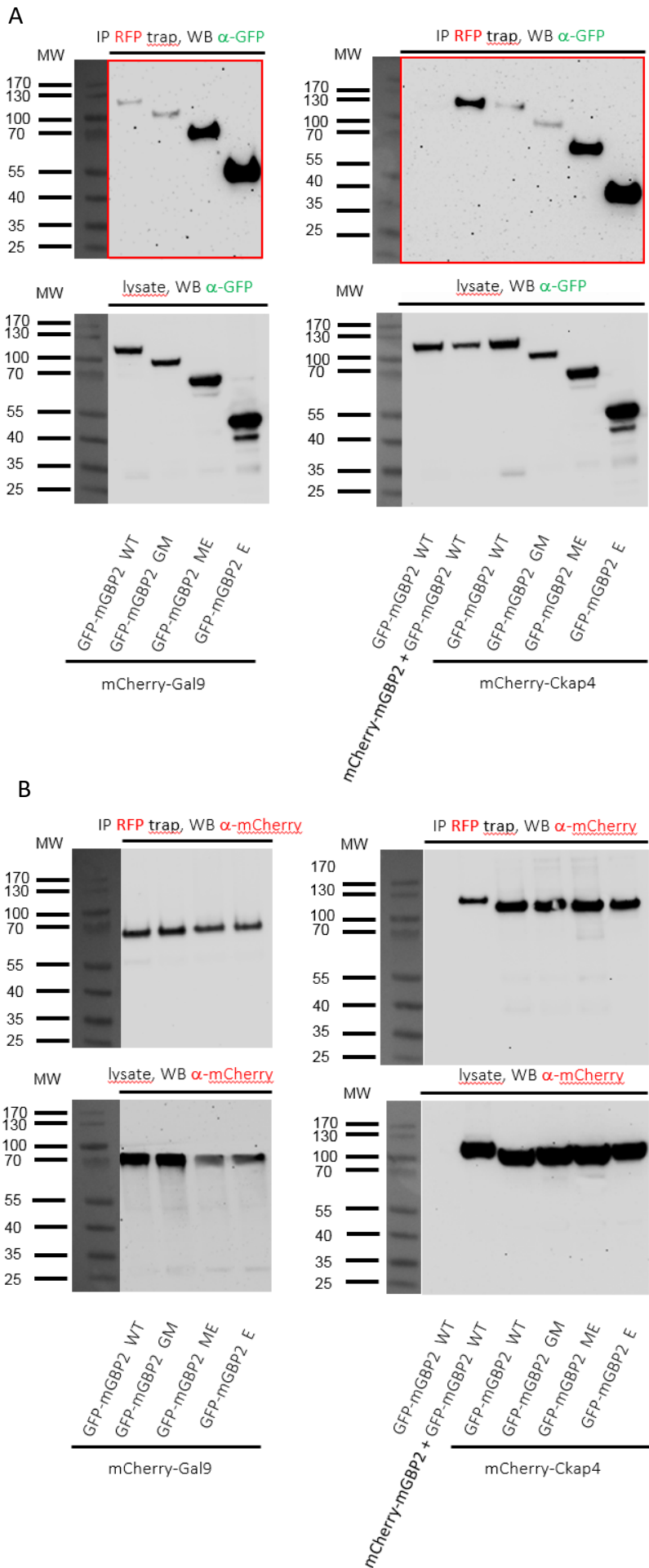
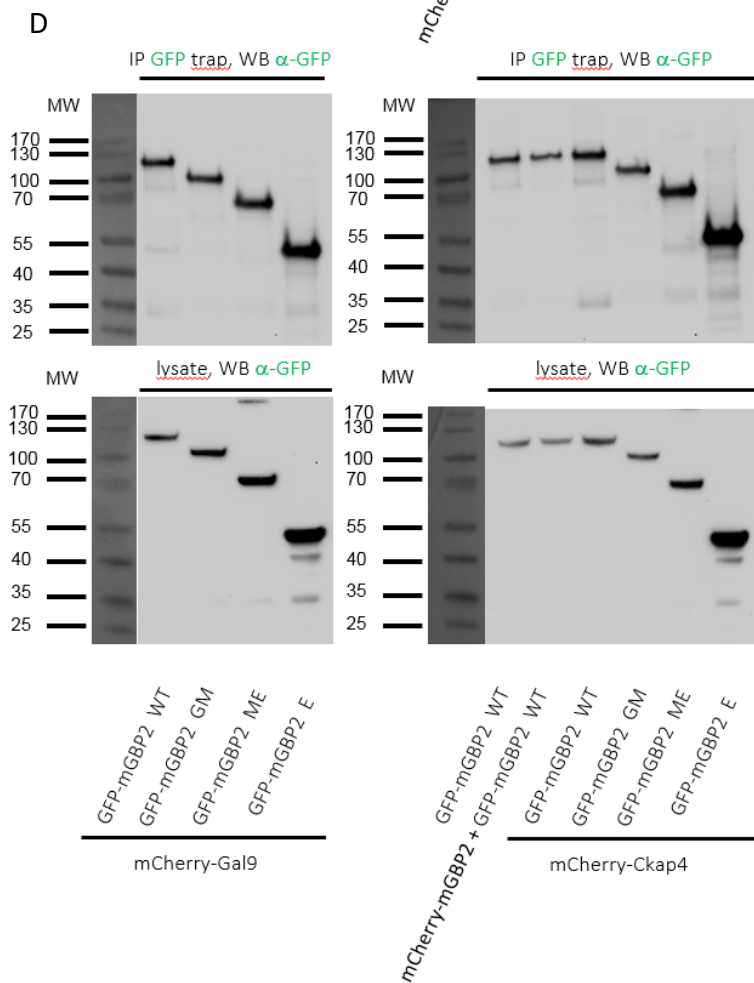
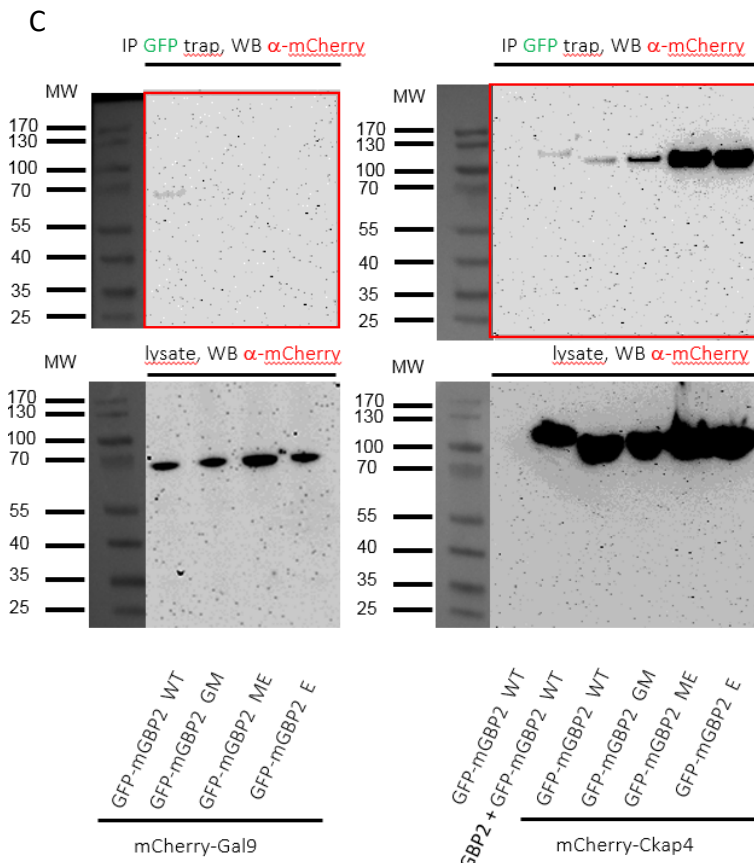


Figure 3.3: Verification of Gal9 and Ckap4 as interaction partners of mGBP2 by IP analysis.

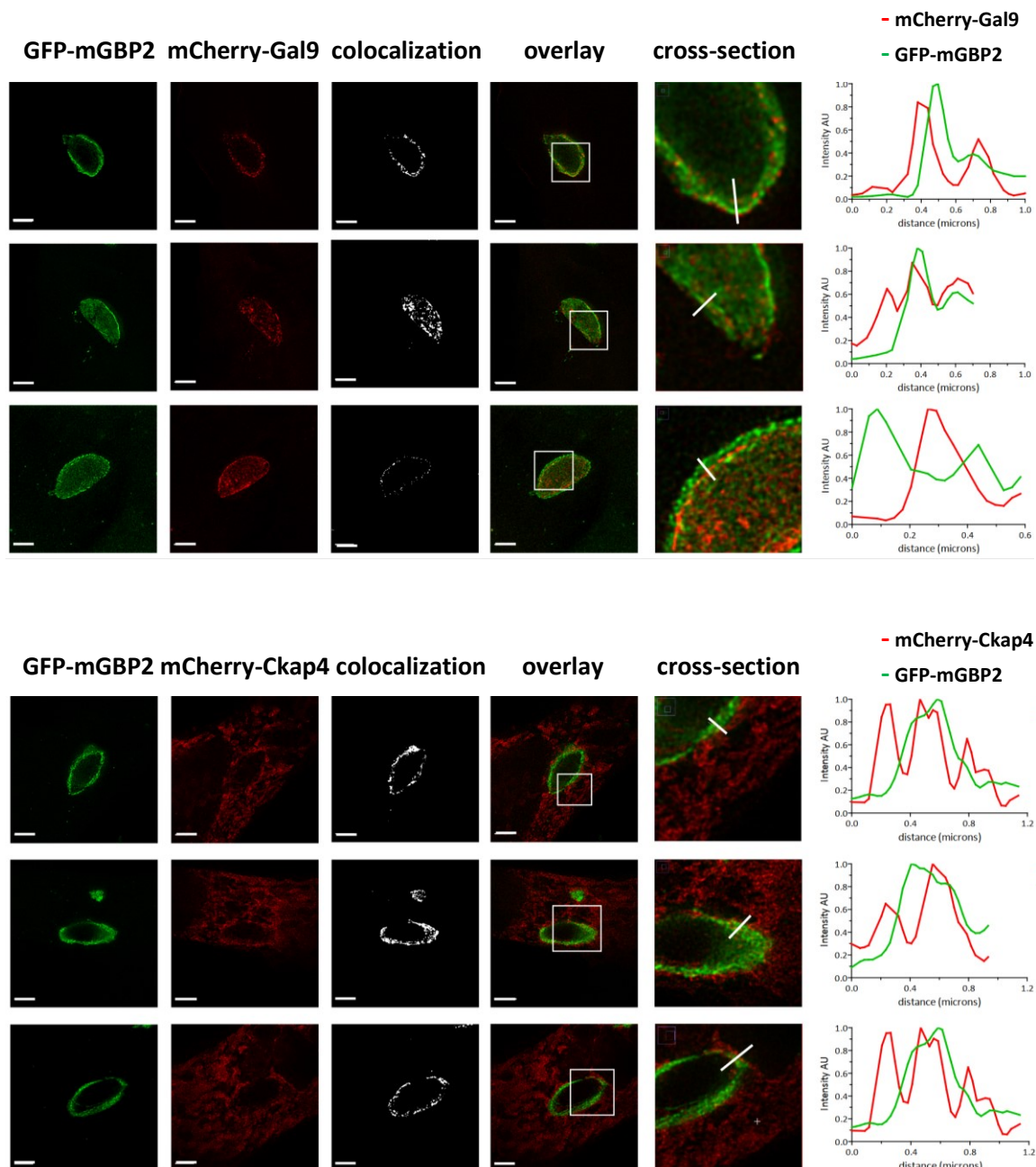
GTP-binding domain and the middle domain (GM), the middle domain and the C-terminal effector domain (ME) or only the C-terminal effector domain (E) (Degrandi et al., 2013). mGBP2^{-/-} MEFs were reconstituted with GFP-mGBP2 WT or one of the indicated mGBP2 truncation mutants as well as one of the N-terminal mCherry fusion proteins: mCherry-mGBP2, mCherry-Gal9 or mCherry-Ckap4. Cells were stimulated with IFN- γ for 16h and infected with *T. gondii* ME49 for 4h. Cells were lysed and postnuclear supernatants were incubated o/n with either RFP-Trap[®] beads (A, B) or with GFP-Trap[®] beads (C, D) at 4°C. IP samples and appropriate cell lysate supernatants were subjected to Western Blotting. Blots were stained with α -GFP or α -mCherry antibodies.



3.2. Subcellular localization of Gal9 and Ckap4 and recruitment to the *T. gondii* PV

3.2.1. Confocal and STED analysis of subcellular localization of Gal9 and Ckap4

In a next step, the colocalization of mGBP2 and Gal9 or Ckap4 at the PVM of *T. gondii* was determined by confocal (Fig. S5) and Stimulated Emission Depletion (STED) microscopy (Fig. 3.4). Doubly transduced mGBP2^{-/-} MEFs co-expressing GFP-mGBP2 with either mCherry-Gal9 or mCherry-Ckap4 were prestimulated with IFN- γ and infected with ME49 *T. gondii* (Fig. 3.4, Fig. S5, S7). GFP-mGBP2 and mCherry-mGBP2 co-expressing MEFs were used as positive controls in colocalization experiments by STED microscopy (Fig. 3.4).



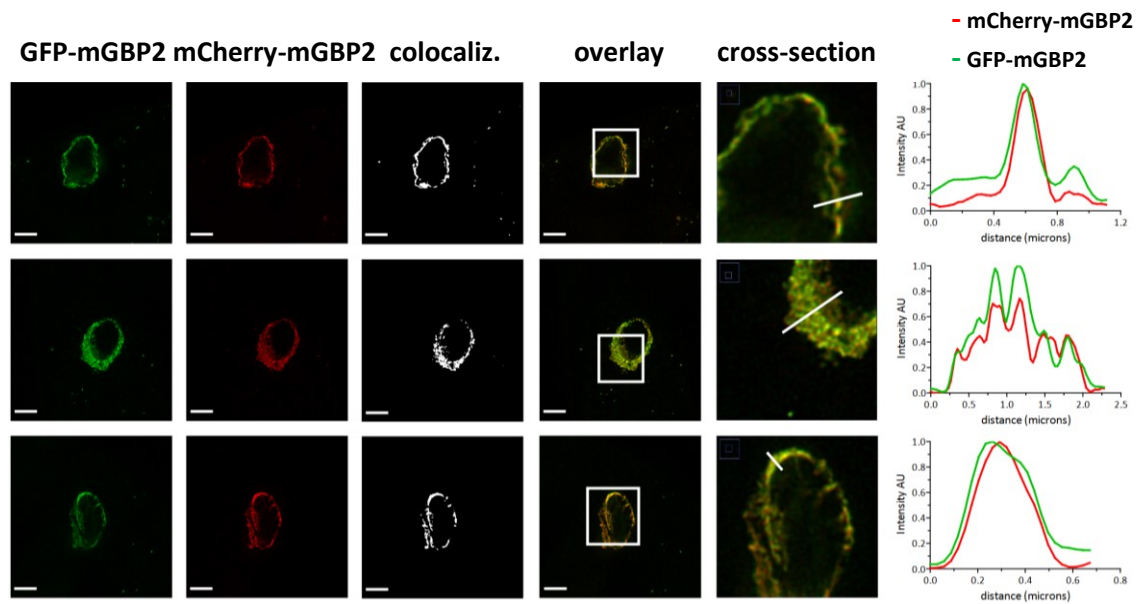


Figure 3.4: Intracellular colocalization of mGBP2 interaction partners Gal9 and Ckap4 at the PVM of *T. gondii*.

Colocalization of mGBP2 with Gal9 or Ckap4 was analysed after transduction of a GFP-mGBP2 fusion construct in mGBP2^{-/-} MEFs and additional transduction of either mCherry-Gal9 or mCherry-Ckap4. GFP-mGBP2 and mCherry-mGBP2 transduced cells were used as a positive control. MEFs were seeded and incubated on glass slides, stimulated with IFN- γ for 16 h and subsequently infected with ME49 *T. gondii* for 2 h. After fixation, infected cells were treated with an α -RFP V_{HH} nanobody conjugated to eGFPBoosterAtto647N and with an α -GFP V_{HH} nanobody conjugated to eGFPBoosterAtto488 for enhancement of the immunofluorescence of mCherry and GFP, respectively. Glass slides were analysed by STED microscopy. 3 representative images from 2 biological replicates of each cell line are shown. Bars 2 μ m. The graphs in the right panel (visualized using GraphPrism software) depict a fluorescence intensity analysis of STED images on the far right with the ImageJ software (Fiji) for Atto488 and Atto647 fluorescence signals along the cross sections of PVMs as indicated. The colocalization thresholds were set to 7500-max for the mCherry and 5000-max for GFP in mCherry-Gal9 and GFP-mGBP2 expressing cells, to 11000-max for the mCherry and 5000-max for GFP in mCherry-Ckap4 and GFP-mGBP2 expressing cells as well as to 13000-max for them mCherry and 2000-max for GFP in mCherry-mGBP2 and GFP-mGBP2 expressing cells.

A distinctive colocalization or close association between mGBP2 and Gal9 and between mGBP2 and Ckap4 could be observed at the PVM already 2 h after infection. Interestingly, mCherry-Gal9 partly colocalized in GFP-mGBP2 containing VLS in uninfected MEFs, whereas a colocalization of mCherry-Ckap4 and GFP-mGBP2 containing VLS could hardly be visualised by confocal microscopy (Fig. S6).

Furthermore, 5 h after infection, different stages of recruitment and accumulation of mGBP2 and its interaction partners at the PVM were observed (Fig. 3.5). Thus, Gal9 and mGBP2 were found to be located together within the intermembranous space of the PV and eventually within the cytosol of the parasite (Fig. 3.5). These results indicate that Gal9 and Ckap4 are interacting together with mGBP2 and suggest that Gal9 and Ckap4 might be intricately involved in the cell autonomous immunity mediated by mGBP2.

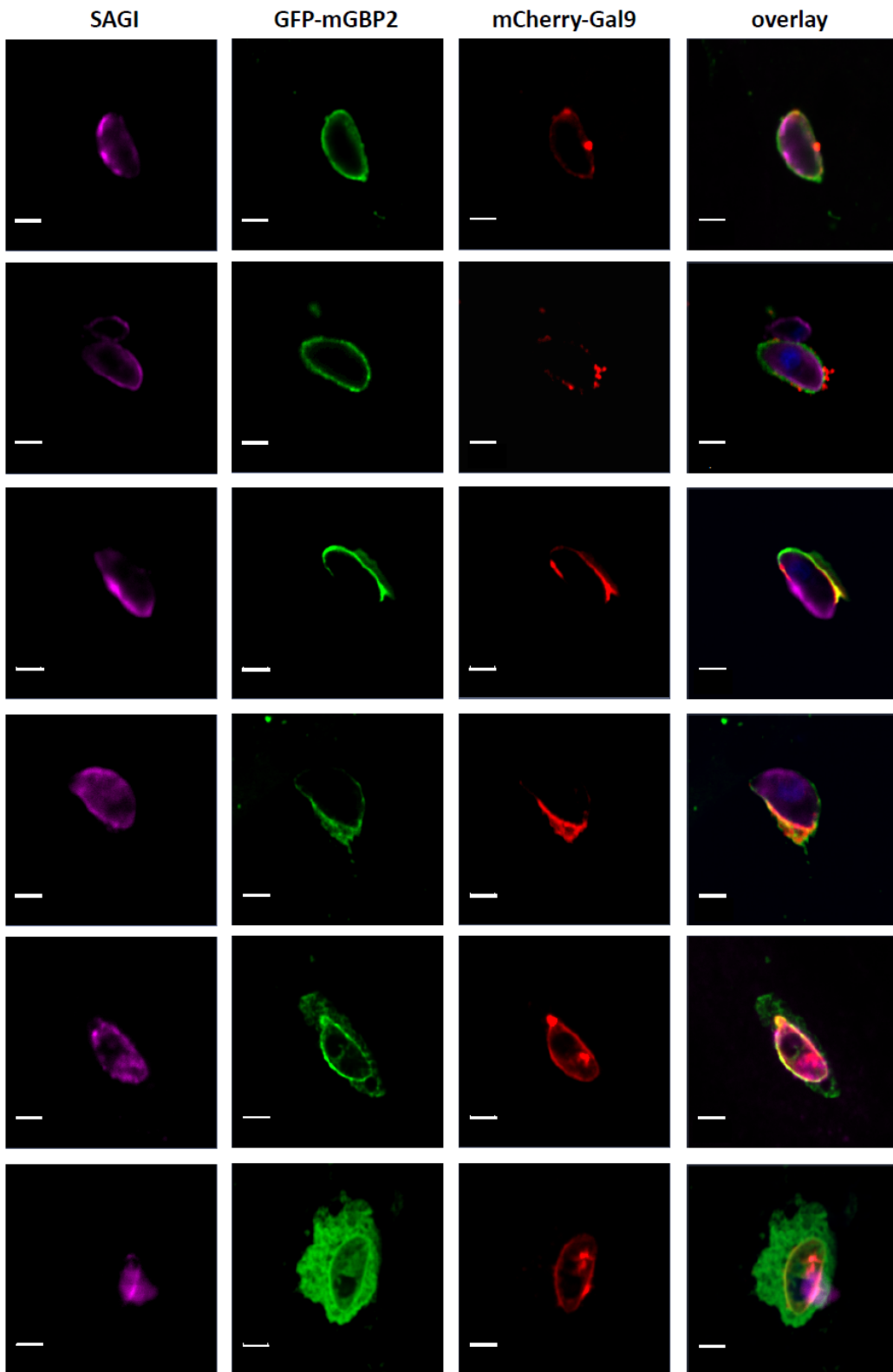


Figure 3.5: Localization of Gal9 and mGBP2 during *T. gondii* infection.

Colocalization of mGBP2 and Gal9 was analysed in GFP-mGBP2 expressing mGBP2^{-/-} MEFs with additional transduction of mCherry-Gal9. MEFs were stimulated with IFN- γ for 16 h and subsequently infected with ME49 *T. gondii* for 5 h. After fixation, *T. gondii* were stained with an α -SAG1 antibody and the cell nuclei were labelled with DAPI. Glass slides were analysed by confocal microscopy. Different stages of infection occurring in parallel are shown. Bars 2 μ m.

3.3. CRISPR/Cas9 mediated knockout of *gal9* and *ckap4* genes in NIH 3T3 fibroblasts

Next, the role of Gal9 and Ckap4 in cell autonomous defence against *T. gondii* were investigated. For this purpose, the *gal9* gene as well as the *ckap4* gene were inactivated applying CRISPR/Cas9 gene editing in NIH 3T3 fibroblasts (Fig. S10). The success of the vector cloning was verified by sequencing for 2 different guide sequences per gene (Tab. 2.2).

Table 2.2: Guide RNA sequences for CRISPR/Cas9 gene editing. *In silico* design of appropriate sgRNAs and genotyping primers was conducted using the CRISPR Design Tool (<http://tools.genome-engineering.org>). The sgRNA guide sequences were subsequently cloned into an expression plasmid pSpCas9(BB) containing both the sgRNA scaffold backbone (BB) and Cas9.

guide RNA	Ckap4	Galectin-9
best	ACC CGT CGG GCG GCG CGG AT	CGG GTT AAT GTA TGG AGA CT
second best	CCC GTC GGG CGG CGC GGA TG	ACC AAT CCA AGG AGG GCT GC

The transfection plasmid was cleaved with the enzyme BbsI, the guide RNA oligos generated from the CRISPR design homepage were phosphorylated with the T4 polynucleotide kinase and finally ligated to the vector via the BbsI interfaces added to the oligos. Then 3T3 fibroblasts were then transfected with the appropriate plasmid, the next day the cells were sorted for the GFP signal and single cells were seeded into 96 wells. Clones were cultured, frozen and genomic DNA isolated. The inactivation of Gal9 and Ckap4 in different clonal NIH 3T3 fibroblast cell lines was confirmed through gene locus sequencing (Fig. 3.6), as well as additional methods such as the Surveyor nuclease assay and Western blotting (WB) for Gal9 (Fig. 3.7 and Fig. 3.8, Fig. S11), and WB analysis using a specific antibody against Ckap4 (Fig. 3.9).

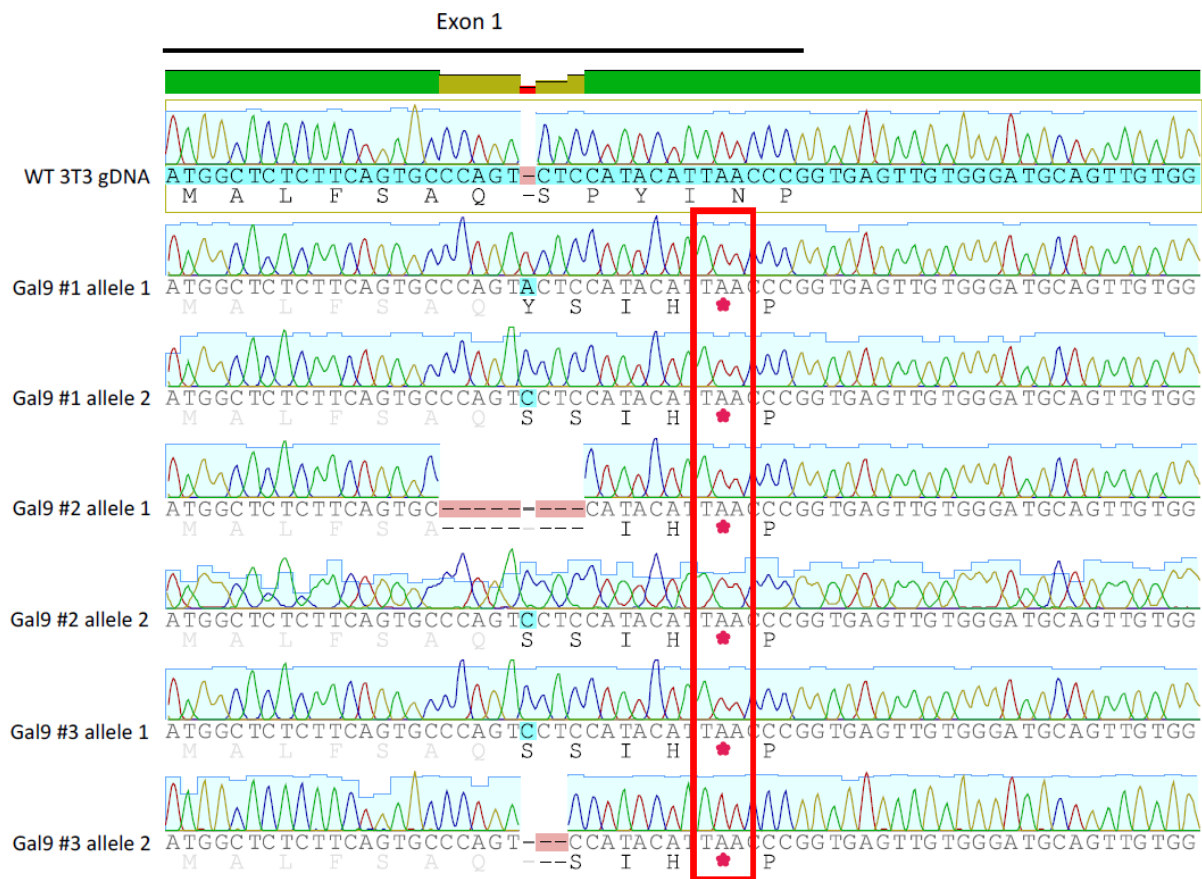


Figure 3.6: CRISPR/Cas9 gene editing of Gal9 and verification of Gal9 inactivation.

CRISPR/Cas9 and sgRNA specific for Gal9 were expressed in NIH 3T3 fibroblasts. Clones were picked and DNA from WT and three CRISPR/Cas9 Gal9 targeted cell clones of NIH 3T3 fibroblasts was isolated and PCR amplified (923 bp). PCR products were cloned into the pCR2.1 TA-cloning vector. The Gal9 mutations were verified by Sanger sequencing. Indels, amino acid sequences and premature stop codons (*) are indicated.

Table 2.2: Primer for detection of CRISPR/Cas9 gene inactivation by Surveyor® Mutation Detection Kit.

CRISPR/Cas9	primer fwd	primer rev	Surveyor endonuclease fragments (bp)		PCR fragment (bp)
Galectin-9	AACTAGATTG GGCCTGCCTC	AGAGATCCCC CTGACTCTGT	176	747	923

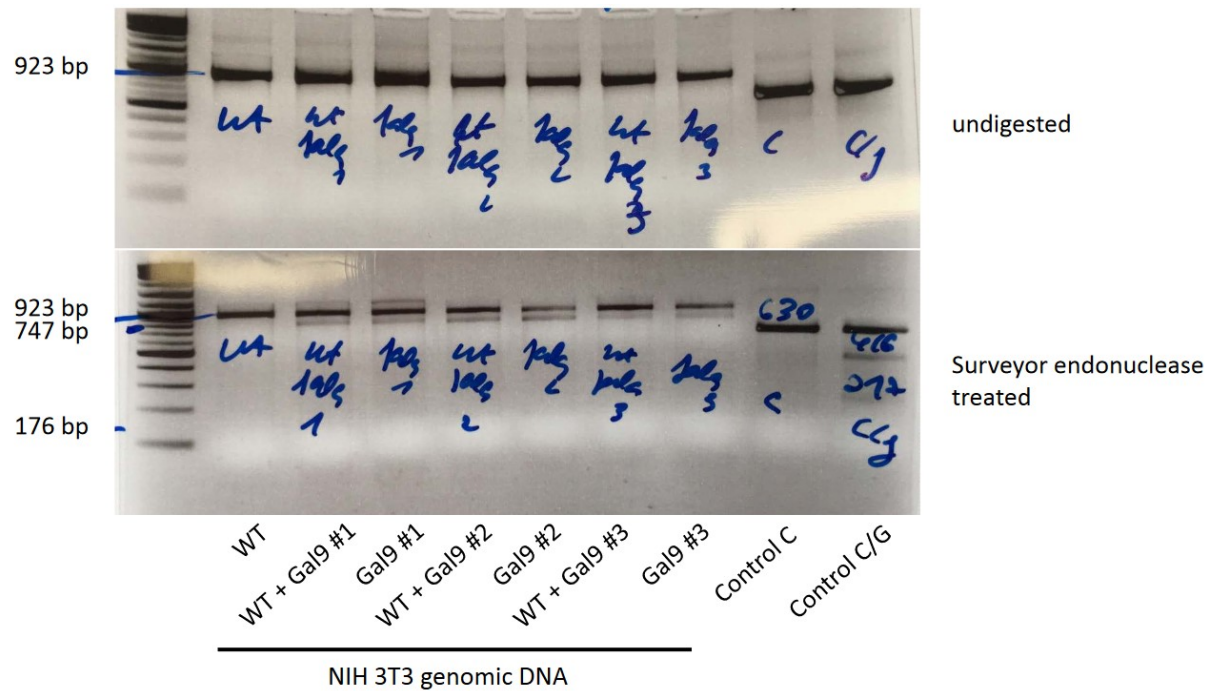


Figure 3.7: Verification of CRISPR/Cas9 Gal9 inactivation using Surveyor® Mutation Detection Kit.

For independent mutation analysis, the Surveyor® Mutation Detection Kit for Standard Gel Electrophoresis was employed. Here, a mismatch-specific DNA endonuclease to scan mutations and polymorphisms in heteroduplex DNA is used. PCR amplicons from Gal9 mutant NIH 3T3 clones (test) and WT (reference) DNA were hybridized and the mixtures of hetero- and homo-duplexes were submitted to Surveyor Nuclease digestion. The reference DNA alone, treated similarly, served as a negative control. DNA fragments were analysed by agarose gel electrophoresis. The formation of new cleavage products, due to the presence of one or more mismatches, is indicated by the presence of additional bands. The relative size of these cleavage products indicates the location of the mismatch or mismatches. Digestion of the kit's own DNA sequences, C and G, is proof of principle.

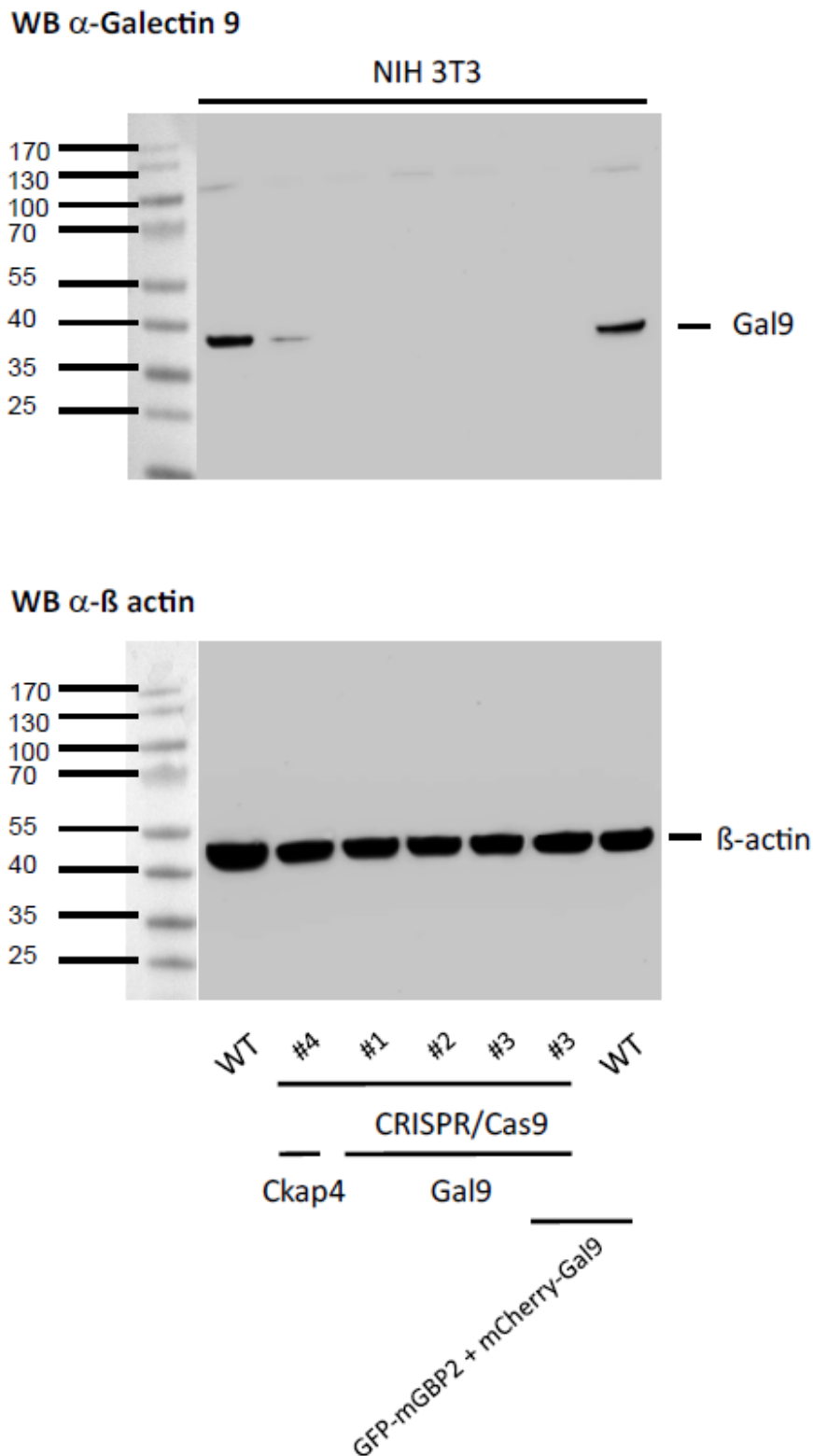


Figure 3.8: Verification of CRISPR/Cas9 Gal9 inactivation by WB analysis.

Postnuclear supernatants of NIH 3T3 cells from different CRISPR/Cas9 Gal9 sgRNA targeted clones and from WT cells were analysed by WB. WT cells and one CRISPR/Cas9 Gal9 sgRNA targeted clone co-expressing GFP-mGBP2 and mCherry-Gal9 served as controls. Cells were stimulated with IFN- γ for 16 h. Blots were stained with polyclonal α -Gal9 from rabbit (Aviva) or α - β -actin antibodies. Density ratios between probe and β -actin control bands in WB stained with polyclonal α -Gal9 antibody were quantified to 0,29 for the WT and 0,22 for the Ckap4 #4 knockout control.

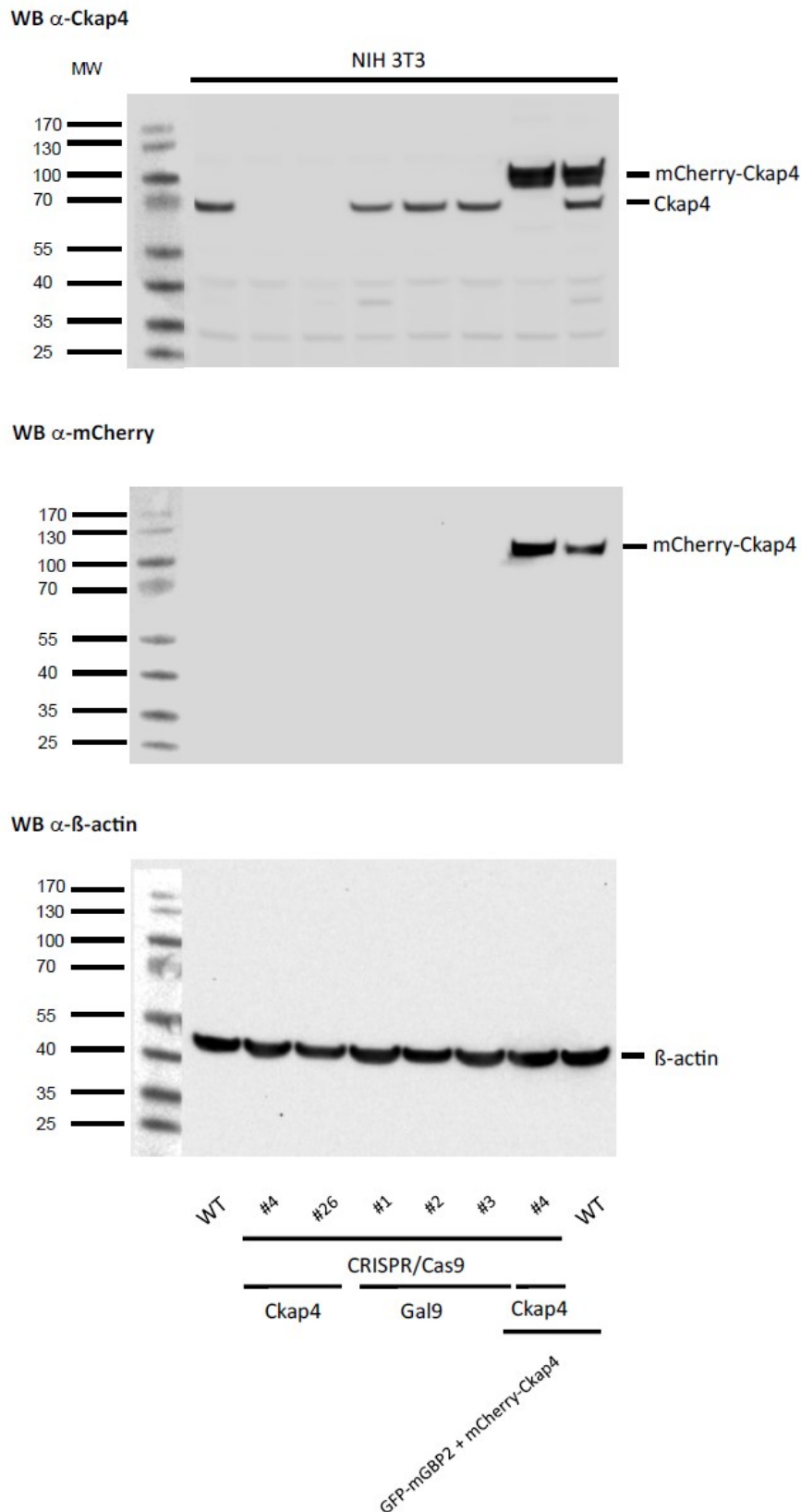


Figure 3.9: Verification of CRISPR/Cas9 Ckap4 inactivation by WB analysis.

CRISPR/Cas9 and sgRNA specific for Ckap4 were expressed in NIH 3T3 fibroblasts. Postnuclear supernatants of NIH 3T3 cells from different CRISPR/Cas9 Ckap4 sgRNA targeted clones versus WT and CRISPR/Cas9 Gal9 sgRNA targeted clones were analysed by WB. WT and one CRISPR/Cas9 Ckap4 sgRNA targeted clones co-expressing GFP-mGBP2 and mCherry-Ckap4 served as controls. Cells were stimulated with IFN- γ for 16 h. Blots were stained with α -Ckap4, α -mCherry or α - β -actin antibodies.

3.4. Recruitment of mGBP2 to the *T. gondii* PV in Gal9 deficient cells.

Subsequently, the involvement of Gal9 in the recruitment of mGBP2 to the *T. gondii* parasitophorous vacuole (PV) was investigated. The function of Ckap4 in cell autonomous immunity against *T. gondii* will be addressed in further studies. Remarkably, a significant decrease in the recruitment efficiency of mGBP2 was observed 2 hours after infection in the targeted fibroblast cell lines lacking Gal9 (Fig. 3.10). Recruitment of mGBP2 could be restored after reconstitution of the fibroblasts with mCherry-Gal9 (Fig. 3.10). Interestingly, the recruitment of Gal9 was also reduced in mGBP2-deficient MEFs, indicating a reciprocal interaction between Gal9 and mGBP2 (Fig. 3.10). These findings suggest that the recruitment of mGBP2 to the *T. gondii* PVM is more efficient in the presence of Gal9.

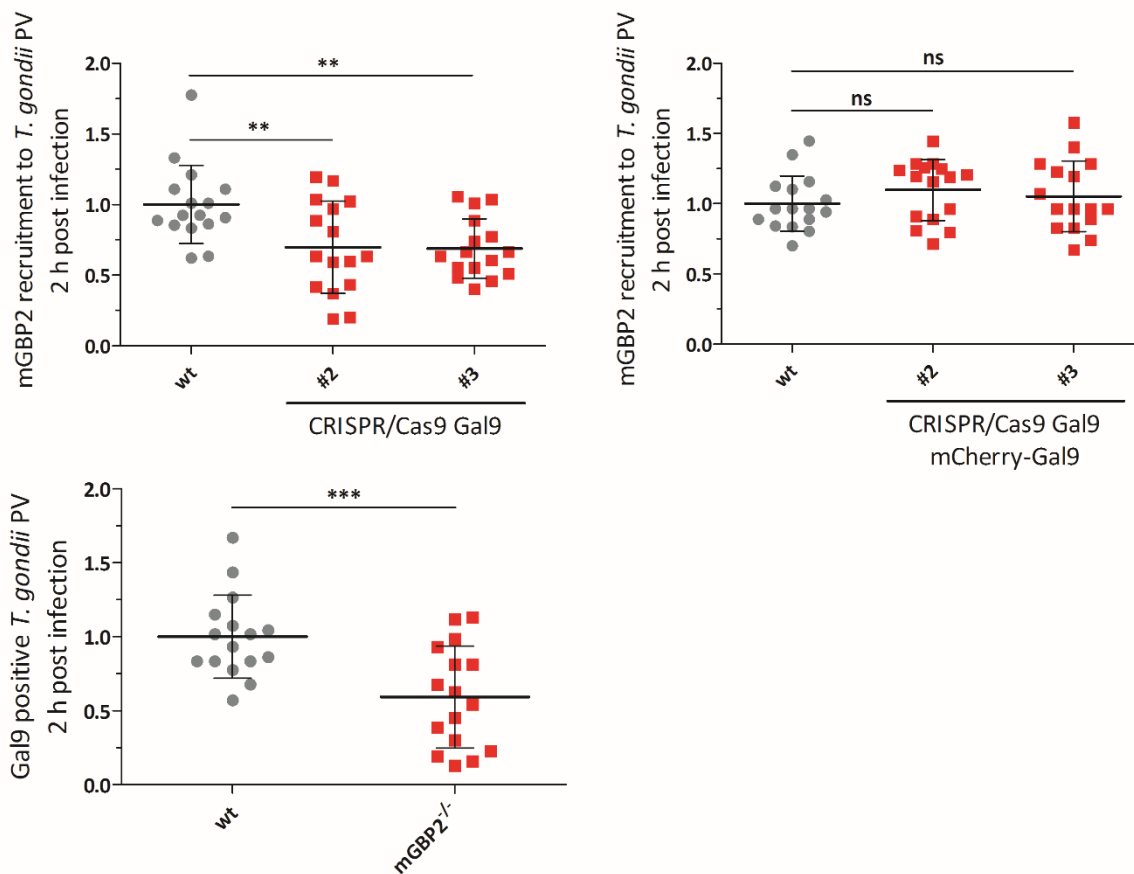


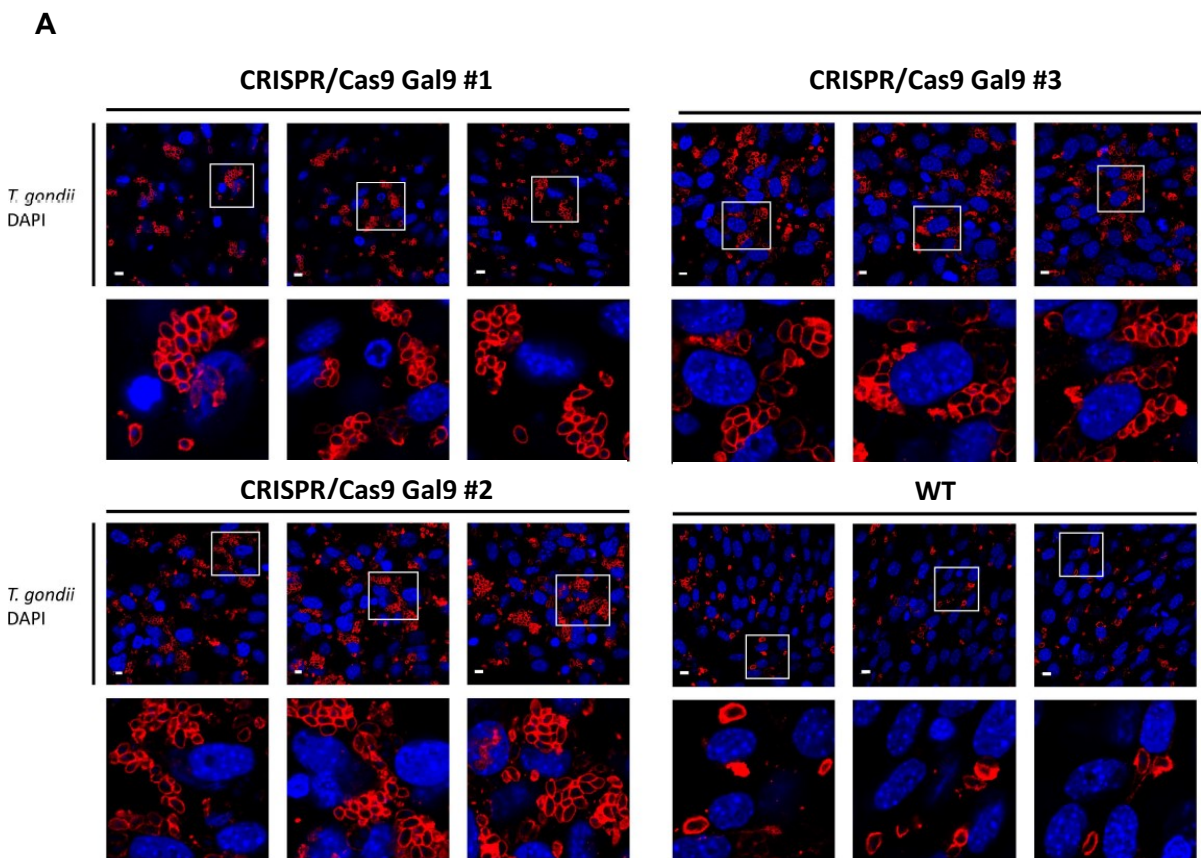
Figure 3.10: Gal9 influences the recruitment of mGBP2 to the PVM of *T. gondii*.

Recruitment of mGBP2 to the PVM was analysed by transduction of a GFP-mGBP2 fusion construct in WT and independent NIH 3T3 cell line clones with verified CRISPR/Cas9 mediated inactivation of Gal9 (see Figs. 3.8/S11). Cells were stimulated with IFN- γ for 16 h and subsequently infected with ME49 *T. gondii* for 2 h. After fixation, *T. gondii* were stained with an α -SAG1 antibody and the nuclei were labelled with DAPI. Glass slides were analysed by confocal microscopy. In each cell line more than 100 PVs were counted. Cumulative analyses from 2 different biological replicates are displayed. The recruitment rate of GFP-mGBP2 in WT cells was set as 1 (100%) and the recruitment rate of mGBP2 in the respective knockout cells was calculated to this

reference. The calculated values are plotted on the y-axis. Also, Gal9 recruitment to the *T. gondii* PV was analysed in mGBP2^{-/-} vs. WT MEFs transduced either with mCherry-Gal9. The rate of Gal9 positive PVMs in WT cells was set as 1 (100%) and related to the respective rates in mGBP2 knockout cells. The calculated values are plotted on the y-axis. Mean values \pm SD are shown. Statistical analysis was performed using the Student's t-test. ***: $p \leq 0.001$; **: $p \leq 0.01$; *: $p \leq 0.05$.

3.5. *T. gondii* replication control by Gal9

In the subsequent step, the impact of Gal9 deficiency on the course of *T. gondii* infection was investigated. The aim was to determine whether Gal9 contribute to cell autonomous immunity against *T. gondii*. To address this, Gal9-deficient fibroblast cell lines were stimulated with IFN- γ , infected with *T. gondii* (ME49) and the replication of the parasite was monitored (Fig. 3.11). Initially, the infection rates in the gene-edited cell lines were compared to wild-type cells to assess whether the inactivation of Gal9 led to increased or decreased infection rates. However, no significant differences in the number of *T. gondii* parasites were detected between the gene-edited cell lines and wild-type fibroblasts 2 hours after infection (Fig. 3.12).



B

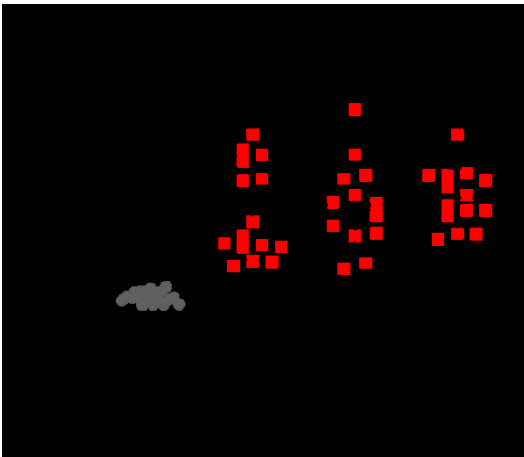


Figure 3.11: Gal9 is required for the intracellular control of replication of *T. gondii*.

WT and independent NIH 3T3 cell line clones with verified CRISPR/Cas9 mediated inactivation of Gal9 were stimulated with IFN- γ for 16 h and subsequently infected with ME49 *T. gondii* for 22 h. (A) After fixation, *T. gondii* were stained with an α -SAGI antibody (red) and the cell nuclei were labelled with DAPI (blue). Glass slides were analysed by confocal microscopy. Bars, 5 μ m. (B) The amounts of rosettes (replicative units) and single parasites inside the PV were determined in WT, Gal9-deficient NIH 3T3 fibroblasts 22 h after infection. In each cell line more than 100 PVs were counted. Cumulative analyses from 2 different biological replicates are displayed. The replication rate in WT cells was set as 1 (100%) and rates in the respective knockout cells was calculated to this reference. The calculated values are plotted on the y-axis. Mean values \pm SD are shown. Statistical analysis was performed using the Student's t-test. ***: $p \leq 0.001$; **: $p \leq 0.01$; *: $p \leq 0.05$.

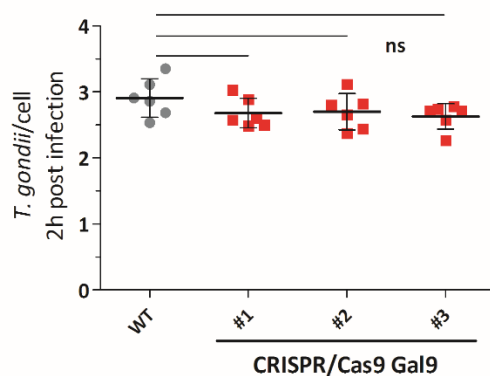


Figure 3.12: Inactivation of Gal9 does not influence infection rates of *T. gondii*.

The infection rates of *T. gondii* ME49 were analysed in WT and independent NIH 3T3 cell line clones with verified Gal9 inactivation. Cells were stimulated with IFN- γ for 16 h and subsequently infected with ME49 *T. gondii*. After fixation, *T. gondii* were stained with the α -SAGI antibody and the cell nuclei were labelled with DAPI. Glass slides were analysed by confocal microscopy. Bars, 5 μ m. The amounts of parasites per cell were quantified 2 h after infection. Mean values \pm SD are shown (lower panel). Statistical analysis was performed using the Student's t-test.

Remarkably, a significant increase in *T. gondii* replication was observed in fibroblasts with Gal9 inactivation, as determined by quantifying the number of *T. gondii* rosettes and single parasites 22 hours after infection (Fig. 3.11).

To confirm the specificity of CRISPR/Cas9 gene inactivation of Gal9, Gal9-deficient cell clones were reconstituted by transduction with mCherry-Gal9 expression constructs, respectively. Importantly, the reconstituted fibroblasts exhibited a comparable level of inhibition in *Toxoplasma* replication as observed in wild-type cells (Fig. 3.13). These results clearly indicate an important role for Gal9 in controlling the intracellular replication of the parasite and suggest that mGBP2 and Gal9 function as supramolecular complexes in the defence against intracellular pathogens.

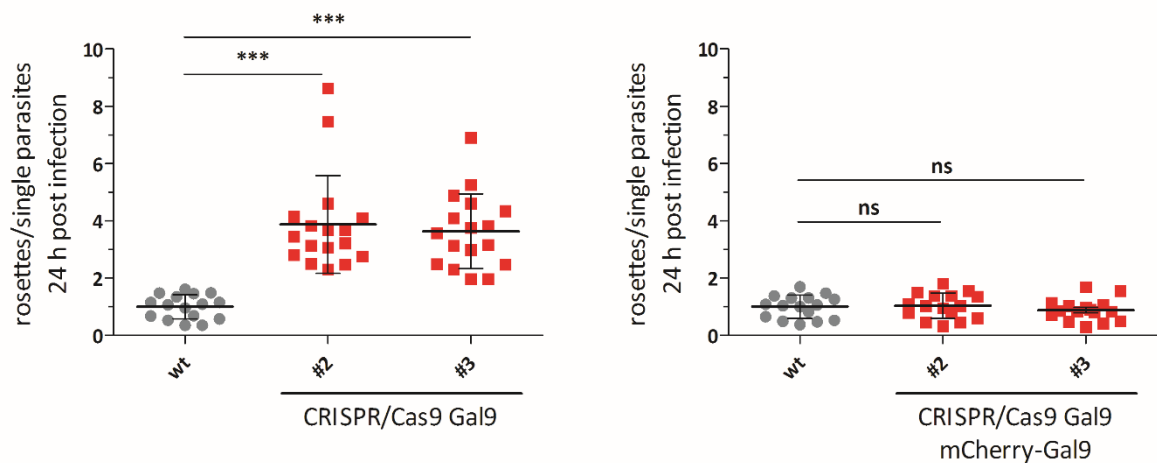


Figure 3.13: Gal9 controls the intracellular replication of *T. gondii*.

WT and independent NIH 3T3 cell line clones with verified CRISPR/Cas9 mediated inactivation of Gal9 cells reconstituted with mCherry-Gal9 were stimulated with IFN- γ for 16 h and subsequently infected with ME49 *T. gondii* for 24 h. After fixation, *T. gondii* were stained with an α -SAG1 antibody and the cell nuclei were labelled with DAPI. Glass slides were analysed by confocal microscopy. The amounts of rosettes and single parasites inside the PV were determined in WT, Gal9-deficient and mCherry-Gal9 reconstituted NIH 3T3 fibroblasts 24 h after infection. Cumulative analyses from 2 different biological replicates are displayed. The replication rate in WT cells was set as 1 (100%) and rates in the respective knockout or reconstituted cells was calculated to this reference. The calculated values are plotted on the y-axis. Mean values \pm SD are shown. Statistical analysis was performed using the Student's t-test. ***: $p \leq 0.001$; **: $p \leq 0.01$; *: $p \leq 0.05$.

4 Discussion

Following infection with *T. gondii*, the innate and adaptive immune systems mount an integrated immune response that results in resistance against this parasite. The innate immunity provides mechanisms that confer initial protection during the acute phase of infection. mGBPs, specifically mGBP2 have been established as a key player in providing cell-autonomous immunity against the intracellular PV resident parasite *T. gondii* (Degrandi et al., 2013; Haldar et al., 2014; Kravets et al., 2016; Kravets et al., 2012; Lindenberg et al., 2017). While it has been shown that mGBPs translocate to PVs, form supramolecular complexes, attack the membrane of the parasite itself, and, consecutively, restrict replication of the intracellular pathogen, the precise molecular mechanisms underlying mGBPs' control of the parasite within the host cell remain largely elusive. In this study, we propose two novel interaction partners of mGBP2, Gal9 and Ckap4, which play a critical role with respect to the recruitment and the antiparasitic function of mGBP2 in the context of cell-autonomous defence against *T. gondii* (for a schematic overview see Fig. S12).

Galectins are a family of nucleocytoplasmic carbohydrate-binding lectins that can directly bind to and eliminate pathogens, by disrupting their surface structures, modulate inflammatory signalling pathways, and promoting processes such as phagocytosis, encapsulation, autophagy, and clearance of pathogens from circulation. Overall, this newfound understanding of galectin functions establishes them not only as pattern recognition receptors but also as crucial effector factors in host defence against microbial pathogens. (Chen et al., 2014; Coers, 2017; Vasta, 2020).

In a previous study, the co-localization of Gal8 with mGBP2-positive *Salmonella* spp. was observed in unprimed bone marrow derived macrophages (BMDMs) (Thurston et al., 2012). The findings suggested that Gal8 functions as a surveillance molecule for monitoring endosomal and lysosomal integrity and detects bacterial invasion of the cytosol by *Listeria* spp. or *Shigella* spp., serving as a versatile receptor for vesicle-damaging pathogens (Thurston et al., 2012). In addition, this study showed that upon recognition of host glycans on damaged phagosomes initially containing *Salmonella typhimurium*, Gal8 promotes autophagic clearance of bacteria-containing vesicles by recruiting NDP52 and its downstream autophagy machinery (Thurston et al., 2016). Interestingly, it was also reported that Gal3, as a member of the Galectin family, and mGBP2 form protein complexes, which associate with vacuoles harbouring secretion system-competent

Legionella pneumophila and *Yersinia pseudotuberculosis* bacteria in response to vacuolar damage (Feeley et al., 2017). In this study, we show that Gal9 interacts and colocalizes with mGBP2 in IFN- γ stimulated MEFs and NIH 3T3 cells in VLS.

Recruitment of Gal9 to the *T. gondii* PV has not been described previously. Furthermore, Gal9 could not only be found at the PVM but also within the intermembranous space between the PVM and the *T. gondii* plasma membrane as well as in the cytosol of the parasites together with mGBP2 approx. 5-6 h post-infection. This indicates that Gal9 and mGBP2 might recruit to the PVM of *T. gondii* in preformed complexes. Mechanistically, a series of events involving mGBP/IRG mediated PVM indentation, PVM vesiculation/disruption, and parasite plasma membrane stripping and denudation, leading ultimately to degradation of the parasite, is proposed by us and others as hallmarks for intracellular *T. gondii* elimination (Kravets et al., 2016; Ling et al., 2006; Martens et al., 2005). It can be suggested that pore forming or denudating activity of these IFN- γ induced GTPases allows Gal9 to transmigrate through the PVM and to recognize β -galactosides on the inner leaflets of the PVM and the parasite, labelling the parasite for further degradation processes.

Parasite glycoconjugates play important roles in host cell invasion, and specific interactions between host galectins and parasite glycoconjugates are considered to be critical for pathogen recognition (Vasta, 2009). Interestingly, glycosylphosphatidylinositols (GPIs) of *T. gondii* (Lekutis et al., 2001) have been shown to be ligands of human Gal3 whereby both glycan and lipid moieties participate in the association of *T. gondii* GPIs with Gal3 (Debierre-Grockiego et al., 2010). GPI-Gal3 interaction, collectively with Toll-like receptors (TLR2 and TLR4), is important for *T. gondii* recognition by macrophages (Debierre-Grockiego et al., 2010). In this context, Gal3, -8, and -9 bind to host glycans in the luminal side of lysed phagosomes or permeated pathogen vacuoles (Mansilla Pareja et al., 2017). A study conducted on the minute virus of mice (MVMp) prototype strain found that both Gal3 and Mgat5, a glycosyltransferase involved in the synthesis of oligosaccharides recognized by Gal3, are essential for efficient cell entry and infection (Garcin et al., 2015). Another study demonstrated that the expression of Gal3 is necessary for the adhesion of *Trypanosoma cruzi* to human cells, facilitating the entry of the parasite into the host cells (Kleshchenko et al., 2004). In addition to Gal3, several other members of the galectin family, such as Gal1, -4, -7, -8, and -14, have been shown to bind to surface proteins of the *T. cruzi* parasite (Pineda et al., 2015). In contrast, the replication of *T. cruzi* was found to be even higher in Gal3 knockout mice compared to WT mice (da Silva et al.,

2017; Pineda et al., 2015). These results can be interpreted from two perspectives: (1) galectins may have redundant functions, and other members of the galectin family could potentially play a role in *T. cruzi* adhesion and invasion; (2) in *in vivo* studies using Gal3^{-/-} mice, the intracellular functions of Gal3 in various cell types may outweigh its extracellular role in specific cell types, making it challenging to confirm certain expected phenotypes *in vivo*. Interestingly, galectins have emerged as important markers for vacuole lysis induced by intracellular bacteria. Upon internalization into host cells, some invasive bacteria like *Salmonella Typhimurium* and *Listeria monocytogenes* may disrupt the endocytic vesicles surrounding them. This disruption exposes the luminal side of the vesicles, including glycans that were originally displayed on the cell surface, to the cytosol. Intracellular Gal3 was characterized as a sensor of vacuolar rupture that occurs when bacteria such as *Shigella flexneri* or *Salmonella enterica* serovar *Typhimurium* actively enter the host cell cytosol (Paz et al., 2010; Santos et al., 2020). Moreover, *S. flexneri* IpaH9.8 labels mGBP2 for degradation (Li et al., 2017). Gal3, -8 and -9 were also shown to associate with *Salmonella*-containing vacuoles (SCV) (Creasey and Isberg, 2012; Pilla et al., 2014; Thurston et al., 2012). The binding of Gal3 to *Helicobacter pylori* occurs through the recognition of the LPS O-antigen (the outer carbohydrate) (Fowler et al., 2006). This binding induces a change in the shape of *H. pylori*, ultimately leading to the death of the bacterial cells (Park et al., 2016). Upon lysosomal damage, mTOR is inhibited for autophagy activation, and this inhibition was found to be controlled by galectins. Gal8 interacts with the Ragulator-Rag SLC38A9 system, while Gal9 interacts with AMPK, leading to the suppression of mTOR activity, which contributes to the autophagic elimination of lysosome-damaging intracellular bacteria, such as *Mycobacterium tuberculosis* (Jia et al., 2018). In addition to Gal8 and Gal9, Gal3 is also involved in the regulation of autophagy during intracellular bacterial infection. Upon endomembrane injury, Gal3 recognises exposed β -galactoside glycoconjugates on damaged membranes and in turn associates with TRIM16. This Gal3-TRIM16 complex serves as a platform for the recruitment of other autophagy regulators, to initiate autophagy and protect cells from invasion by bacteria such *M. tb* (Chauhan et al., 2016). In a similar manner to its effect on TRIM16, Gal3 guides mGBP1 and mGBP2 to intracellular vacuoles damaged by *Yersinia pseudotuberculosis* or *Legionella pneumophila* and facilitates the targeting of these bacteria by ubiquitin and p62, an autophagy receptor (Feeley et al., 2017). Interestingly, it has been observed that Gal3 has an antagonistic function when it is recruited to damaged phagosomes containing *Listeria monocytogenes*. In this context, Gal3 negatively regulates antibacterial autophagy in a manner that is dependent on host N-glycan interactions by inhibiting Gal8 recruitment (Weng et al.,

2018). Another study has shown that adenoviruses can disrupt the endosomal membrane to enter the cytoplasm. This disruption is facilitated by the interaction between the viral capsid PPxY motif and intracellular Gal8. Similar to bacterial infections, this interaction leads to the sequestration of autophagic receptors NDP52 and p62, further modulating the cellular response (Montespan et al., 2017). Here we show that Gal9 is required for the control of the parasite *T. gondii*.

Functionally, the recruitment of mGBP2 to the PVM was reduced in Gal9- inactivated cells and vice versa; the recruitment of Gal9 to the PVM was reduced in mGBP2 deficient cells. In accordance, significantly fewer *Salmonella* were targeted by Gal8 in *Gbp^{chr3-/-}* BMDMs than in wild-type BMDMs (Meunier et al., 2014). Also, the delivery of mGBP1 and mGBP2 to *Legionella*-containing vacuoles (LCV) or *Yersinia*-containing vacuoles is substantially diminished in Gal3- and, to a lesser extent, Gal8-deficient IFN- γ -primed iBMDM (Feeley et al., 2017). In *Salmonella*-infected cells, SCV rupture and Gal3 recruitment was followed by a rapid and massive recruitment of hGBP1 (Santos et al., 2020). Interestingly, a specific polybasic protein motif (PBM: KMRRRK) was identified for hGBP1 which is sufficient to drive significant targeting of hGBP1 to *S. flexneri* recognizing exposed glycans from disrupted, bacteria containing, endosomes. Deletion of the PBM-motive leads to substantially reduced colocalization between Gal3-marked vacuoles and hGBP1 (Piro et al., 2017). mGBP2 lacks such a C-terminal PBM. Nevertheless, the interaction with Gal9 appears to be mostly dependent on the C-terminal domain of mGBP2. Interestingly, both Gal4 and Gal8 recognize blood group B (BGB) antigen on *E. coli* via their C-terminal domains, and both are effective in elimination of BGB-expressing *E. coli* (Stowell et al., 2010). Remarkably, Gal3 and Gal8 exhibit different binding affinities for sialic acid-containing glycans. Gal3, which has a single carbohydrate recognition domain (CRD), is unable to bind to β -galactoside-containing glycoconjugates that are terminally alpha2,6-sialylated (Zhuo and Bellis, 2011). On the other hand, Gal8, which has two CRDs, specifically recognizes sialylated galactosides with high affinity, particularly through its N-terminal CRD (Carlsson et al., 2007). Therefore, alterations in the level of terminal sialylation on host glycans may influence the recruitment of Gal3 and Gal8 to intracellular bacteria, leading to increased accumulation of Gal3 and decreased accumulation of Gal8 on *Listeria monocytogenes*-damaged phagosomes. This differential recruitment presumably contributes to attenuated antibacterial autophagy and enhanced replication of intracellular bacteria (Weng et al., 2018). Based on its structural organization, Gal9 belongs to the tandem-repeat type galectins containing two distinct but homologous CRDs (N-CRD and

C-CRD) covalently connected by a linker peptide (Casals et al., 2018; Liu and Rabinovich, 2010). The impact of the domain composition of Gal9 on its interaction with mGBP2, as well as its role in controlling *T. gondii*, needs to be determined in further analyses.

Rab GDP dissociation inhibitor α (RabGDI α) acts as a suppressor of the mGBP2-Irga6 axis, hereby the lipid-binding activity of RabGDI α is critical for IFN- γ -induced mGBP2-dependent cell-autonomous immunity against ME49 *T. gondii*. RabGDI α deficiency is accompanied by increased recruitment of mGBP2 and Irga6 to the parasite in MEFs and macrophages and results in enhanced IFN- γ -mediated *T. gondii* clearance *in vitro* and *in vivo* (Ohshima et al., 2014). These studies suggest on the one hand GBPs as escorts for distinct anti-pathogenic factors en route to PVs, on the other hand that the recruitment of galectins and GBPs to the PVs might be mutually dependent as part of a coordinated host defence program. This is supported by the significantly increased *T. gondii* proliferation in IFN- γ stimulated Gal9 knockout 3T3 fibroblasts 22-24h post-infection indicating an important role of Gal9 in cell-autonomous *T. gondii* elimination. Studies using Gal3 knockout mice provided evidence that Gal3 is crucial in the experimental infection by *T. gondii* (Bernardes et al. 2006). Infection of Gal3 knockout mice with *T. gondii* resulted in an enhanced T_H1 immune response characterized by increased production of IL-12 by dendritic cells. Similarly, Gal3^{-/-} mice develop more severe pneumococcal pneumonia compared to wild-type mice. However, when recombinant Gal3 is administered to Gal3^{-/-} mice, it reduces the number of *Streptococcus pneumoniae* cell count in the blood and alleviates the severity of infection-induced sepsis (Farnworth et al., 2008). In contrast, IFN- γ -primed Gal3^{-/-} BMDMs restricted *Yersinia and Legionella* bacterial growth, similar to WT BMDMs (Feeley et al., 2017). Interestingly, Gal3 has been shown to have detrimental effects on fungal clearance. In contrast to WT mouse neutrophils, Gal3 knockout neutrophils exhibited enhanced ROS-dependent systemic killing of *Candida albicans*, resulting in reduced fungal burden, improved renal pathology, and lower mortality rates (Wu et al., 2017).

Thus, it might be speculated that the recognition of the lysed PV by Gal9 initiates the uptake of the parasite into autophagosomes or other degradation pathways as it was described for *Salmonella*, where GBPs promote LC3 recruitment via Gal8 (Meunier et al., 2014). Interestingly, *T. gondii* infected Gal3^{-/-} mice develop reduced inflammatory responses in many organs (Bernardes et al., 2006) and succumb to an intraperitoneal infection with *T. gondii* associated with a deficient influx of neutrophils and macrophages into the peritoneal cavity (Alves et al., 2010). Gal3 has been shown to inhibit the ROS-dependent killing of

Candida albicans by neutrophils (Wu et al., 2017) and attenuate the generation of ROS in neutrophils following *T. gondii* infection (Alves et al., 2010; Alves et al., 2013). Therefore, it is plausible that the impact of galectins on antibacterial autophagy is associated with the regulation of cellular ROS production. The function of Gal9 might be the non-redundant to Gal3 and Gal8 in parasitic degradation processes which will be addressed in the future in a Gal9-gene deficient mouse line.

The findings of this study indicate that mGBP2 acts as a scaffold organizing the cell autonomous immunity in concert with Gal9 and thus extends the understanding of molecular host responses in the control of intracellular parasites.

5 Outlook

The identification of additional proteins that interact with mGBP2 could provide valuable insights into the biological function of mGBP2 as part of the cellular response to IFN- γ stimulation in *T. gondii* infection model. These interacting partners could include IFN-induced cellular proteins as well as proteins from intracellular pathogens, such as various ROP kinases and GRA proteins. Improved conditions for immunoprecipitation experiments and subsequent mass spectrometry could be employed to identify these interaction partners. Of particular interest would be elucidating the molecular function of mGBP2 at the parasitophorous vacuole membrane (PVM) of *T. gondii*. Electron microscopic analyses and investigations of protein-membrane interactions using changes in membrane potential in an artificial system could verify a direct association of mGBPs with the *T. gondii* PV. Kinetic observations using live-cell imaging with a confocal laser scanning microscope could determine whether mGBP-positive vacuoles are disrupted during infection. A Gal9-deficient mouse model will be utilized to investigate the in vivo role of Gal9 during *T. gondii* infection. To further support the role of mGBP2 in host defence, it would be interesting to explore additional infection models involving intracellular pathogens. Parameters such as pathogen load and cytokine expression should be compared between mGBP2^{-/-} mice and wild-type animals.

6 Zusammenfassung

Guanylat-bindende Proteine (GBPs) sind eine Familie von großen Interferon-induzierbaren GTPasen, die wichtige Abwehrfunktionen gegen eine Vielzahl intrazellulärer mikrobieller Pathogene ausüben. *Toxoplasma gondii* ist ein invasiver intrazellulärer Apicomplexa-Protozoen-Parasit von globaler Bedeutung. *T. gondii* bildet eine parasitophore Vakuole (PV), die den Parasiten vor den intrazellulären Abwehrmechanismen des Wirtes schützt. Murine GBPs (mGBPs) erkennen die PVs von *T. gondii* und lagern sich zu supramolekularen mGBP-Homo- und Heterokomplexen zusammen, die für die Zerstörung der PV-Membran notwendig sind, was schließlich zur zellautonomen Immunabwehr gegen Pathogene in der Vakuole führt. mGBP2 spielt in Interaktion mit mGBP1 und mGBP3 eine wichtige Rolle in der Immunkontrolle von *T. gondii*. Hier berichten wir über Galectin-9 (Gal9) als wichtigen Interaktionspartner von mGBP2, der für die Immunität gegen *T. gondii* verantwortlich ist. Interessanterweise akkumuliert und kolokalisiert Gal9 mit mGBP2 an der PV von *T. gondii*. Darüber hinaus konnten wir durch CRISPR/Cas9-vermitteltes Gene-Editing zeigen, dass Gal9 für die Wachstumskontrolle von *T. gondii* erforderlich ist. Diese Entdeckungen weisen eindeutig darauf hin, dass Gal9 ein kritischer Faktor für den mGBP2-koordinierten zellulären Immunabwehrmechanismus gegen *T. gondii* ist.

6 Summary

Guanylate binding proteins (GBPs) are a family of large interferon-inducible GTPases that execute essential host defence activities against a wide variety of intracellular microbial pathogens. *Toxoplasma gondii* is an invasive intracellular apicomplexan protozoan parasite of global importance. *T. gondii* establishes a parasitophorous vacuole (PV) that shields the parasite from the host's intracellular defence mechanisms. Murine GBPs (mGBPs) recognise *T. gondii* PVs and assemble into supramolecular mGBP homo- and heterocomplexes that are required for PV membrane disruption eventually resulting in the cell-autonomous immune control of vacuole-resident pathogens. mGBP2, which interacts with mGBP1 and mGBP3, plays an important role in *T. gondii* immune control. To unravel the functions of mGBP2, we report here that galectin-9 (Gal9) is a critical mGBP2 interaction partner involved in immunity to *T. gondii*. Interestingly, Gal9 also accumulates and colocalizes with mGBP2 at the *T. gondii* PV. Furthermore, we demonstrated that Gal9 is required for *T. gondii* growth control by CRISPR/Cas9 mediated gene editing. These discoveries clearly indicate that Gal9 is a critical factor for the mGBP2 coordinated cell autonomous host defence mechanism against *T. gondii*.

7 List of references

- Abbas, A.K., Lichtman, A.H. and von Saunders, S.P. 2007. Cellular and Molecular Immunology.
- Abdullah, N., M. Balakumari, and A.K. Sau. 2010. Dimerization and its role in GMP formation by human guanylate binding proteins. *Biophys J* 99:2235-2244.
- Abreu, R., L. Essler, P. Giri, and F. Quinn. 2020. Interferon-gamma promotes iron export in human macrophages to limit intracellular bacterial replication. *PLoS One* 15:e0240949.
- Adams, L.B., J.B. Hibbs, Jr., R.R. Taintor, and J.L. Krahenbuhl. 1990. Microbiostatic effect of murine-activated macrophages for *Toxoplasma gondii*. Role for synthesis of inorganic nitrogen oxides from L-arginine. *J Immunol* 144:2725-2729.
- Ahmadian, M.R., P. Stege, K. Scheffzek, and A. Wittinghofer. 1997. Confirmation of the arginine-finger hypothesis for the GAP-stimulated GTP-hydrolysis reaction of Ras. *Nat Struct Biol* 4:686-689.
- Ajzenberg, D. 2015. 1995-2015: it is time to celebrate 20 years of (intensive) genotyping of *Toxoplasma gondii* strains. *Future Microbiol* 10:689-691.
- Ajzenberg, D., A.L. Banuls, C. Su, A. Dumetre, M. Demar, B. Carme, and M.L. Darde. 2004. Genetic diversity, clonality and sexuality in *Toxoplasma gondii*. *Int J Parasitol* 34:1185-1196.
- Al-Zeer, M.A., H.M. Al-Younes, D. Lauster, M. Abu Lubad, and T.F. Meyer. 2013. Autophagy restricts *Chlamydia trachomatis* growth in human macrophages via IFNG- inducible guanylate binding proteins. *Autophagy* 9:50-62.
- Alexander, W.S., R. Starr, J.E. Fenner, C.L. Scott, E. Handman, N.S. Sprigg, J.E. Corbin, A.L. Cornish, R. Darwiche, C.M. Owczarek, T.W. Kay, N.A. Nicola, P.J. Hertzog, D. Metcalf, and D.J. Hilton. 1999. SOCS1 is a critical inhibitor of interferon gamma signaling and prevents the potentially fatal neonatal actions of this cytokine. *Cell* 98:597-608.
- Aliberti, J. 2005. Host persistence: exploitation of anti-inflammatory pathways by *Toxoplasma gondii*. *Nat Rev Immunol* 5:162-170.
- Aliberti, J., C. Serhan, and A. Sher. 2002. Parasite-induced lipoxin A4 is an endogenous regulator of IL-12 production and immunopathology in *Toxoplasma gondii* infection. *J Exp Med* 196:1253-1262.
- Aliberti, J., J.G. Valenzuela, V.B. Carruthers, S. Hieny, J. Andersen, H. Charest, C. Reis e Sousa, A. Fairlamb, J.M. Ribeiro, and A. Sher. 2003. Molecular mimicry of a CCR5 binding-domain in the microbial activation of dendritic cells. *Nat Immunol* 4:485-490.
- Alves, C.M., D.A. Silva, A.E. Azzolini, C.M. Marzocchi-Machado, J.V. Carvalho, A.C. Pajuaba, Y.M. Lucisano-Valim, R. Chammas, F.T. Liu, M.C. Roque-Barreira, and J.R. Mineo. 2010. Galectin-3 plays a modulatory role in the life span and activation of murine neutrophils during early *Toxoplasma gondii* infection. *Immunobiology* 215:475-485.
- Alves, C.M., D.A. Silva, A.E. Azzolini, C.M. Marzocchi-Machado, Y.M. Lucisano-Valim, M.C. Roque-Barreira, and J.R. Mineo. 2013. Galectin-3 is essential for reactive

- oxygen species production by peritoneal neutrophils from mice infected with a virulent strain of *Toxoplasma gondii*. *Parasitology* 140:210-219.
- An, R., Y. Tang, L. Chen, H. Cai, D.H. Lai, K. Liu, L. Wan, L. Gong, L. Yu, Q. Luo, J. Shen, Z.R. Lun, F.J. Ayala, and J. Du. 2018. Encephalitis is mediated by ROP18 of *Toxoplasma gondii*, a severe pathogen in AIDS patients. *Proc Natl Acad Sci U S A* 115:E5344-E5352.
- Anderson, P., Y.K. Yip, and J. Vilcek. 1983. Human interferon-gamma is internalized and degraded by cultured fibroblasts. *J Biol Chem* 258:6497-6502.
- Anderson, S.L., J.M. Carton, X. Zhang, and B.Y. Rubin. 1999. Genomic organization and chromosomal localization of a new member of the murine interferon-induced guanylate-binding protein family. *Journal of Interferon and Cytokine Research* 19:487-494.
- Antinori, A., D. Larussa, A. Cingolani, P. Lorenzini, S. Bossolasco, M.G. Finazzi, M. Bongiovanni, G. Guaraldi, S. Grisetti, B. Vigo, B. Gigli, A. Mariano, E.R. Dalle Nogare, M. De Marco, F. Moretti, P. Corsi, N. Abrescia, P. Rellecati, A. Castagna, C. Mussini, A. Ammassari, P. Cinque, A. d'Arminio Monforte, and A. Italian Registry Investigative Neuro. 2004. Prevalence, associated factors, and prognostic determinants of AIDS-related toxoplasmic encephalitis in the era of advanced highly active antiretroviral therapy. *Clin Infect Dis* 39:1681-1691.
- Asundi, V.K., R.C. Stahl, L. Showalter, K.J. Conner, and D.J. Carey. 1994. Molecular cloning and characterization of an isoprenylated 67 kDa protein. *Biochim Biophys Acta* 1217:257-265.
- Aviles, H., J. Stiles, P. O'Donnell, J. Orshal, J. Leid, G. Sonnenfeld, and F. Monroy. 2008. Kinetics of systemic cytokine and brain chemokine gene expression in murine toxoplasma infection. *J Parasitol* 94:1282-1288.
- Ayoade, F., and A.S. Joel Chandranesan. 2023. HIV-1 Associated Toxoplasmosis. In StatPearls. Treasure Island (FL).
- Bach, E.A., M. Aguet, and R.D. Schreiber. 1997. The IFN gamma receptor: a paradigm for cytokine receptor signaling. *Annu Rev Immunol* 15:563-591.
- Baird, N.L., J.L. Bowlin, T.J. Hotz, R.J. Cohrs, and D. Gilden. 2015. Interferon Gamma Prolongs Survival of Varicella-Zoster Virus-Infected Human Neurons In Vitro. *J Virol* 89:7425-7427.
- Bancroft, G.J., R.D. Schreiber, and E.R. Unanue. 1991. Natural immunity: a T-cell-independent pathway of macrophage activation, defined in the scid mouse. *Immunol Rev* 124:5-24.
- Barragan, A., and L.D. Sibley. 2002. Transepithelial migration of *Toxoplasma gondii* is linked to parasite motility and virulence. *J Exp Med* 195:1625-1633.
- Barragan, A., and L.D. Sibley. 2003. Migration of *Toxoplasma gondii* across biological barriers. *Trends Microbiol* 11:426-430.
- Bates, S.R. 2010. P63 (CKAP4) as an SP-A receptor: implications for surfactant turnover. *Cell Physiol Biochem* 25:41-54.
- Batistatou, A., D. Stefanou, E. Arkoumani, and N.J. Agnantis. 2003. The usefulness of p63 as a marker of breast myoepithelial cells. *In Vivo* 17:573-576.

- Beatty, W.L., E.R. Rhoades, D.K. Hsu, F.T. Liu, and D.G. Russell. 2002. Association of a macrophage galactoside-binding protein with Mycobacterium-containing phagosomes. *Cell Microbiol* 4:167-176.
- Beekhuizen, H., and J.S. van de Gevel. 2007. Gamma interferon confers resistance to infection with Staphylococcus aureus in human vascular endothelial cells by cooperative proinflammatory and enhanced intrinsic antibacterial activities. *Infect Immun* 75:5615-5626.
- Behnke, M.S., A. Khan, J.C. Wootton, J.P. Dubey, K. Tang, and L.D. Sibley. 2011. Virulence differences in Toxoplasma mediated by amplification of a family of polymorphic pseudokinases. *Proc Natl Acad Sci U S A* 108:9631-9636.
- Behnke, M.S., J.C. Wootton, M.M. Lehmann, J.B. Radke, O. Lucas, J. Nawas, L.D. Sibley, and M.W. White. 2010. Coordinated progression through two subtranscriptomes underlies the tachyzoite cycle of Toxoplasma gondii. *PLoS One* 5:e12354.
- Bekpen, C., J.P. Hunn, C. Rohde, I. Parvanova, L. Guethlein, D.M. Dunn, E. Glowalla, M. Leptin, and J.C. Howard. 2005. The interferon-inducible p47 (IRG) GTPases in vertebrates: loss of the cell autonomous resistance mechanism in the human lineage. *Genome Biology* 6:
- Bekpen, C., T. Marques-Bonet, C. Alkan, F. Antonacci, M.B. Leogrande, M. Ventura, J.M. Kidd, P. Siswara, J.C. Howard, and E.E. Eichler. 2009. Death and resurrection of the human IRGM gene. *PLoS Genet* 5:e1000403.
- Belkaid, Y., and B.T. Rouse. 2005. Natural regulatory T cells in infectious disease. *Nat Immunol* 6:353-360.
- Belluco, S., G. Simonato, M. Mancin, M. Pietrobelli, and A. Ricci. 2018. Toxoplasma gondii infection and food consumption: A systematic review and meta-analysis of case-controlled studies. *Crit Rev Food Sci Nutr* 58:3085-3096.
- Benard, A., E. Petersen, R. Salamon, G. Chene, R. Gilbert, L.R. Salmi, and G. European Toxo Prevention Study. 2008. Survey of European programmes for the epidemiological surveillance of congenital toxoplasmosis. *Euro Surveill* 13:
- Bernardes, E.S., N.M. Silva, L.P. Ruas, J.R. Mineo, A.M. Loyola, D.K. Hsu, F.T. Liu, R. Chammas, and M.C. Roque-Barreira. 2006. Toxoplasma gondii infection reveals a novel regulatory role for galectin-3 in the interface of innate and adaptive immunity. *Am J Pathol* 168:1910-1920.
- Bernhard, M.C., A. Zwick, T. Mohr, G. Gasparoni, O. Khalmurzaev, V.B. Matveev, P. Loertzer, A. Pryalukhin, A. Hartmann, C.I. Geppert, H. Loertzer, H. Wunderlich, C.M. Naumann, H. Kalthoff, K. Junker, S. Smola, and S. Lohse. 2021. The HPV and p63 Status in Penile Cancer Are Linked with the Infiltration and Therapeutic Availability of Neutrophils. *Mol Cancer Ther* 20:423-437.
- Bhat, N., A. Joe, M. PereiraPerrin, and H.D. Ward. 2007. Cryptosporidium p30, a galactose/N-acetylgalactosamine-specific lectin, mediates infection in vitro. *J Biol Chem* 282:34877-34887.
- Biering, S.B., J. Choi, R.A. Halstrom, H.M. Brown, W.L. Beatty, S. Lee, B.T. McCune, E. Dominici, L.E. Williams, R.C. Orchard, C.B. Wilen, M. Yamamoto, J. Coers, G.A. Taylor, and S. Hwang. 2017. Viral Replication Complexes Are Targeted by LC3-Guided Interferon-Inducible GTPases. *Cell Host Microbe* 22:74-85 e77.

- Black, M.W., and J.C. Boothroyd. 2000. Lytic cycle of *Toxoplasma gondii*. *Microbiol Mol Biol Rev* 64:607-623.
- Blader, I.J., B.I. Coleman, C.T. Chen, and M.J. Gubbels. 2015. Lytic Cycle of *Toxoplasma gondii*: 15 Years Later. *Annu Rev Microbiol* 69:463-485.
- Blader, I.J., and J.P. Saeij. 2009. Communication between *Toxoplasma gondii* and its host: impact on parasite growth, development, immune evasion, and virulence. *APMIS* 117:458-476.
- Bluyssen, H.A., R. Muzaffar, R.J. Vlieststra, A.C. van der Made, S. Leung, G.R. Stark, I.M. Kerr, J. Trapman, and D.E. Levy. 1995. Combinatorial association and abundance of components of interferon-stimulated gene factor 3 dictate the selectivity of interferon responses. *Proc Natl Acad Sci U S A* 92:5645-5649.
- Boehm, U., L. Guethlein, T. Klamp, K. Ozbek, A. Schaub, A. Futterer, K. Pfeffer, and J.C. Howard. 1998. Two families of GTPases dominate the complex cellular response to IFN-gamma. *Journal of Immunology* 161:6715-6723.
- Boehm, U., T. Klamp, M. Groot, and J.C. Howard. 1997. Cellular responses to interferon-gamma. *Annual Review of Immunology* 15:749-795.
- Bogdan, C., J. Mattner, and U. Schleicher. 2004. The role of type I interferons in non-viral infections. *Immunol Rev* 202:33-48.
- Boguski, M.S., and F. McCormick. 1993. Proteins regulating Ras and its relatives. *Nature* 366:643-654.
- Bohne, W., U. Gross, D.J. Ferguson, and J. Heesemann. 1995. Cloning and characterization of a bradyzoite-specifically expressed gene (*hsp30/bag1*) of *Toxoplasma gondii*, related to genes encoding small heat-shock proteins of plants. *Mol Microbiol* 16:1221-1230.
- Bollineni, R.C., C.J. Koehler, R.E. Gislefoss, J.H. Anonsen, and B. Thiede. 2018. Large-scale intact glycopeptide identification by Mascot database search. *Sci Rep* 8:2117.
- Boothroyd, J.C., and M.E. Grigg. 2002. Population biology of *Toxoplasma gondii* and its relevance to human infection: do different strains cause different disease? *Curr Opin Microbiol* 5:438-442.
- Boothroyd, J.C., A. Hehl, L.J. Knoll, and I.D. Manger. 1998. The surface of *Toxoplasma*: more and less. *Int J Parasitol* 28:3-9.
- Bourne, H.R. 1995. GTPases: a family of molecular switches and clocks. *Philos Trans R Soc Lond B Biol Sci* 349:283-289.
- Bourne, H.R. 1997. G proteins. The arginine finger strikes again. *Nature* 389:673-674.
- Bourne, H.R., D.A. Sanders, and F. McCormick. 1991. The GTPase superfamily: conserved structure and molecular mechanism. *Nature* 349:117-127.
- Bourne, H.R., L. Wrischnik, and C. Kenyon. 1990. Ras proteins. Some signal developments. *Nature* 348:678-679.
- Boyle, J.P., B. Rajasekar, J.P.J. Saeij, J.W. Ajioka, M. Berriman, I. Paulsen, D.S. Roos, L.D. Sibley, M.W. White, and J.C. Boothroyd. 2006. Just one cross appears capable of dramatically altering the population biology of a eukaryotic pathogen like *Toxoplasma gondii*. *Proc Natl Acad Sci U S A* 103:10514-10519.
- Boyle, K.B., and F. Randow. 2013. The role of 'eat-me' signals and autophagy cargo receptors in innate immunity. *Curr Opin Microbiol* 16:339-348.

- Braun, L., M.P. Brenier-Pinchart, M. Yogavel, A. Curt-Varesano, R.L. Curt-Bertini, T. Hussain, S. Kieffer-Jaquinod, Y. Coute, H. Pelloux, I. Tardieux, A. Sharma, H. Belrhali, A. Bougdour, and M.A. Hakimi. 2013. A *Toxoplasma dense granule* protein, GRA24, modulates the early immune response to infection by promoting a direct and sustained host p38 MAPK activation. *J Exp Med* 210:2071-2086.
- Briken, V., H. Ruffner, U. Schultz, A. Schwarz, L.F. Reis, I. Strehlow, T. Decker, and P. Staeheli. 1995. Interferon regulatory factor 1 is required for mouse Gbp gene activation by gamma interferon. *Mol Cell Biol* 15:975-982.
- Britzen-Laurent, N., M. Bauer, V. Berton, N. Fischer, A. Syguda, S. Reipschlager, E. Naschberger, C. Herrmann, and M. Sturzl. 2010. Intracellular Trafficking of Guanylate-Binding Proteins Is Regulated by Heterodimerization in a Hierarchical Manner. *Plos One* 5:
- Brunet, J., A.W. Pfaff, A. Abidi, M. Unoki, Y. Nakamura, M. Guinard, J.P. Klein, E. Candolfi, and M. Mousli. 2008. *Toxoplasma gondii* exploits UHRF1 and induces host cell cycle arrest at G2 to enable its proliferation. *Cell Microbiol* 10:908-920.
- Butcher, B.A., B.A. Fox, L.M. Rommereim, S.G. Kim, K.J. Maurer, F. Yarovinsky, D.R. Herbert, D.J. Bzik, and E.Y. Denkers. 2011. *Toxoplasma gondii* rhoptry kinase ROP16 activates STAT3 and STAT6 resulting in cytokine inhibition and arginase-1-dependent growth control. *PLoS Pathog* 7:e1002236.
- Butcher, B.A., R.I. Greene, S.C. Henry, K.L. Annecharico, J.B. Weinberg, E.Y. Denkers, A. Sher, and G.A. Taylor. 2005. p47 GTPases regulate *Toxoplasma gondii* survival in activated macrophages. *Infect Immun* 73:3278-3286.
- Butcher, B.A., L. Kim, P.F. Johnson, and E.Y. Denkers. 2001. *Toxoplasma gondii* tachyzoites inhibit proinflammatory cytokine induction in infected macrophages by preventing nuclear translocation of the transcription factor NF-kappa B. *J Immunol* 167:2193-2201.
- Buxton, D., K.M. Thomson, S. Maley, S. Wright, and H.J. Bos. 1993. Experimental challenge of sheep 18 months after vaccination with a live (S48) *Toxoplasma gondii* vaccine. *Vet Rec* 133:310-312.
- Caamano, J., J. Alexander, L. Craig, R. Bravo, and C.A. Hunter. 1999. The NF-kappa B family member RelB is required for innate and adaptive immunity to *Toxoplasma gondii*. *J Immunol* 163:4453-4461.
- Cai, G., R. Kastelein, and C.A. Hunter. 2000. Interleukin-18 (IL-18) enhances innate IL-12-mediated resistance to *Toxoplasma gondii*. *Infect Immun* 68:6932-6938.
- Canon-Franco, W.A., N. Lopez-Orozco, J.E. Gomez-Marin, and J.P. Dubey. 2014. An overview of seventy years of research (1944-2014) on toxoplasmosis in Colombia, South America. *Parasit Vectors* 7:427.
- Carlsson, S., C.T. Oberg, M.C. Carlsson, A. Sundin, U.J. Nilsson, D. Smith, R.D. Cummings, J. Almkvist, A. Karlsson, and H. Leffler. 2007. Affinity of galectin-8 and its carbohydrate recognition domains for ligands in solution and at the cell surface. *Glycobiology* 17:663-676.
- Carmen, J.C., L. Hardi, and A.P. Sinai. 2006. *Toxoplasma gondii* inhibits ultraviolet light-induced apoptosis through multiple interactions with the mitochondrion-dependent programmed cell death pathway. *Cell Microbiol* 8:301-315.

- Carruthers, V.B. 1999. Armed and dangerous: *Toxoplasma gondii* uses an arsenal of secretory proteins to infect host cells. *Parasitol Int* 48:1-10.
- Carruthers, V.B., and J.C. Boothroyd. 2007. Pulling together: an integrated model of *Toxoplasma* cell invasion. *Current Opinion in Microbiology* 10:82-89.
- Carruthers, V.B., and L.D. Sibley. 1997. Sequential protein secretion from three distinct organelles of *Toxoplasma gondii* accompanies invasion of human fibroblasts. *Eur J Cell Biol* 73:114-123.
- Carruthers, V.B., and F.M. Tomley. 2008. Microneme proteins in apicomplexans. *Subcell Biochem* 47:33-45.
- Carter, C.C., V.Y. Gorbacheva, and D.J. Vestal. 2005. Inhibition of VSV and EMCV replication by the interferon-induced GTPase, mGBP-2: differential requirement for wild-type GTP binding domain. *Archives of Virology* 150:1213-1220.
- Casals, C., M.A. Campanero-Rhodes, B. Garcia-Fojeda, and D. Solis. 2018. The Role of Collectins and Galectins in Lung Innate Immune Defense. *Front Immunol* 9:1998.
- Cerliani, J.P., A.G. Blidner, M.A. Toscano, D.O. Croci, and G.A. Rabinovich. 2017. Translating the 'Sugar Code' into Immune and Vascular Signaling Programs. *Trends Biochem Sci* 42:255-273.
- Charron, A.J., and L.D. Sibley. 2004. Molecular partitioning during host cell penetration by *Toxoplasma gondii*. *Traffic* 5:855-867.
- Chauhan, S., S. Kumar, A. Jain, M. Ponpuak, M.H. Mudd, T. Kimura, S.W. Choi, R. Peters, M. Mandell, J.A. Bruun, T. Johansen, and V. Deretic. 2016. TRIMs and Galectins Globally Cooperate and TRIM16 and Galectin-3 Co-direct Autophagy in Endomembrane Damage Homeostasis. *Dev Cell* 39:13-27.
- Chaussabel, D., R.T. Semnani, M.A. McDowell, D. Sacks, A. Sher, and T.B. Nutman. 2003. Unique gene expression profiles of human macrophages and dendritic cells to phylogenetically distinct parasites. *Blood* 102:672-681.
- Chen, H.Y., I.C. Weng, M.H. Hong, and F.T. Liu. 2014. Galectins as bacterial sensors in the host innate response. *Curr Opin Microbiol* 17:75-81.
- Chen, J., E. Baig, and E.N. Fish. 2004. Diversity and relatedness among the type I interferons. *J Interferon Cytokine Res* 24:687-698.
- Chen, L., D.A. Christian, J.A. Kochanowsky, A.T. Phan, J.T. Clark, S. Wang, C. Berry, J. Oh, X. Chen, D.S. Roos, D.P. Beiting, A.A. Koshy, and C.A. Hunter. 2020. The *Toxoplasma gondii* virulence factor ROP16 acts in cis and trans, and suppresses T cell responses. *J Exp Med* 217:
- Chen, M., L. Yao, L. Zhou, P. Yang, W. Zou, L. Xu, S. Li, and H. Peng. 2022. *Toxoplasma gondii* ROP18(I) inhibits host innate immunity through cGAS-STING signaling. *FASEB J* 36:e22171.
- Cheng, Y.S., R.J. Colonno, and F.H. Yin. 1983. Interferon induction of fibroblast proteins with guanylate binding activity. *J Biol Chem*. 258:7746-7750.
- Cheng, Y.S., C.E. Patterson, and P. Staeheli. 1991. Interferon-induced guanylate-binding proteins lack an N(T)KXD consensus motif and bind GMP in addition to GDP and GTP. *Mol Cell Biol* 11:4717-4725.
- Cho, S.W., S. Kim, J.M. Kim, and J.S. Kim. 2013. Targeted genome engineering in human cells with the Cas9 RNA-guided endonuclease. *Nat Biotechnol* 31:230-232.

- Choi, J., S.B. Biering, and S. Hwang. 2017. Quo vadis? Interferon-inducible GTPases go to their target membranes via the LC3-conjugation system of autophagy. *Small GTPases* 8:199-207.
- Christoph, J., E. Kattner, H.M. Seitz, and I. Reiter-Owona. 2004. [Strategies for the diagnosis and treatment of prenatal toxoplasmosis - a survey]. *Z Geburtshilfe Neonatol* 208:10-16.
- Cirelli, K.M., G. Gorfu, M.A. Hassan, M. Printz, D. Crown, S.H. Leppla, M.E. Grigg, J.P. Saeij, and M. Moayeri. 2014. Inflammasome sensor NLRP1 controls rat macrophage susceptibility to *Toxoplasma gondii*. *PLoS Pathog* 10:e1003927.
- Coers, J. 2013. Self and Non-self Discrimination of Intracellular Membranes by the Innate Immune System. *Plos Pathogens* 9:
- Coers, J. 2017. Sweet host revenge: Galectins and GBPs join forces at broken membranes. *Cell Microbiol* 19:
- Coers, J., I. Bernstein-Hanley, D. Grotzky, I. Parvanova, J.C. Howard, G.A. Taylor, W.F. Dietrich, and M.N. Starnbach. 2008. Chlamydia muridarum evades growth restriction by the IFN-gamma-inducible host resistance factor Irgb10. *J Immunol* 180:6237-6245.
- Coers, J., H.M. Brown, S. Hwang, and G.A. Taylor. 2018. Partners in anti-crime: how interferon-inducible GTPases and autophagy proteins team up in cell-intrinsic host defense. *Curr Opin Immunol* 54:93-101.
- Cohen, S.N., A.C. Chang, and L. Hsu. 1972. Nonchromosomal antibiotic resistance in bacteria: genetic transformation of *Escherichia coli* by R-factor DNA. *Proc Natl Acad Sci U S A* 69:2110-2114.
- Coleman, D.E., A.M. Berghuis, E. Lee, M.E. Linder, A.G. Gilman, and S.R. Sprang. 1994. Structures of active conformations of Gi alpha 1 and the mechanism of GTP hydrolysis. *Science* 265:1405-1412.
- Collazo, C.M., G.S. Yap, G.D. Sempowski, K.C. Lusby, L. Tessarollo, G.F.V. Woude, A. Sher, and G.A. Taylor. 2001. Inactivation of LRG-47 and IRG-47 reveals a family of interferon gamma-inducible genes with essential, pathogen-specific roles in resistance to infection. *Journal of Experimental Medicine* 194:181-187.
- Cooper, A.M., D.K. Dalton, T.A. Stewart, J.P. Griffin, D.G. Russell, and I.M. Orme. 1993. Disseminated tuberculosis in interferon gamma gene-disrupted mice. *J Exp Med* 178:2243-2247.
- Cooper, D., L.V. Norling, and M. Perretti. 2008. Novel insights into the inhibitory effects of Galectin-1 on neutrophil recruitment under flow. *J Leukoc Biol* 83:1459-1466.
- Coppens, I., J.D. Dunn, J.D. Romano, M. Pypaert, H. Zhang, J.C. Boothroyd, and K.A. Joiner. 2006. *Toxoplasma gondii* sequesters lysosomes from mammalian hosts in the vacuolar space. *Cell* 125:261-274.
- Crawford, M.J., N. Thomsen-Zieger, M. Ray, J. Schachtner, D.S. Roos, and F. Seeber. 2006. *Toxoplasma gondii* scavenges host-derived lipoic acid despite its de novo synthesis in the apicoplast. *EMBO J* 25:3214-3222.
- Creasey, E.A., and R.R. Isberg. 2012. The protein SdhA maintains the integrity of the *Legionella*-containing vacuole. *Proc Natl Acad Sci U S A* 109:3481-3486.
- Cristina, N., M.L. Darde, C. Boudin, G. Tavernier, M. Pestre-Alexandre, and P. Ambroise-Thomas. 1995. A DNA fingerprinting method for individual characterization of

- Toxoplasma gondii strains: combination with isoenzymatic characters for determination of linkage groups. *Parasitol Res* 81:32-37.
- Curdt, I., G. Praast, E. Sickinger, J. Schultess, I. Herold, H.B. Braun, S. Bernhardt, G.T. Maine, D.D. Smith, S. Hsu, H.M. Christ, D. Pucci, M. Hausmann, and J. Herzogenrath. 2009. Development of fully automated determination of marker-specific immunoglobulin G (IgG) avidity based on the avidity competition assay format: application for Abbott Architect cytomegalovirus and Toxo IgG Avidity assays. *J Clin Microbiol* 47:603-613.
- da Cunha Correia, C., H. Ramos Lacerda, V.M. de Assis Costa, and A. Mertens de Queiroz Brainer. 2012. Cerebral toxoplasmosis: unusual MRI findings. *Clin Imaging* 36:462-465.
- da Silva, A.A., T.L. Teixeira, S.C. Teixeira, F.C. Machado, M.A. Dos Santos, T.C. Tomiosso, P.C.B. Tavares, R. Brigido, F.A. Martins, N.S.L. Silva, C.C. Rodrigues, M.C. Roque-Barreira, R.A. Mortara, D.S. Lopes, V.M.R. Avila, and C.V. da Silva. 2017. Galectin-3: A Friend but Not a Foe during Trypanosoma cruzi Experimental Infection. *Front Cell Infect Microbiol* 7:463.
- Dalton, D.K., S. Pitts-Meek, S. Keshav, I.S. Figari, A. Bradley, and T.A. Stewart. 1993. Multiple defects of immune cell function in mice with disrupted interferon-gamma genes. *Science* 259:1739-1742.
- Darde, M.L., B. Bouteille, and M. Pestre-Alexandre. 1992. Isoenzyme analysis of 35 Toxoplasma gondii isolates and the biological and epidemiological implications. *J Parasitol* 78:786-794.
- Daubener, W., V. Posdziech, U. Hadding, and C.R. MacKenzie. 1999. Inducible anti-parasitic effector mechanisms in human uroepithelial cells: tryptophan degradation vs. NO production. *Med Microbiol Immunol* 187:143-147.
- Daubener, W., B. Spors, C. Hucke, R. Adam, M. Stins, K.S. Kim, and H. Schrotten. 2001. Restriction of Toxoplasma gondii growth in human brain microvascular endothelial cells by activation of indoleamine 2,3-dioxygenase. *Infect Immun* 69:6527-6531.
- Daugherty, M.D., and H.S. Malik. 2012. Rules of engagement: molecular insights from host-virus arms races. *Annu Rev Genet* 46:677-700.
- Day, P.M., C.D. Thompson, D.R. Lowy, and J.T. Schiller. 2017. Interferon Gamma Prevents Infectious Entry of Human Papillomavirus 16 via an L2-Dependent Mechanism. *J Virol* 91:
- de Souza, W. 2005. Microscopy and cytochemistry of the biogenesis of the parasitophorous vacuole. *Histochem Cell Biol* 123:1-18.
- Debierre-Grockiego, F., M.A. Campos, N. Azzouz, J. Schmidt, U. Bieker, M.G. Resende, D.S. Mansur, R. Weingart, R.R. Schmidt, D.T. Golenbock, R.T. Gazzinelli, and R.T. Schwarz. 2007. Activation of TLR2 and TLR4 by glycosylphosphatidylinositols derived from Toxoplasma gondii. *J Immunol* 179:1129-1137.
- Debierre-Grockiego, F., S. Niehus, B. Coddeville, E. Ellass, F. Poirier, R. Weingart, R.R. Schmidt, J. Mazurier, Y. Guerardel, and R.T. Schwarz. 2010. Binding of Toxoplasma gondii glycosylphosphatidylinositols to galectin-3 is required for their recognition by macrophages. *J Biol Chem* 285:32744-32750.

- Degrandi, D., R. Hoffmann, C. Beuter-Gunia, and K. Pfeffer. 2009. The proinflammatory cytokine-induced IRG1 protein associates with mitochondria. *J Interferon Cytokine Res* 29:55-67.
- Degrandi, D., C. Konermann, C. Beuter-Gunia, A. Kresse, J. Wurthner, S. Kurig, S. Beer, and K. Pfeffer. 2007. Extensive characterization of IFN-induced GTPases mGBP1 to mGBP10 involved in host defense. *Journal of Immunology* 179:7729-7740.
- Degrandi, D., E. Kravets, C. Konermann, C. Beuter-Gunia, V. Klumpers, S. Lahme, E. Wischmann, A.K. Mausberg, S. Beer-Hammer, and K. Pfeffer. 2013. Murine Guanylate Binding Protein 2 (mGBP2) controls *Toxoplasma gondii* replication. *Proceedings of the National Academy of Sciences of the United States of America* 110:294-299.
- Denkers, E.Y. 1999. T lymphocyte-dependent effector mechanisms of immunity to *Toxoplasma gondii*. *Microbes Infect* 1:699-708.
- Denkers, E.Y., and B.A. Butcher. 2005. Sabotage and exploitation in macrophages parasitized by intracellular protozoans. *Trends Parasitol* 21:35-41.
- Denkers, E.Y., and R.T. Gazzinelli. 1998. Regulation and function of T-cell-mediated immunity during *Toxoplasma gondii* infection. *Clin Microbiol Rev* 11:569-588.
- Denzer, K., M.J. Kleijmeer, H.F. Heijnen, W. Stoorvogel, and H.J. Geuze. 2000. Exosome: from internal vesicle of the multivesicular body to intercellular signaling device. *J Cell Sci* 113 Pt 19:3365-3374.
- Du, J., R. An, L. Chen, Y. Shen, Y. Chen, L. Cheng, Z. Jiang, A. Zhang, L. Yu, D. Chu, Y. Shen, Q. Luo, H. Chen, L. Wan, M. Li, X. Xu, and J. Shen. 2022. Withdrawal: *Toxoplasma gondii* virulence factor ROP18 inhibits the host NF-kappaB pathway by promoting p65 degradation. *J Biol Chem* 298:102719.
- Duan, Z., R. Foster, K.A. Brakora, R.Z. Yusuf, and M.V. Seiden. 2006. GBP1 overexpression is associated with a paclitaxel resistance phenotype. *Cancer Chemother Pharmacol* 57:25-33.
- Dubey, J.P. 1987. Toxoplasmosis. *Vet Clin North Am Small Anim Pract* 17:1389-1404.
- Dubey, J.P. 2004. Toxoplasmosis - a waterborne zoonosis. *Vet Parasitol* 126:57-72.
- Dubey, J.P. 2009. History of the discovery of the life cycle of *Toxoplasma gondii*. *Int J Parasitol* 39:877-882.
- Dubey, J.P., and J.K. Frenkel. 1976. Feline toxoplasmosis from acutely infected mice and the development of *Toxoplasma* cysts. *J Protozool* 23:537-546.
- Dubey, J.P., D.S. Lindsay, and C.A. Speer. 1998. Structures of *Toxoplasma gondii* tachyzoites, bradyzoites, and sporozoites and biology and development of tissue cysts. *Clinical Microbiology Reviews* 11:267-+.
- Dubey, J.P., N.L. Miller, and J.K. Frenkel. 1970a. *Toxoplasma gondii* life cycle in cats. *J Am Vet Med Assoc* 157:1767-1770.
- Dubey, J.P., N.L. Miller, and J.K. Frenkel. 1970b. The *Toxoplasma gondii* oocyst from cat feces. *J Exp Med* 132:636-662.
- Dubey, J.P., K.D. Murrell, R. Fayer, and G.A. Schad. 1986. Distribution of *Toxoplasma gondii* tissue cysts in commercial cuts of pork. *J Am Vet Med Assoc* 188:1035-1037.
- Dubey, J.P., C.A. Speer, S.K. Shen, O.C. Kwok, and J.A. Blixt. 1997. Oocyst-induced murine toxoplasmosis: life cycle, pathogenicity, and stage conversion in mice fed *Toxoplasma gondii* oocysts. *J Parasitol* 83:870-882.

- El Hajj, H., M. Lebrun, S.T. Arold, H. Vial, G. Labesse, and J.F. Dubremetz. 2007. ROP18 is a rhoptry kinase controlling the intracellular proliferation of *Toxoplasma gondii*. *PLoS Pathog* 3:e14.
- Etheridge, R.D., A. Alaganan, K. Tang, H.J. Lou, B.E. Turk, and L.D. Sibley. 2014. The *Toxoplasma* pseudokinase ROP5 forms complexes with ROP18 and ROP17 kinases that synergize to control acute virulence in mice. *Cell Host Microbe* 15:537-550.
- Farnworth, S.L., N.C. Henderson, A.C. Mackinnon, K.M. Atkinson, T. Wilkinson, K. Dhaliwal, K. Hayashi, A.J. Simpson, A.G. Rossi, C. Haslett, and T. Sethi. 2008. Galectin-3 reduces the severity of pneumococcal pneumonia by augmenting neutrophil function. *Am J Pathol* 172:395-405.
- Farrar, M.A., and R.D. Schreiber. 1993. The molecular cell biology of interferon-gamma and its receptor. *Annu Rev Immunol* 11:571-611.
- Feeley, E.M., D.M. Pilla-Moffett, E.E. Zwack, A.S. Piro, R. Finethy, J.P. Kolb, J. Martinez, I.E. Brodsky, and J. Coers. 2017. Galectin-3 directs antimicrobial guanylate binding proteins to vacuoles furnished with bacterial secretion systems. *Proc Natl Acad Sci USA* 114:E1698-E1706.
- Feeley, E.M., J.S. Sims, S.P. John, C.R. Chin, T. Pertel, L.M. Chen, G.D. Gaiha, B.J. Ryan, R.O. Donis, S.J. Elledge, and A.L. Brass. 2011. IFITM3 inhibits influenza A virus infection by preventing cytosolic entry. *PLoS Pathog* 7:e1002337.
- Feener, E.P., F. Rosario, S.L. Dunn, Z. Stancheva, and M.G. Myers, Jr. 2004. Tyrosine phosphorylation of Jak2 in the JH2 domain inhibits cytokine signaling. *Mol Cell Biol* 24:4968-4978.
- Feng, S., D. Enosi Tuipulotu, A. Pandey, W. Jing, C. Shen, C. Ngo, M.B. Tessema, F.J. Li, D. Fox, A. Mathur, A. Zhao, R. Wang, K. Pfeffer, D. Degrandi, M. Yamamoto, P.C. Reading, G. Burgio, and S.M. Man. 2022. Pathogen-selective killing by guanylate-binding proteins as a molecular mechanism leading to inflammasome signaling. *Nat Commun* 13:4395.
- Ferguson, D.J. 2009. *Toxoplasma gondii*: 1908-2008, homage to Nicolle, Manceaux and Splendore. *Mem Inst Oswaldo Cruz* 104:133-148.
- Filipe-Santos, O., J. Bustamante, A. Chapgier, G. Vogt, L. de Beaucoudrey, J. Feinberg, E. Jouanguy, S. Boisson-Dupuis, C. Fieschi, C. Picard, and J.L. Casanova. 2006. Inborn errors of IL-12/23- and IFN-gamma-mediated immunity: molecular, cellular, and clinical features. *Semin Immunol* 18:347-361.
- Finethy, R., and J. Coers. 2016. Sensing the enemy, containing the threat: cell-autonomous immunity to *Chlamydia trachomatis*. *FEMS Microbiol Rev* 40:875-893.
- Finethy, R., I. Jorgensen, A.K. Haldar, M.R. de Zoete, T. Strowig, R.A. Flavell, M. Yamamoto, U.M. Nagarajan, E.A. Miao, and J. Coers. 2015. Guanylate binding proteins enable rapid activation of canonical and noncanonical inflammasomes in *Chlamydia*-infected macrophages. *Infect Immun* 83:4740-4749.
- Flannagan, R.S., G. Cosio, and S. Grinstein. 2009. Antimicrobial mechanisms of phagocytes and bacterial evasion strategies. *Nat Rev Microbiol* 7:355-366.
- Fountoulakis, M., M. Zulauf, A. Lustig, and G. Garotta. 1992. Stoichiometry of interaction between interferon gamma and its receptor. *Eur J Biochem* 208:781-787.

- Fowler, M., R.J. Thomas, J. Atherton, I.S. Roberts, and N.J. High. 2006. Galectin-3 binds to *Helicobacter pylori* O-antigen: it is upregulated and rapidly secreted by gastric epithelial cells in response to *H. pylori* adhesion. *Cell Microbiol* 8:44-54.
- Fox, B.A., J.P. Gigley, and D.J. Bzik. 2004. *Toxoplasma gondii* lacks the enzymes required for de novo arginine biosynthesis and arginine starvation triggers cyst formation. *Int J Parasitol* 34:323-331.
- Franck, J., Y.J. Garin, and H. Dumon. 2008. LDBio-Toxo II immunoglobulin G Western blot confirmatory test for anti-toxoplasma antibody detection. *J Clin Microbiol* 46:2334-2338.
- Frederick, J.R., and W.A. Petri, Jr. 2005. Roles for the galactose-/N-acetylgalactosamine-binding lectin of *Entamoeba* in parasite virulence and differentiation. *Glycobiology* 15:53R-59R.
- Frenkel, J.K., J.P. Dubey, and N.L. Miller. 1970. *Toxoplasma gondii* in cats: fecal stages identified as coccidian oocysts. *Science* 167:893-896.
- Fres, J.M., S. Muller, and G.J.K. Praefcke. 2010. Purification of the CaaX-modified, dynamin-related large GTPase hGBP1 by coexpression with farnesyltransferase. *Journal of Lipid Research* 51:2454-2459.
- Frucht, D.M., T. Fukao, C. Bogdan, H. Schindler, J.J. O'Shea, and S. Koyasu. 2001. IFN-gamma production by antigen-presenting cells: mechanisms emerge. *Trends Immunol* 22:556-560.
- Fuentes, I., J.M. Rubio, C. Ramirez, and J. Alvar. 2001. Genotypic characterization of *Toxoplasma gondii* strains associated with human toxoplasmosis in Spain: direct analysis from clinical samples. *J Clin Microbiol* 39:1566-1570.
- Fulcher, J.A., S.T. Hashimi, E.L. Levroney, M. Pang, K.B. Gurney, L.G. Baum, and B. Lee. 2006. Galectin-1-matured human monocyte-derived dendritic cells have enhanced migration through extracellular matrix. *J Immunol* 177:216-226.
- Gao, G., C. Zhu, E. Liu, and I.R. Nabi. 2019. Reticulon and CLIMP-63 regulate nanodomain organization of peripheral ER tubules. *PLoS Biol* 17:e3000355.
- Gao, P.Q., S.H. Sims, D.C. Chang, and A.B. Deisseroth. 1993. Interferon-gamma priming effects in the activation and deactivation of ISGF3 in K562 cells. *J Biol Chem* 268:12380-12387.
- Garcin, P.O., I.R. Nabi, and N. Pante. 2015. Galectin-3 plays a role in minute virus of mice infection. *Virology* 481:63-72.
- Garneau, J.E., M.E. Dupuis, M. Villion, D.A. Romero, R. Barrangou, P. Boyaval, C. Fremaux, P. Horvath, A.H. Magadan, and S. Moineau. 2010. The CRISPR/Cas bacterial immune system cleaves bacteriophage and plasmid DNA. *Nature* 468:67-71.
- Gay, G., L. Braun, M.P. Brenier-Pinchart, J. Vollaire, V. Josserand, R.L. Bertini, A. Varesano, B. Touquet, P.J. De Bock, Y. Coute, I. Tardieux, A. Bougdour, and M.A. Hakimi. 2016. *Toxoplasma gondii* TgIST co-opts host chromatin repressors dampening STAT1-dependent gene regulation and IFN-gamma-mediated host defenses. *J Exp Med* 213:1779-1798.
- Gazzinelli, R.T., S. Hieny, T.A. Wynn, S. Wolf, and A. Sher. 1993. Interleukin 12 is required for the T-lymphocyte-independent induction of interferon gamma by an

- intracellular parasite and induces resistance in T-cell-deficient hosts. *Proc Natl Acad Sci U S A* 90:6115-6119.
- Gazzinelli, R.T., C. Ropert, and M.A. Campos. 2004. Role of the Toll/interleukin-1 receptor signaling pathway in host resistance and pathogenesis during infection with protozoan parasites. *Immunol Rev* 201:9-25.
- Gazzinelli, R.T., M. Wysocka, S. Hieny, T. Scharton-Kersten, A. Cheever, R. Kuhn, W. Muller, G. Trinchieri, and A. Sher. 1996. In the absence of endogenous IL-10, mice acutely infected with *Toxoplasma gondii* succumb to a lethal immune response dependent on CD4⁺ T cells and accompanied by overproduction of IL-12, IFN- γ and TNF- α . *J Immunol* 157:798-805.
- Geyer, M., T. Schweins, C. Herrmann, T. Prisner, A. Wittinghofer, and H.R. Kalbitzer. 1996. Conformational transitions in p21ras and in its complexes with the effector protein Raf-RBD and the GTPase activating protein GAP. *Biochemistry* 35:10308-10320.
- Ghosh, A., G.J.K. Praefcke, L. Renault, A. Wittinghofer, and C. Herrmann. 2006. How guanylate-binding proteins achieve assembly-stimulated processive cleavage of GTP to GMP. *Nature* 440:101-104.
- Gilbert, L.A., S. Ravindran, J.M. Turetzky, J.C. Boothroyd, and P.J. Bradley. 2007. *Toxoplasma gondii* targets a protein phosphatase 2C to the nuclei of infected host cells. *Eukaryot Cell* 6:73-83.
- Goebel, S., U. Gross, and C.G. Luder. 2001. Inhibition of host cell apoptosis by *Toxoplasma gondii* is accompanied by reduced activation of the caspase cascade and alterations of poly(ADP-ribose) polymerase expression. *J Cell Sci* 114:3495-3505.
- Gorbacheva, V.Y., D. Lindner, G.C. Sen, and D.J. Vestal. 2002. The interferon (IFN)-induced GTPase, mGBP-2. Role in IFN- γ -induced murine fibroblast proliferation. *J Biol Chem* 277:6080-6087.
- Gorfu, G., K.M. Cirelli, M.B. Melo, K. Mayer-Barber, D. Crown, B.H. Koller, S. Masters, A. Sher, S.H. Leppla, M. Moayeri, J.P.J. Saeij, and M.E. Grigg. 2014. Dual Role for Inflammasome Sensors NLRP1 and NLRP3 in Murine Resistance to *Toxoplasma gondii*. *Mbio* 5:
- Graham, M.B., D.K. Dalton, D. Giltinan, V.L. Braciale, T.A. Stewart, and T.J. Braciale. 1993. Response to influenza infection in mice with a targeted disruption in the interferon gamma gene. *J Exp Med* 178:1725-1732.
- Gras, L., R.E. Gilbert, M. Wallon, F. Peyron, and M. Cortina-Borja. 2004. Duration of the IgM response in women acquiring *Toxoplasma gondii* during pregnancy: implications for clinical practice and cross-sectional incidence studies. *Epidemiol Infect* 132:541-548.
- Green, A.M., R. Difazio, and J.L. Flynn. 2013. IFN- γ from CD4 T cells is essential for host survival and enhances CD8 T cell function during *Mycobacterium tuberculosis* infection. *J Immunol* 190:270-277.
- Greenlund, A.C., M.A. Farrar, B.L. Viviano, and R.D. Schreiber. 1994. Ligand-induced IFN gamma receptor tyrosine phosphorylation couples the receptor to its signal transduction system (p91). *EMBO J* 13:1591-1600.

- Greenlund, A.C., R.D. Schreiber, D.V. Goeddel, and D. Pennica. 1993. Interferon-gamma induces receptor dimerization in solution and on cells. *J Biol Chem* 268:18103-18110.
- Gregg, B., B.C. Taylor, B. John, E.D. Tait-Wojno, N.M. Girgis, N. Miller, S. Wagage, D.S. Roos, and C.A. Hunter. 2013. Replication and distribution of *Toxoplasma gondii* in the small intestine after oral infection with tissue cysts. *Infect Immun* 81:1635-1643.
- Grube, L., R. Dellen, F. Kruse, H. Schwender, K. Stuhler, and G. Poschmann. 2018. Mining the Secretome of C2C12 Muscle Cells: Data Dependent Experimental Approach To Analyze Protein Secretion Using Label-Free Quantification and Peptide Based Analysis. *J Proteome Res* 17:879-890.
- Gubbels, M.J., C.D. Keroack, S. Dangoudoubiyam, H.L. Worliczek, A.S. Paul, C. Bauwens, B. Elsworth, K. Engelberg, D.K. Howe, I. Coppens, and M.T. Duraisingh. 2020. Fussing About Fission: Defining Variety Among Mainstream and Exotic Apicomplexan Cell Division Modes. *Front Cell Infect Microbiol* 10:269.
- Guenzi, E., K. Topolt, E. Cornali, C. Lubeseder-Martellato, A. Jorg, K. Matzen, C. Zietz, E. Kremmer, F. Nappi, M. Schwemmle, C. Hohenadl, G. Barillari, E. Tschachler, P. Monini, B. Ensoli, and M. Sturzl. 2001. The helical domain of GBP-1 mediates the inhibition of endothelial cell proliferation by inflammatory cytokines. *EMBO J* 20:5568-5577.
- Guenzi, E., K. Topolt, C. Lubeseder-Martellato, A. Jorg, E. Naschberger, R. Benelli, A. Albini, and M. Sturzl. 2003. The guanylate binding protein-1 GTPase controls the invasive and angiogenic capability of endothelial cells through inhibition of MMP-1 expression. *Embo Journal* 22:3772-3782.
- Gupta, N., Y. Manevich, A.S. Kazi, J.Q. Tao, A.B. Fisher, and S.R. Bates. 2006. Identification and characterization of p63 (CKAP4/ERGIC-63/CLIMP-63), a surfactant protein A binding protein, on type II pneumocytes. *American Journal of Physiology-Lung Cellular and Molecular Physiology* 291:L436-L446.
- Gupta, N., M.M. Zahn, I. Coppens, K.A. Joiner, and D.R. Voelker. 2005. Selective disruption of phosphatidylcholine metabolism of the intracellular parasite *Toxoplasma gondii* arrests its growth. *J Biol Chem* 280:16345-16353.
- Gupta, S.L., B.Y. Rubin, and S.L. Holmes. 1979. Interferon action: induction of specific proteins in mouse and human cells by homologous interferons. *Proc Natl Acad Sci USA* 76:4817-4821.
- Hager, K.M., and V.B. Carruthers. 2008. MARveling at parasite invasion. *Trends Parasitol* 24:51-54.
- Hakansson, S., A.J. Charron, and L.D. Sibley. 2001. *Toxoplasma* vacuoles: a two-step process of secretion and fusion forms the parasitophorous vacuole. *Embo Journal* 20:3132-3144.
- Haldar, A.K., C. Foltz, R. Finethy, A.S. Piro, E.M. Feeley, D.M. Pilla-Moffett, M. Komatsu, E.M. Frickel, and J. Coers. 2015. Ubiquitin systems mark pathogen-containing vacuoles as targets for host defense by guanylate binding proteins. *Proceedings of the National Academy of Sciences of the United States of America* 112:E5628-E5637.

- Haldar, A.K., A.S. Piro, R. Finethy, S.T. Espenschied, H.E. Brown, A.M. Giebel, E.M. Frickel, D.E. Nelson, and J. Coers. 2016. Chlamydia trachomatis Is Resistant to Inclusion Ubiquitination and Associated Host Defense in Gamma Interferon-Primed Human Epithelial Cells. *mBio* 7:
- Haldar, A.K., A.S. Piro, D.M. Pilla, M. Yamamoto, and J. Coers. 2014. The E2-Like Conjugation Enzyme Atg3 Promotes Binding of IRG and Gbp Proteins to Chlamydia- and Toxoplasma-Containing Vacuoles and Host Resistance. *Plos One* 9:
- Haldar, A.K., H.A. Saka, A.S. Piro, J.D. Dunn, S.C. Henry, G.A. Taylor, E.M. Frickel, R.H. Valdivia, and J.R. Coers. 2013. IRG and GBP Host Resistance Factors Target Aberrant, "Non-self" Vacuoles Characterized by the Missing of "Self" IRGM Proteins. *Plos Pathogens* 9:
- Haller, O., S. Stertz, and G. Kochs. 2007. The Mx GTPase family of interferon-induced antiviral proteins. *Microbes and Infection* 9:1636-1643.
- Halonen, S.K., G.A. Taylor, and L.M. Weiss. 2001. Gamma interferon-induced inhibition of Toxoplasma gondii in astrocytes is mediated by IGTP. *Infect Immun* 69:5573-5576.
- Halonen, S.K., and E. Weidner. 1994. Overcoating of Toxoplasma parasitophorous vacuoles with host cell vimentin type intermediate filaments. *J Eukaryot Microbiol* 41:65-71.
- Halonen, S.K., and L.M. Weiss. 2013. Toxoplasmosis. *Handb Clin Neurol* 114:125-145.
- Han, B.H., D.J. Park, R.W. Lim, J.H. Im, and H.D. Kim. 1998. Cloning, expression, and characterization of a novel guanylate-binding protein, GBP3 in murine erythroid progenitor cells. *Biochim Biophys Acta* 1384:373-386.
- Hanahan, D., and M. Meselson. 1983. Plasmid screening at high colony density. *Methods Enzymol* 100:333-342.
- Hatakeyama, S. 2017. TRIM Family Proteins: Roles in Autophagy, Immunity, and Carcinogenesis. *Trends Biochem Sci* 42:297-311.
- Haudek, K.C., K.J. Spronk, P.G. Voss, R.J. Patterson, J.L. Wang, and E.J. Arnoys. 2010. Dynamics of galectin-3 in the nucleus and cytoplasm. *Biochim Biophys Acta* 1800:181-189.
- Hayes, M.P., J. Wang, and M.A. Norcross. 1995. Regulation of interleukin-12 expression in human monocytes: selective priming by interferon-gamma of lipopolysaccharide-inducible p35 and p40 genes. *Blood* 86:646-650.
- Hedman, K., M. Lappalainen, I. Seppaia, and O. Makela. 1989. Recent primary toxoplasma infection indicated by a low avidity of specific IgG. *J Infect Dis* 159:736-740.
- Heim, M.H., I.M. Kerr, G.R. Stark, and J.E. Darnell, Jr. 1995. Contribution of STAT SH2 groups to specific interferon signaling by the Jak-STAT pathway. *Science* 267:1347-1349.
- Hernandez, A.V., P. Thota, D. Pellegrino, V. Pasupuleti, V.A. Benites-Zapata, A. Deshpande, A.C. Penalva de Oliveira, and J.E. Vidal. 2017. A systematic review and meta-analysis of the relative efficacy and safety of treatment regimens for HIV-associated cerebral toxoplasmosis: is trimethoprim-sulfamethoxazole a real option? *HIV Med* 18:115-124.

- Heufler, C., F. Koch, U. Stanzl, G. Topar, M. Wysocka, G. Trinchieri, A. Enk, R.M. Steinman, N. Romani, and G. Schuler. 1996. Interleukin-12 is produced by dendritic cells and mediates T helper 1 development as well as interferon-gamma production by T helper 1 cells. *Eur J Immunol* 26:659-668.
- Heukeshoven, J., and R. Dernick. 1988. Improved silver staining procedure for fast staining in PhastSystem Development Unit. I. Staining of sodium dodecyl sulfate gels. *Electrophoresis* 9:28-32.
- Hill, D.E., S. Chirukandoth, and J.P. Dubey. 2005. Biology and epidemiology of *Toxoplasma gondii* in man and animals. *Anim Health Res Rev* 6:41-61.
- Hotop, A., H. Hlobil, and U. Gross. 2012. Efficacy of rapid treatment initiation following primary *Toxoplasma gondii* infection during pregnancy. *Clin Infect Dis* 54:1545-1552.
- Hou, B., A. Benson, L. Kuzmich, A.L. DeFranco, and F. Yarovinsky. 2011. Critical coordination of innate immune defense against *Toxoplasma gondii* by dendritic cells responding via their Toll-like receptors. *Proc Natl Acad Sci U S A* 108:278-283.
- Howe, D.K., S. Honore, F. Derouin, and L.D. Sibley. 1997. Determination of genotypes of *Toxoplasma gondii* strains isolated from patients with toxoplasmosis. *J Clin Microbiol* 35:1411-1414.
- Howe, D.K., and L.D. Sibley. 1995. *Toxoplasma gondii* comprises three clonal lineages: correlation of parasite genotype with human disease. *J Infect Dis* 172:1561-1566.
- Howe, D.K., B.C. Summers, and L.D. Sibley. 1996. Acute virulence in mice is associated with markers on chromosome VIII in *Toxoplasma gondii*. *Infect Immun* 64:5193-5198.
- Hu, X., and L.B. Ivashkiv. 2009. Cross-regulation of signaling pathways by interferon-gamma: implications for immune responses and autoimmune diseases. *Immunity* 31:539-550.
- Huang, R.P., J.X. Wu, Y. Fan, and E.D. Adamson. 1996. UV activates growth factor receptors via reactive oxygen intermediates. *J Cell Biol* 133:211-220.
- Huang, S., W. Hendriks, A. Althage, S. Hemmi, H. Bluethmann, R. Kamijo, J. Vilcek, R.M. Zinkernagel, and M. Aguet. 1993. Immune response in mice that lack the interferon-gamma receptor. *Science* 259:1742-1745.
- Huang, S., Q. Meng, A. Maminska, and J.D. MacMicking. 2019. Cell-autonomous immunity by IFN-induced GBPs in animals and plants. *Curr Opin Immunol* 60:71-80.
- Huett, A., R.J. Heath, J. Begun, S.O. Sassi, L.A. Baxt, J.M. Vyas, M.B. Goldberg, and R.J. Xavier. 2012. The LRR and RING Domain Protein LRSAM1 Is an E3 Ligase Crucial for Ubiquitin-Dependent Autophagy of Intracellular *Salmonella Typhimurium*. *Cell Host & Microbe* 12:778-790.
- Hunn, J.P., C.G. Feng, A. Sher, and J.C. Howard. 2011. The immunity-related GTPases in mammals: a fast-evolving cell-autonomous resistance system against intracellular pathogens. *Mamm Genome* 22:43-54.
- Hunter, C.A., R. Chizzonite, and J.S. Remington. 1995. IL-1 beta is required for IL-12 to induce production of IFN-gamma by NK cells. A role for IL-1 beta in the T cell-

- independent mechanism of resistance against intracellular pathogens. *J Immunol* 155:4347-4354.
- Hunter, C.A., and L.D. Sibley. 2012. Modulation of innate immunity by *Toxoplasma gondii* virulence effectors. *Nature Reviews Microbiology* 10:766-778.
- Hwang, I.Y., J.H. Quan, M.H. Ahn, H.A. Ahmed, G.H. Cha, D.W. Shin, and Y.H. Lee. 2010. *Toxoplasma gondii* infection inhibits the mitochondrial apoptosis through induction of Bcl-2 and HSP70. *Parasitol Res* 107:1313-1321.
- Igarashi, K., G. Garotta, L. Ozmen, A. Ziemiecki, A.F. Wilks, A.G. Harpur, A.C. Lerner, and D.S. Finbloom. 1994. Interferon-gamma induces tyrosine phosphorylation of interferon-gamma receptor and regulated association of protein tyrosine kinases, Jak1 and Jak2, with its receptor. *J Biol Chem* 269:14333-14336.
- Innes, E.A. 2010. Vaccination against *Toxoplasma gondii*: an increasing priority for collaborative research? *Expert Rev Vaccines* 9:1117-1119.
- Innes, E.A., C. Hamilton, J.L. Garcia, A. Chryssafidis, and D. Smith. 2019. A one health approach to vaccines against *Toxoplasma gondii*. *Food Waterborne Parasitol* 15:e00053.
- Jabado, N., A. Jankowski, S. Dougaparsad, V. Picard, S. Grinstein, and P. Gros. 2000. Natural resistance to intracellular infections: natural resistance-associated macrophage protein 1 (Nramp1) functions as a pH-dependent manganese transporter at the phagosomal membrane. *J Exp Med* 192:1237-1248.
- Jankovic, D., M.C. Kullberg, C.G. Feng, R.S. Goldszmid, C.M. Collazo, M. Wilson, T.A. Wynn, M. Kamanaka, R.A. Flavell, and A. Sher. 2007. Conventional T-bet(+)Foxp3(-) Th1 cells are the major source of host-protective regulatory IL-10 during intracellular protozoan infection. *J Exp Med* 204:273-283.
- Jia, J., Y.P. Abudu, A. Claude-Taupin, Y. Gu, S. Kumar, S.W. Choi, R. Peters, M.H. Mudd, L. Allers, M. Salemi, B. Phinney, T. Johansen, and V. Deretic. 2018. Galectins Control mTOR in Response to Endomembrane Damage. *Mol Cell* 70:120-135 e128.
- Johnston, A.C., A. Piro, B. Clough, M. Siew, S. Virreira Winter, J. Coers, and E.M. Frickel. 2016. Human GBP1 does not localize to pathogen vacuoles but restricts *Toxoplasma gondii*. *Cell Microbiol* 18:1056-1064.
- Joiner, K.A., and D.S. Roos. 2002. Secretory traffic in the eukaryotic parasite *Toxoplasma gondii*: less is more. *J Cell Biol* 157:557-563.
- Jones, J., A. Lopez, and M. Wilson. 2003. Congenital toxoplasmosis. *Am Fam Physician* 67:2131-2138.
- Jones, J.L., D. Kruszon-Moran, M. Wilson, G. McQuillan, T. Navin, and J.B. McAuley. 2001. *Toxoplasma gondii* infection in the United States: seroprevalence and risk factors. *Am J Epidemiol* 154:357-365.
- Jones, L.A., J. Alexander, and C.W. Roberts. 2006. Ocular toxoplasmosis: in the storm of the eye. *Parasite Immunol* 28:635-642.
- Jongert, E., C.W. Roberts, N. Gargano, E. Forster-Waldl, and E. Petersen. 2009. Vaccines against *Toxoplasma gondii*: challenges and opportunities. *Mem Inst Oswaldo Cruz* 104:252-266.
- Jorgovanovic, D., M. Song, L. Wang, and Y. Zhang. 2020. Roles of IFN-gamma in tumor progression and regression: a review. *Biomark Res* 8:49.

- Jouanguy, E., R. Doffinger, S. Dupuis, A. Pallier, F. Altare, and J.L. Casanova. 1999. IL-12 and IFN-gamma in host defense against mycobacteria and salmonella in mice and men. *Curr Opin Immunol* 11:346-351.
- Kang, K.M., G.S. Lee, J.H. Lee, I.W. Choi, D.W. Shin, and Y.H. Lee. 2004. Effects of iNOS inhibitor on IFN-gamma production and apoptosis of splenocytes in genetically different strains of mice infected with *Toxoplasma gondii*. *Korean J Parasitol* 42:175-183.
- Karaghiosoff, M., H. Neubauer, C. Lassnig, P. Kovarik, H. Schindler, H. Pircher, B. McCoy, C. Bogdan, T. Decker, G. Brem, K. Pfeffer, and M. Muller. 2000. Partial impairment of cytokine responses in Tyk2-deficient mice. *Immunity* 13:549-560.
- Karlsson, A., P. Follin, H. Leffler, and C. Dahlgren. 1998. Galectin-3 activates the NADPH-oxidase in exudated but not peripheral blood neutrophils. *Blood* 91:3430-3438.
- Kashio, Y., K. Nakamura, M.J. Abedin, M. Seki, N. Nishi, N. Yoshida, T. Nakamura, and M. Hirashima. 2003. Galectin-9 induces apoptosis through the calcium-calpain-caspase-1 pathway. *Journal of Immunology* 170:3631-3636.
- Kasper, L.H. 1989. Identification of stage-specific antigens of *Toxoplasma gondii*. *Infect Immun* 57:668-672.
- Kerr, I.M., and G.R. Stark. 1991. The control of interferon-inducible gene expression. *FEBS Lett* 285:194-198.
- Khaminets, A., J.P. Hunn, S. Konen-Waisman, Y.O. Zhao, D. Preukschat, J. Coers, J.P. Boyle, Y.C. Ong, J.C. Boothroyd, G. Reichmann, and J.C. Howard. 2010. Coordinated loading of IRG resistance GTPases on to the *Toxoplasma gondii* parasitophorous vacuole. *Cellular Microbiology* 12:939-961.
- Kikuchi, A., K. Fumoto, and H. Kimura. 2017. The Dickkopf1-cytoskeleton-associated protein 4 axis creates a novel signalling pathway and may represent a molecular target for cancer therapy. *Br J Pharmacol* 174:4651-4665.
- Kim, B.H., J.D. Chee, C.J. Bradfield, E.S. Park, P. Kumar, and J.D. MacMicking. 2016. Interferon-induced guanylate-binding proteins in inflammasome activation and host defense. *Nat Immunol* 17:481-489.
- Kim, B.H., A.R. Shenoy, P. Kumar, R. Das, S. Tiwari, and J.D. MacMicking. 2011. A Family of IFN-gamma-Inducible 65-kD GTPases Protects Against Bacterial Infection. *Science* 332:717-721.
- Kim, K., and L.M. Weiss. 2004. *Toxoplasma gondii*: the model apicomplexan. *Int J Parasitol* 34:423-432.
- Kim, K., and L.M. Weiss. 2008. *Toxoplasma*: the next 100years. *Microbes Infect* 10:978-984.
- Kim, S.K., A.E. Fouts, and J.C. Boothroyd. 2007. *Toxoplasma gondii* dysregulates IFN-gamma-inducible gene expression in human fibroblasts: insights from a genome-wide transcriptional profiling. *J Immunol* 178:5154-5165.
- Kimura, H., K. Fumoto, K. Shojima, S. Nojima, Y. Osugi, H. Tomihara, H. Eguchi, Y. Shintani, H. Endo, M. Inoue, Y. Doki, M. Okumura, E. Morii, and A. Kikuchi. 2016. CKAP4 is a Dickkopf1 receptor and is involved in tumor progression. *J Clin Invest* 126:2689-2705.

- Kinsella, B.T., R.A. Erdman, and W.A. Maltese. 1991. Posttranslational modification of Ha-ras p21 by farnesyl versus geranylgeranyl isoprenoids is determined by the COOH-terminal amino acid. *Proc Natl Acad Sci U S A* 88:8934-8938.
- Kleshchenko, Y.Y., T.N. Moody, V.A. Furtak, J. Ochieng, M.F. Lima, and F. Villalta. 2004. Human galectin-3 promotes Trypanosoma cruzi adhesion to human coronary artery smooth muscle cells. *Infect Immun* 72:6717-6721.
- Klibi, J., T. Niki, A. Riedel, C. Pioche-Durieu, S. Souquere, E. Rubinstein, S. Le Moulec, J. Guigay, M. Hirashima, F. Guemira, D. Adhikary, J. Mautner, and P. Busson. 2009. Blood diffusion and Th1-suppressive effects of galectin-9-containing exosomes released by Epstein-Barr virus-infected nasopharyngeal carcinoma cells. *Blood* 113:1957-1966.
- Knight, E., Jr., and B.D. Korant. 1979. Fibroblast interferon induces synthesis of four proteins in human fibroblast cells. *Proc Natl Acad Sci U S A* 76:1824-1827.
- Kochanowsky, J.A., K.K. Thomas, and A.A. Koshy. 2021. ROP16-Mediated Activation of STAT6 Suppresses Host Cell Reactive Oxygen Species Production, Facilitating Type III Toxoplasma gondii Growth and Survival. *mBio* 12:
- Kokordelis, P., B. Kramer, C. Korner, C. Boesecke, E. Voigt, P. Ingiliz, A. Glassner, M. Eisenhardt, F. Wolter, D. Kaczmarek, H.D. Nischalke, J.K. Rockstroh, U. Spengler, and J. Nattermann. 2014. An effective interferon-gamma-mediated inhibition of hepatitis C virus replication by natural killer cells is associated with spontaneous clearance of acute hepatitis C in human immunodeficiency virus-positive patients. *Hepatology* 59:814-827.
- Konen-Waisman, S., and J.C. Howard. 2007. Cell-autonomous immunity to Toxoplasma gondii in mouse and man. *Microbes Infect* 9:1652-1661.
- Konermann, C. 2008. Die Rolle der IFN-gamma induzierten 65 kDa Guanylat-bindenden Proteine mGBP1 bis mGBP5 als Effektmoleküle bei der Erregerabwehr. In Heinrich-Heine University Düsseldorf.**
- Konermann, C., A. Kresse, C. Beuter-Gunia, J. Wurthner, D. Degrandi, K. Pfeffer, and S. Beer. 2007. In silico and in vitro characterization of mGBP4 splice variants. *DNA Cell Biol* 26:847-851.
- Koo, G.C., and Y.H. Gan. 2006. The innate interferon gamma response of BALB/c and C57BL/6 mice to in vitro Burkholderia pseudomallei infection. *BMC Immunol* 7:19.
- Krapp, C., D. Hotter, A. Gawanbacht, P.J. McLaren, S.F. Kluge, C.M. Sturzel, K. Mack, E. Reith, S. Engelhart, A. Ciuffi, V. Hornung, D. Sauter, A. Telenti, and F. Kirchhoff. 2016. Guanylate Binding Protein (GBP) 5 Is an Interferon-Inducible Inhibitor of HIV-1 Infectivity. *Cell Host Microbe* 19:504-514.
- Kravets, D.E. 2012. Charakterisierung des murinen Guanylat-bindenden Proteins 2 (mGBP2). In Heinrich-Heine University Düsseldorf.
- Kravets, E., D. Degrandi, Q. Ma, T.O. Peulen, V. Klumpers, S. Felekyan, R. Kuhnemuth, S. Weidtkamp-Peters, C.A. Seidel, and K. Pfeffer. 2016. Guanylate binding proteins directly attack Toxoplasma gondii via supramolecular complexes. *Elife* 5:
- Kravets, E., D. Degrandi, S. Weidtkamp-Peters, B. Ries, C. Konermann, S. Felekyan, J.M. Dargazanli, G.J.K. Praefcke, C.A.M. Seidel, L. Schmitt, S.H.J. Smits, and K. Pfeffer. 2012. The GTPase Activity of Murine Guanylate-binding Protein 2 (mGBP2)

- Controls the Intracellular Localization and Recruitment to the Parasitophorous Vacuole of *Toxoplasma gondii*. *Journal of Biological Chemistry* 287:27452-27466.
- Kresse, A., C. Konermann, D. Degrandi, C. Beuter-Gunia, J. Wuerthner, K. Pfeffer, and S. Beer. 2008. Analyses of murine GBP homology clusters based on in silico, in vitro and in vivo studies. *Bmc Genomics* 9:
- Kroemer, G., and B. Levine. 2008. Autophagic cell death: the story of a misnomer. *Nat Rev Mol Cell Biol* 9:1004-1010.
- Kunzelmann, S., G.J. Praefcke, and C. Herrmann. 2005. Nucleotide binding and self-stimulated GTPase activity of human guanylate-binding protein 1 (hGBP1). *Methods Enzymol* 404:512-527.
- Kunzelmann, S., G.J. Praefcke, and C. Herrmann. 2006. Transient kinetic investigation of GTP hydrolysis catalyzed by interferon-gamma-induced hGBP1 (human guanylate binding protein 1). *J Biol Chem* 281:28627-28635.
- Laliberte, J., and V.B. Carruthers. 2008. Host cell manipulation by the human pathogen *Toxoplasma gondii*. *Cellular and Molecular Life Sciences* 65:1900-1915.
- Lambert, H., I. Dellacasa-Lindberg, and A. Barragan. 2011. Migratory responses of leukocytes infected with *Toxoplasma gondii*. *Microbes Infect* 13:96-102.
- Lang, C., M. Algner, N. Beinert, U. Gross, and C.G. Luder. 2006. Diverse mechanisms employed by *Toxoplasma gondii* to inhibit IFN-gamma-induced major histocompatibility complex class II gene expression. *Microbes Infect* 8:1994-2005.
- Lang, C., U. Gross, and C.G. Luder. 2007. Subversion of innate and adaptive immune responses by *Toxoplasma gondii*. *Parasitol Res* 100:191-203.
- Lederer, J.A., V.L. Perez, L. DesRoches, S.M. Kim, A.K. Abbas, and A.H. Lichtman. 1996. Cytokine transcriptional events during helper T cell subset differentiation. *J Exp Med* 184:397-406.
- Legewie, L., J. Loschwitz, N. Steffens, M. Prescher, X. Wang, S.H.J. Smits, L. Schmitt, B. Strodel, D. Degrandi, and K. Pfeffer. 2019. Biochemical and structural characterization of murine GBP7, a guanylate binding protein with an elongated C-terminal tail. *Biochem J* 476:3161-3182.
- Lekutis, C., D.J. Ferguson, M.E. Grigg, M. Camps, and J.C. Boothroyd. 2001. Surface antigens of *Toxoplasma gondii*: variations on a theme. *Int J Parasitol* 31:1285-1292.
- Li, G., J. Zhang, Y. Sun, H. Wang, and Y. Wang. 2009. The evolutionarily dynamic IFN-inducible GTPase proteins play conserved immune functions in vertebrates and cephalochordates. *Mol Biol Evol* 26:1619-1630.
- Li, K., L. Yao, J. Wang, H. Song, Y.H. Zhang, X. Bai, K. Zhang, D.M. Zhou, D. Ai, and Y. Zhu. 2022. SARS-CoV-2 Spike protein promotes vWF secretion and thrombosis via endothelial cytoskeleton-associated protein 4 (CKAP4). *Signal Transduct Target Ther* 7:332.
- Li, P., Q. Du, Z. Cao, Z. Guo, J. Evankovich, W. Yan, Y. Chang, L. Shao, D.B. Stolz, A. Tsung, and D.A. Geller. 2012. Interferon-gamma induces autophagy with growth inhibition and cell death in human hepatocellular carcinoma (HCC) cells through interferon-regulatory factor-1 (IRF-1). *Cancer Lett* 314:213-222.
- Li, P., W. Jiang, Q. Yu, W. Liu, P. Zhou, J. Li, J. Xu, B. Xu, F. Wang, and F. Shao. 2017. Ubiquitination and degradation of GBPs by a *Shigella* effector to suppress host defence. *Nature* 551:378-383.

- Li, S.X., J. Li, L.W. Dong, and Z.Y. Guo. 2020. Cytoskeleton-Associated Protein 4, a Promising Biomarker for Tumor Diagnosis and Therapy. *Front Mol Biosci* 7:552056.
- Li, Y., M. Komai-Koma, D.S. Gilchrist, D.K. Hsu, F.T. Liu, T. Springall, and D. Xu. 2008. Galectin-3 is a negative regulator of lipopolysaccharide-mediated inflammation. *J Immunol* 181:2781-2789.
- Lilue, J., U.B. Muller, T. Steinfeldt, and J.C. Howard. 2013. Reciprocal virulence and resistance polymorphism in the relationship between *Toxoplasma gondii* and the house mouse. *Elife* 2:e01298.
- Lima, T.S., and M.B. Lodoen. 2019. Mechanisms of Human Innate Immune Evasion by *Toxoplasma gondii*. *Front Cell Infect Microbiol* 9:103.
- Lindenberg, V., K. Molleken, E. Kravets, S. Stallmann, J.H. Hegemann, D. Degrandi, and K. Pfeffer. 2017. Broad recruitment of mGBP family members to Chlamydia trachomatis inclusions. *PLoS One* 12:e0185273.
- Ling, Y.M., M.H. Shaw, C. Ayala, I. Coppens, G.A. Taylor, D.J. Ferguson, and G.S. Yap. 2006. Vacuolar and plasma membrane stripping and autophagic elimination of *Toxoplasma gondii* in primed effector macrophages. *J.Exp.Med.* 203:2063-2071.
- Lingelbach, K., and K.A. Joiner. 1998. The parasitophorous vacuole membrane surrounding Plasmodium and Toxoplasma: an unusual compartment in infected cells. *J Cell Sci* 111 (Pt 11):1467-1475.
- Liu, F.T., R.J. Patterson, and J.L. Wang. 2002. Intracellular functions of galectins. *Biochim Biophys Acta* 1572:263-273.
- Liu, F.T., and G.A. Rabinovich. 2010. Galectins: regulators of acute and chronic inflammation. *Ann N Y Acad Sci* 1183:158-182.
- Lubeseder-Martellato, C., E. Guenzi, A. Jorg, K. Topolt, E. Naschberger, E. Kremmer, C. Zietz, E. Tschachler, P. Hutzler, M. Schwemmler, K. Matzen, T. Grimm, B. Ensoli, and M. Sturzl. 2002. Guanylate-binding protein-1 expression is selectively induced by inflammatory cytokines and is an activation marker of endothelial cells during inflammatory diseases. *Am J Pathol* 161:1749-1759.
- Lubitz, F.P., D. Degrandi, K. Pfeffer, and A.K. Mausberg. 2013. In Astrocytes the Accumulation of the Immunity-Related GTPases Irga6 and Irgb6 at the Vacuole of *Toxoplasma gondii* Is Dependent on the Parasite Virulence. *Scientific World Journal*
- Luder, C.G., M. Algnier, C. Lang, N. Bleicher, and U. Gross. 2003. Reduced expression of the inducible nitric oxide synthase after infection with *Toxoplasma gondii* facilitates parasite replication in activated murine macrophages. *Int J Parasitol* 33:833-844.
- Luder, C.G., T. Lang, B. Beuerle, and U. Gross. 1998. Down-regulation of MHC class II molecules and inability to up-regulate class I molecules in murine macrophages after infection with *Toxoplasma gondii*. *Clin Exp Immunol* 112:308-316.
- Luder, C.G., and F. Seeber. 2001. *Toxoplasma gondii* and MHC-restricted antigen presentation: on degradation, transport and modulation. *Int J Parasitol* 31:1355-1369.
- Luder, C.G., W. Walter, B. Beuerle, M.J. Maeurer, and U. Gross. 2001. *Toxoplasma gondii* down-regulates MHC class II gene expression and antigen presentation by murine

- macrophages via interference with nuclear translocation of STAT1alpha. *Eur J Immunol* 31:1475-1484.
- Luder, C.G.K., and T. Rahman. 2017. Impact of the host on Toxoplasma stage differentiation. *Microb Cell* 4:203-211.
- Luft, B.J., and J.S. Remington. 1992. Toxoplasmic encephalitis in AIDS. *Clin Infect Dis* 15:211-222.
- Luo, M., Y.J. Chen, Y. Xie, Q.R. Wang, Y.N. Xiang, N.Y. Long, W.X. Yang, Y. Zhao, and J.J. Zhou. 2022. Dickkopf-related protein 1/cytoskeleton-associated protein 4 signaling activation by Helicobacter pylori-induced activator protein-1 promotes gastric tumorigenesis via the PI3K/AKT/mTOR pathway. *World J Gastroenterol* 28:6769-6787.
- Macatonia, S.E., N.A. Hosken, M. Litton, P. Vieira, C.S. Hsieh, J.A. Culpepper, M. Wysocka, G. Trinchieri, K.M. Murphy, and A. O'Garra. 1995. Dendritic cells produce IL-12 and direct the development of Th1 cells from naive CD4+ T cells. *J Immunol* 154:5071-5079.
- MacMicking, J.D. 2004. IFN-inducible GTPases and immunity to intracellular pathogens. *Trends Immunol* 25:601-609.
- MacMicking, J.D. 2012. Interferon-inducible effector mechanisms in cell-autonomous immunity. *Nature Reviews Immunology* 12:367-382.
- MacMicking, J.D., G.A. Taylor, and J.D. McKinney. 2003. Immune control of tuberculosis by IFN-gamma-inducible LRG-47. *Science* 302:654-659.
- Maenz, M., D. Schluter, O. Liesenfeld, G. Schares, U. Gross, and U. Pleyer. 2014. Ocular toxoplasmosis past, present and new aspects of an old disease. *Prog Retin Eye Res* 39:77-106.
- Magi, B., and L. Migliorini. 2011. Western blotting for the diagnosis of congenital toxoplasmosis. *New Microbiol* 34:93-95.
- Man, S.M., R. Karki, R.K.S. Malireddi, G. Neale, P. Vogel, M. Yamamoto, M. Lamkanfi, and T.D. Kanneganti. 2015. The transcription factor IRF1 and guanylate-binding proteins target activation of the AIM2 inflammasome by Francisella infection. *Nature Immunology* 16:467-U174.
- Mandelbrot, L., F. Kieffer, R. Sitta, H. Laurichesse-Delmas, N. Winer, L. Mesnard, A. Berrebi, G. Le Bouar, J.P. Bory, A.G. Cordier, Y. Ville, F. Perrotin, J.M. Jouannic, F. Biquard, C. d'Ercole, V. Houfflin-Debarge, I. Villena, R. Thiebaut, and T.S. Group. 2018. Prenatal therapy with pyrimethamine + sulfadiazine vs spiramycin to reduce placental transmission of toxoplasmosis: a multicenter, randomized trial. *Am J Obstet Gynecol* 219:386 e381-386 e389.
- Mansilla Pareja, M.E., A. Bongiovanni, F. Lafont, and M.I. Colombo. 2017. Alterations of the Coxiella burnetii Replicative Vacuole Membrane Integrity and Interplay with the Autophagy Pathway. *Front Cell Infect Microbiol* 7:112.
- Martens, S., and J. Howard. 2006. The interferon-inducible GTPases. *Annu Rev Cell Dev Biol* 22:559-589.
- Martens, S., I. Parvanova, J. Zerrahn, G. Griffiths, G. Schell, G. Reichmann, and J.C. Howard. 2005. Disruption of Toxoplasma gondii parasitophorous vacuoles by the mouse p47-resistance GTPases. *Plos Pathogens* 1:187-201.

- Martin, A.M., T. Liu, B.C. Lynn, and A.P. Sinai. 2007. The *Toxoplasma gondii* parasitophorous vacuole membrane: transactions across the border. *J Eukaryot Microbiol* 54:25-28.
- Martorelli Di Genova, B., S.K. Wilson, J.P. Dubey, and L.J. Knoll. 2019. Intestinal delta-6-desaturase activity determines host range for *Toxoplasma* sexual reproduction. *PLoS Biol* 17:e3000364.
- Matsuura, A., J. Tsukada, T. Mizobe, T. Higashi, F. Mouri, R. Tanikawa, A. Yamauchi, M. Hirashima, and Y. Tanaka. 2009. Intracellular galectin-9 activates inflammatory cytokines in monocytes. *Genes Cells* 14:511-521.
- Matta, S.K., N. Rinkenberger, I.R. Dunay, and L.D. Sibley. 2021. *Toxoplasma gondii* infection and its implications within the central nervous system. *Nat Rev Microbiol* 19:467-480.
- Mazzone, F., V.E. Simons, L. van Geelen, M. Frank, A. Mandi, T. Kurtan, K. Pfeffer, and R. Kalscheuer. 2022. In Vitro Biological Activity of Natural Products from the Endophytic Fungus *Paraboeremia selaginellae* against *Toxoplasma gondii*. *Antibiotics (Basel)* 11:
- Merkt, F.K., F. Mazzone, S.S. Sazzadeh, L. Bonda, L.K.E. Hinz, I. Gruber, K. Buchholz, C. Janiak, K. Pfeffer, and T.J.J. Muller. 2021. Fluorescent Indolo[3,2-a]phenazines against *Toxoplasma gondii*: Concise Synthesis by Gold-Catalyzed Cycloisomerization with 1,2-Silyl Migration and ipso-Iodination Suzuki Sequence. *Chemistry* 27:9774-9781.
- Messmer-Blust, A.F., S. Balasubramanian, V.Y. Gorbacheva, J.A. Jeyaratnam, and D.J. Vestal. 2010. The interferon-gamma-induced murine guanylate-binding protein-2 inhibits rac activation during cell spreading on fibronectin and after platelet-derived growth factor treatment: role for phosphatidylinositol 3-kinase. *Mol Biol Cell* 21:2514-2528.
- Meunier, E., and P. Broz. 2016. Interferon-inducible GTPases in cell autonomous and innate immunity. *Cell Microbiol* 18:168-180.
- Meunier, E., M.S. Dick, R.F. Dreier, N. Schurmann, D.K. Broz, S. Warming, M. Roose-Girma, D. Bumann, N. Kayagaki, K. Takeda, M. Yamamoto, and P. Broz. 2014. Caspase-11 activation requires lysis of pathogen-containing vacuoles by IFN-induced GTPases. *Nature* 509:366-+.
- Meunier, E., P. Wallet, R.F. Dreier, S. Costanzo, L. Anton, S. Ruhl, S. Dussurgey, M.S. Dick, A. Kistner, M. Rigard, D. Degrandi, K. Pfeffer, M. Yamamoto, T. Henry, and P. Broz. 2015. Guanylate-binding proteins promote activation of the AIM2 inflammasome during infection with *Francisella novicida*. *Nature Immunology* 16:476-U185.
- Miller, C.H., S.G. Maher, and H.A. Young. 2009. Clinical Use of Interferon-gamma. *Ann N Y Acad Sci* 1182:69-79.
- Minns, L.A., L.C. Menard, D.M. Foureau, S. Darche, C. Ronet, D.W. Mielcarz, D. Buzoni-Gatel, and L.H. Kasper. 2006. TLR9 is required for the gut-associated lymphoid tissue response following oral infection of *Toxoplasma gondii*. *J Immunol* 176:7589-7597.
- Miranda, F.J.B., B.C. Rocha, M.C.A. Pereira, L.M.N. Pereira, E.H.M. de Souza, A.P. Marino, P.A.C. Costa, D.V. Vasconcelos-Santos, L.R.V. Antonelli, and R.T.

- Gazzinelli. 2021. Toxoplasma gondii-Induced Neutrophil Extracellular Traps Amplify the Innate and Adaptive Response. *mBio* 12:e0130721.
- Mittal, R., M.R. Ahmadian, R.S. Goody, and A. Wittinghofer. 1996. Formation of a transition-state analog of the Ras GTPase reaction by Ras-GDP, tetrafluoroaluminate, and GTPase-activating proteins. *Science* 273:115-117.
- Miyairi, I., V.R. Tatireddigari, O.S. Mahdi, L.A. Rose, R.J. Belland, L. Lu, R.W. Williams, and G.I. Byrne. 2007. The p47 GTPases Iigp2 and Irgb10 regulate innate immunity and inflammation to murine Chlamydia psittaci infection. *J Immunol* 179:1814-1824.
- Mizushima, N., Y. Ohsumi, and T. Yoshimori. 2002. Autophagosome formation in mammalian cells. *Cell Struct Funct* 27:421-429.
- Molestina, R.E., N. El-Guendy, and A.P. Sinai. 2008. Infection with Toxoplasma gondii results in dysregulation of the host cell cycle. *Cell Microbiol* 10:1153-1165.
- Molestina, R.E., T.M. Payne, I. Coppens, and A.P. Sinai. 2003. Activation of NF-kappaB by Toxoplasma gondii correlates with increased expression of antiapoptotic genes and localization of phosphorylated IkappaB to the parasitophorous vacuole membrane. *J Cell Sci* 116:4359-4371.
- Molestina, R.E., and A.P. Sinai. 2005a. Detection of a novel parasite kinase activity at the Toxoplasma gondii parasitophorous vacuole membrane capable of phosphorylating host IkappaBalpha. *Cell Microbiol* 7:351-362.
- Molestina, R.E., and A.P. Sinai. 2005b. Host and parasite-derived IKK activities direct distinct temporal phases of NF-kappaB activation and target gene expression following Toxoplasma gondii infection. *J Cell Sci* 118:5785-5796.
- Montespan, C., S.A. Marvin, S. Austin, A.M. Burrage, B. Roger, F. Rayne, M. Faure, E.M. Campbell, C. Schneider, R. Reimer, K. Grunewald, C.M. Wiethoff, and H. Wodrich. 2017. Multi-layered control of Galectin-8 mediated autophagy during adenovirus cell entry through a conserved PPxY motif in the viral capsid. *PLoS Pathog* 13:e1006217.
- Montoya, J.G. 2002. Laboratory diagnosis of Toxoplasma gondii infection and toxoplasmosis. *J Infect Dis* 185 Suppl 1:S73-82.
- Montoya, J.G., A. Berry, F. Rosso, and J.S. Remington. 2007. The differential agglutination test as a diagnostic aid in cases of toxoplasmic lymphadenitis. *J Clin Microbiol* 45:1463-1468.
- Montoya, J.G., and O. Liesenfeld. 2004. Toxoplasmosis. *Lancet* 363:1965-1976.
- Montoya, J.G., and J.S. Remington. 2008. Management of Toxoplasma gondii infection during pregnancy. *Clinical Infectious Diseases* 47:554-566.
- Moore, S.L., M.D. Schaber, S.D. Mosser, E. Rands, M.B. O'Hara, V.M. Garsky, M.S. Marshall, D.L. Pompliano, and J.B. Gibbs. 1991. Sequence dependence of protein isoprenylation. *J Biol Chem* 266:14603-14610.
- Mordue, D.G., N. Desai, M. Dustin, and L.D. Sibley. 1999a. Invasion by Toxoplasma gondii establishes a moving junction that selectively excludes host cell plasma membrane proteins on the basis of their membrane anchoring. *J Exp Med* 190:1783-1792.
- Mordue, D.G., S. Hakansson, I. Niesman, and L.D. Sibley. 1999b. Toxoplasma gondii resides in a vacuole that avoids fusion with host cell endocytic and exocytic vesicular trafficking pathways. *Exp Parasitol* 92:87-99.

- Mordue, D.G., F. Monroy, M. La Regina, C.A. Dinarello, and L.D. Sibley. 2001. Acute toxoplasmosis leads to lethal overproduction of Th1 cytokines. *J Immunol* 167:4574-4584.
- Muller, U., U. Steinhoff, L.F. Reis, S. Hemmi, J. Pavlovic, R.M. Zinkernagel, and M. Aguet. 1994. Functional role of type I and type II interferons in antiviral defense. *Science* 264:1918-1921.
- Mullis, P.E., and P.M. Brickell. 1992. The use of the polymerase chain reaction in prenatal diagnosis of growth hormone gene deletions. *Clin Endocrinol (Oxf)* 37:89-95.
- Mun, H.S., F. Aosai, K. Norose, L.X. Piao, H. Fang, S. Akira, and A. Yano. 2005. Toll-like receptor 4 mediates tolerance in macrophages stimulated with *Toxoplasma gondii*-derived heat shock protein 70. *Infect Immun* 73:4634-4642.
- Murphy, K.M., Travers, P. and Walport, M. 2009. Janeway Immunologie.
- Murray, P.J. 2007. The JAK-STAT signaling pathway: input and output integration. *J Immunol* 178:2623-2629.
- Murray, P.J. 2016. Amino acid auxotrophy as a system of immunological control nodes. *Nat Immunol* 17:132-139.
- Murray, P.J., R.A. Young, and G.Q. Daley. 1998. Hematopoietic remodeling in interferon-gamma-deficient mice infected with mycobacteria. *Blood* 91:2914-2924.
- Nantais, D.E., M. Schwemmler, J.T. Stickney, D.J. Vestal, and J.E. Buss. 1996. Prenylation of an interferon-gamma-induced GTP-binding protein: the human guanylate binding protein, huGBP1. *J Leukoc Biol* 60:423-431.
- Naranjo-Galvis, C.A., K.Y. Cardona-Londono, M. Orrego-Cardozo, and X. Elcoroaristizabal-Martin. 2022. *Toxoplasma gondii* infection and peripheral-blood gene expression profiling of older people reveals dysregulation of cytokines and identifies hub genes as potential therapeutic targets. *Heliyon* 8:e10576.
- Naschberger, E., R.S. Croner, S. Merkel, A. Dimmler, P. Tripal, K.U. Amann, E. Kremmer, W.M. Brueckl, T. Papadopoulos, C. Hohenadl, W. Hohenberger, and M. Sturzl. 2008. Angiostatic immune reaction in colorectal carcinoma: Impact on survival and perspectives for antiangiogenic therapy. *Int J Cancer* 123:2120-2129.
- Nash, P.B., M.B. Purner, R.P. Leon, P. Clarke, R.C. Duke, and T.J. Curiel. 1998. *Toxoplasma gondii*-infected cells are resistant to multiple inducers of apoptosis. *J Immunol* 160:1824-1830.
- Nassar, N., G.R. Hoffman, D. Manor, J.C. Clardy, and R.A. Cerione. 1998. Structures of Cdc42 bound to the active and catalytically compromised forms of Cdc42GAP. *Nat Struct Biol* 5:1047-1052.
- Nelson, M.M., A.R. Jones, J.C. Carmen, A.P. Sinai, R. Burchmore, and J.M. Wastling. 2008. Modulation of the host cell proteome by the intracellular apicomplexan parasite *Toxoplasma gondii*. *Infect Immun* 76:828-844.
- Neun, R., M.F. Richter, P. Staeheli, and M. Schwemmler. 1996. GTPase properties of the interferon-induced human guanylate-binding protein 2. *FEBS Lett* 390:69-72.
- Nguyen, T.T., Y. Hu, D.P. Widney, R.A. Mar, and J.B. Smith. 2002. Murine GBP-5, a new member of the murine guanylate-binding protein family, is coordinately regulated with other GBPs in vivo and in vitro. *J Interferon Cytokine Res* 22:899-909.
- Nishikawa, Y., O. Kawase, O. Vielemeyer, H. Suzuki, K.A. Joiner, X. Xuan, and H. Nagasawa. 2007. *Toxoplasma gondii* infection induces apoptosis in noninfected

- macrophages: role of nitric oxide and other soluble factors. *Parasite Immunol* 29:375-385.
- Nishiyama, S., A. Pradipta, J.S. Ma, M. Sasai, and M. Yamamoto. 2020. T cell-derived interferon-gamma is required for host defense to *Toxoplasma gondii*. *Parasitol Int* 75:102049.
- Noda, C., H. Kimura, K. Arasaki, M. Matsushita, A. Yamamoto, Y. Wakana, H. Inoue, and M. Tagaya. 2014. Valosin-containing protein-interacting membrane protein (VIMP) links the endoplasmic reticulum with microtubules in concert with cytoskeleton-linking membrane protein (CLIMP)-63. *J Biol Chem* 289:24304-24313.
- Nordmann, A., L. Wixler, Y. Boergeling, V. Wixler, and S. Ludwig. 2012. A new splice variant of the human guanylate-binding protein 3 mediates anti-influenza activity through inhibition of viral transcription and replication. *Faseb Journal* 26:1290-1300.
- Odberg-Ferragut, C., M. Soete, A. Engels, B. Samyn, A. Loyens, J. Van Beeumen, D. Camus, and J.F. Dubremetz. 1996. Molecular cloning of the *Toxoplasma gondii* sag4 gene encoding an 18 kDa bradyzoite specific surface protein. *Mol Biochem Parasitol* 82:237-244.
- Ohshima, J., Y. Lee, M. Sasai, T. Saitoh, J.S. Ma, N. Kamiyama, Y. Matsuura, S. Pann-Ghill, M. Hayashi, S. Ebisu, K. Takeda, S. Akira, and M. Yamamoto. 2014. Role of Mouse and Human Autophagy Proteins in IFN-gamma-Induced Cell-Autonomous Responses against *Toxoplasma gondii*. *Journal of Immunology* 192:3328-3335.
- Ohshima, J., M. Sasai, J. Liu, K. Yamashita, J.S. Ma, Y. Lee, H. Bando, J.C. Howard, S. Ebisu, M. Hayashi, K. Takeda, D.M. Standley, E.M. Frickel, and M. Yamamoto. 2015. RabGDIalpha is a negative regulator of interferon-gamma-inducible GTPase-dependent cell-autonomous immunity to *Toxoplasma gondii*. *Proc Natl Acad Sci U S A* 112:E4581-4590.
- Olariu, T.R., J.S. Remington, R. McLeod, A. Alam, and J.G. Montoya. 2011. Severe congenital toxoplasmosis in the United States: clinical and serologic findings in untreated infants. *Pediatr Infect Dis J* 30:1056-1061.
- Olias, P., R.D. Etheridge, Y. Zhang, M.J. Holtzman, and L.D. Sibley. 2016. *Toxoplasma* Effector Recruits the Mi-2/NuRD Complex to Repress STAT1 Transcription and Block IFN-gamma-Dependent Gene Expression. *Cell Host Microbe* 20:72-82.
- Olszewski, M.A., J. Gray, and D.J. Vestal. 2006. In silico genomic analysis of the human and murine guanylate-binding protein (GBP) gene clusters. *Journal of Interferon and Cytokine Research* 26:328-352.
- Ong, Y.C., M.L. Reese, and J.C. Boothroyd. 2010. *Toxoplasma* rhoptry protein 16 (ROP16) subverts host function by direct tyrosine phosphorylation of STAT6. *J Biol Chem* 285:28731-28740.
- Orange, J.S., B. Wang, C. Terhorst, and C.A. Biron. 1995. Requirement for natural killer cell-produced interferon gamma in defense against murine cytomegalovirus infection and enhancement of this defense pathway by interleukin 12 administration. *J Exp Med* 182:1045-1056.
- Ortiz-Alegria, L.B., H. Caballero-Ortega, I. Canedo-Solares, C.P. Rico-Torres, A. Sahagun-Ruiz, M.E. Medina-Escutia, and D. Correa. 2010. Congenital toxoplasmosis:

- candidate host immune genes relevant for vertical transmission and pathogenesis. *Genes Immun* 11:363-373.
- Osugi, Y., K. Fumoto, and A. Kikuchi. 2019. CKAP4 Regulates Cell Migration via the Interaction with and Recycling of Integrin. *Mol Cell Biol* 39:
- Ottenhoff, T.H., F.A. Verreck, E.G. Lichtenauer-Kaligis, M.A. Hoeve, O. Sanal, and J.T. van Dissel. 2002. Genetics, cytokines and human infectious disease: lessons from weakly pathogenic mycobacteria and salmonellae. *Nat Genet* 32:97-105.
- Pai, E.F., W. Kabsch, U. Krengel, K.C. Holmes, J. John, and A. Wittinghofer. 1989. Structure of the guanine-nucleotide-binding domain of the Ha-ras oncogene product p21 in the triphosphate conformation. *Nature* 341:209-214.
- Palfy, G., D.K. Menyhard, and A. Perczel. 2020. Dynamically encoded reactivity of Ras enzymes: opening new frontiers for drug discovery. *Cancer Metastasis Rev* 39:1075-1089.
- Paludan, S.R. 2000. Synergistic action of pro-inflammatory agents: cellular and molecular aspects. *J Leukoc Biol* 67:18-25.
- Paquet, C., M.H. Yudin, O. Society of, and C. Gynaecologists of. 2013. Toxoplasmosis in pregnancy: prevention, screening, and treatment. *J Obstet Gynaecol Can* 35:78-81.
- Park, A.M., S. Hagiwara, D.K. Hsu, F.T. Liu, and O. Yoshie. 2016. Galectin-3 Plays an Important Role in Innate Immunity to Gastric Infection by *Helicobacter pylori*. *Infect Immun* 84:1184-1193.
- Parkes, M., J.C. Barrett, N.J. Prescott, M. Tremelling, C.A. Anderson, S.A. Fisher, R.G. Roberts, E.R. Nimmo, F.R. Cummings, D. Soars, H. Drummond, C.W. Lees, S.A. Khawaja, R. Bagnall, D.A. Burke, C.E. Todhunter, T. Ahmad, C.M. Onnie, W. McArdle, D. Strachan, G. Bethel, C. Bryan, C.M. Lewis, P. Deloukas, A. Forbes, J. Sanderson, D.P. Jewell, J. Satsangi, J.C. Mansfield, C. Wellcome Trust Case Control, L. Cardon, and C.G. Mathew. 2007. Sequence variants in the autophagy gene IRGM and multiple other replicating loci contribute to Crohn's disease susceptibility. *Nat Genet* 39:830-832.
- Parmley, S.F., U. Gross, A. Sucharczuk, T. Windeck, G.D. Sgarlato, and J.S. Remington. 1994. Two alleles of the gene encoding surface antigen P22 in 25 strains of *Toxoplasma gondii*. *J Parasitol* 80:293-301.
- Parmley, S.F., L.M. Weiss, and S. Yang. 1995. Cloning of a bradyzoite-specific gene of *Toxoplasma gondii* encoding a cytoplasmic antigen. *Mol Biochem Parasitol* 73:253-257.
- Pawlowski, N., A. Khaminets, J.P. Hunn, N. Papic, A. Schmidt, R.C. Uthaiyah, R. Lange, G. Vopper, S. Martens, E. Wolf, and J.C. Howard. 2011. The activation mechanism of Irga6, an interferon-inducible GTPase contributing to mouse resistance against *Toxoplasma gondii*. *Bmc Biology* 9:
- Payne, R.A., J.M. Francis, and W. Kwantes. 1984. Comparison of a latex agglutination test with other serological tests for the measurement of antibodies to *Toxoplasma gondii*. *J Clin Pathol* 37:1293-1297.
- Payne, T.M., R.E. Molestina, and A.P. Sinai. 2003. Inhibition of caspase activation and a requirement for NF-kappaB function in the *Toxoplasma gondii*-mediated blockade of host apoptosis. *J Cell Sci* 116:4345-4358.

- Paz, I., M. Sachse, N. Dupont, J. Mounier, C. Cederfur, J. Enninga, H. Leffler, F. Poirier, M.C. Prevost, F. Lafont, and P. Sansonetti. 2010. Galectin-3, a marker for vacuole lysis by invasive pathogens. *Cell Microbiol* 12:530-544.
- Peloux, Y., P. Couzineau, H. Baufine-Ducrocq, J.L. Tayot, and D. Jacquot. 1973. [Direct agglutination test for toxoplasma. Role of immunoglobulins 19S and 7S. Preliminary notes]. *Ann Biol Clin (Paris)* 31:185-192.
- Pereira, K.S., R.M. Franco, and D.A. Leal. 2010. Transmission of toxoplasmosis (*Toxoplasma gondii*) by foods. *Adv Food Nutr Res* 60:1-19.
- Perez, E.E., J. Wang, J.C. Miller, Y. Jouvenot, K.A. Kim, O. Liu, N. Wang, G. Lee, V.V. Bartsevich, Y.L. Lee, D.Y. Guschin, I. Rupniewski, A.J. Waite, C. Carpenito, R.G. Carroll, J.S. Orange, F.D. Urnov, E.J. Rebar, D. Ando, P.D. Gregory, J.L. Riley, M.C. Holmes, and C.H. June. 2008. Establishment of HIV-1 resistance in CD4+ T cells by genome editing using zinc-finger nucleases. *Nat Biotechnol* 26:808-816.
- Pestka, S., C.D. Krause, and M.R. Walter. 2004. Interferons, interferon-like cytokines, and their receptors. *Immunol Rev* 202:8-32.
- Pfefferkorn, E.R., and P.M. Guyre. 1984. Inhibition of growth of *Toxoplasma gondii* in cultured fibroblasts by human recombinant gamma interferon. *Infect Immun* 44:211-216.
- Pfrepfer, K.I., G. Enders, M. Gohl, D. Krczal, H. Hlobil, D. Wassenberg, and E. Soutschek. 2005. Seroreactivity to and avidity for recombinant antigens in toxoplasmosis. *Clin Diagn Lab Immunol* 12:977-982.
- Phelps, E.D., K.R. Sweeney, and I.J. Blader. 2008. *Toxoplasma gondii* rhoptry discharge correlates with activation of the early growth response 2 host cell transcription factor. *Infect Immun* 76:4703-4712.
- Pifer, R., A. Benson, C.R. Sturge, and F. Yarovinsky. 2011. UNC93B1 is essential for TLR11 activation and IL-12-dependent host resistance to *Toxoplasma gondii*. *J Biol Chem* 286:3307-3314.
- Pilla-Moffett, D., M.F. Barber, G.A. Taylor, and J. Coers. 2016. Interferon-Inducible GTPases in Host Resistance, Inflammation and Disease. *J Mol Biol* 428:3495-3513.
- Pilla, D.M., J.A. Hagar, A.K. Haldar, A.K. Mason, D. Degrandi, K. Pfeffer, R.K. Ernst, M. Yamamoto, E.A. Miao, and J. Coers. 2014. Guanylate binding proteins promote caspase-11-dependent pyroptosis in response to cytoplasmic LPS. *Proceedings of the National Academy of Sciences of the United States of America* 111:6046-6051.
- Pineda, M.A., H. Cuervo, M. Fresno, M. Soto, and P. Bonay. 2015. Lack of Galectin-3 Prevents Cardiac Fibrosis and Effective Immune Responses in a Murine Model of *Trypanosoma cruzi* Infection. *J Infect Dis* 212:1160-1171.
- Pinon, J.M., H. Dumon, C. Chemla, J. Franck, E. Petersen, M. Lebech, J. Zufferey, M.H. Bessieres, P. Marty, R. Holliman, J. Johnson, V. Luyasu, B. Lecolier, E. Guy, D.H. Joynson, A. Decoster, G. Enders, H. Pelloux, and E. Candolfi. 2001. Strategy for diagnosis of congenital toxoplasmosis: evaluation of methods comparing mothers and newborns and standard methods for postnatal detection of immunoglobulin G, M, and A antibodies. *J Clin Microbiol* 39:2267-2271.
- Piro, A.S., D. Hernandez, S. Luoma, E.M. Feeley, R. Finethy, A. Yirga, E.M. Frickel, C.F. Lesser, and J. Coers. 2017. Detection of Cytosolic *Shigella flexneri* via a C-Terminal Triple-Arginine Motif of GBP1 Inhibits Actin-Based Motility. *mBio* 8:

- Platanias, L.C. 2005. Introduction: interferon signals: what is classical and what is nonclassical? *J Interferon Cytokine Res* 25:732.
- Pleyer, U., U. Gross, D. Schluter, H. Wilking, and F. Seeber. 2019. Toxoplasmosis in Germany. *Dtsch Arztebl Int* 116:435-444.
- Pollard, A.M., K.N. Onatolu, L. Hiller, K. Haldar, and L.J. Knoll. 2008. Highly polymorphic family of glycosylphosphatidylinositol-anchored surface antigens with evidence of developmental regulation in *Toxoplasma gondii*. *Infect Immun* 76:103-110.
- Poschmann, G., K. Seyfarth, D. Besong Agbo, H.W. Klafki, J. Rozman, W. Wurst, J. Wiltfang, H.E. Meyer, M. Klingenspor, and K. Stuhler. 2014. High-fat diet induced isoform changes of the Parkinson's disease protein DJ-1. *J Proteome Res* 13:2339-2351.
- Praefcke, G.J.K., M. Geyer, M. Schwemmler, H.R. Kalbitzer, and C. Herrmann. 1999. Nucleotide-binding characteristics of human guanylate-binding protein 1 (hGBP1) and identification of the third GTP-binding motif. *Journal of Molecular Biology* 292:321-332.
- Praefcke, G.J.K., and H.T. McMahon. 2004. The dynamin superfamily: Universal membrane tubulation and fission molecules? *Nature Reviews Molecular Cell Biology* 5:133-147.
- Prakash, B., G.J.K. Praefcke, L. Renault, A. Wittinghofer, and C. Herrmann. 2000a. Structure of human guanylate-binding protein 1 representing a unique class of GTP-binding proteins. *Nature* 403:567-571.
- Prakash, B., L. Renault, G.J.K. Praefcke, C. Herrmann, and A. Wittinghofer. 2000b. Triphosphate structure of guanylate-binding protein 1 and implications for nucleotide binding and GTPase mechanism. *Embo Journal* 19:4555-4564.
- Prejean, C., and O.R. Colamonici. 2000. Role of the cytoplasmic domains of the type I interferon receptor subunits in signaling. *Semin Cancer Biol* 10:83-92.
- Rabinovich, G.A., F.T. Liu, M. Hirashima, and A. Anderson. 2007. An emerging role for galectins in tuning the immune response: lessons from experimental models of inflammatory disease, autoimmunity and cancer. *Scand J Immunol* 66:143-158.
- Rabinovich, G.A., and M.A. Toscano. 2009. Turning 'sweet' on immunity: galectin-glycan interactions in immune tolerance and inflammation. *Nat Rev Immunol* 9:338-352.
- Ran, F.A., P.D. Hsu, J. Wright, V. Agarwala, D.A. Scott, and F. Zhang. 2013. Genome engineering using the CRISPR-Cas9 system. *Nat Protoc* 8:2281-2308.
- Reese, M.L., G.M. Zeiner, J.P. Saeij, J.C. Boothroyd, and J.P. Boyle. 2011. Polymorphic family of injected pseudokinases is paramount in *Toxoplasma* virulence. *Proc Natl Acad Sci U S A* 108:9625-9630.
- Reiner, S.L., and R.M. Locksley. 1995. The regulation of immunity to *Leishmania major*. *Annu Rev Immunol* 13:151-177.
- Reis e Sousa, C., S. Hieny, T. Scharon-Kersten, D. Jankovic, H. Charest, R.N. Germain, and A. Sher. 1997. In vivo microbial stimulation induces rapid CD40 ligand-independent production of interleukin 12 by dendritic cells and their redistribution to T cell areas. *J Exp Med* 186:1819-1829.
- Remington, J.S., P. Thulliez, and J.G. Montoya. 2004. Recent developments for diagnosis of toxoplasmosis. *J Clin Microbiol* 42:941-945.

- Renart, J., and I.V. Sandoval. 1984. Western blots. *Methods Enzymol* 104:455-460.
- Rioux, J.D., R.J. Xavier, K.D. Taylor, M.S. Silverberg, P. Goyette, A. Huett, T. Green, P. Kuballa, M.M. Barmada, L.W. Datta, Y.Y. Shugart, A.M. Griffiths, S.R. Targan, A.F. Ippoliti, E.J. Bernard, L. Mei, D.L. Nicolae, M. Regueiro, L.P. Schumm, A.H. Steinhart, J.I. Rotter, R.H. Duerr, J.H. Cho, M.J. Daly, and S.R. Brant. 2007. Genome-wide association study identifies new susceptibility loci for Crohn disease and implicates autophagy in disease pathogenesis. *Nat Genet* 39:596-604.
- Robben, P.M., D.G. Mordue, S.M. Truscott, K. Takeda, S. Akira, and L.D. Sibley. 2004. Production of IL-12 by macrophages infected with *Toxoplasma gondii* depends on the parasite genotype. *J Immunol* 172:3686-3694.
- Robert-Koch-Institut. 2016. Vorkommen und Bedeutung von *Toxoplasma gondii* in Deutschland - Ergebnisse der serologischen Untersuchungen innerhalb der Studie zur Gesundheit Erwachsener in Deutschland DEGS; .**
- Rorman, E., C.S. Zamir, I. Rilkis, and H. Ben-David. 2006. Congenital toxoplasmosis--prenatal aspects of *Toxoplasma gondii* infection. *Reprod Toxicol* 21:458-472.
- Rosowski, E.E., Q.P. Nguyen, A. Camejo, E. Spooner, and J.P. Saeij. 2014. *Toxoplasma gondii* Inhibits gamma interferon (IFN-gamma)- and IFN-beta-induced host cell STAT1 transcriptional activity by increasing the association of STAT1 with DNA. *Infect Immun* 82:706-719.
- Rothfuchs, A.G., C. Trumstedt, H. Wigzell, and M.E. Rottenberg. 2004. Intracellular bacterial infection-induced IFN-gamma is critically but not solely dependent on Toll-like receptor 4-myeloid differentiation factor 88-IFN-alpha beta-STAT1 signaling. *J Immunol* 172:6345-6353.
- Rupper, A.C., and J.A. Cardelli. 2008. Induction of guanylate binding protein 5 by gamma interferon increases susceptibility to *Salmonella enterica* serovar typhimurium-induced pyroptosis in RAW 264.7 cells. *Infection and Immunity* 76:2304-2315.
- Saadatnia, G., and M. Golkar. 2012. A review on human toxoplasmosis. *Scand J Infect Dis* 44:805-814.
- Saeij, J.P., J.P. Boyle, S. Collier, S. Taylor, L.D. Sibley, E.T. Brooke-Powell, J.W. Ajioka, and J.C. Boothroyd. 2006. Polymorphic secreted kinases are key virulence factors in toxoplasmosis. *Science* 314:1780-1783.
- Saeij, J.P., S. Collier, J.P. Boyle, M.E. Jerome, M.W. White, and J.C. Boothroyd. 2007. *Toxoplasma* co-opts host gene expression by injection of a polymorphic kinase homologue. *Nature* 445:324-327.
- Saeij, J.P., and E.M. Frickel. 2017. Exposing *Toxoplasma gondii* hiding inside the vacuole: a role for GBPs, autophagy and host cell death. *Curr Opin Microbiol* 40:72-80.
- Sanchez, S.G., and S. Besteiro. 2021. The pathogenicity and virulence of *Toxoplasma gondii*. *Virulence* 12:3095-3114.
- Sano, H., D.K. Hsu, J.R. Apgar, L. Yu, B.B. Sharma, I. Kuwabara, S. Izui, and F.T. Liu. 2003. Critical role of galectin-3 in phagocytosis by macrophages. *J Clin Invest* 112:389-397.
- Santos, J.C., D. Boucher, L.K. Schneider, B. Demarco, M. Dilucca, K. Shkarina, R. Heilig, K.W. Chen, R.Y.H. Lim, and P. Broz. 2020. Human GBP1 binds LPS to initiate assembly of a caspase-4 activating platform on cytosolic bacteria. *Nat Commun* 11:3276.

- Santos, J.C., and P. Broz. 2018. Sensing of invading pathogens by GBPs: At the crossroads between cell-autonomous and innate immunity. *J Leukoc Biol*
- Santos, J.C., M.S. Dick, B. Lagrange, D. Degrandi, K. Pfeffer, M. Yamamoto, E. Meunier, P. Pelczar, T. Henry, and P. Broz. 2018. LPS targets host guanylate-binding proteins to the bacterial outer membrane for non-canonical inflammasome activation. *EMBO J* 37:
- Scanga, C.A., J. Aliberti, D. Jankovic, F. Tilloy, S. Bennouna, E.Y. Denkers, R. Medzhitov, and A. Sher. 2002. Cutting edge: MyD88 is required for resistance to *Toxoplasma gondii* infection and regulates parasite-induced IL-12 production by dendritic cells. *Journal of Immunology* 168:5997-6001.
- Scharton-Kersten, T.M., T.A. Wynn, E.Y. Denkers, S. Bala, E. Grunvald, S. Hieny, R.T. Gazzinelli, and A. Sher. 1996. In the absence of endogenous IFN-gamma, mice develop unimpaired IL-12 responses to *Toxoplasma gondii* while failing to control acute infection. *J Immunol* 157:4045-4054.
- Scharton-Kersten, T.M., G. Yap, J. Magram, and A. Sher. 1997. Inducible nitric oxide is essential for host control of persistent but not acute infection with the intracellular pathogen *Toxoplasma gondii*. *J Exp Med* 185:1261-1273.
- Scheffzek, K., M.R. Ahmadian, W. Kabsch, L. Wiesmuller, A. Lautwein, F. Schmitz, and A. Wittinghofer. 1997. The Ras-RasGAP complex: structural basis for GTPase activation and its loss in oncogenic Ras mutants. *Science* 277:333-338.
- Schluter, D., and A. Barragan. 2019. Advances and Challenges in Understanding Cerebral Toxoplasmosis. *Front Immunol* 10:242.
- Schnoor, M., A. Betanzos, D.A. Weber, and C.A. Parkos. 2009. Guanylate-binding protein-1 is expressed at tight junctions of intestinal epithelial cells in response to interferon-gamma and regulates barrier function through effects on apoptosis. *Mucosal Immunol* 2:33-42.
- Schroder, K., P.J. Hertzog, T. Ravasi, and D.A. Hume. 2004. Interferon-gamma: an overview of signals, mechanisms and functions. *J Leukoc Biol* 75:163-189.
- Schwab, J.C., C.J. Beckers, and K.A. Joiner. 1994. The parasitophorous vacuole membrane surrounding intracellular *Toxoplasma gondii* functions as a molecular sieve. *Proc Natl Acad Sci USA* 91:509-513.
- Schweizer, A., M. Ericsson, T. Bachi, G. Griffiths, and H.P. Hauri. 1993. Characterization of a novel 63 kDa membrane protein. Implications for the organization of the ER-to-Golgi pathway. *J Cell Sci* 104 (Pt 3):671-683.
- Schwemmler, M., B. Kaspers, A. Irion, P. Staeheli, and U. Schultz. 1996. Chicken guanylate-binding protein. Conservation of GTPase activity and induction by cytokines. *J Biol Chem* 271:10304-10308.
- Schwemmler, M., and P. Staeheli. 1994. The Interferon-Induced 67-Kda Guanylate-Binding Protein (Hgbp1) Is A Gtpase That Converts Gtp to Gmp. *Journal of Biological Chemistry* 269:11299-11305.
- Seabra, M.C., and G.L. James. 1998. Prenylation assays for small GTPases. *Methods Mol Biol* 84:251-260.
- Seder, R.A., W.E. Paul, M.M. Davis, and B. Fazekas de St Groth. 1992. The presence of interleukin 4 during in vitro priming determines the lymphokine-producing

- potential of CD4+ T cells from T cell receptor transgenic mice. *J Exp Med* 176:1091-1098.
- Sehgal, A., S. Bettiol, M. Pypaert, M.R. Wenk, A. Kaasch, I.J. Blader, K.A. Joiner, and I. Coppens. 2005. Peculiarities of host cholesterol transport to the unique intracellular vacuole containing *Toxoplasma*. *Traffic* 6:1125-1141.
- Selleck, E.M., S.J. Fentress, W.L. Beatty, D. Degrandi, K. Pfeffer, H.W. Virgin, J.D. MacMicking, and L.D. Sibley. 2013. Guanylate-binding Protein 1 (Gbp1) Contributes to Cell-autonomous Immunity against *Toxoplasma gondii*. *Plos Pathogens* 9:
- Shapira, S., O.S. Harb, J. Margarit, M. Matrajt, J. Han, A. Hoffmann, B. Freedman, M.J. May, D.S. Roos, and C.A. Hunter. 2005. Initiation and termination of NF-kappaB signaling by the intracellular protozoan parasite *Toxoplasma gondii*. *J Cell Sci* 118:3501-3508.
- Shenoy, A.R., D.A. Wellington, P. Kumar, H. Kassa, C.J. Booth, P. Cresswell, and J.D. MacMicking. 2012. GBP5 Promotes NLRP3 Inflammasome Assembly and Immunity in Mammals. *Science* 336:481-485.
- Sher, A., and R.L. Coffman. 1992. Regulation of immunity to parasites by T cells and T cell-derived cytokines. *Annu Rev Immunol* 10:385-409.
- Shi, W., C. Xue, X.Z. Su, and F. Lu. 2018. The roles of galectins in parasitic infections. *Acta Trop* 177:97-104.
- Shydlovskiy, S., A.Y. Zienert, S. Ince, C. Dovengerds, A. Hohendahl, J.M. Dargazanli, A. Blum, S.D. Gunther, N. Kladt, M. Sturzl, A.C. Schauss, M. Kutsch, A. Roux, G.J.K. Praefcke, and C. Herrmann. 2017. Nucleotide-dependent farnesyl switch orchestrates polymerization and membrane binding of human guanylate-binding protein 1. *Proc Natl Acad Sci U S A* 114:E5559-E5568.
- Sibley, L.D. 1993. Interactions between *Toxoplasma gondii* and its mammalian host cells. *Semin Cell Biol* 4:335-344.
- Sibley, L.D. 2011. Invasion and intracellular survival by protozoan parasites. *Immunol Rev* 240:72-91.
- Sibley, L.D., and J.W. Ajioka. 2008. Population structure of *Toxoplasma gondii*: clonal expansion driven by infrequent recombination and selective sweeps. *Annu Rev Microbiol* 62:329-351.
- Sibley, L.D., and N.W. Andrews. 2000. Cell invasion by un-palatable parasites. *Traffic* 1:100-106.
- Sibley, L.D., and J.C. Boothroyd. 1992. Virulent strains of *Toxoplasma gondii* comprise a single clonal lineage. *Nature* 359:82-85.
- Sibley, L.D., A. Khan, J.W. Ajioka, and B.M. Rosenthal. 2009. Genetic diversity of *Toxoplasma gondii* in animals and humans. *Philos Trans R Soc Lond B Biol Sci* 364:2749-2761.
- Sibley, L.D., I.R. Niesman, S.F. Parmley, and M.F. Cesbron-Delauw. 1995. Regulated secretion of multi-lamellar vesicles leads to formation of a tubulo-vesicular network in host-cell vacuoles occupied by *Toxoplasma gondii*. *J Cell Sci* 108 (Pt 4):1669-1677.

- Silva, N.M., J.C. Vieira, C.M. Carneiro, and W.L. Tafuri. 2009. Toxoplasma gondii: the role of IFN-gamma, TNFRp55 and iNOS in inflammatory changes during infection. *Exp Parasitol* 123:65-72.
- Sims, S.H., Y. Cha, M.F. Romine, P.Q. Gao, K. Gottlieb, and A.B. Deisseroth. 1993. A novel interferon-inducible domain: structural and functional analysis of the human interferon regulatory factor 1 gene promoter. *Mol Cell Biol* 13:690-702.
- Sinai, A.P., and K.A. Joiner. 1997. Safe haven: the cell biology of nonfusogenic pathogen vacuoles. *Annu Rev Microbiol* 51:415-462.
- Sinai, A.P., T.M. Payne, J.C. Carmen, L. Hardi, S.J. Watson, and R.E. Molestina. 2004. Mechanisms underlying the manipulation of host apoptotic pathways by Toxoplasma gondii. *Int J Parasitol* 34:381-391.
- Sinai, A.P., P. Webster, and K.A. Joiner. 1997. Association of host cell endoplasmic reticulum and mitochondria with the Toxoplasma gondii parasitophorous vacuole membrane: a high affinity interaction. *J Cell Sci* 110 (Pt 17):2117-2128.
- Singh, S.B., A.S. Davis, G.A. Taylor, and V. Deretic. 2006. Human IRGM induces autophagy to eliminate intracellular mycobacteria. *Science* 313:1438-1441.
- Singh, S.B., W. Ornatowski, I. Vergne, J. Naylor, M. Delgado, E. Roberts, M. Ponpuak, S. Master, M. Pilli, E. White, M. Komatsu, and V. Deretic. 2010. Human IRGM regulates autophagy and cell-autonomous immunity functions through mitochondria. *Nat Cell Biol* 12:1154-1165.
- Sisto, M., L. Lorusso, G. Ingravallo, R. Tamma, B. Nico, D. Ribatti, S. Ruggieri, and S. Lisi. 2018. Reduced myoflament component in primary Sjogren's syndrome salivary gland myoepithelial cells. *J Mol Histol* 49:111-121.
- Skariah, S., A.A. Sultan, and D.G. Mordue. 2022. IFN-induced cell-autonomous immune mechanisms in the control of intracellular protozoa. *Parasitol Res* 121:1559-1571.
- Smith, J.E. 1995. A ubiquitous intracellular parasite: the cellular biology of Toxoplasma gondii. *Int J Parasitol* 25:1301-1309.
- Smith, P.K., R.I. Krohn, G.T. Hermanson, A.K. Mallia, F.H. Gartner, M.D. Provenzano, E.K. Fujimoto, N.M. Goeke, B.J. Olson, and D.C. Klenk. 1985. Measurement of protein using bicinchoninic acid. *Anal Biochem* 150:76-85.
- Snyder, L.M., C.M. Doherty, H.L. Mercer, and E.Y. Denkers. 2021. Induction of IL-12p40 and type 1 immunity by Toxoplasma gondii in the absence of the TLR-MyD88 signaling cascade. *PLoS Pathog* 17:e1009970.
- Song, M.M., and K. Shuai. 1998. The suppressor of cytokine signaling (SOCS) 1 and SOCS3 but not SOCS2 proteins inhibit interferon-mediated antiviral and antiproliferative activities. *J Biol Chem* 273:35056-35062.
- Steffens, N., C. Beuter-Gunia, E. Kravets, A. Reich, L. Legewie, K. Pfeffer, and D. Grandi. 2020. Essential Role of mGBP7 for Survival of Toxoplasma gondii Infection. *mBio* 11:
- Steinfeldt, T., S. Konen-Waisman, L. Tong, N. Pawlowski, T. Lamkemeyer, L.D. Sibley, J.P. Hunn, and J.C. Howard. 2010. Phosphorylation of Mouse Immunity-Related GTPase (IRG) Resistance Proteins Is an Evasion Strategy for Virulent Toxoplasma gondii. *Plos Biology* 8:
- Stepick-Biek, P., P. Thulliez, F.G. Araujo, and J.S. Remington. 1990. IgA antibodies for diagnosis of acute congenital and acquired toxoplasmosis. *J Infect Dis* 162:270-273.

- Stickney, J.T., and J.E. Buss. 2000. Murine guanylate-binding protein: Incomplete geranylgeranyl isoprenoid modification of an interferon-gamma-inducible guanosine triphosphate-binding protein. *Molecular Biology of the Cell* 11:2191-2200.
- Stowell, S.R., C.M. Arthur, M. Dias-Baruffi, L.C. Rodrigues, J.P. Gourdine, J. Heimburg-Molinaro, T. Ju, R.J. Molinaro, C. Rivera-Marrero, B. Xia, D.F. Smith, and R.D. Cummings. 2010. Innate immune lectins kill bacteria expressing blood group antigen. *Nat Med* 16:295-301.
- Stratmann, B., B. Engelbrecht, B.C. Espelage, N. Klusmeier, J. Tiemann, T. Gawlowski, Y. Mattern, M. Eisenacher, H.E. Meyer, N. Rabbani, P.J. Thornalley, D. Tschoepe, G. Poschmann, and K. Stuhler. 2016. Glyoxalase 1-knockdown in human aortic endothelial cells - effect on the proteome and endothelial function estimates. *Sci Rep* 6:37737.
- Su, C., D.K. Howe, J.P. Dubey, J.W. Ajioka, and L.D. Sibley. 2002. Identification of quantitative trait loci controlling acute virulence in *Toxoplasma gondii*. *Proc Natl Acad Sci U S A* 99:10753-10758.
- Suzuki, Y. 2002. Immunopathogenesis of cerebral toxoplasmosis. *J Infect Dis* 186 Suppl 2:S234-240.
- Suzuki, Y., M.A. Orellana, R.D. Schreiber, and J.S. Remington. 1988. Interferon-gamma: the major mediator of resistance against *Toxoplasma gondii*. *Science* 240:516-518.
- Szabo, S.J., B.M. Sullivan, S.L. Peng, and L.H. Glimcher. 2003. Molecular mechanisms regulating Th1 immune responses. *Annu Rev Immunol* 21:713-758.
- Taylor, G.A. 2007. IRG proteins: key mediators of interferon-regulated host resistance to intracellular pathogens. *Cellular Microbiology* 9:1099-1107.
- Taylor, G.A., C.G. Feng, and A. Sher. 2004. p47 GTPases: regulators of immunity to intracellular pathogens. *Nat Rev Immunol* 4:100-109.
- Taylor, G.A., M. Jeffers, D.A. Largaespada, N.A. Jenkins, N.G. Copeland, and G.F. Vande Woude. 1996. Identification of a novel GTPase, the inducibly expressed GTPase, that accumulates in response to interferon gamma. *J Biol Chem* 271:20399-20405.
- Taylor, S., A. Barragan, C. Su, B. Fux, S.J. Fentress, K. Tang, W.L. Beatty, H.E. Hajj, M. Jerome, M.S. Behnke, M. White, J.C. Wootton, and L.D. Sibley. 2006. A secreted serine-threonine kinase determines virulence in the eukaryotic pathogen *Toxoplasma gondii*. *Science* 314:1776-1780.
- Tenter, A.M., A.R. Heckeroth, and L.M. Weiss. 2000. *Toxoplasma gondii*: from animals to humans. *Int J Parasitol* 30:1217-1258.
- Thevenaz, P., U.E. Ruttimann, and M. Unser. 1998. A pyramid approach to subpixel registration based on intensity. *IEEE Trans Image Process* 7:27-41.
- Thurston, T.L., K.B. Boyle, M. Allen, B.J. Ravenhill, M. Karpiyevich, S. Bloor, A. Kaul, J. Noad, A. Foeglein, S.A. Matthews, D. Komander, M. Bycroft, and F. Randow. 2016. Recruitment of TBK1 to cytosol-invading *Salmonella* induces WIPI2-dependent antibacterial autophagy. *EMBO J* 35:1779-1792.
- Thurston, T.L., M.P. Wandel, N. von Muhlinen, A. Foeglein, and F. Randow. 2012. Galectin 8 targets damaged vesicles for autophagy to defend cells against bacterial invasion. *Nature* 482:414-418.

- Tietzel, I., C. El-Haibi, and R.A. Carabeo. 2009. Human Guanylate Binding Proteins Potentiate the Anti-Chlamydia Effects of Interferon-gamma. *Plos One* 4:
- Tiwari, S., H.P. Choi, T. Matsuzawa, M. Pypaert, and J.D. MacMicking. 2009. Targeting of the GTPase Irgm1 to the phagosomal membrane via PtdIns(3,4)P-2 and PtdIns(3,4,5)P-3 promotes immunity to mycobacteria. *Nature Immunology* 10:907-U144.
- Towbin, H., T. Staehelin, and J. Gordon. 1979. Electrophoretic transfer of proteins from polyacrylamide gels to nitrocellulose sheets: procedure and some applications. *Proc Natl Acad Sci U S A* 76:4350-4354.
- Tretina, K., E.S. Park, A. Maminska, and J.D. MacMicking. 2019. Interferon-induced guanylate-binding proteins: Guardians of host defense in health and disease. *J Exp Med* 216:482-500.
- Trinchieri, G. 1995. Interleukin-12 and interferon-gamma. Do they always go together? *Am J Pathol* 147:1534-1538.
- Tsuboi, Y., H. Abe, R. Nakagawa, S. Oomizu, K. Watanabe, N. Nishi, T. Nakamura, A. Yamauchi, and M. Hirashima. 2007. Galectin-9 protects mice from the Shwartzman reaction by attracting prostaglandin E2-producing polymorphonuclear leukocytes. *Clin Immunol* 124:221-233.
- Tuffy, K.M., and S. Lobo Planey. 2012. Cytoskeleton-Associated Protein 4: Functions Beyond the Endoplasmic Reticulum in Physiology and Disease. *International Scholarly Research Notices* 10.5402:11.
- Upadhyaya, A., S. Jalali, M. Tyagi, and D.C. Parameswarappa. 2023. Intravitreal Clindamycin as an Adjuvant Therapy in Congenital Toxoplasma Retinochoroiditis in a Neonate - A Case Report. *Ocul Immunol Inflamm* 1-4.
- Uthaiyah, R.C., G.J. Praefcke, J.C. Howard, and C. Herrmann. 2003. IIGP1, an interferon-gamma-inducible 47-kDa GTPase of the mouse, showing cooperative enzymatic activity and GTP-dependent multimerization. *J Biol Chem* 278:29336-29343.
- Varella, I.S., I.C. Canti, B.R. Santos, A.Z. Coppini, L.C. Argondizzo, C. Tonin, and M.B. Wagner. 2009. Prevalence of acute toxoplasmosis infection among 41,112 pregnant women and the mother-to-child transmission rate in a public hospital in South Brazil. *Mem Inst Oswaldo Cruz* 104:383-388.
- Varinou, L., K. Ramsauer, M. Karaghiosoff, T. Kolbe, K. Pfeffer, M. Muller, and T. Decker. 2003. Phosphorylation of the Stat1 transactivation domain is required for full-fledged IFN-gamma-dependent innate immunity. *Immunity* 19:793-802.
- Vasta, G.R. 2009. Roles of galectins in infection. *Nat Rev Microbiol* 7:424-438.
- Vasta, G.R. 2012. Galectins as Pattern Recognition Receptors: Structure, Function, and Evolution. *Current Topics in Innate Immunity* 1:946:21-36.
- Vasta, G.R. 2020. Galectins in Host-Pathogen Interactions: Structural, Functional and Evolutionary Aspects. *Adv Exp Med Biol* 1204:169-196.
- Vedrenne, C., D.R. Klopfenstein, and H.P. Hauri. 2005. Phosphorylation controls CLIMP-63-mediated anchoring of the endoplasmic reticulum to microtubules. *Mol Biol Cell* 16:1928-1937.
- Vestal, D.J., J.E. Buss, G.S. Kelner, D. Maciejewski, V.K. Asundi, and R.A. Maki. 1996. Rat p67 GBP is induced by interferon-gamma and isoprenoid-modified in macrophages. *Biochem Biophys Res Commun* 224:528-534.

- Vestal, D.J., J.E. Buss, S.R. McKercher, N.A. Jenkins, N.G. Copeland, G.S. Kelner, V.K. Asundi, and R.A. Maki. 1998. Murine GBP-2: A new IFN-gamma-induced member of the GBP family of GTPases isolated from macrophages. *Journal of Interferon and Cytokine Research* 18:977-985.
- Vestal, D.J., V.Y. Gorbacheva, and G.C. Sen. 2000. Different subcellular localizations for the related interferon-induced GTPases, MuGBP-1 and MuGBP-2: Implications for different functions? *Journal of Interferon and Cytokine Research* 20:991-1000.
- Vetter, I.R., and A. Wittinghofer. 2001. The guanine nucleotide-binding switch in three dimensions. *Science* 294:1299-1304.
- Virreira Winter, S., W. Niedelman, K.D. Jensen, E.E. Rosowski, L. Julien, E. Spooner, K. Caradonna, B.A. Burleigh, J.P.J. Saeij, H.L. Ploegh, and E.M. Frickel. 2011. Determinants of GBP Recruitment to *Toxoplasma gondii* Vacuoles and the Parasitic Factors That Control It. *Plos One* 6:
- von Itzstein, M., M. Plebanski, B.M. Cooke, and R.L. Coppel. 2008. Hot, sweet and sticky: the glycobiology of *Plasmodium falciparum*. *Trends Parasitol* 24:210-218.
- Vopel, T., S. Kunzelmann, and C. Herrmann. 2009. Nucleotide dependent cysteine reactivity of hGBP1 uncovers a domain movement during GTP hydrolysis. *Febs Letters* 583:1923-1927.
- Vopel, T., A. Syguda, N. Britzen-Laurent, S. Kunzelmann, M.B. Ludemann, C. Dovengerds, M. Sturzl, and C. Herrmann. 2010. Mechanism of GTPase-Activity-Induced Self-Assembly of Human Guanylate Binding Protein 1. *Journal of Molecular Biology* 400:63-70.
- Walker, M.E., E.E. Hjort, S.S. Smith, A. Tripathi, J.E. Hornick, E.H. Hinchcliffe, W. Archer, and K.M. Hager. 2008. *Toxoplasma gondii* actively remodels the microtubule network in host cells. *Microbes Infect* 10:1440-1449.
- Wang, Z.E., S.L. Reiner, S. Zheng, D.K. Dalton, and R.M. Locksley. 1994. CD4+ effector cells default to the Th2 pathway in interferon gamma-deficient mice infected with *Leishmania major*. *J Exp Med* 179:1367-1371.
- Wang, Z.J., S.M. Yu, J.M. Gao, P. Zhang, G. Hide, M. Yamamoto, D.H. Lai, and Z.R. Lun. 2021. High resistance to *Toxoplasma gondii* infection in inducible nitric oxide synthase knockout rats. *iScience* 24:103280.
- Warnock, D.E., and S.L. Schmid. 1996. Dynamin GTPase, a force-generating molecular switch. *Bioessays* 18:885-893.
- Wehner, M., and C. Herrmann. 2010. Biochemical properties of the human guanylate binding protein 5 and a tumor-specific truncated splice variant. *Febs Journal* 277:1597-1605.
- Wehner, M., S. Kunzelmann, and C. Herrmann. 2012. The guanine cap of human guanylate-binding protein 1 is responsible for dimerization and self-activation of GTP hydrolysis. *Febs Journal* 279:203-210.
- Weinlander, K., E. Naschberger, M.H. Lehmann, P. Tripal, W. Paster, H. Stockinger, C. Hohenadl, and M. Sturzl. 2008. Guanylate binding protein-1 inhibits spreading and migration of endothelial cells through induction of integrin alpha4 expression. *FASEB J* 22:4168-4178.

- Weng, I.C., H.L. Chen, T.H. Lo, W.H. Lin, H.Y. Chen, D.K. Hsu, and F.T. Liu. 2018. Cytosolic galectin-3 and -8 regulate antibacterial autophagy through differential recognition of host glycans on damaged phagosomes. *Glycobiology* 28:392-405.
- Wenner, C.A., M.L. Guler, S.E. Macatonia, A. O'Garra, and K.M. Murphy. 1996. Roles of IFN-gamma and IFN-alpha in IL-12-induced T helper cell-1 development. *J Immunol* 156:1442-1447.
- Wennerberg, K., K.L. Rossman, and C.J. Der. 2005. The Ras superfamily at a glance. *J Cell Sci* 118:843-846.
- Wilking, H., M. Thamm, K. Stark, T. Aebischer, and F. Seeber. 2016. Prevalence, incidence estimations, and risk factors of *Toxoplasma gondii* infection in Germany: a representative, cross-sectional, serological study. *Sci Rep* 6:22551.
- Wittinghofer, A., and P. Gierschik. 2000. Highlight: GTP binding proteins--central regulators in cell biology. *Biol Chem* 381:355.
- Wong, S.Y., and J.S. Remington. 1993. Biology of *Toxoplasma gondii*. *AIDS* 7:299-316.
- Wu, L., X. Wang, Y. Li, Y. Liu, D. Su, T. Fu, F. Guo, L. Gu, X. Jiang, S. Chen, and J. Cao. 2016. *Toxoplasma gondii* ROP18: potential to manipulate host cell mitochondrial apoptosis. *Parasitol Res* 115:2415-2422.
- Wu, S.Y., J.H. Huang, W.Y. Chen, Y.C. Chan, C.H. Lin, Y.C. Chen, F.T. Liu, and B.A. Wu-Hsieh. 2017. Cell Intrinsic Galectin-3 Attenuates Neutrophil ROS-Dependent Killing of *Candida* by Modulating CR3 Downstream Syk Activation. *Front Immunol* 8:48.
- Wynn, T.A., C.M. Nicolet, and D.M. Paulnock. 1991. Identification and characterization of a new gene family induced during macrophage activation. *J Immunol* 147:4384-4392.
- Yamamoto, M., M. Okuyama, J.S. Ma, T. Kimura, N. Kamiyama, H. Saiga, J. Ohshima, M. Sasai, H. Kayama, T. Okamoto, D.C.S. Huang, D. Soldati-Favre, K. Horie, J. Takeda, and K. Takeda. 2012. A Cluster of Interferon-gamma-Inducible p65 GTPases Plays a Critical Role in Host Defense against *Toxoplasma gondii*. *Immunity* 37:302-313.
- Yamamoto, Y.I., V. Huber, and S. Hoshino-Shimizi. 1997. Identification of *Toxoplasma gondii* antigens involved in the IgM and IgG indirect hemagglutination tests for the diagnosis of toxoplasmosis. *Rev Inst Med Trop Sao Paulo* 39:149-154.
- Yang, L.L., R.M. Li, X.H. Pan, M. Qian, and B. Du. 2012. [Construction of P2Y6 constitutive knock down breast cancer cell line and evaluation of its proliferation]. *Xi Bao Yu Fen Zi Mian Yi Xue Za Zhi* 28:510-513.
- Yang, R.Y., G.A. Rabinovich, and F.T. Liu. 2008. Galectins: structure, function and therapeutic potential. *Expert Rev Mol Med* 10:e17.
- Yang, S., and S.F. Parmley. 1995. A bradyzoite stage-specifically expressed gene of *Toxoplasma gondii* encodes a polypeptide homologous to lactate dehydrogenase. *Mol Biochem Parasitol* 73:291-294.
- Yap, G., M. Pesin, and A. Sher. 2000. Cutting edge: IL-12 is required for the maintenance of IFN-gamma production in T cells mediating chronic resistance to the intracellular pathogen, *Toxoplasma gondii*. *J Immunol* 165:628-631.
- Yap, G.S., and A. Sher. 1999. Cell-mediated immunity to *Toxoplasma gondii*: initiation, regulation and effector function. *Immunobiology* 201:240-247.

- Yarovinsky, F., D.K. Zhang, J.F. Andersen, G.L. Bannenberg, C.N. Serhan, M.S. Hayden, S. Hieny, F.S. Sutterwala, R.A. Flavell, S. Ghosh, and A. Sher. 2005. TLR11 activation of dendritic cells by a protozoan profilin-like protein. *Science* 308:1626-1629.
- Yokoyama, K., G.W. Goodwin, F. Ghomashchi, J.A. Glomset, and M.H. Gelb. 1991. A protein geranylgeranyltransferase from bovine brain: implications for protein prenylation specificity. *Proc Natl Acad Sci USA* 88:5302-5306.
- Yoshida, A., Y. Koide, M. Uchijima, and T.O. Yoshida. 1994. IFN-gamma induces IL-12 mRNA expression by a murine macrophage cell line, J774. *Biochem Biophys Res Commun* 198:857-861.
- You, M., D.H. Yu, and G.S. Feng. 1999. Shp-2 tyrosine phosphatase functions as a negative regulator of the interferon-stimulated Jak/STAT pathway. *Mol Cell Biol* 19:2416-2424.
- Youn, J.H., H.W. Nam, D.J. Kim, Y.M. Park, W.K. Kim, W.S. Kim, and W.Y. Choi. 1991. Cell cycle-dependent entry of *Toxoplasma gondii* into synchronized HL-60 cells. *Kisaengchunghak Chapchi* 29:121-128.
- Zantl, N., A. Uebe, B. Neumann, H. Wagner, J.R. Siewert, B. Holzmann, C.D. Heidecke, and K. Pfeffer. 1998. Essential role of gamma interferon in survival of colon ascendens stent peritonitis, a novel murine model of abdominal sepsis. *Infect Immun* 66:2300-2309.
- Zhang, F.L., and P.J. Casey. 1996. Protein prenylation: molecular mechanisms and functional consequences. *Annu Rev Biochem* 65:241-269.
- Zhang, G., and A. Tandon. 2012. Quantitative assessment on the cloning efficiencies of lentiviral transfer vectors with a unique clone site. *Sci Rep* 2:1-8.
- Zhang, J., S.L. Planey, C. Ceballos, S.M. Stevens, Jr., S.K. Keay, and D.A. Zacharias. 2008. Identification of CKAP4/p63 as a major substrate of the palmitoyl acyltransferase DHHC2, a putative tumor suppressor, using a novel proteomics method. *Mol Cell Proteomics* 7:1378-1388.
- Zhang, X.F., J. Settleman, J.M. Kyriakis, E. Takeuchi-Suzuki, S.J. Elledge, M.S. Marshall, J.T. Bruder, U.R. Rapp, and J. Avruch. 1993. Normal and oncogenic p21ras proteins bind to the amino-terminal regulatory domain of c-Raf-1. *Nature* 364:308-313.
- Zhao, X.Y., and S.E. Ewald. 2020. The molecular biology and immune control of chronic *Toxoplasma gondii* infection. *J Clin Invest* 130:3370-3380.
- Zhao, Y., and G.S. Yap. 2014. *Toxoplasma*'s arms race with the host interferon response: a menage a trois of ROPs. *Cell Host Microbe* 15:517-518.
- Zhao, Y.O., C. Rohde, J.T. Lilue, S. Konen-Waisman, A. Khaminets, J.P. Hunn, and J.C. Howard. 2009. *Toxoplasma gondii* and the immunity-related GTPase (IRG) resistance system in mice - A Review. *Memorias do Instituto Oswaldo Cruz* 104:234-240.
- Zhao, Z.J., B. Fux, M. Goodwin, I.R. Dunay, D. Strong, B.C. Miller, K. Cadwell, M.A. Delgado, M. Ponpuak, K.G. Green, R.E. Schmidt, N. Mizushima, V. Deretic, L.D. Sibley, and H.W. Virgin. 2008. Autophagosome-independent Essential Function for the Autophagy Protein Atg5 in Cellular Immunity to Intracellular Pathogens. *Cell Host & Microbe* 4:458-469.

- Zhou, X.W., B.F. Kafsack, R.N. Cole, P. Beckett, R.F. Shen, and V.B. Carruthers. 2005. The opportunistic pathogen *Toxoplasma gondii* deploys a diverse legion of invasion and survival proteins. *J Biol Chem* 280:34233-34244.
- Zhuo, Y., and S.L. Bellis. 2011. Emerging role of alpha2,6-sialic acid as a negative regulator of galectin binding and function. *J Biol Chem* 286:5935-5941.
- Zimmermann, S., P.J. Murray, K. Heeg, and A.H. Dalpke. 2006. Induction of suppressor of cytokine signaling-1 by *Toxoplasma gondii* contributes to immune evasion in macrophages by blocking IFN-gamma signaling. *J Immunol* 176:1840-1847.
- Zinkernagel, A.S., R.S. Johnson, and V. Nizet. 2007. Hypoxia inducible factor (HIF) function in innate immunity and infection. *J Mol Med (Berl)* 85:1339-1346.
- Zufferey, R., T. Dull, R.J. Mandel, A. Bukovsky, D. Quiroz, L. Naldini, and D. Trono. 1998. Self-inactivating lentivirus vector for safe and efficient in vivo gene delivery. *J Virol* 72:9873-9880.
- Zuniga, E., A. Gruppi, J. Hirabayashi, K.I. Kasai, and G.A. Rabinovich. 2001. Regulated expression and effect of galectin-1 on *Trypanosoma cruzi*-infected macrophages: modulation of microbicidal activity and survival. *Infect Immun* 69:6804-6812.

Acknowledgement

First and foremost, I would like to thank my family for their unconditional and devoted support during both the good and the turbulent times of my life. I would also like to thank Prof. Dr. Klaus Pfeffer and Dr. Daniel Degrandi, my boss and supervisor, who have accompanied my career with advice and support over many years.

Appendix

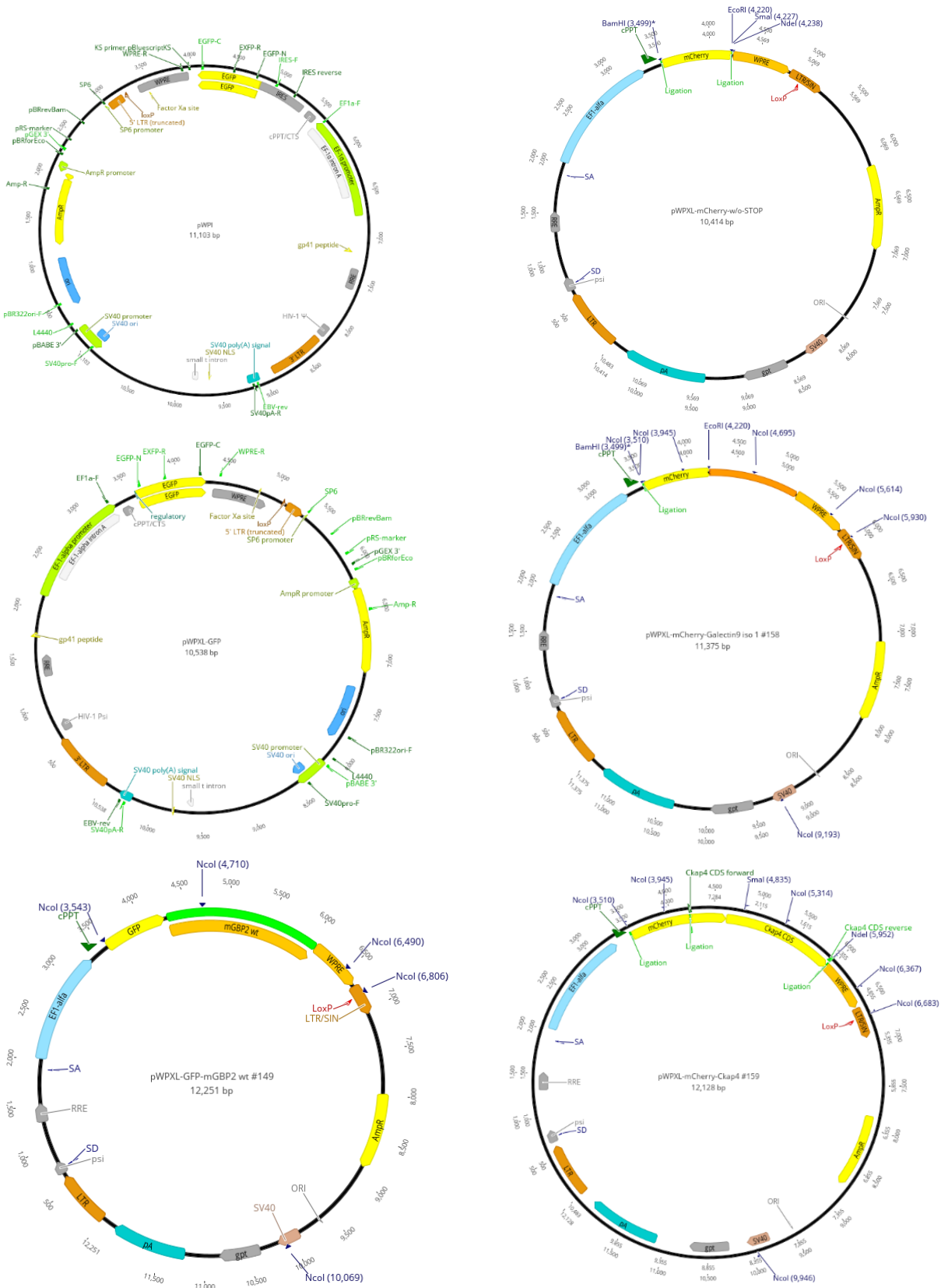


Figure S1: Expression plasmids for interaction partner analysis of mGBP2.
 The construction and visualization of the vectors were carried out using the Geneious software.

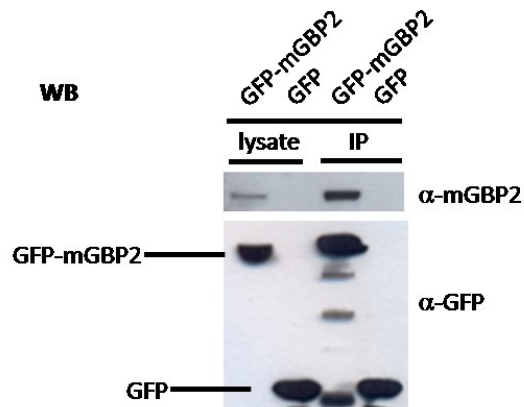
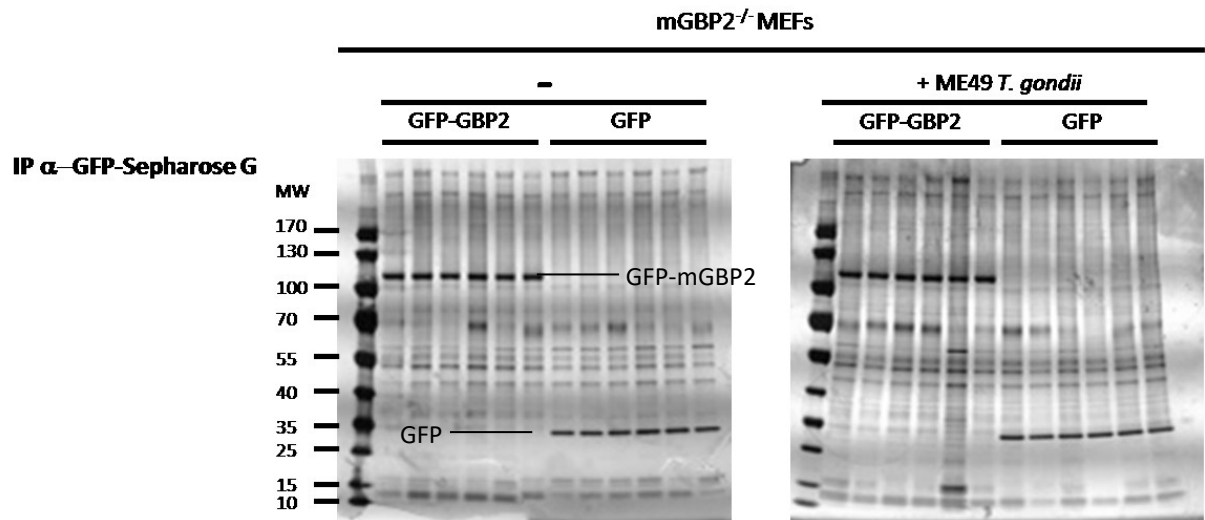
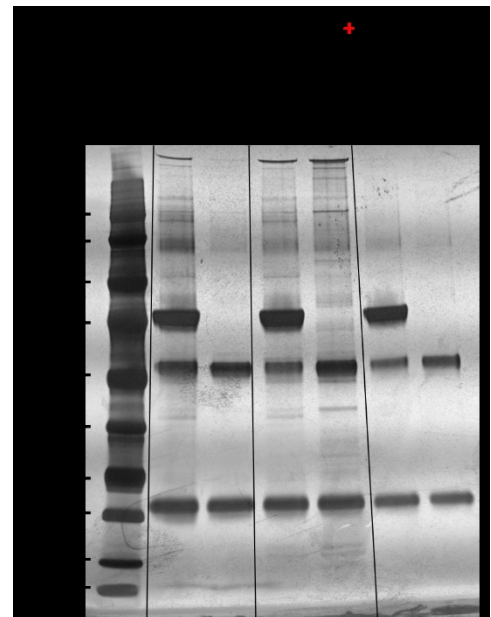
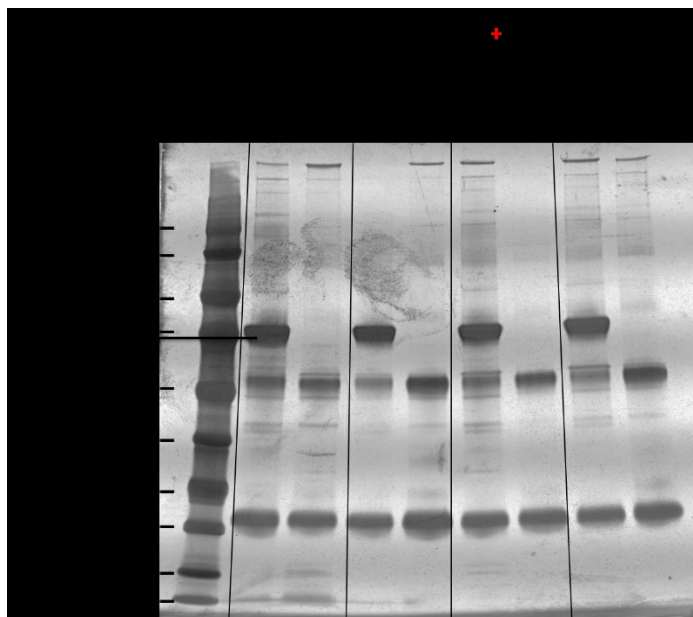


Figure S2: Identification and validation of mGBP2 interaction partners.

mGBP2^{-/-} MEFs were reconstituted with GFP-mGBP2 or a GFP-only expressing control vector and stimulated with IFN- γ for 16 h, infected for 2 h with ME49 *T. gondii* or left uninfected. Subsequently, cells were lysed and postnuclear supernatants were incubated o/n with α -GFP antibody coupled agarose beads at 4°C for IP. One part of IP samples was separated via 10% SDS-PAGE and labelled using silver staining (upper row). Another part of the IP samples was subjected to Western Blotting and immune staining with an α -mGBP2 antiserum or an α -GFP antibody (lower row). A third part of these IP samples was transferred to the MS analysis (see main text).



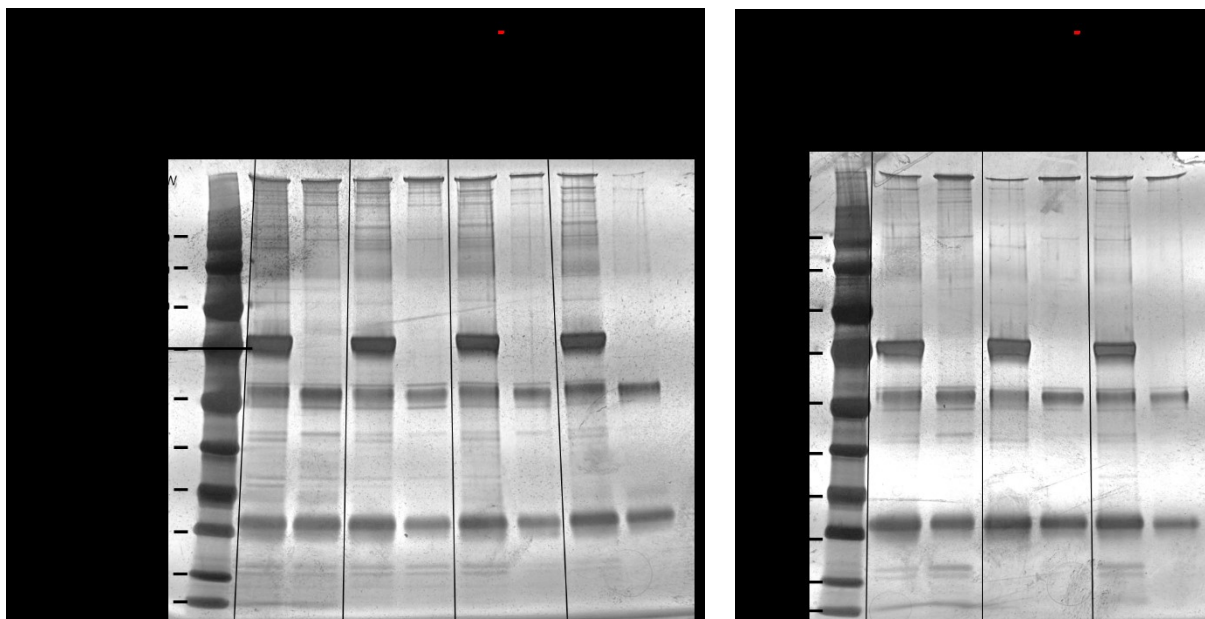


Figure S3: Identification of mGBP2 interaction partners.

mGBP2^{-/-} MEFs were reconstituted with HA-mGBP2 or a control pWPI vector and either treated with IFN- γ for 16 h or left untreated. Additionally, cells were stimulated for 16 h either with 100 mM Bafilomycin A1 (endosomal acidification and autophagy inhibitor), 1 μ M Wortmannin (PI3 kinase inhibitor), 100 mM Concanamycin (autophagy inhibitor), 2 μ M MG132 (proteasome inhibitor), or Lactacystin (proteasome inhibitor). Subsequently, cells were lysed and postnuclear supernatants were incubated o/n with α -HA antibody coupled agarose beads at 4°C for IP. IP samples were separated via 10% SDS-PAGE and labelled using silver staining.

Table S1: List and known function of mass spectrometry-identified potential interaction partners of mGBP2.

Protein	known function
THBS1	Adhesive glycoprotein, mediates activation of macrophages in fungal infections, interacts with <i>Trypanosoma cruzi</i> surface calreticulin
Anxa5/6	Calcium-dependent phospholipid-binding proteins, exocytosis and endocytosis, cellular signal transduction, inflammation, endosomal aggregation, and vesicle fusion.
Ddx21	DEXD/H-box RNA helicases, RNA recognition, anti-viral and anti-microbial activity
Ddx5/6	
Dhx9	
Isg15	Ubiquitin-like protein, RIG-I-like receptor signalling pathway, antiviral and antiparasitic activity.
LAMP2	Membrane-bound glycoprotein, protection, maintenance, and adhesion of lysosomes, receptor for chaperone-mediated autophagy
Tnpo1	Nucleus-cytoplasm transport
Kpnb1/a2	Nucleus-cytoplasm, RNA transport
Ckap4	Protein processing in the ER
iNOS	Microbial immune defence
Ifitm3	Antiviral immune defence
Nampt	Nicotinamide metabolism, stress response
Npm3	Nuclear chaperone phosphoprotein

Aifm1	Mitochondrial protein involved cytochrome c induced in apoptosis, mitochondrial bioenergetics, and oxidative stress response
Eif3e	Subunit of the eukaryotic translation initiation factor 3 complex, plays a crucial role in the initiation of protein synthesis
Cathepsin D	Lysosomal protease, involved in tissue remodelling, antigen presentation, and autophagy
Galectin 9	Carbohydrate-binding protein, involved in immune regulation and inflammation

Table S2: List and validation status of mass spectrometry-identified potential interaction partners of mGBP2.

Interaction-partner	Size [bp]	TOPO 2.1	pWPXL mCherry / GFP	Virus	Cell line	Colocalization	IP
Anxa5	960	+	+	+	+	+	+
Anxa6 iso 1	2022	+	+	+			
Anxa6 iso 2	2004	+	+	+			
Ckap4	1728	+	+	+	+	+	+
Copa	3675	+	+	+			
Ddx5	1848	+	+	+			
Ddx6	1452	+	+	+			
Ddx21	2556	+	+	+			
Eif3e	1341		+	+			
Galectin 9 iso 1	1059	+	+	+	+	+	+
Ifitm3	414	+	+	+			
iNOS	3435	+	+				
ISG15	486	+	+	+	+	+	+
Kpna2	1590	+	+	+			
Kpnb1	2631	+	+	+			
Nampt	1476	+	+	+			
Npm3	528	+	+	+			
Thbs1	3616	+	+	+			
Tnpo1 iso 1	2697	+	+	+			
Tnpo1 iso 2	2673	+	+	+			
Cathepsin D	1233	+		+	+	+	
Lamp2 iso 1	1248	+		+	+		
Lamp2 iso 2	1248	+		+	+		
Aifm1	1844			+	+		

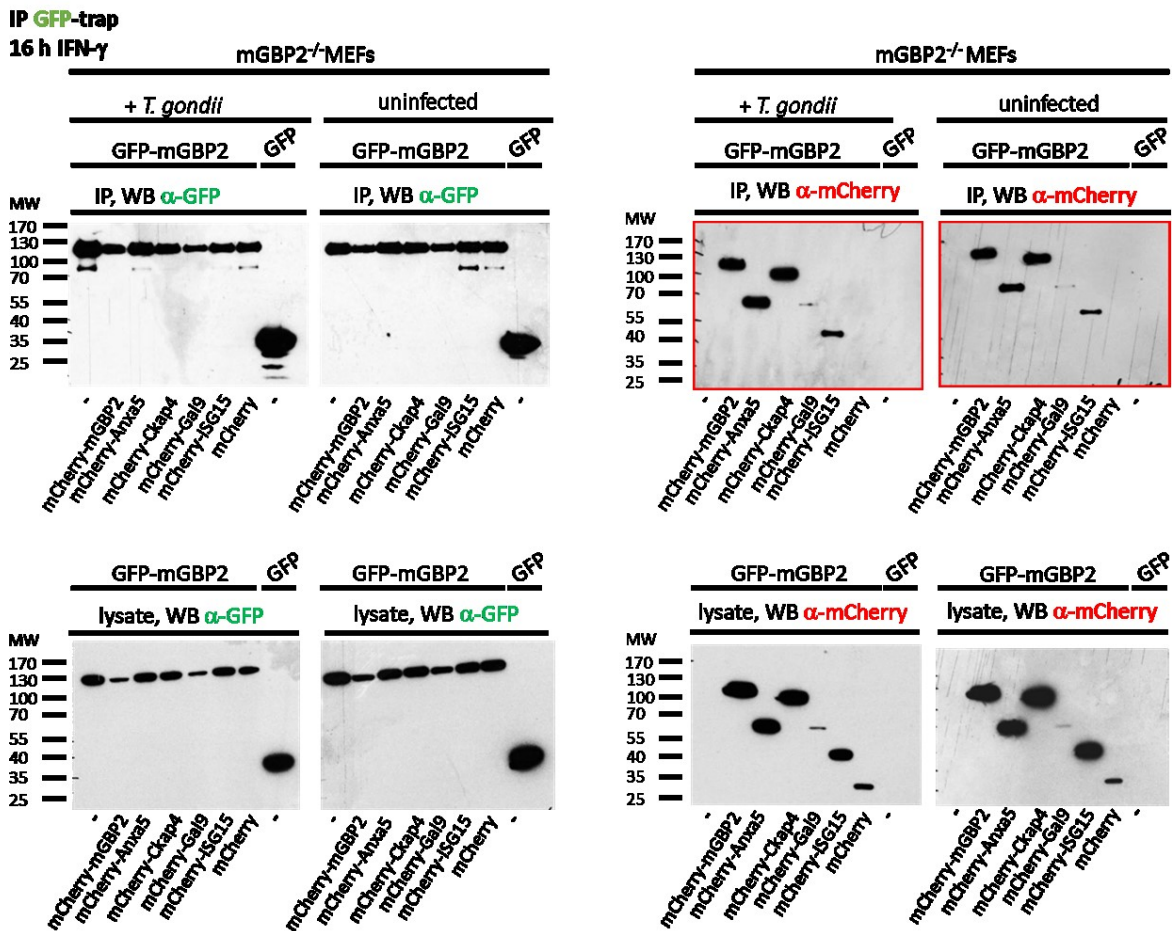


Figure S4: Verification of MS-identified interaction partners of mGBP2 by IP analysis.

mGBP2^{-/-} MEFs were reconstituted with GFP-mGBP2 or a GFP-only expressing control vector and additionally transduced with mCherry fusion constructs of MS identified interaction partners of mGBP2 or with only mCherry expressing vector, and stimulated with IFN- γ for 16 h, infected for 2 h with ME49 *T. gondii* or left uninfected. Subsequently, cells were lysed and postnuclear supernatants were incubated for 1h with GFP-Trap® beads at 4°C for IP. The IP samples were subjected to Western Blotting and immune staining with an α -GFP or an α -mCherry antibodies.

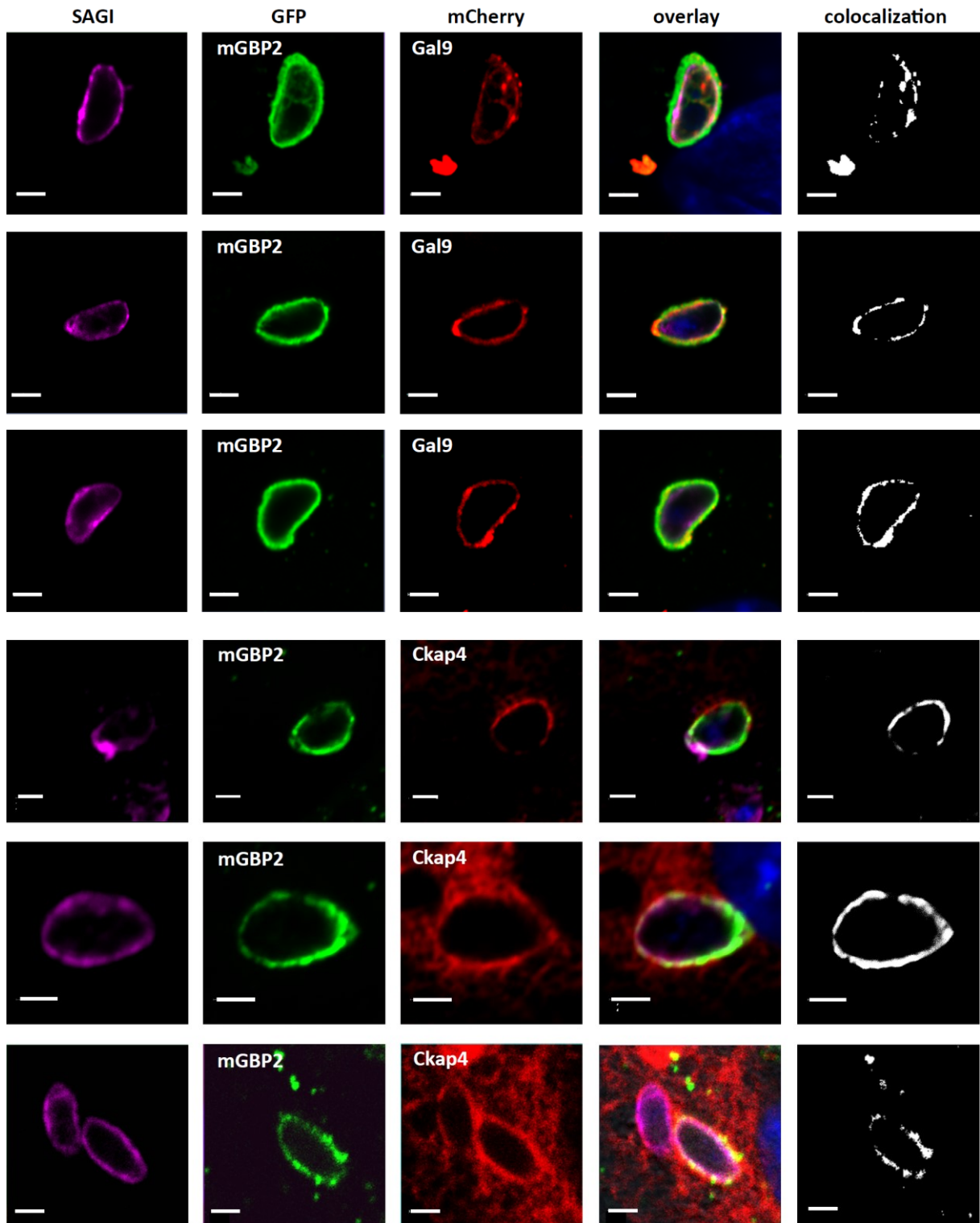


Figure S5: Intracellular colocalization of mGBP2 with the interaction partners Gal9 and Ckap4.

Colocalization of GFP-mGBP2 with mCherry-Gal9 or mCherry-Ckap4 was analysed in mGBP2^{-/-} MEFs reconstituted with the indicated fusion proteins. Cells were stimulated with IFN- γ for 16 h and subsequently infected with ME49 *T. gondii* for 2 h. After fixation, *T. gondii* were stained with an α -SAG1 antibody and the cell nuclei were labelled with DAPI. Glass slides were analysed by confocal microscopy. Bars 5 μ m. The right column depicts the results for a colocalization analysis using the Image Visualization and Analysis Software (Imaris) for GFP and mCherry fluorescence.

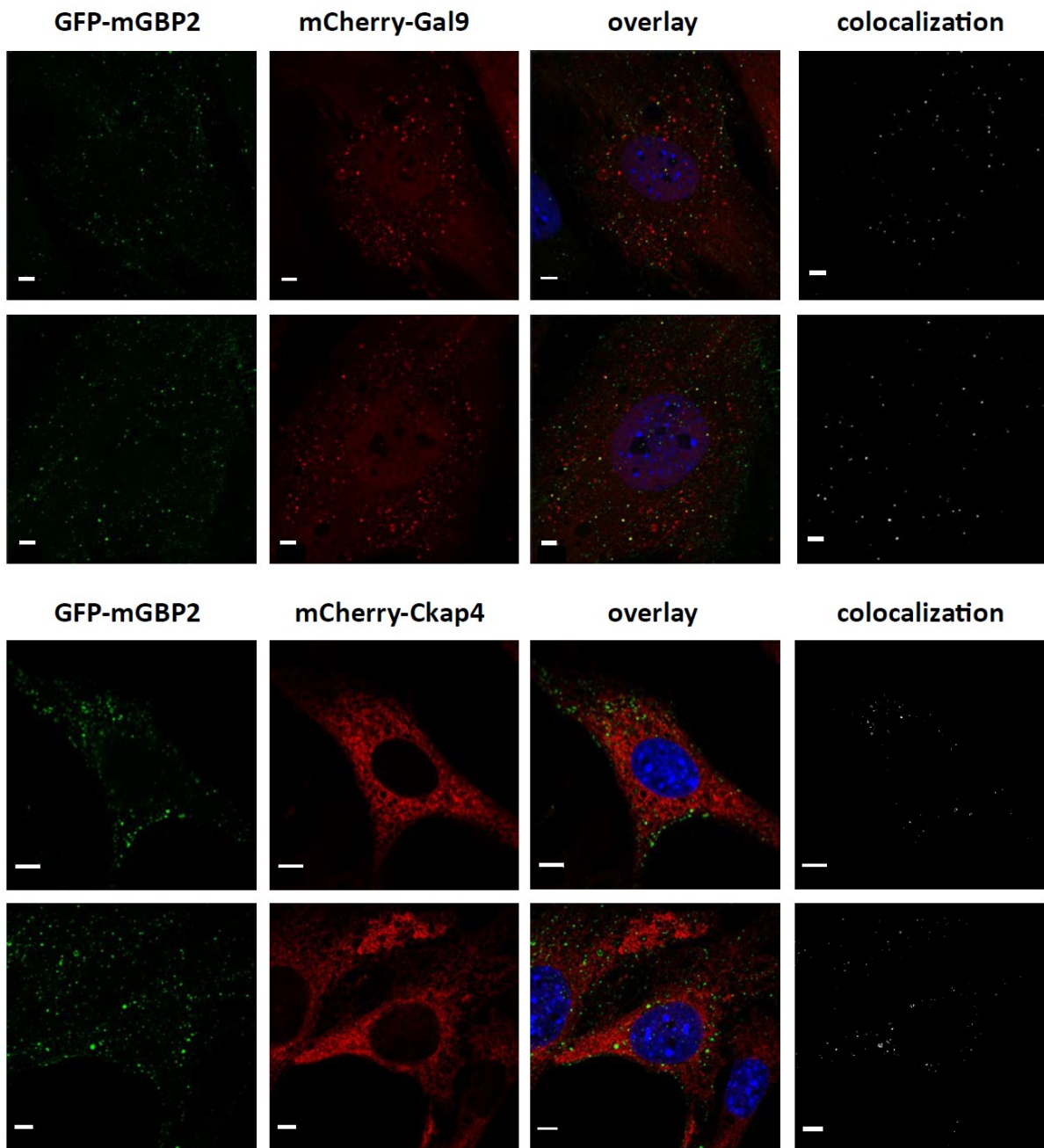


Figure S6. Intracellular colocalization of mGBP2 with the interaction partners Gal9 and Ckap4.

Colocalization of GFP-mGBP2 with mCherry-Gal9 or mCherry-Ckap4 was analysed in mGBP2^{-/-} MEFs reconstituted with the indicated fusion proteins. Cells were stimulated with IFN- γ for 16 h. After fixation, cell nuclei were labelled with DAPI. Glass slides were analysed by confocal microscopy. Bars 5 μ m. The right column depicts the results for a colocalization analysis using the Image Visualization and Analysis Software (Imaris) for GFP and mCherry fluorescence.

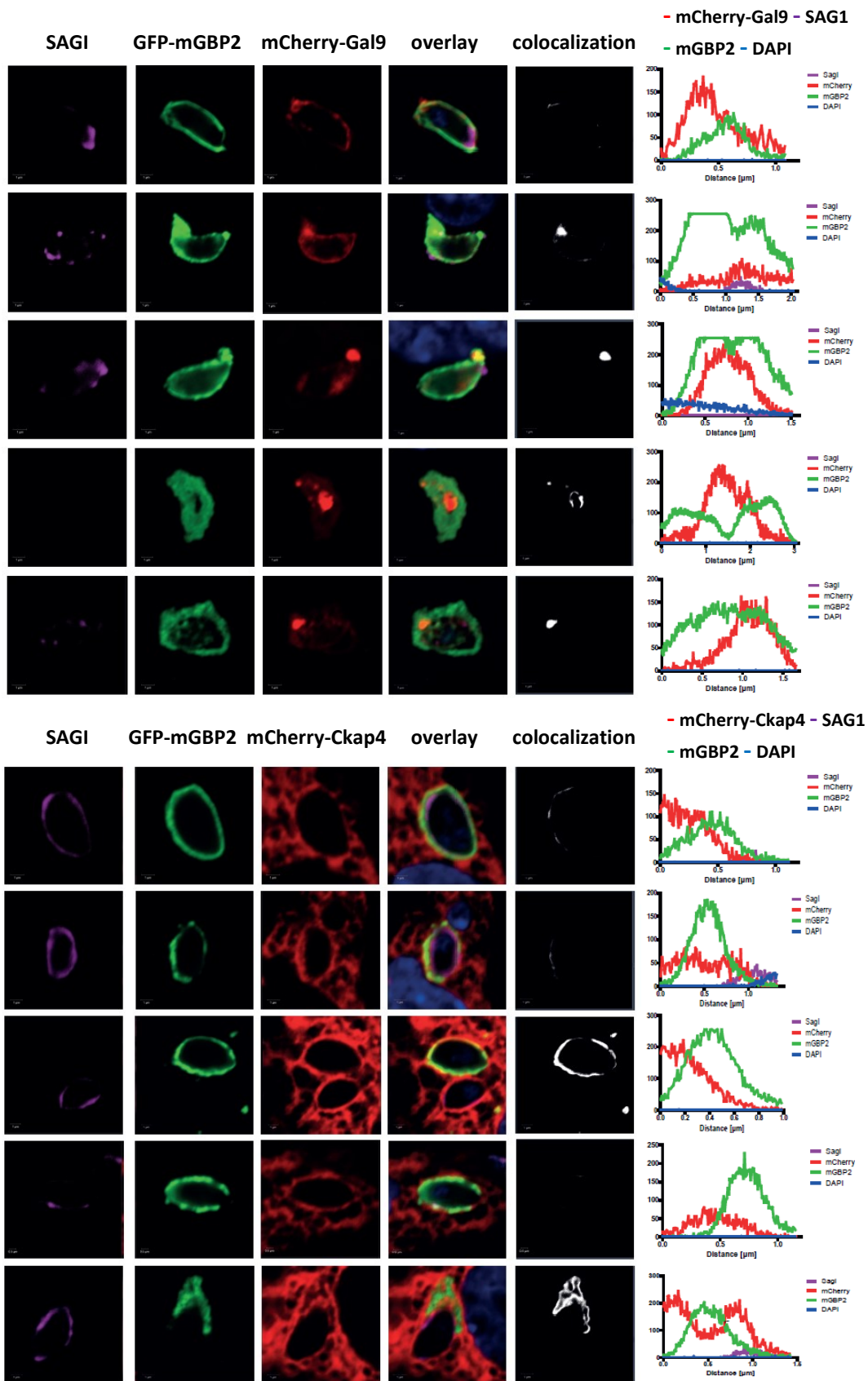
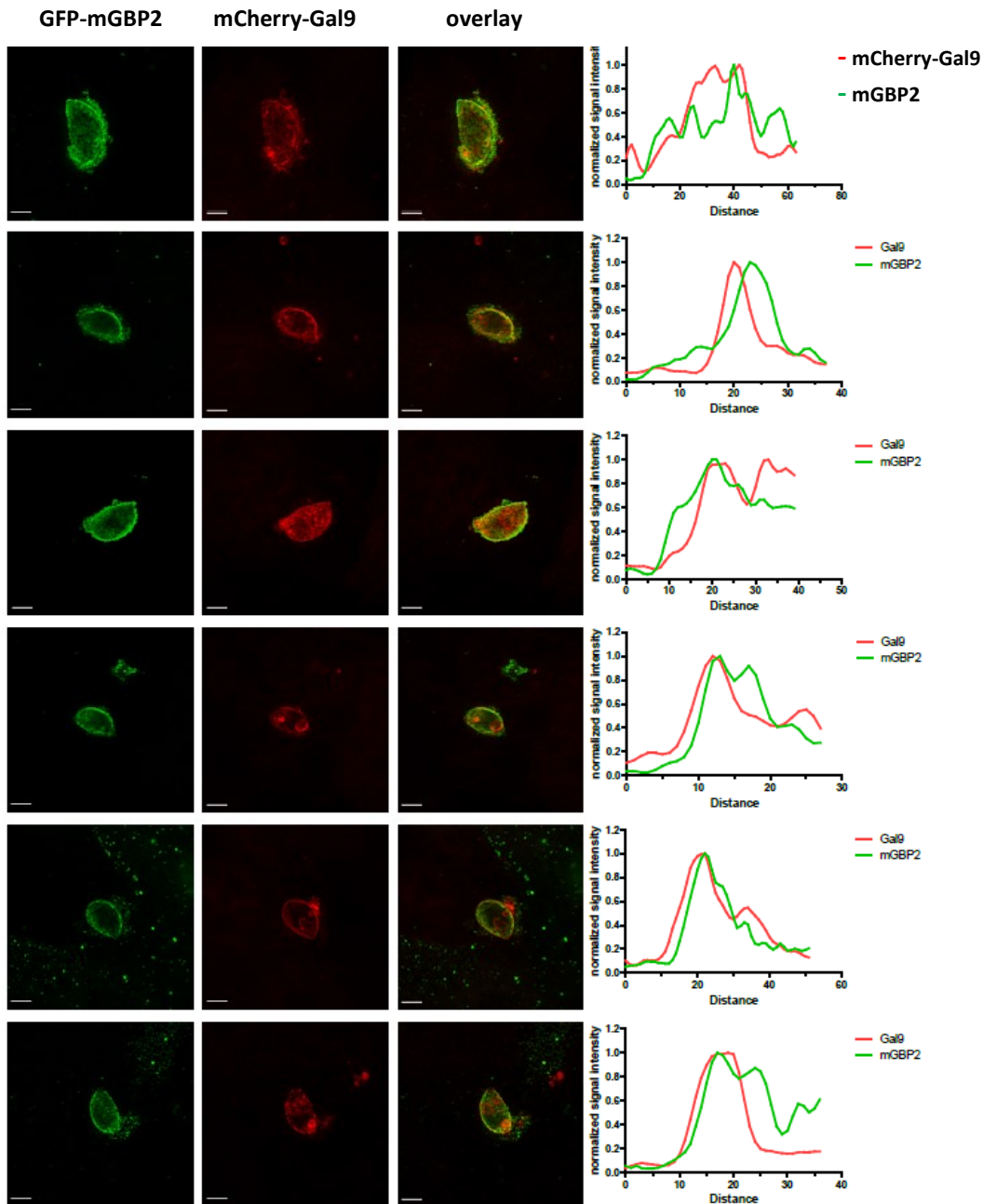


Figure S7: Intracellular colocalization of mGBP2 with the interaction partners Gal9 and Ckap4.

Colocalization of GFP-mGBP2 with mCherry-Gal9 or mCherry-Ckap4 was analysed in mGBP2^{-/-} MEFs reconstituted with the indicated fusion proteins. Cells were stimulated with IFN- γ for 16 h and subsequently infected with ME49 *T. gondii* for 2 h. Living cells were treated with SNAP-Cell 647-SiR substrate at 37°C, 5% CO₂ for 30 minutes to label the mCherry-fusion protein. After fixation, *T. gondii* were stained with an α -

SAG1 antibody and the cell nuclei were labelled with DAPI. Glass slides were analysed by confocal microscopy. The “colocalization” column depicts the results for a colocalization analysis using the Image Visualization and Analysis Software (Imaris) for GFP and mCherry fluorescence. The graphs in the right panel (visualized using GraphPrism software) depict a fluorescence intensity analysis of confocal images on the far right with the ImageJ software (Fiji) for GFP and mCherry fluorescence signals along the cross sections of PVMs.



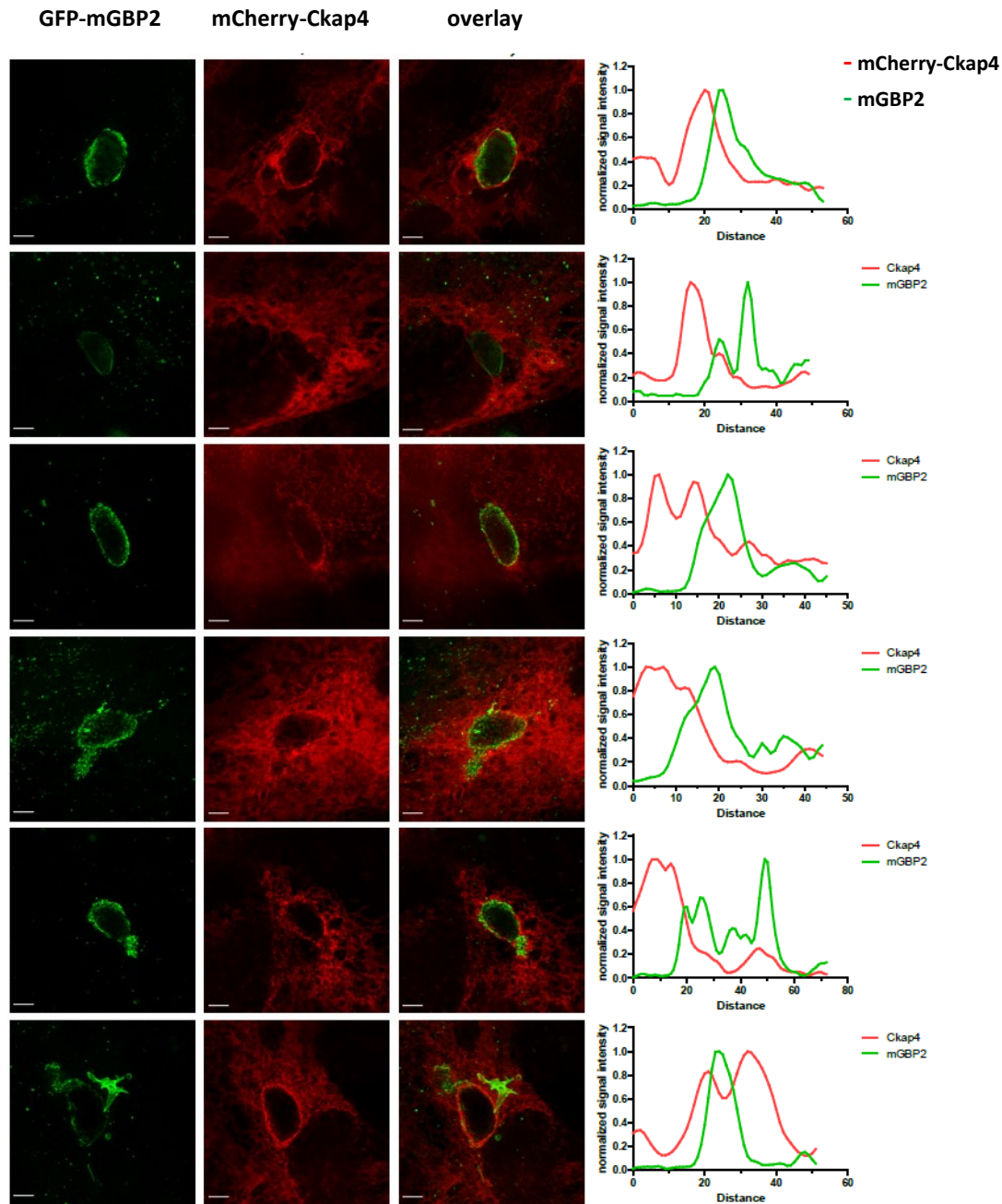


Figure S8: Intracellular colocalization of mGBP2 with the interaction partners Gal9 and Ckap4. STED microscopy.

Colocalization of GFP-mGBP2 with mCherry-Gal9 or mCherry-Ckap4 was analysed in mGBP2^{-/-} MEFs reconstituted with the indicated fusion proteins. Cells were stimulated with IFN- γ for 16 h and subsequently infected with ME49 *T. gondii* for 2 h. Living cells were treated with SNAP-Cell 647-SiR substrate at 37°C, 5% CO₂ for 30 minutes to label the mCherry-fusion protein. After fixation, infected cells were treated with an α -RFP V_HH nanobody conjugated to eGFPBoosterAtto647N for enhancement of the immunofluorescence of mCherry. Glass slides were analysed by STED microscopy. The graphs in the right panel (visualized using GraphPrism software) depict a fluorescence intensity analysis of STED images on the far right with the ImageJ software (Fiji) for GFP and mCherry fluorescence signals along the cross sections of PVMs.

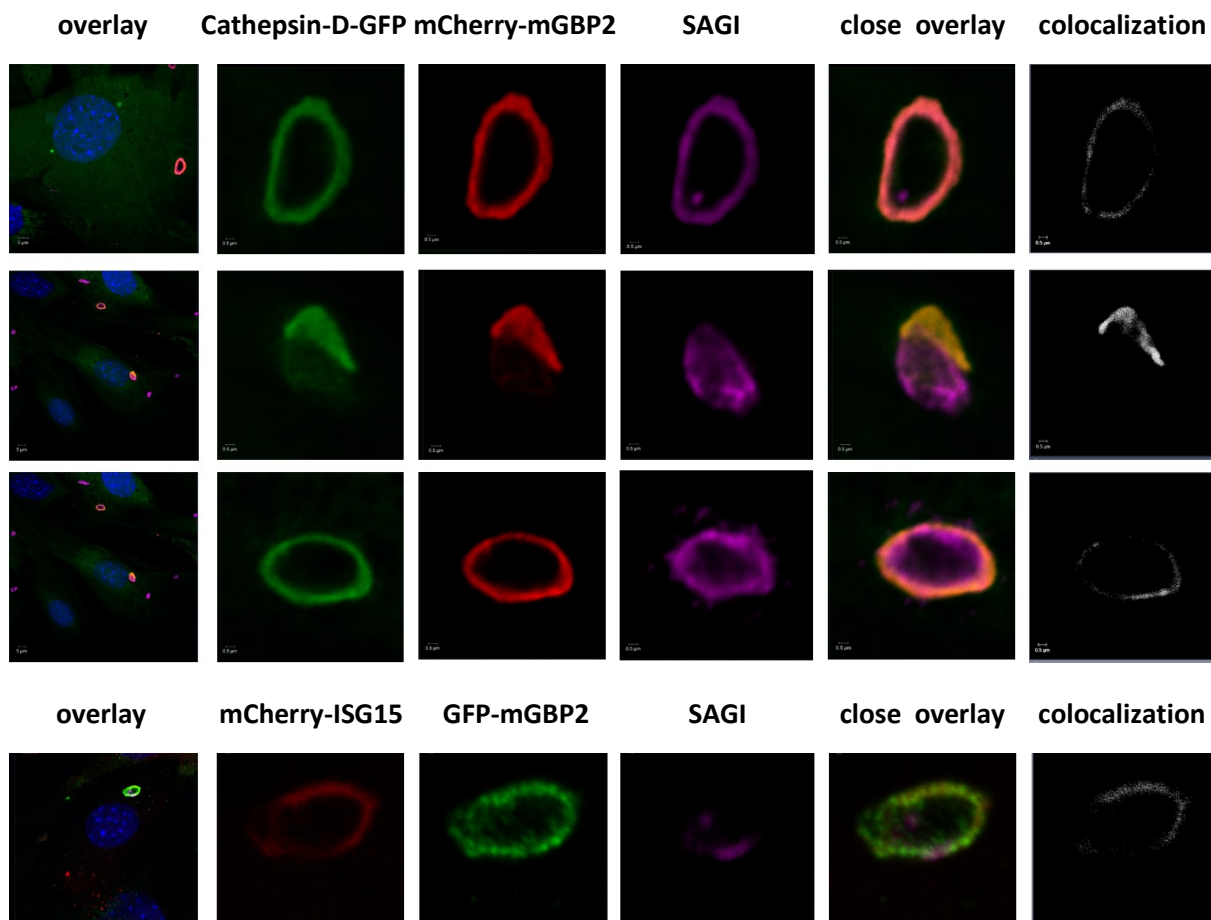


Figure S9: Intracellular colocalization of mGBP2 with the interaction partners Cathepsin-D and ISG15. Confocal microscopy.

Colocalization of either mCherry-mGBP2 with Cathepsin-D-GFP or GFP-mGBP2 with mCherry-ISG15 was analysed in mGBP2^{-/-} MEFs reconstituted with the indicated fusion proteins. Cells were stimulated with IFN- γ for 16 h and subsequently infected with ME49 *T. gondii* for 2 h. After fixation, *T. gondii* were stained with an α -SAG1 antibody and the cell nuclei were labelled with DAPI. Bars 5 and 0.5 μ m. The right column depicts the results for a colocalization analysis using the Image Visualization and Analysis Software (Zeiss) for GFP and mCherry fluorescence.

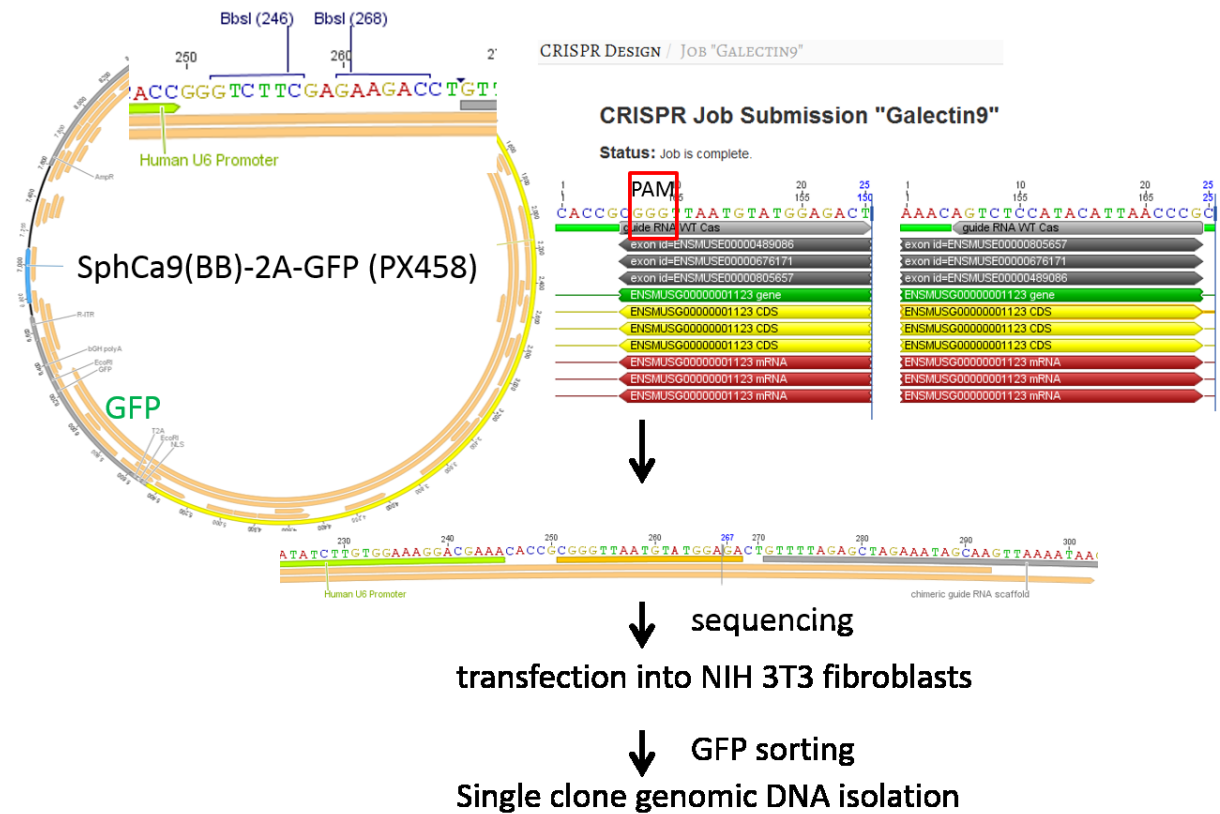


Figure S10: CRISPR/Cas9 cloning strategy.

The experimental is presented, outlining the steps involved in vector design, construction, validation, and cell line expansion. *In silico* design of appropriate sgRNAs (here exemplarily depicted for *gal9* gene knockout) and genotyping primers was conducted using the CRISPR Design Tool (<http://tools.genome-engineering.org>). The sgRNA guide sequences were subsequently cloned into an expression plasmid containing both the sgRNA scaffold backbone (BB) and Cas9, known as pSpCas9(BB). This resulting plasmid is denoted as pSpCas9(sgRNA). Verified pSpCas9(sgRNA) plasmids, were then transfected into 3T3 fibroblasts to assess their ability to induce targeted cleavage. Finally, transfected cells were sorted for GFP and underwent clonal expansion to generate isogenic cell lines with predetermined mutations.

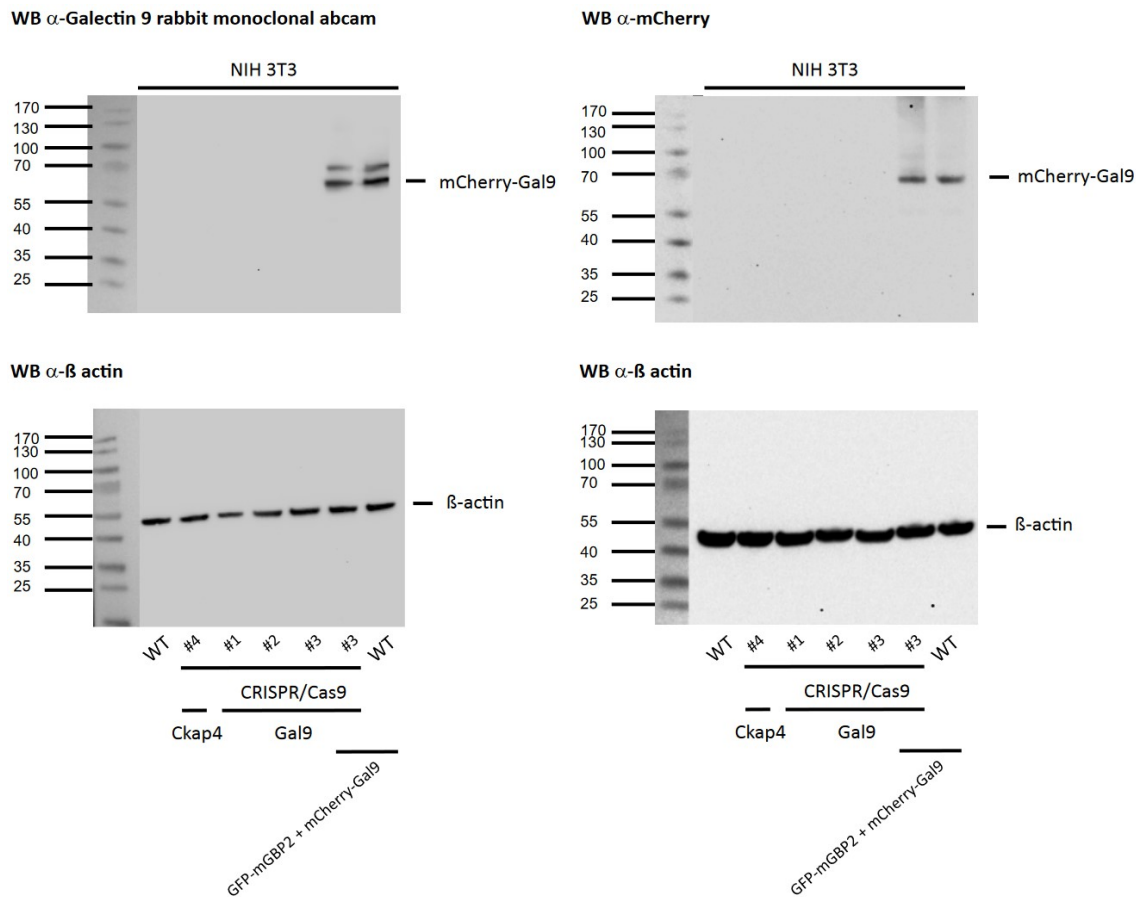


Figure S11: Verification of CRISPR/Cas9 Gal9 inactivation by WB analysis.

Postnuclear supernatants of NIH 3T3 cells from different CRISPR/Cas9 Gal9 sgRNA targeted clones and from WT cells were analysed by WB. WT cells and one CRISPR/Cas9 Gal9 sgRNA targeted clone co-expressing GFP-mGBP2 and mCherry-Gal9 served as controls. Cells were stimulated with IFN- γ for 16 h. Blots were stained with monoclonal α -Gal9 from rabbit (abcam) (upper left panel), α -mCherry (upper right panel) or α - β -actin antibodies (lower panel).

Table S3: Recruitment rates of Gal9 to PV of *T. gondii* in IFN- γ stimulated WT compared to mGBP2^{-/-} MEF 2 h post infection.

WT MEFs				mGBP2 ^{-/-} MEFs			
<i>T. gondii</i>	mCherry-Gal9	ratio	normalized	<i>T. gondii</i>	mCherry-Gal9	ratio	normalized
13	4	0,31	0,83	12	1	0,08	0,23
13	8	0,62	1,67	14	2	0,14	0,39
17	9	0,53	1,44	17	1	0,06	0,16
19	4	0,21	0,57	14	1	0,07	0,19
16	6	0,38	1,02	12	2	0,17	0,45
15	7	0,47	1,27	21	1	0,05	0,13
14	4	0,29	0,78	11	4	0,36	0,99
13	4	0,31	0,83	13	3	0,23	0,63
13	4	0,31	0,83	12	5	0,42	1,13
16	4	0,25	0,68	12	3	0,25	0,68
13	5	0,38	1,04	30	9	0,30	0,81
53	21	0,40	1,07	10	3	0,30	0,81
32	12	0,38	1,02	17	7	0,41	1,12
33	14	0,42	1,15	35	7	0,20	0,54
32	11	0,34	0,93	32	11	0,34	0,93
44	14	0,32	0,86	27	3	0,11	0,30

Table S4: Recruitment rates of mGBP2 to PV of *T. gondii* in IFN- γ stimulated WT NIH 3T3 fibroblasts compared to cells with specific gene inactivation mutants 2 h post infection.

WT GFP-mGBP2 3T3				CRISPR Gal9 #2 + GFP mGBP2 3T3			
<i>T. gondii</i>	GFP-mGBP2	ratio	normalized	<i>T. gondii</i>	GFP-mGBP2	ratio	normalized
10	8	0,80	1,78	19	10	0,53	1,17
11	5	0,45	1,01	16	3	0,19	0,42
12	5	0,42	0,92	15	7	0,47	1,04
16	8	0,50	1,11	16	7	0,44	0,97
12	5	0,42	0,92	12	2	0,17	0,37
10	6	0,60	1,33	14	4	0,29	0,63
12	6	0,50	1,11	13	7	0,54	1,19
11	5	0,45	1,01	10	4	0,40	0,89
11	6	0,55	1,21	14	4	0,29	0,63
16	6	0,38	0,83	13	6	0,46	1,02
21	6	0,29	0,63	22	8	0,36	0,81
25	10	0,40	0,89	23	2	0,09	0,19
25	7	0,28	0,62	22	2	0,09	0,20
18	7	0,39	0,86	37	10	0,27	0,60
22	9	0,41	0,91	46	9	0,20	0,43
26	10	0,38	0,85	30	8	0,27	0,59
CRISPR Gal9 #3 + GFP mGBP2							
<i>T. gondii</i>	GFP-mGBP2	ratio	normalized				
21	10	0,48	1,06				
13	3	0,23	0,51				
12	4	0,33	0,74				
16	4	0,25	0,55				
15	6	0,40	0,89				
11	3	0,27	0,61				
14	4	0,29	0,63				
11	5	0,45	1,01				
15	7	0,47	1,04				
12	3	0,25	0,55				
22	4	0,18	0,40				
20	6	0,30	0,67				
30	9	0,30	0,67				
29	6	0,21	0,46				
46	10	0,22	0,48				
23	8	0,35	0,77				

Table S5: Recruitment rates of mGBP2 to PV of *T. gondii* in IFN- γ stimulated WT NIH 3T3 fibroblasts compared to cells with specific gene inactivation mutants, followed by plasmidic gene reconstitution 2 h post infection.

WT GFP-mGBP2 + mCherry-Gal9				CRISPR Gal9 #2 + GFP mGBP2 + mCherry-Gal9			
<i>T. gondii</i>	GFP-mGBP2	ratio	normalized	<i>T. gondii</i>	GFP-mGBP2	ratio	normalized
14	8	0,57	1,10	12	9	0,75	1,45
14	7	0,50	0,96	15	9	0,60	1,16
12	9	0,75	1,45	12	6	0,50	0,96
10	7	0,70	1,35	17	11	0,65	1,25
12	6	0,50	0,96	15	10	0,67	1,29
15	9	0,60	1,16	15	10	0,67	1,29
12	5	0,42	0,80	16	10	0,63	1,20
12	7	0,58	1,12	14	9	0,64	1,24

13	6	0,46	0,89	13	6	0,46	0,89
15	8	0,53	1,03	23	15	0,65	1,26
26	12	0,46	0,89	46	17	0,37	0,71
39	17	0,44	0,84	21	13	0,62	1,19
43	21	0,49	0,94	36	17	0,47	0,91
30	13	0,43	0,84	34	14	0,41	0,79
36	18	0,50	0,96	31	13	0,42	0,81
44	16	0,36	0,70	47	29	0,62	1,19
CRISPR Gal9 #3 + GFP mGBP2 + mCherry-Gal9							
<i>T. gondii</i>	GFP- mGBP2	ratio	normalized				
12	8	0,67	1,29				
12	8	0,67	1,29				
14	6	0,43	0,83				
10	5	0,50	0,96				
11	9	0,82	1,58				
14	6	0,43	0,83				
16	8	0,50	0,96				
10	5	0,50	0,96				
11	8	0,73	1,40				
10	5	0,50	0,96				
22	14	0,64	1,23				
27	15	0,56	1,07				
26	12	0,46	0,89				
26	10	0,38	0,74				
21	13	0,62	1,19				
23	8	0,35	0,67				

Table S6: Replication rates of *T. gondii* in IFN- γ stimulated NIH 3T3 fibroblasts compared to cells with specific gene inactivation mutants 22 h post infection.

WT				CRISPR Gal9 #1			
singles	rosettes	ratio	normalized	singles	rosettes	ratio	normalized
100	65	0,65	1,08	52	100	1,92	1,99
100	52	0,52	0,86	63	100	1,59	1,64
100	71	0,71	1,18	53	100	1,89	1,95
100	57	0,57	0,95	66	100	1,52	1,57
100	60	0,60	1,00	54	100	1,85	1,91
100	56	0,56	0,93	33	101	3,06	3,16
101	83	0,82	0,85	29	101	3,48	3,60
100	83	0,83	0,86	30	101	3,37	3,48
95	101	1,06	1,10	28	100	3,57	3,69
103	85	0,83	0,85	33	100	3,03	3,13
90	100	1,11	1,15	26	100	3,85	3,98
95	100	1,05	1,09	47	100	2,13	2,12
103	110	1,07	1,10	52	100	1,92	1,91
95	100	0,95	0,94	60	100	1,67	1,66
100	100	1,00	0,99	44	105	2,39	2,37
100	91	1,10	1,09				
105	106	0,99	0,98				
99	100	0,99	0,98				
CRISPR Gal9 #2				CRISPR Gal9 #3			
singles	rosettes	ratio	normalized	singles	rosettes	ratio	normalized
55	115	2,09	2,16	51	101	1,98	2,05
64	100	1,56	1,62	33	100	3,03	3,13

68	100	1,47	1,52	32	100	3,13	3,23
29	101	3,48	3,60	52	108	2,08	2,15
24	103	4,29	4,44	26	100	3,85	3,98
32	100	3,13	3,23	36	100	2,78	2,87
36	100	2,78	2,87	40	100	2,50	2,58
38	100	2,63	2,72	32	101	3,16	3,26
33	101	3,06	3,16	32	100	3,13	3,23
47	100	2,13	2,12	40	100	2,50	2,58
44	102	2,32	2,30	33	100	3,03	3,01
37	102	2,76	2,74	46	100	2,17	2,16
40	100	2,50	2,49	37	100	2,70	2,69
				41	102	2,49	2,47

Table S7: Replication rates of *T. gondii* in IFN- γ stimulated, GFP-mGBP2 expressing NIH 3T3 fibroblasts compared to cells with specific gene inactivation mutants, and replication rates in the cells lines followed by plasmidic gene reconstitution 24 h post infection.

WT GFP-mGBP2				CRISPR Gal9 #2 + GFP mGBP2			
rosettes	singles	ratio	normalized	rosettes	singles	ratio	normalized
2	13	0,15	0,35	11	9	1,22	2,81
2	13	0,15	0,35	12	11	1,09	2,51
7	11	0,64	1,46	12	9	1,33	3,07
5	12	0,42	0,96	12	12	1,00	2,30
6	12	0,50	1,15	14	10	1,40	3,22
6	12	0,50	1,15	12	10	1,20	2,76
5	17	0,29	0,68	14	13	1,08	2,48
7	15	0,47	1,07	15	10	1,50	3,45
6	20	0,30	0,69	15	11	1,36	3,14
9	14	0,64	1,48	20	12	1,67	3,84
7	12	0,58	1,34	24	15	1,60	3,68
3	13	0,23	0,53	13	4	3,25	7,48
14	20	0,70	1,61	15	4	3,75	8,63
5	20	0,25	0,58	18	10	1,80	4,14
11	17	0,65	1,49	16	10	1,60	3,68
10	21	0,48	1,10	16	9	1,78	4,09
				16	8	2,00	4,60
CRISPR Gal9 #3 + GFP mGBP2				WT GFP-mGBP2 + mCherry-Gal9			
rosettes	singles	ratio	normalized	rosettes	singles	ratio	normalized
15	15	1,00	2,30	4	15	0,27	0,48
12	14	0,86	1,97	4	19	0,21	0,38
14	13	1,08	2,48	5	11	0,45	0,82
14	7	2,00	4,60	7	10	0,70	1,27
11	8	1,38	3,16	9	11	0,82	1,48
14	9	1,56	3,58	3	11	0,27	0,49
12	14	0,86	1,97	8	11	0,73	1,32
13	10	1,30	2,99	6	10	0,60	1,09
16	7	2,29	5,26	13	17	0,76	1,38
15	11	1,36	3,14	4	11	0,36	0,66
13	12	1,08	2,49	5	17	0,29	0,53
15	9	1,67	3,84	10	18	0,56	1,00
17	8	2,13	4,89	10	17	0,59	1,06
17	9	1,89	4,35	15	16	0,94	1,70
18	11	1,64	3,77	8	14	0,57	1,03
16	9	1,78	4,09	13	18	0,72	1,31
15	5	3,00	6,90				

CRISPR Gal9 #2 GFP-mGBP2 + mCherry-Gal9				CRISPR Gal9 #3 GFP-mGBP2 + mCherry-Gal9			
rosettes	singles	ratio	normalized	rosettes	singles	ratio	normalized
10	12	0,83	1,51	5	19	0,26	0,48
3	12	0,25	0,45	2	12	0,17	0,30
8	14	0,57	1,03	3	11	0,27	0,49
14	14	1,00	1,81	5	11	0,45	0,82
4	16	0,25	0,45	6	13	0,46	0,83
12	16	0,75	1,36	3	13	0,23	0,42
5	11	0,45	0,82	4	10	0,40	0,72
10	13	0,77	1,39	8	16	0,50	0,90
5	15	0,33	0,60	7	13	0,54	0,97
12	14	0,86	1,55	8	14	0,57	1,03
7	16	0,44	0,79	12	19	0,63	1,14
10	19	0,53	0,95	14	15	0,93	1,69
8	14	0,57	1,03	8	17	0,47	0,85
13	17	0,76	1,38	12	14	0,86	1,55
4	22	0,18	0,33	11	24	0,46	0,83
11	18	0,61	1,11	10	17	0,59	1,06

Table S8: Infection rates of *T. gondii* in IFN- γ stimulated WT NIH 3T3 fibroblasts compared to cells with specific gene inactivation mutants 2 h post infection.

WT	CRISPR Gal9 #1	CRISPR Gal9 #2	CRISPR Gal9 #3	CRISPR Ckap4 #4	CRISPR Ckap4 #26
2,86	2,49	2,38	2,74	3,03	2,38
2,54	2,57	2,65	2,27	2,89	2,31
3,11	2,89	2,44	2,71	2,51	2,83
2,68	2,50	2,82	2,71	3,42	2,89
3,35	3,02	2,80	2,57	2,66	3,09
2,91	2,60	3,12	2,78	2,86	2,31

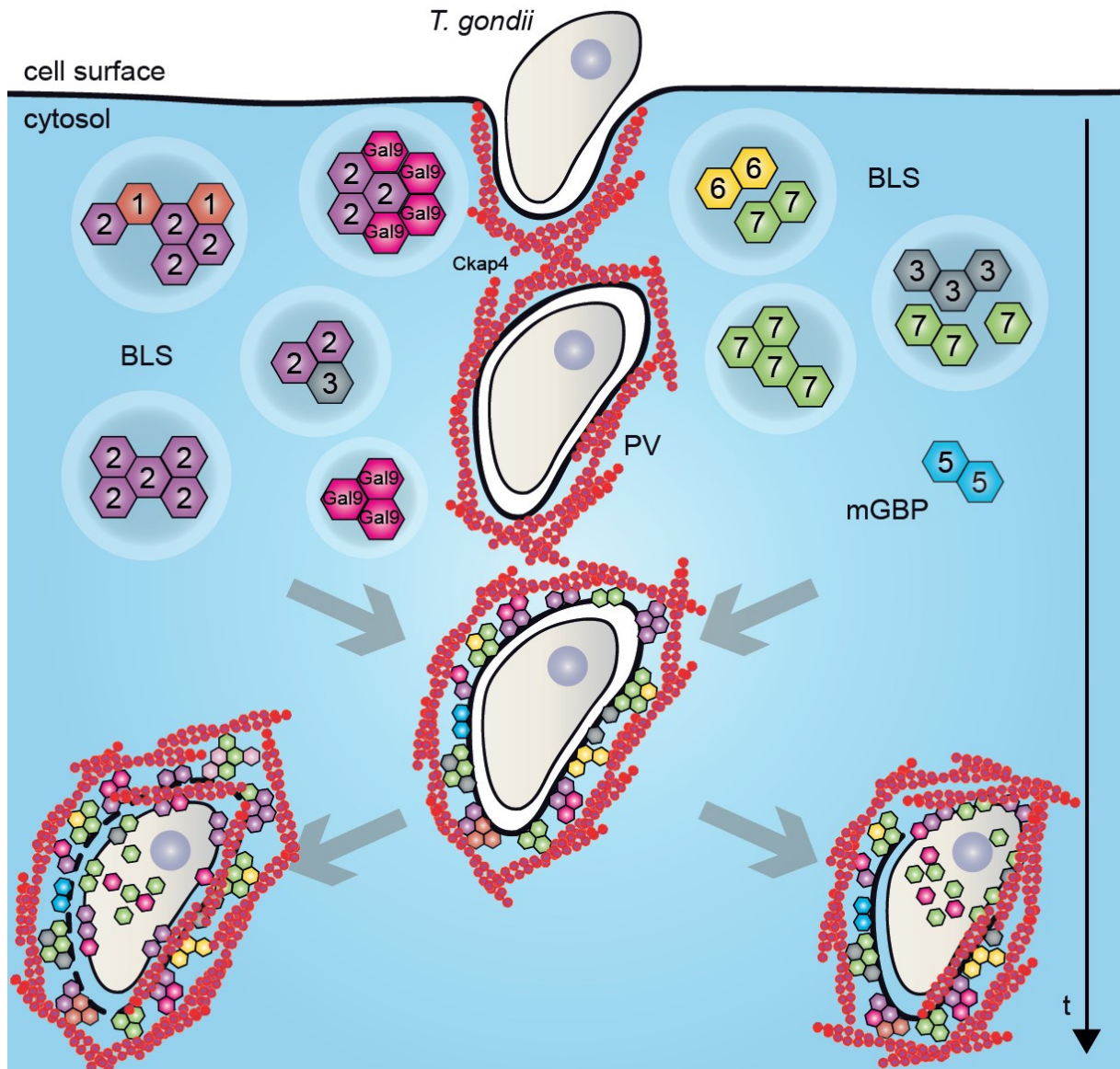


Figure S12: Schematic view of mGBPs, Gal9, and Ckap4 dynamics and multimerization in *T. gondii* infected cells. For details see Results and Discussion.

Table S9: List and validation status of *T. gondii* virulence factors as potential interaction partners of mGBP2.

<i>T. gondii</i> virulence factors	Size [bp]	pWPXL GFP C-term.	pWPXL mCherry N-term.	Virus	MEF cell line on mGBP2 ^{-/-} GFP-mGBP2/mCherry-mGBP2 background
ROP5 BK iso2	1621-1654		+	+	
ROP5 ME49 iso1/2			+	+	
ROP16 BK	2120		+	+	
ROP16 ME49			+	+	

ROP17 BK	1831		+	+	
ROP17 ME49			+	+	
ROP18 BK iso1	1623-1756		+	+	
ROP18 ME49 iso1/2/3			+	+	
GRA7 BK iso1/2	755	+	+	+	+
GRA7 ME49 iso1/2		+	+	+	+
GRA15 BK	2430-2685	+	+	+	+
GRA15 ME49		+	+	+	+
GRA25 BK	948	+	+	+	+
GRA25 ME49		+	+	+	+

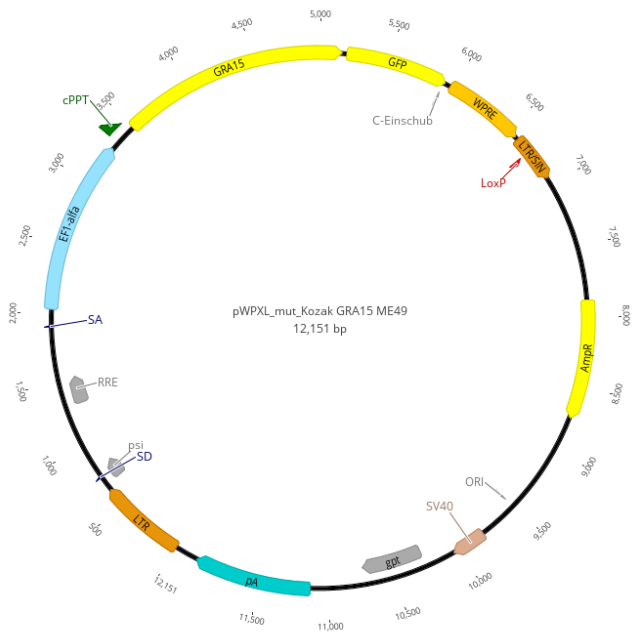


Figure S13: Expression plasmids for *T. gondii* virulence factors.

The construction and visualization of the vector was carried out using the Geneious software.

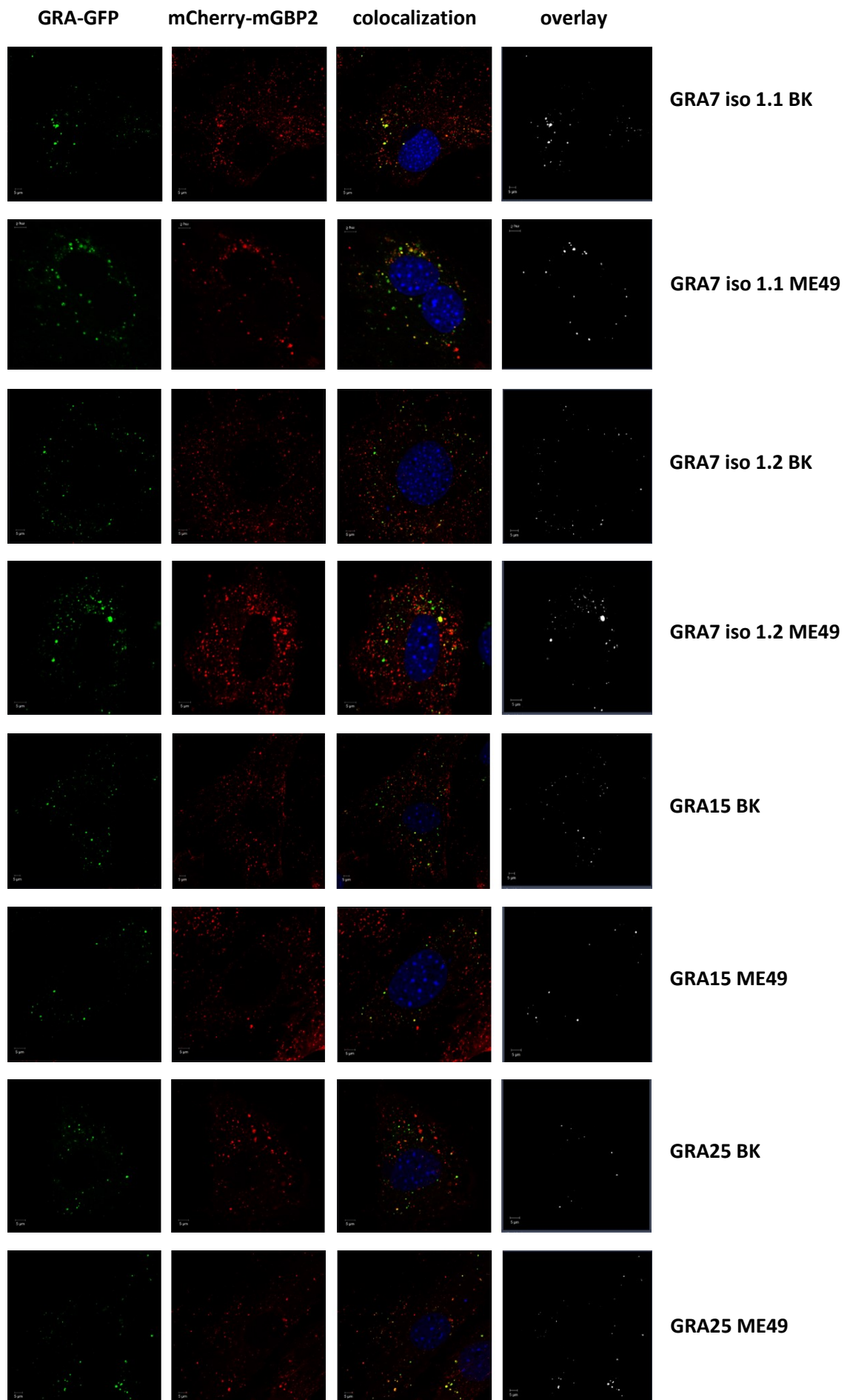
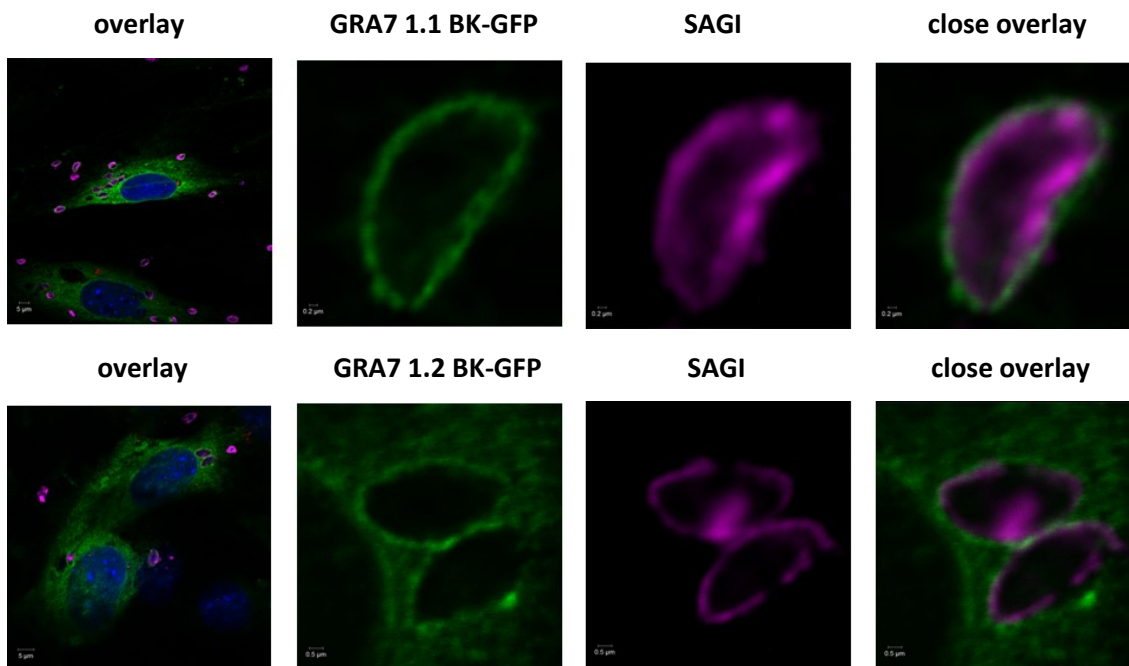
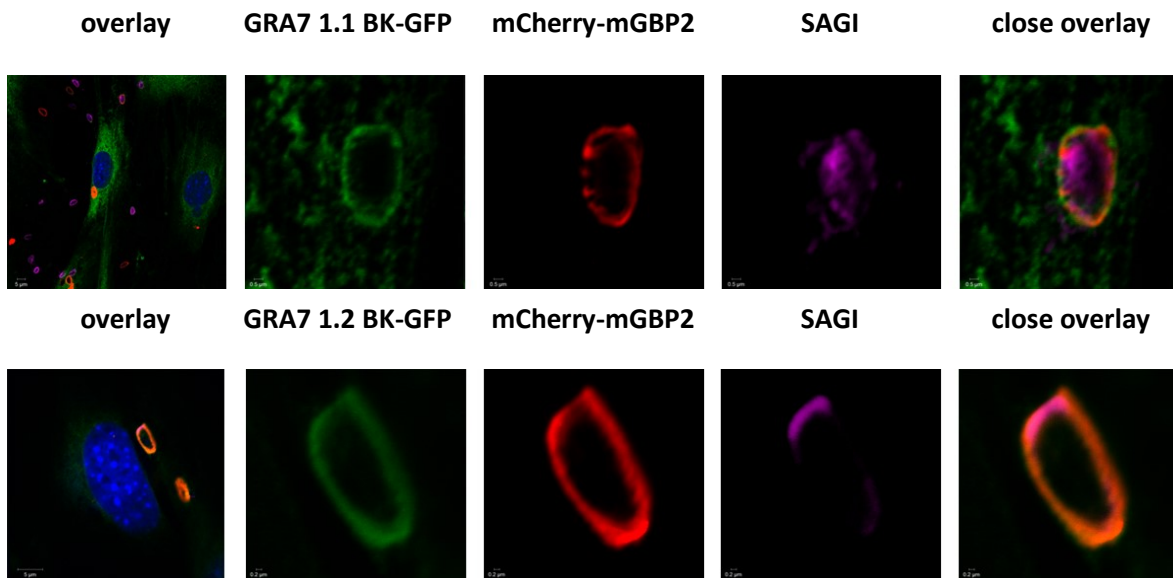


Figure S14: Intracellular colocalization of mGBP2 with GRA proteins of *T. gondii* in uninfected cells.

Colocalization of GRA7/15/25-GFP with mCherry-mGBP2 was analysed in mGBP2^{-/-} MEFs reconstituted with the indicated fusion proteins. Cells were stimulated with IFN- γ for 16 h. After fixation, cell nuclei were labelled with DAPI. Glass slides were analysed by confocal microscopy. Bars 5 μ m.

**Figure S15: Intracellular colocalization of GRA proteins with SAGI protein of *T. gondii*.**

Colocalization of GRA7-GFP with SAGI was analysed in mGBP2^{-/-} MEFs reconstituted with the indicated fusion proteins. Cells were infected with ME49 *T. gondii* for 2 h without IFN- γ prestimulation. After fixation, *T. gondii* were stained with an α -SAG1 antibody and the cell nuclei were labelled with DAPI. Glass slides were analysed by confocal microscopy. Bars 0.2, 0.5 and 5 μ m.

**Figure S16: Intracellular colocalization of mGBP2 with GRA proteins of *T. gondii* in *T. gondii* infected cells.**

Colocalization of GRA-GFP with mCherry-mGBP2 was analysed in mGBP2^{-/-} MEFs reconstituted with the indicated fusion proteins. Cells were stimulated with IFN- γ for 16 h and subsequently infected with ME49 *T. gondii* for 2 h. After fixation, *T. gondii* were stained with an α -SAG1 antibody and the cell nuclei were labelled with DAPI. Glass slides were analysed by confocal microscopy. Bars 0.2, 0.5 and 5 μ m.

Declaration of independence

I declare in lieu of an oath that this dissertation has been written by me independently and without unauthorised outside help, in compliance with the "Principles for Ensuring Good Scientific Practice at the Heinrich Heine University Düsseldorf". Furthermore, this dissertation has not been submitted to any other institution either in the present form or in a similar form.

Most of the methods required for the preparation of this thesis were carried out independently by the author.

The following methods were carried out in cooperation with:

STED microscopy (Dr. Stefanie Weidtkamp-Peters. Dr. Sebastian Hänsch: Centre of Advanced Imaging, Heinrich Heine University Düsseldorf).

Mass spectrometric analyses (Dr. Gereon Poschmann; Molecular Proteomics Laboratory (MPL), Biologisch-Medizinisches Forschungszentrum (BMFZ), Heinrich Heine University Düsseldorf).

Düsseldorf, 01.08.2024

Dr. rer. nat. Elisabeth Kravets

Curriculum vitae

Personal data

Name Elisabeth Kravets
Date of birth 03.05.1983
in Frunze/Bishkek (Kirgizstan)
Nationality German
Marital status Single
Address Beckbuschstraße 7, 40474 Düsseldorf

Course of education

1989-94 Gymnasium, Frunze/Bishkek (Kirgizstan)

1995-2003 Gymnasium auf der Gartenstraße, Mönchengladbach

06/2003 A-levels, acquired on Gymnasium auf der Gartenstraße, Mönchengladbach

10/2003-06/2008 Biochemistry studies at the Heinrich Heine University Düsseldorf
Degree: Master of Science

01/2009-12/2012 Doctoral thesis at the Institute for Medical Microbiology and Hospital Hygiene of the Heinrich Heine University Düsseldorf
Degree: PhD, Dr.rer.nat. with the grade *summa cum laude*

10/2016-11/22 Medical studies at the Heinrich Heine University Düsseldorf
Degree: Approbation

11/2016-08/2023 Doctoral thesis at the Institute for Medical Microbiology and Hospital Hygiene of the Heinrich Heine University Düsseldorf
Degree: PhD, Dr.med. with the grade